

# Iowa Research Online

---

## Biotransformation and photolysis of 2,4-dinitroanisole, 3-nitro-1,2,4-triazol-5-one, and nitroguanidine

Schroer, Hunter William

<https://iro.uiowa.edu/esploro/outputs/doctoral/Biotransformation-and-photolysis-of-24-dinitroanisole-3-nitro-124-triazol-5-one/9983776982702771/filesAndLinks?index=0>

---

Schroer, H. W. (2019). Biotransformation and photolysis of 2,4-dinitroanisole, 3-nitro-1,2,4-triazol-5-one, and nitroguanidine [University of Iowa]. <https://doi.org/10.17077/etd.rn3l166x>

---

<https://iro.uiowa.edu>  
Free to read and download  
Copyright © 2018 Hunter William Schroer  
Downloaded on 2025/01/24 16:15:59 -0600

BIOTRANSFORMATION AND PHOTOLYSIS OF 2,4-DINITROANISOLE, 3-NITRO-  
1,2,4-TRIAZOL-5-ONE, AND NITROGUANIDINE

by

Hunter William Schroer

A thesis submitted in partial fulfillment  
of the requirements for the Doctor of Philosophy  
degree in Civil and Environmental Engineering in the  
Graduate College of  
The University of Iowa

May 2018

Thesis Supervisor: Assistant Professor Craig L. Just

Graduate College  
The University of Iowa  
Iowa City, Iowa

CERTIFICATE OF APPROVAL

---

PH.D. THESIS

---

This is to certify that the Ph.D. thesis of

Hunter William Schroer

has been approved by the Examining Committee for  
the thesis requirement for the Doctor of Philosophy degree  
in Civil and Environmental Engineering at the May 2018 graduation.

Thesis Committee:

---

Craig L. Just, Thesis Supervisor

---

David M. Cwiertny

---

Gregory H. LeFevre

---

Hans-Joachim Lehmler

---

Jerald L. Schnoor

To my parents,  
who taught me the value of hard work and perseverance

The great American flag is wrapped in drag with explosives  
Compulsive disorder, sons and daughters  
Barricaded blocks and borders  
Look what you taught us!

Kendrick Lamar  
XXX

To live simply is to live gently, keeping in mind always the needs of the planet, other creatures, and the generations to come. In doing this we lose nothing, because the interests of the whole naturally include our own. . . . In claiming nothing for [ourselves, we] have everything, for everything is [ours] to enjoy as part of the whole.

Ekknath Easwaran  
*Original Goodness: On the Beatitudes of the Sermon on the Mount*

## ACKNOWLEDGEMENTS

Many thanks to my collaborators Hans-Joachim Lehmler and Xueshu Li for their synthesis of NTO and isotope-labeled DNAN as well as helpful critique of manuscripts. I am greatly indebted to Katie Langenfeld, Esteban Londono, Kate Drees, Becca Mattson, Kendra Markland, Cecilia Wolf, Alora Kraus and Hannah Langenfeld for their lab work that made all of my experiments possible. Special thanks to Ellen Black, Becca Mattson, and Kendra Markland for their ideas and inspiration as well as encouragement to stay the course when (almost) every experiment failed. I would like to thank Deb Williard, Drew Latta, and Eric Jetter for technical lab assistance. Thanks to Michelle Scherer for teaching me some of the art of technical communication. Thanks to Tim Mattes for helpful discussions. I am grateful to Vic Parcell and Lynn Teesch at the University of Iowa High Resolution Mass Spectrometry Facility as well as Stephen Harvey at the University of Minnesota Center for Mass Spectrometry and Proteomics for help with accurate mass analysis. Thanks to the Environmental Engineering & Science group at University of Iowa, who made graduate school much more fun than it could have been. I am deeply thankful for Craig Just, who recruited me to be his student and supported me every step of the way. Finally, I am grateful to my wife, Audrey, who was my rock and constant cheerleader.

## ABSTRACT

Nitroaromatic explosives have contaminated millions of acres of soil and water across the globe since World War II with known mutagenic, carcinogenic, and ecotoxicological effects. Recently, the U.S. Army initiated a shift away from traditional explosive compounds, such as trinitrotoluene (TNT) and hexahydrotrinitrotriazine (RDX), towards new, insensitive high explosive formulations. The new formulations approved for use include “IMX-101” and “IMX-104,” which contain 2,4-dinitroanisole (DNAN), 3-nitro-1,2,4-triazol-5-one (NTO), and nitroguanidine (NQ). These mixtures are less prone to accidental detonation making storage, transport, and implementation of these formulations safer for soldiers. Furthermore, initial research indicates that these compounds are less toxic than the older analogues. Despite the apparent benefits, the new explosives have higher solubility (approximately 3-300 times) than the compounds they are replacing, and NTO and NQ are fairly recalcitrant to aerobic biodegradation. The refractory nature and high solubility of the compounds raises concerns about leaching and water contamination considering the previous scale of environmental contamination from production and use of legacy explosives, while feasible strategies for cleaning up the new chemicals from soil and water have not been developed. Therefore, there is a critical need for understanding of the mechanisms of biodegradation these compounds will undergo in the environment and in engineered systems. In addition, a number of questions remain about the photochemistry of the compounds and how they may transform in sunlit surface water.

Accordingly, this thesis examines biological transformations of DNAN and NTO in vegetative, fungal, and bacterial organisms, as well as photolysis of NTO and NQ in aqueous solution and DNAN in plant leaves. I identified 34 novel biotransformation

products of DNAN using stable-isotope labeled DNAN and high resolution mass spectrometry. Most identified biotransformation products were the result of a nitro-group reduction as the first metabolic step. *Arabidopsis* plants, a *Rhizobium* bacterium, and a *Penicillium* fungus all further metabolized DNAN to produce large, conjugated compounds, and no mineralization was observed in the systems studied. All three organisms reduced both *para*- and *ortho*-nitro groups of DNAN, with a dramatic preference for *ortho* reduction. I found that photodegradation of DNAN and its plant metabolites within *Arabidopsis* leaves could impact the phytoremediation of DNAN and other contaminants. Soil slurries acclimated to nitroaromatic wastewater degraded DNAN with and without carbon and nitrogen amendments and NTO with added carbon. Organisms capable of degrading DNAN and NTO were isolated, and NTO was transformed to urea, amino-triazolone, and hydroxyl-triazolone. Photolysis of NTO sensitized singlet oxygen formation and yielded hydroxyl-triazolone, nitrite, nitrate, and ammonium. The rate of photolysis of NTO increased over the neutral pH range, and natural organic matter quenched the photolysis of NTO. An unknown volatile product accumulated in the headspace of sealed reactors after NTO photolysis. Singlet oxygen degraded NTO and formed nitrite in stoichiometric yield. Photolysis of NQ produced nitrite and nitrate, but at high pH, the reaction occurred much faster than at neutral pH, and the mass balance of inorganic nitrogen was much lower. Further work should be done to investigate the mechanisms of and products from NTO and NQ photolysis.



## **PUBLIC ABSTRACT**

Nitroaromatic explosives have contaminated millions of acres of soil and water across the globe since World War II with known mutagenic, carcinogenic, and ecotoxicological effects. Recently, the U.S. Army initiated a shift away from traditional explosive compounds, such as trinitrotoluene (TNT) and hexahydrotrinitrotriazine (RDX), towards new, insensitive high explosive formulations including 2,4-dinitroanisole (DNAN), nitrotriazolone (NTO), and nitroguanidine (NQ). These mixtures are less prone to accidental detonation making storage, transport, and implementation of these formulations safer for soldiers, and research indicates that these compounds are less toxic than the older analogues. Despite the apparent benefits, the new explosives have higher solubility in water (approximately 3-300 times) than the compounds they are replacing, and are fairly recalcitrant to aerobic biodegradation, raising concerns about leaching and water contamination considering the previous scale of environmental contamination.

Accordingly, this thesis examines metabolism of the explosives in vegetative, fungal, and bacterial organisms, as well as light-mediated destruction of the compounds in order to find practical technologies for cleaning up the explosives in the environment. I identified 34 new biotransformation products of DNAN, indicating that biological transformation and toxicity assessment of DNAN will be complex. Plants were shown to take up or transform DNAN, NTO, and NQ, and may be viable as a remediation technology. Finally, light breaks down DNAN inside plant leaves and NTO and NQ in water. Therefore, destruction by sunlight may be an important route for attenuation of the compounds in sunlit surface water.

## TABLE OF CONTENTS

LIST OF TABLES .....	ix
LIST OF FIGURES .....	x
CHAPTER 1: INTRODUCTION .....	1
CHAPTER 2: STABLE ISOTOPE-ENABLED PATHWAY ELUCIDATION OF 2,4-DINITROANISOLE METABOLIZED BY RHIZOBIUM LICHTII .....	10
CHAPTER 3: BIOTRANSFORMATION OF 2,4-DINITROANISOLE BY A FUNGAL PENICILLIUM SP. ....	23
CHAPTER 4: METABOLISM AND PHOTOLYSIS OF 2,4-DINITROANISOLE IN ARABIDOPSIS .....	55
CHAPTER 5: PHOTOLYSIS OF 3-NITRO-1,2,4-TRIAZOL-5-ONE AND NITROGUANIDINE: MECHANISMS AND PRODUCTS .....	88
CHAPTER 6: BIOTRANSFORMATION OF NTO AND DNAN BY ACCLIMATED SOIL SLURRIES AND ISOLATED SOIL BACTERIA .....	115
CHAPTER 7: CONCLUSIONS .....	137
APPENDIX A: CHEMICAL SYNTHESIS AND CHARACTERIZATION.....	143
APPENDIX B: SUPPLEMENTARY RESULTS.....	151
REFERENCES .....	156

## LIST OF TABLES

Table 1.	Water solubility of traditional and insensitive high explosives. ....	2
Table 2.	Accurate masses of DNAN metabolites and corresponding molecular formulas as determined by ESI LC-MS/QToF. ....	18
Table 3.	LC-MS/MS parameters for quantitation of DNAN and other metabolites in <i>Penicillium</i> media using a six-standard, external calibration curve. Peak areas of M306, M276, and M254 were collected in lieu of absolute quantification. ....	30
Table 4.	XCMS Online parameters for untargeted metabolomics analysis .....	31
Table 5.	Transformations of various DNAN metabolites resulting from 16 hours of incubation of strain KH1. ....	35
Table 6.	DNAN metabolites determined from LC-QToF. Each accurate mass value is the average of six biological replicates.....	38
Table 7.	[ <sup>15</sup> N <sub>2</sub> ]DNAN metabolites determined from LC-QToF. Accurate mass values are the mean of 3 biological replicates. ....	41
Table 8.	[ <sup>13</sup> C <sub>6</sub> ]DNAN metabolites determined from LC-QToF. Accurate mass values are the mean of 3 biological replicates. ....	44
Table 9.	Chemicals and reagents utilized.....	57
Table 10.	LC-QQQ parameters .....	64
Table 11.	Summary of phase II DNAN metabolites identified in <i>Arabidopsis</i> .....	71
Table 12.	Summary of [ <sup>15</sup> N <sub>2</sub> ]DNAN metabolites identified in <i>Arabidopsis</i> .....	74
Table 13.	Summary of [ <sup>13</sup> C <sub>6</sub> ]DNAN metabolites identified in <i>Arabidopsis</i> .....	75
Table 14.	Summary of guanidine nitration experiments (100 μM guanidine, 25 mM pH 7 PO <sub>4</sub> <sup>-</sup> buffer, 8 h exposure).....	114
Table 15.	Constituents in IAAAP wastewater (provided by IAAAP staff). ....	118

## LIST OF FIGURES

Figure 1.	IHE explosives referenced in this work and used in formulations “IMX-101” and “IMX-104.”.....	3
Figure 2.	Unlabeled DNAN and stable isotope-labeled versions of DNAN used in this work. ....	11
Figure 3.	Degradation over 24 h by <i>R. lichtii</i> exposed to 5 mg L <sup>-1</sup> DNAN with and without 5 mM fructose (C) and ammonium nitrate (N). Control indicates DNAN + C + N without <i>R. lichtii</i> . Error bars denote one standard deviation (n = 3).....	16
Figure 4.	Sulfated amine metabolite of DNAN (m/z 247) evidenced by ESI <sup>-</sup> LC-MS/MS mass fragments at m/z 152, 122, 80, and 46 (black bars) corresponding to the molecular structures shown. A sulfated amine of [ <sup>15</sup> N <sub>2</sub> ]DNAN (m/z 249) had fragments at m/z 154, 123, 80, and 47 (green bars), and a sulfated amine of [ <sup>13</sup> C <sub>6</sub> ]DNAN (m/z 253) had fragments at m/z 158, 128, 80, and 46 (blue bars). ....	17
Figure 5.	Exact mass spectra of sulfated and acylated DNAN metabolites. (A) Sulfated hydroxylamine metabolites of DNAN (m/z 262.9984), [ <sup>15</sup> N <sub>2</sub> ]DNAN (m/z 264.9904), and [ <sup>13</sup> C <sub>6</sub> ]DNAN (m/z 269.0167) were evidenced by ESI <sup>-</sup> LC-MS/QToF. (B) Acetylated amines of DNAN (m/z 195.0410), [ <sup>15</sup> N <sub>2</sub> ]DNAN (m/z 197.0360), and [ <sup>13</sup> C <sub>6</sub> ]DNAN (m/z 201.0615) showed methyl group losses resulting in ions at m/z 180.0177, 182.0123, and 186.0378, respectively.....	19
Figure 6.	Formation of 4-ANAN by <i>R. lichtii</i> (A) ESI <sup>+</sup> LC-MS/MS provided evidence of two monoamino metabolites of DNAN (m/z 169, black line), [ <sup>15</sup> N <sub>2</sub> ]DNAN (m/z 171, orange line), and [ <sup>13</sup> C <sub>6</sub> ]DNAN (m/z 175, green line) corresponding to the structures shown. (B) The para-substituted amino metabolite (4-ANAN) of DNAN was confirmed by mass fragments corresponding to methyl loss (M - CH <sub>3</sub> ) and nitro group loss (M - HNO <sub>2</sub> ). Both 2-ANAN and 4-ANAN were confirmed by true standards. ....	20
Figure 7.	Putative DNAN transformation pathway of <i>R. lichtii</i> . M1–5 could result from reduction of either nitro group, although ortho reduction is indicated in the diagram. Letters indicate the number of isomers detected: a = 1, b = 2, and c = 5. ....	22

Figure 8.	Time series of (A) 10 mg/L DNAN degradation and (B) metabolite formation over 21 days of incubation at 30 °C with <i>Penicillium</i> sp. KH1 in the metabolomics experiment. Error bars represent one standard deviation from the mean. Metabolomics analysis was executed on media after ten days of incubation with an additional DNAN spike after seven days.....	33
Figure 9.	Time series of (A) 10 mg/L DNAN degradation and (B) metabolite formation over fourteen days of incubation at 30 °C with <i>Penicillium</i> sp. KH1 (n=3, <sup>a</sup> denotes n=2). The sum of 2-ANAN, 2-ANP, 4-ANAN, 4-ANP, DNP and 2-NAc-NAN in the killed control is represented with closed blue triangles (n=1). Error bars represent one standard deviation from the mean. ....	34
Figure 10.	Proposed DNAN transformation pathways for <i>Penicillium</i> sp. KH1. Brackets indicate the intermediate compound was not detected. An “X” over an arrow indicates the reaction was not observed when incubated with the starting substrate for 8 and 16 hours. An “a” indicates an isomer of M196 of unknown structure.....	37
Figure 11.	LC-MS chromatogram of <i>m/z</i> 195 in ESI <sup>-</sup> mode illustrating that isomeric starting substrates confirm five isomers of M196 resulting from either <i>ortho</i> ( <i>o</i> ) or <i>para</i> ( <i>p</i> ) nitro-reduction of DNAN.....	48
Figure 12.	Possible structures for the six isomers of M196 and reactions required for formation from the corresponding amino-nitrophenol.....	49
Figure 13.	LC-MS (SIM) peak areas over time of <i>m/z</i> 195 in ESI <sup>-</sup> mode for metabolite (A) M196b and (B) M196d produced from DNAN by <i>Penicillium</i> sp. KH1. Error bars are one standard deviation from the mean (n=3, n=2 days 5, 6, and 14). The open triangles are the concentrations in the killed control media (n=1). ....	51
Figure 14.	Concentration trends of (A) sulfated and (B) malonylated DNAN metabolites as demonstrated by LC-MS/MS peak areas. Error bars represent one standard deviation from the mean (n=3, n=2 days 5, 6 and 14). ....	52
Figure 15.	Irradiance of Suntest CPS+ at 750 W/m <sup>2</sup> and growth chamber lights .....	61
Figure 16.	DNAN uptake kinetics at varying initial concentrations (n=3) .....	68
Figure 17.	DNAN mass in hydroponic media and <i>Arabidopsis</i> whole plant tissue .....	69
Figure 18.	Mass of DNAN and phase I metabolites in plant tissues and media .....	70

Figure 19.	Proposed relationships between some identified DNAN metabolites in <i>Arabidopsis</i> .....	76
Figure 20.	Hydrolysis of metabolite M330 to yield 2-ANAN .....	77
Figure 21.	Metabolite formation over time in whole plant tissues.....	78
Figure 22.	DNAN and M330 in <i>Arabidopsis</i> leaves during exposure to simulated sunlight .....	82
Figure 23.	$^{15}\text{NO}_2^-$ measured in leaf extracts exposed to simulated sunlight or in the dark .....	83
Figure 24.	Principal components plot of photolyzed leaves (teal circles) compared to dark-control leaves (black circles) .....	84
Figure 25.	A) molar extinction coefficient of NTO from pH 5 to 9 and B) spectral irradiance of the solar simulator ( $750 \text{ W/m}^2$ ) and the 200 W Xe/Hg lamp with a 400 nm cutoff filter.....	93
Figure 26.	Observed pseudo-first-order rates and half-life of direct photolysis of NTO from pH 5-12 (25 mM buffer, $10 \mu\text{M}$ NTO, sparged with air). Error bars are 95% confidence intervals and are not shown when within the symbol. ....	94
Figure 27.	Rates of indirect photolysis of NTO with respect to SRNOM concentration ( $10 \mu\text{M}$ NTO, 5 mM borate buffer, pH 8.5). Rates are corrected for light screening, and error bars are 95% confidence intervals. A one-way ANOVA determined a statistical significance among rates ( $p < 0.001$ ) and letters indicate significantly different groups by a post-hoc Tukey multiple comparisons test ( $\alpha = 0.05$ ). ....	95
Figure 28.	Probing mechanisms of NTO ( $10 \mu\text{M}$ ) direct photolysis. A) direct photolysis of NTO with varied dissolved oxygen regimes. B) direct photolysis of NTO with and without quenchers of singlet oxygen (1 mM sodium azide) or excited triplet states (5 mM sorbic acid). Lines are linear regression of natural log-transformed data. ....	96
Figure 29.	Production of $^1\text{O}_2$ by NTO as demonstrated by A) photodegradation of $20 \mu\text{M}$ FFA in the presence of varying concentrations of NTO and 1 mM sodium azide (pH 8.5) and B) photolysis of NTO in $\text{D}_2\text{O}$ and $\text{H}_2\text{O}$ (pH 7, pD 7.4). ....	97

Figure 30.	Observed, pseudo-first-order rate constants of NTO direct photolysis with initial concentrations spanning four orders of magnitude (pH 8, 25 mM phosphate buffer). Error bars are 95% confidence intervals and are not displayed when within the symbols. A one-way ANOVA determined a statistical significance among rates ( $p < 0.001$ ) and letters indicate significantly different groups by a post-hoc Tukey multiple comparisons test ( $\alpha = 0.05$ ).....	98
Figure 31.	Determination of 2 <sup>nd</sup> -order reaction rate constants of NTO with A) singlet oxygen using FFA as a probe and B) hydroxyl radical using pCBA and a competition kinetics approach. Solid lines are linear regression and dotted lines are 95% confidence intervals. ....	99
Figure 32.	Effect of nitrite on A) NTO and B) hydroxyl-triazolone photolysis.....	100
Figure 33.	Photolysis and inorganic nitrogen products from photolysis of 100 $\mu$ M NTO under varying initial conditions. ....	101
Figure 34.	A) Molar absorptivity of NQ and irradiance of solar simulator. B) UV-Vis absorbance of 100 $\mu$ M NQ solution after photolysis for the indicated time. ....	107
Figure 35.	Variation in A) molar absorptivity from pH 5-9 and B) pseudo-first-order rate constant of NQ photolysis (750 W/m <sup>2</sup> , 35 °C) from pH 2-12. ....	108
Figure 36.	Production of nitrite and nitrate after five hours of NQ photolysis (100 $\mu$ M, 25 mM buffer).....	109
Figure 37.	Summary of nitrite and nitrate yield from data in Figure 36 after 95% degradation of NQ. ....	110
Figure 38.	Preliminary experiments with photo-sensitizers to determine if NQ is reactive with any photo-produced reactive intermediates, i.e., if NQ would be subject to indirect photolysis. ....	111
Figure 39.	Photolysis of 100 $\mu$ M NQ in the presence and absence of 500 $\mu$ M guanidine and nitrite. Lines are linear regression of the log-normalized data. ....	112

Figure 40.	Preliminary NTO (5 mg L <sup>-1</sup> ) degradation in minimal salts media by acclimated soil slurries. (A) n = 2 and error bars are standard deviation of the mean. Error bars are not shown when they fall inside the symbol and (B) is concentration of NTO in the soil slurries (n = 1) with carbon (C; 10 mM glucose and 5 mM succinate) and nitrogen (N; 5 mM NH <sub>4</sub> Cl), which were spiked again with NTO after nine days (indicated by the vertical dashed line). The organisms in this study were isolated from the soil slurry with added carbon and nitrogen in (B) after 16 days (indicated by the arrow). .....	119
Figure 41.	Screening for NTO degradation in MSM media with 10 mM glucose, 5 mM succinate, and 5 mM NH <sub>4</sub> Cl by organisms isolated from soil slurries. The type of media the organism was isolated on is indicated in the label for each organism, and the organism numbers are arbitrary. ....	120
Figure 42.	Data from Figure 41, averaged by organism as identified by DNA sequencing.....	121
Figure 43.	Neither <i>Bacillus</i> isolate (B1, panel A; B2, panel B) degraded NTO (5 mg L <sup>-1</sup> ) in minimal salts media when it was the sole source of carbon (C; 10 mM glucose and 5 mM succinate) or nitrogen (N; 5 mM NH <sub>4</sub> Cl). The data were not corrected for evaporation.....	123
Figure 44.	Degradation of NTO and resulting transformation products in minimal salts media containing 10 mM glucose, 5 mM succinate, and 5 mM NH <sub>4</sub> Cl. A) Strain B1 produces urazole and ATO. B) Strain B2 produces some ATO and some unknown products. ....	124
Figure 45.	Degradation of urazole (left) and ATO (right) in minimal salts media containing 10 mM glucose, 5 mM succinate, and 5 mM NH <sub>4</sub> Cl by <i>Bacillus</i> sp. isolate 1 to form urea. ....	125
Figure 46.	Degradation of ATO into unknown products by <i>Bacillus</i> sp. 2 in minimal salts medium with 10 mM glucose, 5 mM succinate, and 5 mM NH <sub>4</sub> Cl. ....	126
Figure 47.	Putative degradation pathways of NTO by <i>Bacillus</i> spp. 1 and 2 (B1 and B2, respectively).....	127
Figure 48.	NTO degradation by acclimated soil slurries in minimal salts media with various carbon (C, 10 mM glucose and 5 mM succinate) and nitrogen (N, 5 mM NH <sub>4</sub> Cl) regimes (n = 3). Additional carbon and nitrogen were added at 15 days as indicated by the vertical dashed line. The NTO control contained 500 mg L <sup>-1</sup> sodium azide. ....	128



Figure 49.	Degradation of DNAN by acclimated soil slurries with various carbon (C, 10 mM glucose and 5 mM succinate) and nitrogen (N, 5 mM NH <sub>4</sub> Cl) regimes in MSM media. Unamended contains DNAN and MSM, while the killed control contains DNAN, MSM, and 5 mg L <sup>-1</sup> sodium azide. ....	132
Figure 50.	DNAN degradation in minimal salts media without added carbon or nitrogen from Figure 49 over a longer time period. Serial dilutions of the unamended soil slurries were taken after 54 days (after 98% DNAN degradation). ....	133
Figure 51.	Degradation of DNAN (left panel) and resulting sum of 2-ANAN and 4-ANAN (right panel) in liquid media by soil slurry isolates grown on R2A agar. ....	134
Figure 52.	Degradation of DNAN (left panel) and resulting sum of 2-ANAN and 4-ANAN (right panel) in liquid media by soil slurry isolates grown on LB agar. ....	135
Figure A1.	LC-MS scan from <i>m/z</i> 40-500 in positive electrospray ionization mode showing the purity of 2-NAc-NAN synthesized as described in Chapter 2 (blank is in red). ....	144
Figure A2.	<sup>1</sup> H NMR spectrum of 2-NAc-NAN. ....	145
Figure A3.	<sup>13</sup> C NMR spectrum of 2-NAc-NAN. ....	146
Figure A4.	<sup>1</sup> H NMR of 1,2,4-triazolone (TO). ....	147
Figure A5.	<sup>13</sup> C NMR of 1,2,4-triazolone (TO). ....	148
Figure A6.	<sup>1</sup> H NMR of 3-nitro-1,2,4-triazol-5-one (NTO). ....	149
Figure A7.	<sup>13</sup> C NMR of 3-nitro-1,2,4-triazol-5-one (NTO). ....	150
Figure A8.	High resolution mass spectra of 3-nitro-1,2,4-triazol-5-one (NTO). ....	150
Figure B1.	Radioactivity in liquid chromatography fractions from willow tree root and leaf extracts after four days of exposure to [ <sup>14</sup> C <sub>6</sub> ]DNAN. ....	151

Figure B2.	<p>Uptake or root transformation of NTO by switch grass (<i>Panicum virgatum</i> ‘Alamo’). Grass was grown from seed by overnight stratification in DI water at 4 °C, and then grown in potting soil for 6 weeks. Four individual grasses were selected and transferred to 50 mL hydroponic 0.25x Hoaglands solution in a 100 mL, black-painted beaker sealed with a foam plug for two weeks of acclimation. Then, the four replicate grasses were exposed to 10 mg L<sup>-1</sup> NTO in 0.25x Hoaglands solution for 17 days, and samples were withdrawn and analyzed by HPLC over time to evaluate uptake and transformation by the switchgrass. Standard error of the means falls within the symbols. ....</p>	152
Figure B3.	<p>Degradation of 10 mg L<sup>-1</sup> NTO in solution by the <i>Penicillium</i> sp. featured in chapter 3 of the thesis. Nitrite, nitrate, and urea were qualitatively identified to form from the reaction. ....</p>	153
Figure B4.	<p>Uptake of 5 mg L<sup>-1</sup> NQ from 0.25x Hoaglands solution by switchgrass (<i>Panicum virgatum</i> ‘Alamo’) and accumulation in leaf and root tissues over 12 days .....</p>	154

## CHAPTER 1:INTRODUCTION

### Background and Rationale

Over 15 million acres in the United States of America – an area the size of the state of West Virginia – are suspected or known to be contaminated with military munitions.<sup>1</sup> Due to the extensive manufacture and use of munitions explosives, the compounds can enter the environment through a variety of channels including: unexploded ordinance at training ranges, permitted disposal or spills at manufacturing facilities, and release at storage and disposal locations.<sup>2</sup> Release of explosives to the environment is concerning due the documented negative health effects attributed to this class of compounds.<sup>2-4</sup> For example, trinitrotoluene (TNT) is classified as a priority pollutant by the U.S. EPA due to mutagenic and carcinogenic characteristics.<sup>3</sup> Therefore, the widespread use and release of explosive chemicals is a critical concern for the health of humans and ecosystems, and viable remediation and treatment methods must be developed for these compounds.

Munitions are high-energy chemicals that are typically organic and nitroaromatic. The nitro groups that impart explosive performance to munitions chemicals are highly electronegative, withdrawing electrons from and lending stability to associated aromatic moieties.<sup>5</sup> The specific chemical functionalities of the nitro groups define the nitroaromatic explosives as generally recalcitrant to oxidation, making remediation of the munitions compounds difficult and expensive.<sup>4,6</sup> Due to oxidative recalcitrance, the compounds are often reduced from nitro- to amino-containing compounds, *via* reactive nitroso moieties. Once reduced, the amino-containing compounds can bind reversibly and irreversibly to humic matter in soils, making assessment of mass balances difficult in practice.<sup>7</sup> To further complicate the remediation and fate of munitions in the environment, the reduced amino-containing compounds are often more toxic to flora and fauna, generally making this remediation pathway undesirable.<sup>3</sup>

Due to the difficulties of natural attenuation or bioremediation of explosives, treatment has often been accomplished by cost- and energy-intensive methods such as burn-in-place or soil excavation with combustion, or landfilling.<sup>3</sup> Given the labor and energy demands of these methods, some alternative technologies have been investigated. For example, initial studies resulted in EPA approval of composting TNT-contaminated soil. However,

further studies have shown that TNT metabolites and extracts from composted TNT waste remain highly mutagenic.<sup>8,9</sup> Bioremediation has been investigated with some laboratory success in fungal and bacterial systems. In addition, phytoremediation (using green plants or vegetation to clean up contaminated soil and water) has been investigated as a cheaper alternative to *ex situ* methods. Hybrid poplar trees have been the most studied organisms for phytoremediation of explosives due to high growth rates and extensive root systems for trapping and pumping contaminated water.<sup>10-14</sup> *Arabidopsis thaliana* has been engineered to contain an RDX-degrading cytochrome P450, which enhanced phytoremediation of RDX contaminated soil and decreased phytotoxicity of the explosive.<sup>15</sup> Glucotransferases and glutathione transferases in *Arabidopsis* have also been shown to detoxify TNT.<sup>5, 16</sup> Multiple additional species of plants have been shown to take up and transform TNT, RDX, and HMX in soil and in hydroponic systems. Overall, remediation of explosives with biotic systems is a promising *in situ* approach that has the potential to effectively contain and degrade the explosives.

While there has been extensive study of treatment and remediation of legacy explosives, these compounds are being phased out in favor of new compounds called insensitive high explosives (IHE). IHE are less prone to accidental detonation than traditional explosive compounds such as TNT and hexahydrotrinitrotriazine (RDX).<sup>17</sup> The increased safety of the new explosives protects soldiers and simplifies transport logistics; however, the environmental fate of the compounds remains relatively unstudied.<sup>18, 19</sup> The new formulations approved for use include “IMX-101” and “IMX-104,” which contain 2,4-dinitroanisole (DNAN), 3-nitro-1,2,4-triazol-5-one (NTO), nitroguanidine (NQ), and RDX (Figure 1). The high aqueous

solubility of the newer compounds compared to older explosives currently makes them a risk for soil and groundwater contamination (Table 1).<sup>20</sup> In addition to concerns about environmental transport,

Table 1. Water solubility of traditional and insensitive high explosives.

Compound	Solubility (mg L <sup>-1</sup> )	Log <i>K</i> <sub>ow</sub> <sup>a</sup>
TNT	100	1.7
RDX	62	-2.2
DNAN	276	1.6
NQ	3,800	-1.3
NTO	16,642	-1.4

<sup>a</sup>calculated using ACD/ChemSketch 2015.2.5

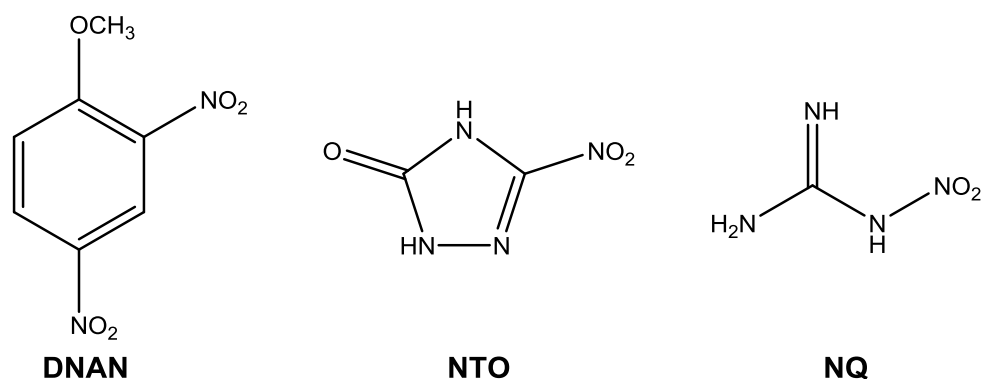


Figure 1. IHE explosives referenced in this work and used in formulations “IMX-101” and “IMX-104.”

DNAN is toxic to bacteria, earthworms, plants, and mammals.<sup>17, 21</sup> The previous scale of environmental contamination from legacy explosives warrants concern over the widespread release of the newly-implemented explosives.<sup>2</sup> In addition, more unexploded ordinance remains after IHE detonation when compared to traditional explosives, and the compounds dissolve quickly on firing ranges, in order of their solubilities in water.<sup>20, 22, 23</sup>

### Biotic Transformation and Toxicity of IHE

#### DNAN

In general, the new IHE are more amenable to biodegradation than the legacy explosives. The most common transformation route of DNAN is *ortho*-nitro group reduction to 2-amino-4-nitroanisole (2-ANAN).<sup>19, 24-27</sup> Further reduction to 2,4-diaminoanisole has been observed and is more favorable under anaerobic conditions.<sup>19, 25, 26, 28-30</sup> One study has demonstrated mineralization of DNAN by an isolated *Nocardioides* sp. *via* demethylation to 2,4-dinitrophenol (DNP).<sup>31</sup> Recently, this bacterium was utilized in reactors and endogenous soils and was shown to effectively remediate DNAN in engineered systems.<sup>32</sup> Chapter two demonstrates a bacterium that performs acetylation, formylation, and sulfation of DNAN after reduction of the nitro groups, identifying eleven metabolites that were previously unknown.<sup>27</sup> In the same study, I demonstrated that initial reduction of the *para*-nitro group is possible with this soil- and plant-associated microbe.

This reduction pathway was previously unobserved, but has now been seen in soil microcosms.<sup>26, 27</sup> In an isolated fungal system also originating from plant tissues (*Penicillium* sp.), I identified 13 additional novel metabolites of DNAN (Chapter 3).<sup>33</sup> These compounds result from malonylation, acetylation, hydroxylation, and sulfation of reduced and demethylated DNAN metabolites.

In bulk soil slurries and activated sludge, DNAN was transformed rather slowly under aerobic and microaerophilic conditions without carbon and nitrogen amendments (Chapter 6).<sup>25, 26, 28</sup> Anaerobic conditions enhance DNAN degradation, facilitating reduction of both nitro groups.<sup>25, 26</sup> In sludge and soil, azo- and azoxy-dimers of reduced DNAN were also detected, including methyl and methylene conjugates.<sup>25, 26, 28</sup> Similar reduction and dimerization reactions have been well-characterized for TNT.<sup>34, 35</sup> Preliminary plant uptake studies have indicated that the phytotoxicity of DNAN could be higher than TNT based on ryegrass seedling emergence.<sup>17</sup> Grass extracts contained DNAN and acid-extractable 2-ANAN indicating conjugation of the reduced product, but no further metabolites were identified.<sup>17, 36</sup> Our preliminary data indicates demethylation and hydroxylation of DNAN and further conjugation of mono- and di-saccharide moieties in willow tree cuttings (unpublished). DNAN was taken up quickly and readily translocated to leaves and stems as confirmed by [<sup>14</sup>C]DNAN incubations (see Appendix B). *Arabidopsis* takes up DNAN and readily transforms DNAN to large, soluble transformation products (Chapter 4).<sup>37</sup>

Overall, DNAN is the most toxic of the IHE constituents.<sup>38</sup> The toxicity of DNAN, and two of its amino derivatives towards nitrifiers, aerobic heterotrophs, methanogens and the bioluminescent bacterium, *Aliivibrio fischeri* has been investigated.<sup>24</sup> The results indicated that reduction to diaminoanisole (uncommon under aerobic conditions) was required to lower DNAN toxicity. A follow up study indicated that azo dimers were more toxic to *A. fischeri* and methanogens than DNAN, and methanogens were inhibited by the intermediate amino and nitroso reduction products.<sup>39</sup> DNAN or DNAN transformation products were also toxic to ryegrass, zebrafish embryos, algae, earthworms, rats, aquatic invertebrates, fish, and tadpoles, although, in general, the toxicity is lower than for TNT, which it is replacing.<sup>17, 40-43</sup>

## NTO

NTO has been less studied than DNAN. NTO behaves as an organic acid and has a pKa of 3.76.<sup>20</sup> In terms of transformation, oxidation of NTO to 3-hydroxy-1,2,4-triazol-5-one (urazole) was observed in hepatic microsomes under aerobic conditions.<sup>44</sup> NTO was mineralized by *Bacillus licheniformis* in a batch culture as confirmed by <sup>14</sup>C labeling, but the process required a pH of 6 for reduction to aminotriazolone (ATO) with an adjustment to pH 8 for ATO mineralization.<sup>45</sup> Identified products included CO<sub>2</sub> and urea. In a separate study with NTO degradation in batch, NTO was observed to be degraded by an enriched microbial culture.<sup>46</sup> A denitrated triazolone product was proposed, but mass spectral evidence indicated no such transformation.<sup>46</sup> The aerobic nature of the previous two studies was questioned by Krzmarzick et al., who observed no NTO degradation in aerobic soil slurries.<sup>18</sup> Krzmarzick et al. found rapid reduction to ATO under anaerobic conditions, with no further transformation. Interestingly, ATO was quickly degraded to inorganic nitrogen under *aerobic* conditions. Therefore, NTO degradation in soil may require anaerobic and subsequent aerobic conditions for complete mineralization. Besides bacterial degradation, a preliminary study claimed NTO was not detected in plant biomass grown in IMX-101 contaminated soil, however the limit of quantification was not determined, and no transformation products were examined.<sup>36</sup> Preliminary experiments suggest that NTO is taken up or transformed by switchgrass (Appendix B). Preliminary data from an incubation of NTO with a *Penicillium* sp. resulted in mineralization of NTO to urea, nitrite, and nitrate under aerobic conditions (Appendix B).

The toxicity of NTO appears to be much lower than traditional nitroaromatic explosives. The mutagenic potential of NTO was tested under a variety of conditions, and the results indicated no potential for genetic hazards due to the compound.<sup>47</sup> In an aqueous toxicity investigation, NTO was classified as “practically non-toxic” to unicellular algae and *Ceriodaphnia dubia*.<sup>48</sup> In addition, DNAN and NTO were found to be less toxic and have less bioaccumulation potential than TNT to *Rana pipiens* tadpoles.<sup>43, 49</sup> NTO was found to have no endocrine disrupting properties in uterotrophic bioassays in rats.<sup>50</sup> However, a more in-depth study found evidence of reproductive toxicity to male rats caused by NTO. The results indicated that NTO could affect steroidogenesis or have direct testicular toxicity in mammals.<sup>51</sup> NTO inhibited methanogenesis, and ATO was toxic to

*Daphnia magna*.<sup>52</sup> Finally, a study of photolysis of IMX-101 and the individual constituents indicates a 100-times increase in toxicity of NTO to *Ceriodaphnia dubia* after photolysis, but questions remain about the underlying cause of the toxicity increase.<sup>38</sup>

## NQ

Nitroguanidine has historically been used as a rocket propellant and is now being repurposed for IMX-101.<sup>53</sup> The toxicity of NQ is low across the domains of life, from bacteria and aquatic invertebrates to plants and mammals.<sup>54-58</sup> Interestingly, photolysis increases the toxicity of NQ to fathead minnows, algae, and *Daphnia magna*, as well as to *Ceriodaphnia dubia* by 1000 times for yet unknown reasons.<sup>38, 55</sup> In non-contaminated soil, slurries augmented with carbon induced complete NQ degradation in about six days, while adding carbon and nitrogen only produced moderate degradation.<sup>53</sup> Unamended soil did not degrade NQ in this study or others.<sup>59-61</sup> An organism capable of mineralizing NQ was isolated from the soil slurry with added carbon, and was demonstrated to produce ammonia and N<sub>2</sub>O from NQ.<sup>53</sup> Surface water microcosms transformed NQ with the addition of nutrients, and degradation occurred slowly under anaerobic conditions amended with nutrients.<sup>56</sup> Soil columns did not fully transform NQ and land application was discouraged by Williams et al.<sup>60</sup> In terms of plant uptake and transformation, tall fescue and soybean took up NQ under hydroponic and soil conditions, with no transformation products detected.<sup>57</sup> We found that switchgrass took up NQ into the blades, with no transformation and a full mass balance (Appendix B).

## Abiotic Transformation and Treatment of IHE

### DNAN

In a study of the photolysis of DNAN, reaction products included nitrite and nitrate, indicating photo-oxidation could represent a major pathway of DNAN attenuation in shallow surface waters and shallow soil.<sup>62</sup> Another reaction product identified was 2,4-dinitrophenol, and various other hydroxyl-substituted products were proposed. More recently, Perreault et al. identified methoxynitrophenol formation from renitration of DNAN photoproducts during photolysis in IMX-101 mixtures.<sup>23</sup> Interestingly, dissolved organic matter had little effect on the photolysis of DNAN. The photolysis half-life of



DNAN was fast ( $\leq 1$  day), and therefore, photo-oxidation could represent an economical and effective remediation alternative.<sup>62</sup> DNAN is observed not to hydrolyze under environmentally relevant conditions.<sup>63, 64</sup> DNAN has been transformed to DNP without additional substrates using an immobilized demethylase enzyme.<sup>65</sup> Sorption to lignin and granular activated carbon have been proposed for removing DNAN from process waters and appear effective.<sup>66, 67</sup> The sorption of DNAN and its amino derivatives was investigated in soil columns.<sup>19</sup> Reduction of the nitro groups was shown to increase irreversible soil binding and sorption tendency, in agreement with previous studies of reactive amine-containing TNT transformation products.<sup>7</sup> In a study of soil microcosms with [<sup>14</sup>C]DNAN, some DNAN was irreversibly incorporated into humus material, with a strong correlation between <sup>14</sup>C incorporation and the fraction of organic carbon in the soil. Horseradish peroxidase amendment also increased the propensity of <sup>14</sup>C binding to soil.<sup>68</sup> Iron coupled to electron shuttling organisms has been demonstrated to reduce DNAN.<sup>69</sup> Finally, zero-valent iron was used to reduce DNAN waste before Fenton's oxidation and polishing with a biological treatment scheme.<sup>70</sup> DNAN reduction products can be oxidized by manganese oxides and DNAN can be reduced by various iron redox systems.<sup>71-73</sup>

### *NTO*

Electrochemical and Fenton's oxidation of NTO yields complete mineralization.<sup>74, 75</sup> In terms of environmental mobility, NTO was shown to weakly sorb to soil slurries, as expected from the high solubility.<sup>76</sup> Some loss of NTO was observed in live soils relative to autoclaved soils, which the authors attribute to biodegradation, but no transformation products were identified. Autoclaving is known to reduce ferrous iron, which can oxidize soil organic matter and promote reduction of the NTO.<sup>77</sup> Therefore, NTO may have been removed by abiotic processes rather than biodegradation in this case.<sup>76</sup> A study on DNAN and NTO interactions with clay minerals and metal oxides indicated that ATO could be transformed by a Mn-oxide.<sup>78</sup> No transformation products were identified, however. Additionally, little is known about the sorptive properties of the major NTO transformation product, ATO. One study demonstrated the kinetics of iron-copper reduction of NTO and DNAN, but no transformation products were identified.<sup>79</sup> NTO photolysis is relatively slow in the absence of a catalyst but is greatly enhanced with the

addition of  $\text{TiO}_2$ .<sup>23, 74</sup> No previous studies have been carried out on the indirect photolysis of NTO and only two studies addressed photolysis of mixtures of DNAN, NQ, and NTO, with some questions remaining.<sup>23, 38</sup> For example, the products that cause aquatic toxicity after NTO and NQ photolysis are still unknown. In addition, the mechanism of NTO-enhanced nitration of guanidine to form NQ in the presence of  $\text{TiO}_2$  is also unclear. These questions are investigated in chapter five.

## *NQ*

NQ is labile to photodegradation (Chapter 5). Haag et al. claimed the major product was hydroxyguanidine, while Burrows et al. observed guanidine, urea and cyanoguanidine.<sup>56, 80</sup> More recently, Perreault et al. observed guanidine as the stoichiometric product from NQ photolysis in unbuffered solution.<sup>23</sup> However, Noss and Chyrek observed guanidine formation during photolysis at low pH, but a lower mass balance and unknown products at higher pH.<sup>81</sup> These conflicting reports left questions about the pH dependence and product distribution of NQ photolysis, which are examined further in chapter five. NQ is apparently recalcitrant to hydrogen peroxide and ozone oxidation.<sup>81</sup> Under anaerobic conditions, NQ was reduced to nitrosoguanidine, which was then abiotically transformed in sludge.<sup>82</sup>

## **Thesis Organization**

The thesis is structured as follows. Chapters two and three are studies of biotransformation of the explosive DNAN by a bacterium and fungus, respectively. These two organisms were isolated from hybrid willow trees in an attempt to discover endophytic organisms that would be capable of degrading the explosive. In theory, the willow tree could provide an environmental niche where the organisms could survive and thrive, while the tree also pumped explosive-contaminated water to the organisms for the organisms to degrade. Chapter four is a study of biotransformation and subsequent photolysis of DNAN within the model plant *Arabidopsis thaliana*. This study was conducted to demonstrate that plants can take up and transform the explosive. Information on transformation products is useful for field monitoring and to demonstrate that measuring the parent compound may not be an accurate indicator of how much explosive

was taken up by the plant. Further, this study demonstrates that DNAN and its plant metabolites can be photolyzed inside plant leaves, further detoxifying the compound, but complicating the analysis and mass balance assessment of DNAN in the field. Chapter five is a study of NTO and NQ photolysis in simulated sunlight. The purpose was to examine transformation kinetics and mechanisms of the two compounds for potential treatment by UV or if the compounds contaminate sunlit surface waters. Chapter six examines transformation of NTO and DNAN by isolated organisms and bulk soil slurries acclimated to nitroaromatic wastewater in an attempt to isolate explosive-degrading organisms useful for remediation.

## CHAPTER 2: STABLE ISOTOPE-ENABLED PATHWAY ELUCIDATION OF 2,4-DINITROANISOLE METABOLIZED BY RHIZOBIUM LICHTII

This chapter has been peer-reviewed and published in *Environmental Science & Technology Letters*, **2015**, 2 (12), pp 362–366

### Introduction

Plant-based remediation (phytoremediation) has been studied extensively for traditional explosives<sup>6, 11, 83, 84</sup> and may prove useful for IMX. Furthermore, the study of endophytes (i.e. organisms that inhabit plants asymptotically) is increasing, given their ability to degrade xenobiotics naturally or via bio-augmentation.<sup>85-87</sup> In this study, we: 1) isolated and identified a hybrid willow tree endophyte capable of degrading DNAN, and 2) identified several DNAN transformation products using [<sup>15</sup>N] and [<sup>13</sup>C] stable isotope metabolic profiling.

### Experimental

#### *Chemicals*

Dinitroanisole (98%) was from Sigma (St. Louis, MO). Liquid chromatography solvents (Optima), 2-methoxy-5-nitroaniline (2-ANAN) (98%) and 4-methoxy-3-nitroaniline (4-ANAN) (97%) were supplied by Fisher (Waltham, MA).

*Synthesis and characterization of isotope-labeled DNAN – This work performed by Xueshu Li and Hans-Joachim Lehmler*

[<sup>13</sup>C<sub>6</sub>]-DNAN and [<sup>15</sup>N<sub>2</sub>]-DNAN (Figure 2) were synthesized by nitration of the corresponding anisole with propionyl nitrate generated *in situ* from propionic anhydride and nitric acid. Treatment of [<sup>13</sup>C<sub>6</sub>]-anisole with fuming nitric acid gave [<sup>13</sup>C<sub>6</sub>]-DNAN (purity >99%) and treatment of non-labeled anisole with <sup>15</sup>N-nitric acid gave [<sup>15</sup>N<sub>2</sub>]-DNAN (purity >99%). Structural confirmation and purity analysis was done by <sup>1</sup>H and <sup>13</sup>C nuclear magnetic resonance spectroscopy, liquid chromatography-high resolution mass spectrometry and by gas chromatography-mass spectrometry.<sup>27</sup>

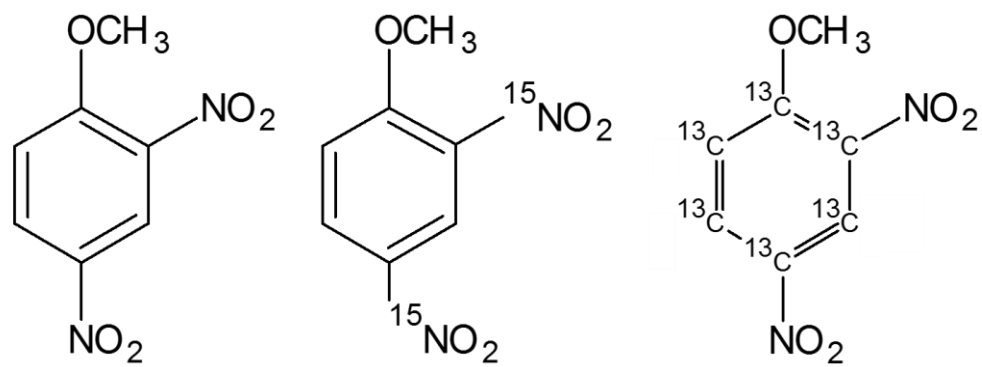


Figure 2. Unlabeled DNAN and stable isotope-labeled versions of DNAN used in this work.

### *Plant tissue endophyte extraction*

Willow tree cuttings (*Salix 'Iowa Willow'*) were obtained from Ecolotree (North Liberty, Iowa). Cuttings averaging 23 cm were maintained in a Hoagland's nutrient solution at 27 °C and under a photoperiod of 16 h light and 8 h dark. Portions of the leaves, stems, and roots were removed and surface sterilized to kill epiphytic bacteria. Surface sterilization was completed by soaking the specimen for five minutes in soapy water, and then thoroughly rinsing with potable water until the soap was removed. The specimens were soaked in 70% ethanol solution for 30 seconds and rinsed with sterilized, deionized water. The specimens were then submerged in a 0.1% Tween 80 (Sigma) and 6.25% hypochlorite solution for fifteen minutes with occasional, gentle mixing. The specimen was rinsed five times with sterilized, deionized water. The final rinse water was plated on an R2A media plate and incubated at 30°C for two weeks to verify the sterilization method's effectiveness.<sup>88-90</sup> In a sterile, laminar-flow hood, the surface sterilized specimen was cut into 5-mm sized pieces and submerged in 150 mL sterilized, deionized water with agitation (125 rpm) for 24 to 48 h at 26°C in the dark. In an attempt to isolate *Methylobacterium* (see ref. 83), 100 µL of the plant solution were spread on a minimal media consisting of, per liter of deionized water: 1.74 g K<sub>2</sub>HPO<sub>4</sub>, 1.38 g NaH<sub>2</sub>PO<sub>4</sub> · H<sub>2</sub>O, 0.54 g Na<sub>2</sub>SO<sub>4</sub>, 0.20 g MgSO<sub>4</sub> · 7H<sub>2</sub>O, 25 mg CaCl<sub>2</sub>·2H<sub>2</sub>O, 3.5 mg FeCl<sub>2</sub>·4H<sub>2</sub>O, 5 µg CuSO<sub>4</sub>·5H<sub>2</sub>O, 10 µg MgSO<sub>4</sub>·5H<sub>2</sub>O, 10 µg Na<sub>2</sub>MoO<sub>4</sub>·2H<sub>2</sub>O, 10 µg H<sub>3</sub>BO<sub>3</sub>, 70 µg ZnSO<sub>4</sub>·7H<sub>2</sub>O, and 5 µg CoCl<sub>2</sub>·6H<sub>2</sub>O, 9 g agar, supplemented with 5% CH<sub>3</sub>OH as a carbon source and 1.20 g/L NH<sub>4</sub>NO<sub>3</sub> as a nitrogen source. The plates were incubated at 30°C in the dark. Growing colonies were isolated by further streaking on the same minimal media. Pink *Methylobacterium* (see ref. 83) and white *Rhizobium* grew on this media.

### *Isolated endophyte exposure to DNAN*

In order to identify 2,4-dinitroanisole degrading bacteria, the colonies of *Methylobacteria* and *Rhizobium* were streaked onto plates with minimal medium plates supplemented with 1 mg/L 2,4-dinitroanisole (DNAN) as the sole source of carbon and nitrogen and stored in the dark at 30°C. Plates with a noticeable amount of growth were streaked onto R2A medium plates to accelerate growth and then re-exposed to DNAN on

minimal medium plates supplemented with 5 mg/L DNAN as the sole carbon and nitrogen source and stored in the dark at 30°C. Again, growing colonies were streaked onto R2A plates and stored in the dark at 30°C. The white *Rhizobium* colonies were the only organisms observed to grow on DNAN after about two weeks, so we selected them for further study. The bacteria were then maintained in minimal medium solution supplemented with 40 g/L glucose as the carbon source and 1.20 g/L ammonium nitrate as the nitrogen source for biomass growth or streaked onto R2A plates and stored in the dark at 30°C for 36 h, then stored in the dark at 4°C.

*Endophyte isolation and identification – This work performed by Katherine Langenfeld*

Isolated colonies that grew on plates with 5 mg L<sup>-1</sup> DNAN as the sole source of carbon and nitrogen were streaked onto R2A medium and stored in the dark at 30°C. Genomic DNA was extracted using a PowerWater DNA Isolation Kit (MoBio Laboratories, Inc., Carlsbad, CA) followed by 16S rRNA PCR (universal 1492r, 27f primers) (Mastercycler Model Eppgradient, Eppendorf, Hauppauge, NY). Annealing conditions were 2 min at 94°C followed by 30, 1-min cycles 94°C, then 1 min at 55°C, and the 1 min at 72°C, before 7 minutes at 72°C prior to cooling at 4°C. The amplified DNA was purified (QIAquick PCR Purification Kit, QIAGEN, Valencia, CA) and sequenced at the Iowa Institute of Human Genetics Genomics Division. The sequenced DNA was identified as *Rhizobium* by the blastn suite (National Center for Biotechnology Information, Bethesda, MD) and deposited under accession number KT881311 as *Rhizobium lichtii*. The cultures were maintained in minimal medium solution (without agar) supplemented with 40 g/L glucose and 1.20 g/L ammonium nitrate for growing biomass or streaked onto R2A plates and stored in the dark at 30°C.

*Degradation of DNAN, [<sup>13</sup>C<sub>6</sub>]-DNAN, and [<sup>15</sup>N<sub>2</sub>]-DNAN*

Pure *R. lichtii* cultures were grown overnight in rich media and exposed to 5 mg L<sup>-1</sup> DNAN in triplicate with and without added carbon and nitrogen. Samples were taken every two hours, filtered (0.2µm) and diluted 4:1 with methanol. The bioreactors were sterilized, foam-stoppered, serum vials (30 mL) containing minimal medium (25 mL) inoculated by 1 mL of *R. lichtii* solution with three cultures amended with fructose and

ammonium nitrate (5 mM). Controls were inoculated with 1 mL of sterile deionized water and all bioreactors were incubated at 30°C in the dark. In a second experiment to identify DNAN metabolites, *R. lichtii* was incubated separately with DNAN, [<sup>13</sup>C<sub>6</sub>]-DNAN or [<sup>15</sup>N<sub>2</sub>]-DNAN amended with 5 mM fructose and ammonium nitrate. After 24 hours, three extracellular samples, each incubated with a different stable isotope of DNAN, were filtered (0.2 μm), combined to a final volume of 200 μL containing 10% acetonitrile and analyzed for accurate mass data.

### *Analytical methods*

Samples were analyzed using an Agilent (Santa Clara, CA) liquid chromatography system and 6460 triple quadrupole mass spectrometer (LC-MS/MS). For DNAN, 80:20 methanol:water with 1 mM ammonium acetate (0.25 mL min<sup>-1</sup>) through a Zorbax C18 column (3x150 mm, 5 μm) at 35°C and a 10 min run time was used. For non-labeled DNAN, the MS/MS transition was 183>109 in negative ion electrospray ionization (ESI<sup>-</sup>) mode.<sup>91</sup> For metabolites, full and product ion scans were typically run with a linear gradient (10 to 90% methanol) over 15 min, with a 10 min hold and a 10 min return to 10% methanol. For positive ion mode (ESI<sup>+</sup>) analysis, 5 mM of formic acid was used with methanol as the organic solvent.

Accurate mass determinations were made on a Waters (Milford, MA) Acquity ultra performance liquid chromatography system followed by a Waters QToF-premier mass spectrometer. An Acquity UPLC HSS T3 column (2.1x100 mm, 1.8 μm) heated to 60 °C (0.6 mL min<sup>-1</sup>) was used. Leucine enkephalin was infused (10 μL min<sup>-1</sup>) as the lock mass. The mobile phase was 95% deionized water (A) and 5% acetonitrile (B), both containing 5 mM ammonium acetate. The gradient was as follows: 0 min, 0% B; linear to 10 min, 100% B; 15 min 100% B. ESI<sup>-</sup> mode, a mass to charge (m/z) range of 50-600, a scan rate of 0.15 s scan<sup>-1</sup> and a cone voltage of 35 volts were utilized.



## Results and Discussion

### *DNAN Degradation and Metabolite Identification*

*R. lichtii* cultures with added fructose and ammonium nitrate completely removed 5 mg L<sup>-1</sup> of DNAN within 24 hours while cultures without added carbon or nitrogen removed approximately half of the DNAN (Figure 2).

Accurate mass analysis revealed DNAN metabolites with ion formulas of C<sub>7</sub>H<sub>7</sub>N<sub>2</sub>O<sub>6</sub>S, C<sub>7</sub>H<sub>7</sub>N<sub>2</sub>O<sub>7</sub>S, C<sub>9</sub>H<sub>9</sub>N<sub>2</sub>O<sub>5</sub>, C<sub>8</sub>H<sub>7</sub>N<sub>2</sub>O<sub>4</sub>, and C<sub>9</sub>H<sub>9</sub>N<sub>2</sub>O<sub>4</sub> (Table 2). The formulas representing additions of sulfur and oxygen suggest sulfation of DNAN (C<sub>7</sub>H<sub>6</sub>N<sub>2</sub>O<sub>5</sub>) after nitro group reduction to an amine (M1a-e, Table 2)(Figure 4) or hydroxylamine (M2a-b, Table 2)(Figure 5A). The formulas representing additions of carbon, hydrogen and oxygen suggest an acetylation product (M3-5, Table 2)(Figure 5B). Two metabolites (C<sub>8</sub>H<sub>7</sub>N<sub>2</sub>O<sub>4</sub> and C<sub>9</sub>H<sub>9</sub>N<sub>2</sub>O<sub>4</sub>) appeared to be combinations of acetylation and/or methylation (M3 and M5, Table 2). Accurate masses of DNAN metabolites and corresponding molecular formulas as determined by ESI- LC-MS/QToF).

Five DNAN metabolite isomers (M1a-e, Table 2), corresponding to the C<sub>7</sub>H<sub>8</sub>N<sub>2</sub>O<sub>6</sub>S formula determined by accurate mass, were detected by ESI- LC-MS/QToF. These isomers exhibited similar mass spectra including identical nitro group (m/z 46) fragments for DNAN and [<sup>13</sup>C<sub>6</sub>]-DNAN and a single mass shifted (m/z 47) nitro group loss for [<sup>15</sup>N<sub>2</sub>]-DNAN (Figure 3). The sulfate group fragment (m/z 80) was identical for DNAN, [<sup>15</sup>N<sub>2</sub>]-DNAN and [<sup>13</sup>C<sub>6</sub>]-DNAN. Other mass fragments confirmed an intact aromatic ring and a nitro group reduction to the corresponding amine (Figure 4). The data suggest an unknown SO<sub>3</sub><sup>-</sup> addition for metabolites M1a, M1b and M1d and amine group sulfation for metabolites M1c and M1e (Figure 4), but mass spectrometry does not enable exact structural determination.

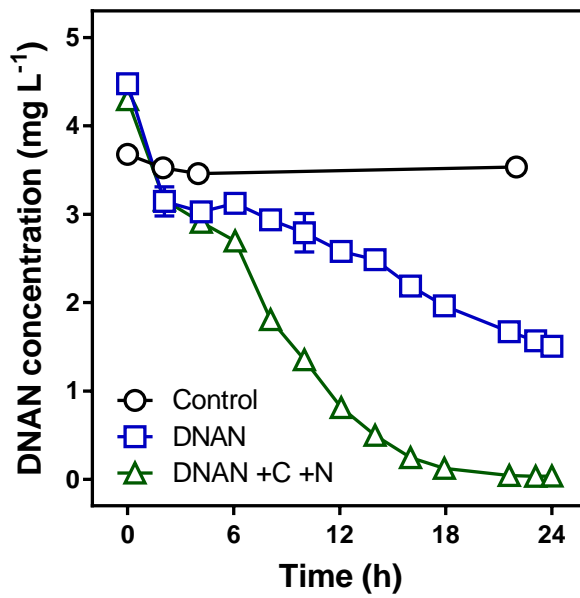


Figure 3. Degradation over 24 h by *R. lichtii* exposed to 5 mg L<sup>-1</sup> DNAN with and without 5 mM fructose (C) and ammonium nitrate (N). Control indicates DNAN + C + N without *R. lichtii*. Error bars denote one standard deviation (n = 3).

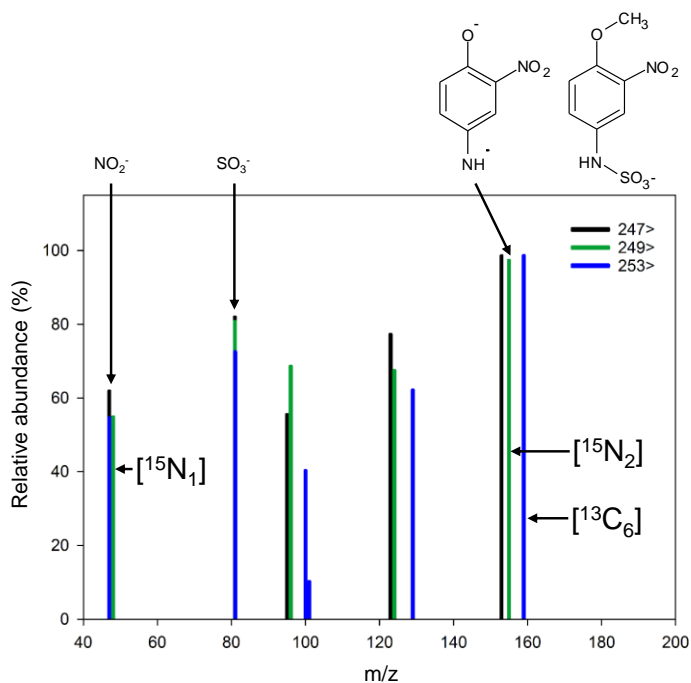


Figure 4. Sulfated amine metabolite of DNAN ( $m/z$  247) evidenced by ESI<sup>-</sup> LC-MS/MS mass fragments at  $m/z$  152, 122, 80, and 46 (black bars) corresponding to the molecular structures shown. A sulfated amine of [<sup>15</sup>N<sub>2</sub>]DNAN ( $m/z$  249) had fragments at  $m/z$  154, 123, 80, and 47 (green bars), and a sulfated amine of [<sup>13</sup>C<sub>6</sub>]DNAN ( $m/z$  253) had fragments at  $m/z$  158, 128, 80, and 46 (blue bars).

Table 2. Accurate masses of DNAN metabolites and corresponding molecular formulas as determined by ESI<sup>-</sup> LC-MS/QToF.

Ion Formula	Proposed ion	Metabolite	Retention time, min	Accurate mass, m/z	Deviation, mDa (ppm)
C <sub>7</sub> H <sub>7</sub> N <sub>2</sub> O <sub>6</sub> S	[M-H] <sup>-</sup>	M1a	0.81	247.0058	3.3 (13.4)
		[ <sup>15</sup> N <sub>2</sub> ]-		*	*
		[ <sup>13</sup> C <sub>6</sub> ]-		253.0264	3.8 (15)
		M1b	1.23	247.0037	1.2 (4.9)
		[ <sup>15</sup> N <sub>2</sub> ]-		249.0012	4.6 (18.5)
		[ <sup>13</sup> C <sub>6</sub> ]-		253.0253	2.7 (10.7)
		M1c	1.39	247.0031	0.6 (2.4)
		[ <sup>15</sup> N <sub>2</sub> ]-		248.9986	2.0 (8.0)
		[ <sup>13</sup> C <sub>6</sub> ]-		253.0237	1.1 (4.3)
		M1d	1.42	247.0026	0.1 (0.4)
		[ <sup>15</sup> N <sub>2</sub> ]-		248.9978	1.2 (4.8)
		[ <sup>13</sup> C <sub>6</sub> ]-		253.0234	0.8 (3.2)
		M1e	1.75	247.0036	1.1 (4.5)
		[ <sup>15</sup> N <sub>2</sub> ]-		248.9965	-0.1 (-0.4)
		[ <sup>13</sup> C <sub>6</sub> ]-		253.0226	0.0 (0.0)
C <sub>7</sub> H <sub>7</sub> N <sub>2</sub> O <sub>7</sub> S	[M-H] <sup>-</sup>	M2a	1.30	262.9984	1.0 (3.8)
		[ <sup>15</sup> N <sub>2</sub> ]-		264.9904	-1.1 (-4.2)
		[ <sup>13</sup> C <sub>6</sub> ]-		269.0167	-0.8 (3.0)
		M2b	1.37	262.9979	0.5 (1.9)
		[ <sup>15</sup> N <sub>2</sub> ]-		264.9914	-0.1 (-0.4)
		[ <sup>13</sup> C <sub>6</sub> ]-		269.0191	1.6 (5.9)
C <sub>9</sub> H <sub>9</sub> N <sub>2</sub> O <sub>5</sub>	[M-H] <sup>-</sup>	M3	2.49	225.0492	-1.9 (-8.4)
		[ <sup>15</sup> N <sub>2</sub> ]-		227.0456	0.4 (1.8)
		[ <sup>13</sup> C <sub>6</sub> ]-		231.0734	2.1 (9.1)
C <sub>8</sub> H <sub>7</sub> N <sub>2</sub> O <sub>4</sub>	[M-H] <sup>-</sup>	M4a	2.75	195.0410	0.4 (2.1)
		[ <sup>15</sup> N <sub>2</sub> ]-		197.0360	1.3 (6.6)
		[ <sup>13</sup> C <sub>6</sub> ]-		201.0615	0.8 (4.0)
		M4b	3.23	195.0430	2.4 (12.3)
		[ <sup>15</sup> N <sub>2</sub> ]-		197.0348	0.1 (0.5)
		[ <sup>13</sup> C <sub>6</sub> ]-		201.0590	-1.7 (-8.5)
C <sub>9</sub> H <sub>9</sub> N <sub>2</sub> O <sub>4</sub>	[M-H] <sup>-</sup>	M5	2.98	209.0602	4.0 (19.1)
		[ <sup>15</sup> N <sub>2</sub> ]-		211.0521	1.8 (8.5)
		[ <sup>13</sup> C <sub>6</sub> ]-		215.0765	0.1 (0.5)

\*Denotes below detection limit

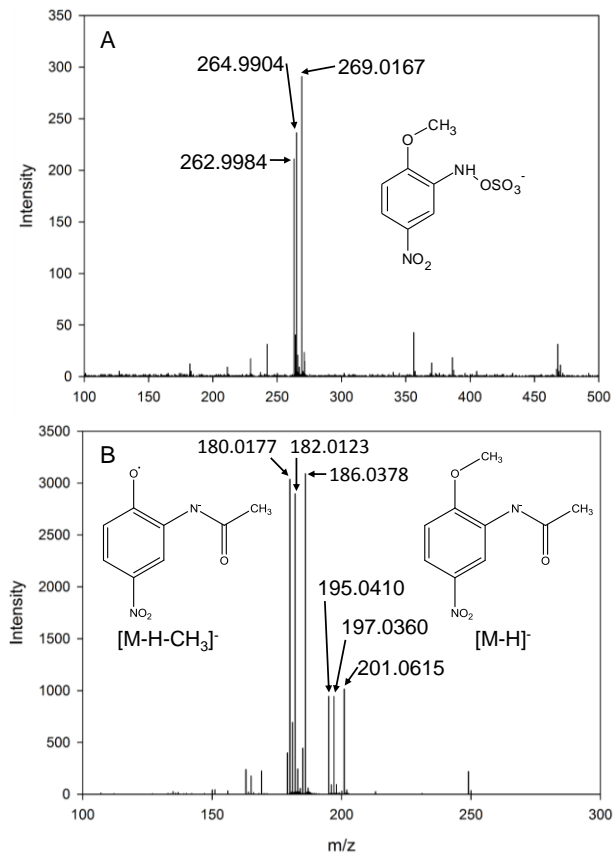


Figure 5. Exact mass spectra of sulfated and acetylated DNAN metabolites. (A) Sulfated hydroxylamine metabolites of DNAN (m/z 262.9984), [ $^{15}N_2$ ]DNAN (m/z 264.9904), and [ $^{13}C_6$ ]DNAN (m/z 269.0167) were evidenced by ESI LC-MS/QToF. (B) Acetylated amines of DNAN (m/z 195.0410), [ $^{15}N_2$ ]DNAN (m/z 197.0360), and [ $^{13}C_6$ ]DNAN (m/z 201.0615) showed methyl group losses resulting in ions at m/z 180.0177, 182.0123, and 186.0378, respectively.

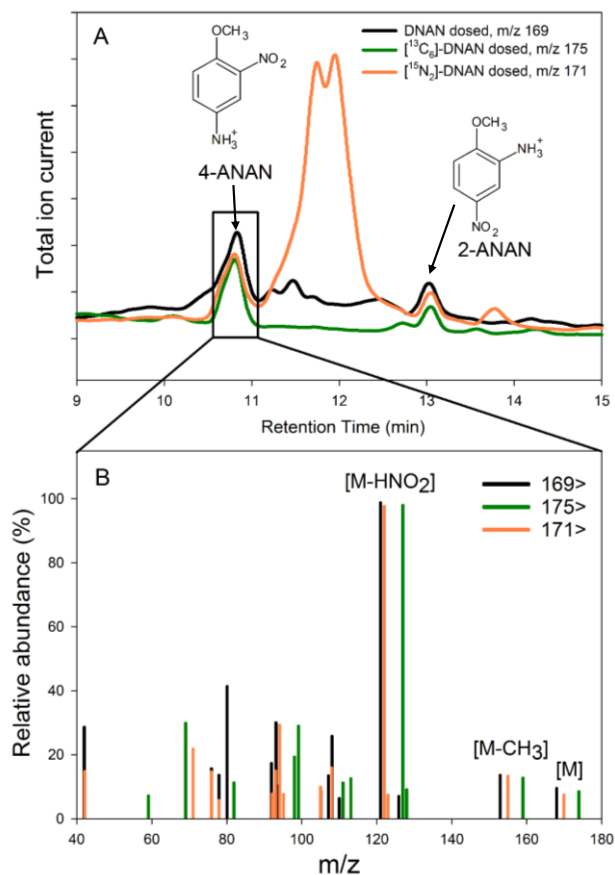


Figure 6. Formation of 4-ANAN by *R. litchii*(A) ESI<sup>+</sup> LC-MS/MS provided evidence of two monoamino metabolites of DNAN (m/z 169, black line),  $[^{15}\text{N}_2]$ DNAN (m/z 171, orange line), and  $[^{13}\text{C}_6]$ DNAN (m/z 175, green line) corresponding to the structures shown. (B) The para-substituted amino metabolite (4-ANAN) of DNAN was confirmed by mass fragments corresponding to methyl loss (M – CH<sub>3</sub>) and nitro group loss (M – HNO<sub>2</sub>). Both 2-ANAN and 4-ANAN were confirmed by true standards.

The formation of acetylated DNAN metabolites (M3, M4a, M4b and M5) has been previously observed<sup>5</sup>, and could have been catalyzed by aryl-N-acetyltransferases (NAT) known to acetylate aryl-amines and aryl-hydroxylamines.<sup>92</sup> The NAT gene in *Mycobacterium tuberculosis* is located in the same operon as enzymes capable of degrading aromatics.<sup>93</sup> NAT genes have been found across all domains of life and even in the Rhizobiales, *Mesorhizobium loti*.<sup>94</sup>

*Novel para-position transformation of DNAN to 4-amino-2-nitroanisole.*

In this study, we detected 2-amino-4-nitroanisole (2-ANAN), which is a common transformation product of DNAN.<sup>19, 24, 25</sup> Conversely, the formation of 4-amino-2-nitroanisole (4-ANAN) resulting from *para* nitro group reduction of DNAN has not been reported. True standards and ESI<sup>+</sup> LC-MS/MS confirmed the presence of 2-ANAN and 4-ANAN in the DNAN-incubated samples (Figure 5). The peaks at 10.8 and 13.1 min (Figure 6A) had mass shifts consistent with an aminonitroanisole (m/z 169), a [<sup>15</sup>N<sub>2</sub>]-aminonitroanisole (m/z 171) and a [<sup>13</sup>C<sub>6</sub>]-aminonitroanisole (m/z 175). Tandem mass spectra confirmed the structure of each aminonitroanisole (4-ANAN, Figure 6B).

Similarly, a DNAN metabolite detected at m/z 183, 185 and 189 is proposed as 2-hydroxylamino-4-nitroanisole (2-HA-NAN) or 4-hydroxylamino-2-nitroanisole (4-HA-NAN) within the putative DNAN transformation pathway (

).

The ability to culture *R. lichtii* on solid and in liquid media suggests promise for bioaugmenting soils contaminated with DNAN. A longer incubation with DNAN as the sole carbon and nitrogen source could result in DNAN mineralization, especially considering that the microbe could grow on DNAN as the sole source of carbon and nitrogen. However, the broad range of DNAN metabolites identified in this study and the lack of aromatic ring alteration with carbon and nitrogen added in this short assay suggests that the degradation pathway should be more fully elucidated before field-scale implementation of phytoremediation or bioaugmentation with *R. lichtii*.

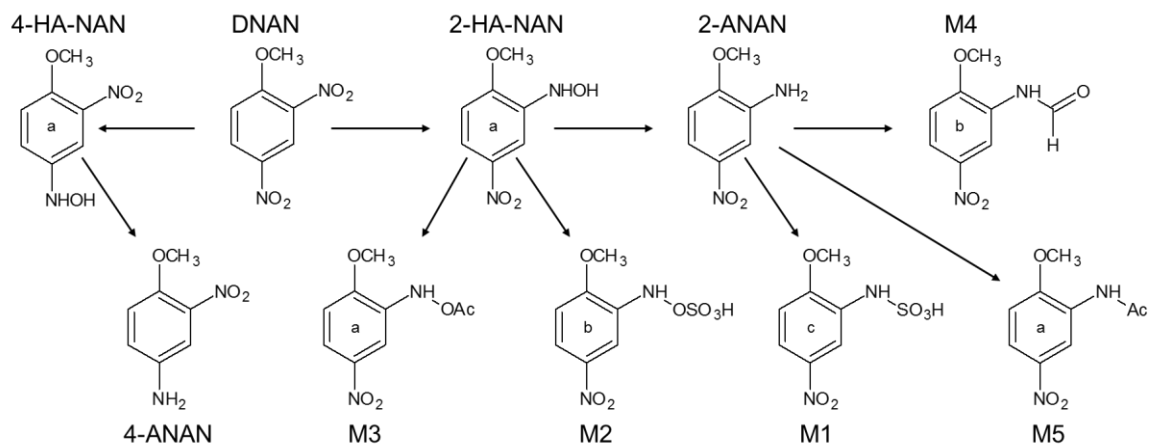


Figure 7. Putative DNAN transformation pathway of *R. lichtii*. M1–5 could result from reduction of either nitro group, although ortho reduction is indicated in the diagram. Letters indicate the number of isomers detected: a = 1, b = 2, and c = 5.



## CHAPTER 3:BIOTRANSFORMATION OF 2,4-DINITROANISOLE BY A FUNGAL PENICILLIUM SP.

This chapter has been peer-reviewed and published in *Biodegradation*, **2017**, 28 (95), doi:10.1007/s10532-016-9780-7.

### Introduction

Insensitive munitions explosives (IMX) are new formulations designed to minimize the risk of unintended detonation. IMX formulations are being implemented by the US Army to phase out traditional explosives containing trinitrotoluene (TNT) and hexahydrotrinitrotriazine (RDX) <sup>17</sup>. The increased safety of IMX mixtures comes at a potential environmental expense as the individual IMX constituents, such as 2,4-dinitroanisole (DNAN), are more water-soluble than TNT and RDX. For example, DNAN has a solubility in water of 276 mg/L compared to 100 mg/L for TNT<sup>20, 95</sup>. Army-approved formulation IMX-101 contains 43% DNAN, 37% nitroguanidine and 20% 3-nitro-1,2,4-triazol-5-one (NTO) by volume, while IMX-104 consists of 32% DNAN, 53% NTO, and 15% RDX <sup>20</sup>. The high percentage of DNAN in these formulations and the estimated 50 million acres affected by legacy explosives in the United States alone<sup>2</sup> raise concerns about the widespread release of this compound and its transformation products (TPs). In addition, DNAN has a relatively unknown ecosystem fate and toxicity<sup>43</sup>. Therefore, the new explosives and their TPs pose a contamination risk to groundwater and ecosystems and require further characterization of transformation and transport in the environment<sup>20, 95</sup>.

Fungi of many taxa have been shown to degrade xenobiotics of all types, including nitroaromatic explosives<sup>96-98</sup>. Fungi can often mineralize recalcitrant compounds, but may also create previously unknown TPs<sup>96, 99</sup>. Fungal bioreactors have been proposed for treating liquid waste streams, and fungal bioremediation (mycoremediation) has been demonstrated for various compounds in solid waste<sup>98, 100</sup>. In addition, fungi are ubiquitous in the environment and play an important role in ecosystem nutrient cycling <sup>98</sup>. Consequently, it is important to characterize fungal transformations of contaminants to assess new TPs and the possibility of remediation of soil and solids with fungal cultures. Microorganisms isolated from inside plant tissues (i.e., endophytes) may prove useful for bioaugmentation and enhancing plant-based remediation<sup>85, 89</sup>. Endophytic bacteria isolated

from hybrid poplar and willow tree tissues have even been shown to degrade DNAN and other explosives<sup>27, 90</sup>. While DNAN has been mineralized by a *Nocardioides* sp.<sup>31</sup>, complete biological mineralization of DNAN remains unusual, and fungal TPs have not yet been identified. Here, we (1) isolate and identify an endophytic fungus that can degrade DNAN and (2) characterize the transformation products of DNAN from the isolated fungus.

## Experimental section

### *Chemicals*

2,4-Dinitroanisole (98%) was purchased from Sigma (St. Louis, MO). [<sup>13</sup>C<sub>6</sub>]DNAN (>99%) and [<sup>15</sup>N<sub>2</sub>]DNAN (>99%) were synthesized as previously described<sup>27</sup>. A 2,4-dinitrophenol analytical standard (USPH1401), 4-methoxy-3-nitroaniline [4-ANAN (97%)], 2-methoxy-5-nitroaniline [2-ANAN (98+%)], 4-amino-2-nitrophenol (99%), and 2-amino-4-nitrophenol (99%) were purchased from Fisher Scientific (Waltham, MA). All reagents were ACS reagent grade or better and liquid chromatography solvents were Fisher Optima grade.

### *Synthesis of 2-(N-acetyl)amino-4-nitroanisole – NMR characterization performed by Xueshu Li and Hans-Joachim Lehmler*

2-(*N*-acetyl)amino-4-nitroanisole (2-NAc-NAN) was synthesized as described by Ayyangar and Srinivasan<sup>101</sup>. Briefly, 2-amino-4-nitroanisole (50 mmol) was combined with 50 mmol pyridine and 55 mmol acetic anhydride and the mixture was stirred and heated in a boiling water bath for 3 hours. The mixture was poured into water, and the product was filtered and washed with water. The product was recrystallized twice with water:ethanol (1:1, v/v) to produce 8.63 g (82% yield) of yellow solid, mp 178-179 °C (lit. 178 °C<sup>101</sup>). The purity was >99% as determined by liquid chromatography mass spectrometry (LC-MS) with positive electrospray ionization (ESI<sup>+</sup>). High resolution, quadrupole time-of-flight mass spectrometry (LC-QToF) (ESI<sup>+</sup>) revealed an exact mass of 211.0719, consistent with the calculated mass of 211.0723 for the expected formula [C<sub>9</sub>H<sub>10</sub>N<sub>2</sub>O<sub>4</sub> + H]<sup>+</sup>. <sup>1</sup>H and <sup>13</sup>C NMR spectra were recorded on a Bruker DRX-400 spectrometer in the University of Iowa Central NMR Research Facility (Iowa City, IA)

using tetramethylsilane as internal standard. The  $^1\text{H}$  and  $^{13}\text{C}$  chemical shifts are consistent with the proposed structure:  $^1\text{H}$  NMR (400 MHz,  $\text{CDCl}_3$ ):  $\delta$  9.26 (s, 1H), 7.96 (d,  $J = 8.7$  Hz, 1H), 7.81 (s, 1H), 6.92 (d,  $J = 8.7$  Hz, 1H), 4.00 (s, 3H), 2.25 (s, 3H) ppm.  $^{13}\text{C}$  NMR (100 MHz,  $\text{CDCl}_3$ )  $\delta$  168.3, 152.2, 141.6, 127.8, 119.7, 114.9, 109.1, 56.4, 24.8 ppm (see Appendix A).

### *Fungus isolation*

Willow tree cuttings (*Salix* ‘Iowa Willow’) were obtained from Ecolotree (North Liberty, Iowa). Cuttings averaging 23 cm were maintained in a Hoagland’s nutrient solution at 27 °C and under a photoperiod of 16 h light and 8 h dark. Portions of the leaves, stems, and roots were removed and surface-sterilized to kill epiphytic microorganisms. Surface sterilization was completed by soaking the specimens for five minutes in soapy water, and then thoroughly rinsing with tap water until the soap was removed. The specimens were soaked in 70% ethanol solution for 30 seconds and rinsed with sterilized, deionized water. The specimens were then submerged in a 0.1% Tween 80 (Sigma) and 6.25% hypochlorite solution for fifteen minutes with occasional, gentle mixing. The specimens was rinsed five times with sterilized, deionized water. Surface-sterilized roots and leaves were then shaken in sterile water for 24 hours at 0.22 x  $g$  and 26 °C. An aliquot of 100  $\mu\text{L}$  was plated on malt extract agar (MP Biomedicals, Santa Ana, CA) and incubated at 30 °C in the dark. Small (<1 cm) disks of mycelium were excised from the edge of growing colonies and transferred to new plates at least four times in order to isolate a fungal strain. Strains were maintained on malt extract agar. A spore solution was collected by inoculating 100 mL of malt extract agar in a 1 L flask with a mycelial disk. After seven days of growth, 20 mL of sterile deionized (DI) water was added, the flask was swirled and then the spore solution was aseptically funneled into a sterile serum bottle and stored at 4 °C. The spore solution was serially diluted and plated on malt extract agar to determine the concentration of colony forming units (CFU). The concentration of the spore solution was determined to be  $1.21 \times 10^6$  CFU/mL.

*Identification of Penicillium sp. KH1 – This work performed by Katherine Langenfeld*

Fungal DNA was extracted using 100  $\mu\text{m}$  glass beads and a Bead Beater (BioSpec Products).<sup>102</sup> 18S rRNA primer pairs EF3-EF4 (1.4 kb) and EF4-fung5 (0.5 kb) were used separately in the polymerase chain reaction (PCR) (Mastercycler Model Eppgradient, Eppendorf, Hauppauge, NY).<sup>103</sup> The amplified DNA was purified (QIAquick PCR Purification Kit, QIAGEN, Valencia, CA) and PCR product concentrations were determined using a Qubit® dsDNA HS Assay Kit and Qubit® 2.0 Fluorometer (Life Technologies, Eugene, OR). 148.4 ng PCR purified product and 15 pmol primer, EF4 and fung5 primers were combined in RNase free water to make 11.0  $\mu\text{L}$  of template and primer solution. The template and primer solutions were delivered to the Iowa Institute of Human Genetics Genomics Division to be sequenced on the Applied Biosystems Model 3730 DNA Sequencer. Prior to cycle sequencing, the facility combined 0.5  $\mu\text{L}$  DMSO, 0.45  $\mu\text{L}$  Applied Biosystems Sequencing Big Dye Terminator (BDT) Mix, 0.05  $\mu\text{L}$  dGTP BDT reaction mix, 2.0  $\mu\text{L}$  2.5x buffer, 1.5  $\mu\text{L}$  water, and 5.5  $\mu\text{L}$  template and primer. The DNA sequence results were submitted to the blastn suite (National Center for Biotechnology Information, Bethesda, MD) to identify the fungus and the sequence was submitted to GENBANK under accession number KU866421 as *Penicillium sp.* strain KH1.

*Biodegradation pathway elucidation experiment*

The medium used for this study was a simple glucose peptone (GP) medium composed of 20 g glucose, 5 g peptone, 2 g yeast extract, 1 g  $\text{K}_2\text{HPO}_4$ , and 0.5 g  $\text{MgSO}_4 \cdot 7\text{H}_2\text{O}$  per liter of deionized (DI) water<sup>99</sup>. The incubations (30 °C) were performed in sterilized amber serum bottles (125 mL) containing 20 mL of the medium and 100  $\mu\text{L}$  of a solution of *Penicillium sp.* KH1 spores ( $1.21 \times 10^6$  colony forming units per mL). The serum bottles were sealed with Micropore tape (3M, St. Paul, MN) and loosely covered with aluminum foil. After seven days of biomass pre-growth, the medium was decanted while retaining the biomass, and new medium (20 mL) was added. Six total bioreactors were treated with DNAN: three contained medium with 5 mg/L DNAN and 5 mg/L [ $^{13}\text{C}_6$ ]DNAN, while three contained medium with 5 mg/L DNAN and 5 mg/L [ $^{15}\text{N}_2$ ]DNAN. Three bioreactors containing fungus but no DNAN served as biological

controls with an absence of DNAN metabolites. A second spike of the same media (10 mL) was added to each reactor after seven days of DNAN exposure.

Samples were collected at 2, 4, 6, 8, 16, 24, 32, 40, and 48 hours and then 1-3 day intervals. For each sample, 0.5-1.5 mL of medium was collected with a needle syringe and filtered through a 0.2  $\mu\text{m}$  nylon filter (Pall Life Sciences, Port Washington, NY). For analysis, 400  $\mu\text{L}$  of filtrate from the sample after 10 days of exposure was added to 600  $\mu\text{L}$  of solvent (95% DI water and 5% acetonitrile containing 5 mM ammonium acetate).

#### *Negative and killed controls for the untargeted metabolomics experiment*

In the untargeted metabolomics experiment, two additional control conditions were utilized. These control bioreactors were prepared in the same manner as those described in the “untargeted metabolomics experiment” methods section of the manuscript but were not utilized for metabolomics analysis. Two control bioreactors, autoclaved after six days, contained media and 10 mg/L DNAN (“sorption control”, Fig. S1); and two control bioreactors contained media, 10 mg/L DNAN, but no fungal spores (“negative control”, Fig. S1). Controls were decanted after seven days and refilled (20 mL). Controls were sampled after seven and twenty-one days of incubation with DNAN.

#### *Degradation kinetics and pathway elucidation using metabolites as substrates*

To resolve isomeric metabolites and to determine metabolite formation over time, *Penicillium* sp. KH1 (20  $\mu\text{L}$  of spore solution) was pre-grown for seven days at 30  $^{\circ}\text{C}$  in GP medium (2 mL) in sterilized test tubes (100 x 13 mm) with a glass wool plug and a metal cap. After biomass growth, samples were decanted and refilled with medium containing 10 mg/L DNAN (n=36). Controls included autoclaved biomass dosed with 10 mg/L DNAN (n=36) and spiked medium containing no fungal spores (n=21). At each time point, three bioreactors from each condition were sacrificially sampled by freezing at -80  $^{\circ}\text{C}$  until further processing. Sample preparation involved thawing the test tubes in a 20  $^{\circ}\text{C}$  water bath before filtering the media with a 0.22  $\mu\text{m}$  PES syringe filter (Chemglass Life Sciences, Vineland, NJ). For LC-MS analyses, 250  $\mu\text{L}$  of sample filtrate was added to 50  $\mu\text{L}$  of acetonitrile and 700  $\mu\text{L}$  of DI water. One sample each from the treatment was lost for days 5, 6, and 14 during sample preparation for analysis.

Separate bioreactors were dosed with 5 mg/L of each of the following (n=2, each): 2,4-dinitrophenol (DNP), 2-amino-4-nitroanisole (2-ANAN), 4-amino-2-nitroanisole (4-ANAN), 2-amino-4-nitrophenol (2-ANP), 4-amino-2-nitrophenol (4-ANP) and 2-(*N*-acetyl)amino-4-nitroanisole (2-NAc-NAN). Each of these metabolites was observed in the initial biodegradation pathway experiment and served as primary substrates to further elucidate and confirm the metabolic pathways<sup>99</sup>. One bioreactor from each of the alternative primary substrates was sacrificially sampled after eight and 16 hours of incubation. Samples were frozen at -80 °C and filtered and diluted as above. Spores used for all experiments were never previously exposed to DNAN, ensuring that the fungal enzymatic systems were not previously adapted to or induced by DNAN degradation.

To correct for media evaporation, a follow-up experiment was conducted under the same conditions with no added DNAN. Three bioreactors contained autoclaved fungus, three contained live fungus and one contained only media. The reactors were weighed periodically, and a linear regression was applied to each condition and used to correct the observed concentrations and peak areas of metabolites.

### *Analytical methods*

Tandem mass spectrometry (LC-MS/MS) was performed on an Agilent (Santa Clara, CA) 1260 liquid chromatograph coupled to an Agilent 6460 triple-quadrupole MS with a Jetstream ESI source. Samples in the auto-sampler tray were maintained at 8 °C. An Agilent Zorbax XDB (2.1 x 50 mm, 3.5 µm) column (35 °C) at 500 µL/min was used with mobile phase (A) as 95% DI water with 5% acetonitrile (ACN) and mobile phase (B) as 95% ACN and 5% DI water. Both mobile phases contained 5 mM of ammonium hydroxide and ammonium acetate. For DNAN analysis, the mobile phase gradient was: 0 min, 10% B; linear to 5 min, 95% B; 7 min, 95% B; 7.1 min 10% B; 12 min 10% B. DNAN and other metabolites were quantified in ESI negative (ESI<sup>-</sup>) and ESI<sup>+</sup> modes and qualified with a second fragment ion using the mass transitions outlined in Table 4. Samples were quantitated using a six-standard, external calibration curve run during each batch. Agilent MassHunter Quantitative Analysis software was used to fit a power regression model to the curve in order to extend the range of quantification to 3-4 orders of magnitude of concentration ( $R^2 > 0.998$  for all analytes). The limits of detection

(LODs) are listed in Table 4. Three to four quality control injections of the standards were made during each batch run to ensure consistent detector response, and samples were injected in a random order during each batch of 25-75 samples. A DI water blank was run every five samples to ensure there was no carry-over or contamination during analysis runs. For quantitation of reduced DNAN metabolites, the solvent system consisted of (A) DI water and (B) acetonitrile both containing 0.1% formic acid with the same column and flow rate. The mobile phase gradient was: 0 min, 5% B; 2 min, 5% B; linear to 8 min, 35% B; linear to 10 min, 95% B; 10.1 min 5% B; 15 min 5% B.

Accurate mass data were collected on a Waters (Milford, MA) Acquity ultraperformance liquid chromatograph (UPLC) followed by a Waters QToF Premier MS. An Acquity UPLC HSS T3 column (2.1 mm x 100 mm, 1.8  $\mu$ m) heated to 60 °C (0.6 mL/min) was used. Leucine enkephalin was infused (10  $\mu$ L/min) as the lock mass. Samples were analyzed (in separate runs) by both ESI<sup>-</sup> and ESI<sup>+</sup> mode. A mass to charge ( $m/z$ ) range of 40–600, a scan rate of 0.2 s/scan and a sampling cone voltage of 30 were used for ESI<sup>-</sup> mode. A scan rate of 0.15 s/scan and a sampling cone voltage of 23 were used for ESI<sup>+</sup> mode. Samples in the auto-sampler tray were maintained at 8 °C. The mobile phase was (A) 95% DI water with 5% acetonitrile and (B) 95% acetonitrile and 5% DI water, both containing 5 mM ammonium acetate for ESI<sup>-</sup>. For ESI<sup>+</sup> mode, 0.05% formic acid was added to both mobile phases. The mobile phase gradient was: 0 min, 0% B; linear to 7 min, 100% B; 9 min, 100% B; 9.1 min 0% B; 13 min 0% B. The desolvation gas (400 °C) flow was 800 L/h and the capillary voltage was 2.5 kV.

Accurate mass, full-scan data were collected for ten minutes, converted to netCDF format by Databridge software and uploaded to XCMS Online<sup>104</sup> for an untargeted metabolomics approach to metabolite elucidation. The XCMS software takes raw, full-scan mass spectrometric data and reconstructs chromatograms of each ion detected. The reconstructed chromatograms were compared to determine differences between control and dosed fungus media based on magnitude, retention time, and mass-to-charge ratio for every ion detected in the samples. This study only examined compounds resulting from DNAN as confirmed by stable-isotope labeled substrates, and, as such, was not a comprehensive metabolomics investigation. Full XCMS Online parameters are detailed in Table 3. Two combinations of DNAN isotopes were used to allow unambiguous

identification of metabolites derived from DNAN and to provide orthogonal data sets. Elemental formulas were assigned using Waters MassLynx software and data from the averaged accurate mass data from all biological replicates.

### Statistical analysis

Raw, time-series data were compared for significant differences using a two-sided, matched-pairs Student's t-test ( $\alpha = 0.05$ ,  $p < 0.05$ ). An F-test ( $\alpha = 0.05$ ) was used to test linear regressions for significant deviations ( $p < 0.05$ ) from a null slope. Figures were produced and statistical analysis was conducted using GraphPad Prism 7.00.

Table 3. LC-MS/MS parameters for quantitation of DNAN and other metabolites in *Penicillium* media using a six-standard, external calibration curve. Peak areas of M306, M276, and M254 were collected in lieu of absolute quantification.

	RT (min)	parent ion	Quantitation ion (collision energy)	Qualification ion (collision energy)	Cell accelerator voltage	ESI mode	LOD (ppb)
2,4-dinitroanisole (DNAN)	2.2	183.0	109.1 (30)	123.0 (23)	1	-	1.5
[ <sup>13</sup> C <sub>6</sub> ]dinitroanisole ([ <sup>13</sup> C <sub>6</sub> ]DNAN)	2.2	189.0	114.0 (30)	129.0 (23)	1	-	1.5
[ <sup>15</sup> N <sub>2</sub> ]dinitroanisole ([ <sup>15</sup> N <sub>2</sub> ]DNAN)	2.2	185.0	110.0 (30)	123.0 (23)	1	-	1.5
2,4-dinitrophenol (DNP)	1.6	183.0	109.1 (30)	123.0 (23)	1	-	0.15
2-amino-4-nitroanisole (2-ANAN)	5.3	169.1	123.0 (15)	80.0 (30)	7	+	1
4-amino-2-nitroanisole (4-ANAN)	1.6	169.1	122.0 (15)	77.0 (35)	7	+	<1
2-amino-4-nitrophenol (2-ANP)	1.9	155.1	109.1 (20)	92.0 (40)	1	+	1
4-amino-2-nitrophenol (4-ANP)	1.0	155.1	109.1 (20)	80.1 (40)	1	+	5
2-N-acetyl-4-nitroanisole (2-NAc-NAN)	7.2	210.9	169.0 (10)	123.0 (20)	4	+	<1
M306	1.8	305.0	225 (5)	N/A	5	-	N/A
M276	6.8	275.1	195.0 (5)	N/A	5	-	N/A
M254	1.4 (a) 2.9 (b)	253.0	167.0 (15)	N/A	5	-	N/A



Table 4. XCMS Online parameters for untargeted metabolomics analysis

Feature detection	Method	matchedFilter
	FWHM	6
	step	0.1
	max # chrom. Peaks	50
	mzdiff	0.01
	S/N raio cutoff	10
Retention time correction	method	obiwarp
	profStep	1
Alignment	minfrac	0.5
	bw	5
	mzwid	0.015
	minsamp	1
	max	300
Statistics	Statistical Test	unpaired parametric t-test
	p-value threshold (highly significant features)	0.01
	fold change threshold	1.5
	p-value threshold (significant features)	0.5
Miscellaneous	Correct mass calibration gaps	Yes
	Bypass file sanity check	No

## Results & Discussion

### *DNAN reduction, demethylation, and degradation kinetics*

A fungal sp. isolated from willow tree cuttings that was able to degrade DNAN in rich medium was identified as a *Penicillium* sp. by the 18s ribosomal DNA gene. *Penicillium* is in the phylum Ascomycota and fellow ascomycetes have been shown to mineralize lignin and possess laccases, powerful oxidative enzymes useful for bioremediation<sup>105, 106</sup>. While most of the studies on fungal metabolism of xenobiotics focuses on *Phanerochaete chrysosporium*<sup>96, 97</sup>, *Penicillium* have been shown to degrade 100% of TNT in liquid media and to detoxify aromatic amines in soil<sup>107, 108</sup>.

A nominal quantity of 10 mg/L DNAN was degraded quickly in solution by *Penicillium* sp. KH1 (Figure 9A). The degradation followed pseudo-first-order kinetics with a rate constant of  $0.47 \pm 0.03 \text{ d}^{-1}$ . This rate ( $t_{1/2} = 35 \text{ h}$ ) is considerably slower than that observed by an isolated DNAN-mineralizing bacteria, *Nocardioides* sp. JS1661 ( $t_{1/2} < 1 \text{ h}$ ); however, the half-life of DNAN degradation by the *Penicillium* sp. was on the same order of magnitude as aerobic soil slurries with added carbon and nitrogen ( $t_{1/2} \approx 96 \text{ h}$ ) and aerobic sludge with added carbon ( $t_{1/2} \approx 50 \text{ h}$ )<sup>25, 28</sup>.

An initial 8-hour sorption phase was observed in both control conditions. Up to eight hours, DNAN sorbed to the glassware in the negative control, but the slope of a least-squares linear regression from eight hours until 14 d was not significantly different from zero ( $p = 0.6745$ ,  $n = 21$ ), indicating that the concentration of DNAN did not change. There was also a significant difference ( $p < 0.0001$ ,  $n = 7$  pairs) in DNAN concentrations between the two control conditions, indicating that less DNAN was in the bulk media when the inactive biomass was present. The killed control provided evidence for sorption – rather than transformation – because molar concentrations of reduced and/or demethylated metabolites represented less than 0.9% of the original DNAN (Figure 9A). The slope of the killed control was different from zero after eight hours ( $p = 0.0191$ ,  $n = 12$ ). This finding indicates that some spores may have survived autoclaving or that some enzymes could still be intact to degrade DNAN. However, DNAN concentrations in the treatment were significantly different than the killed control over 14 days ( $p < 0.0001$ ,  $n = 12$  pairs).

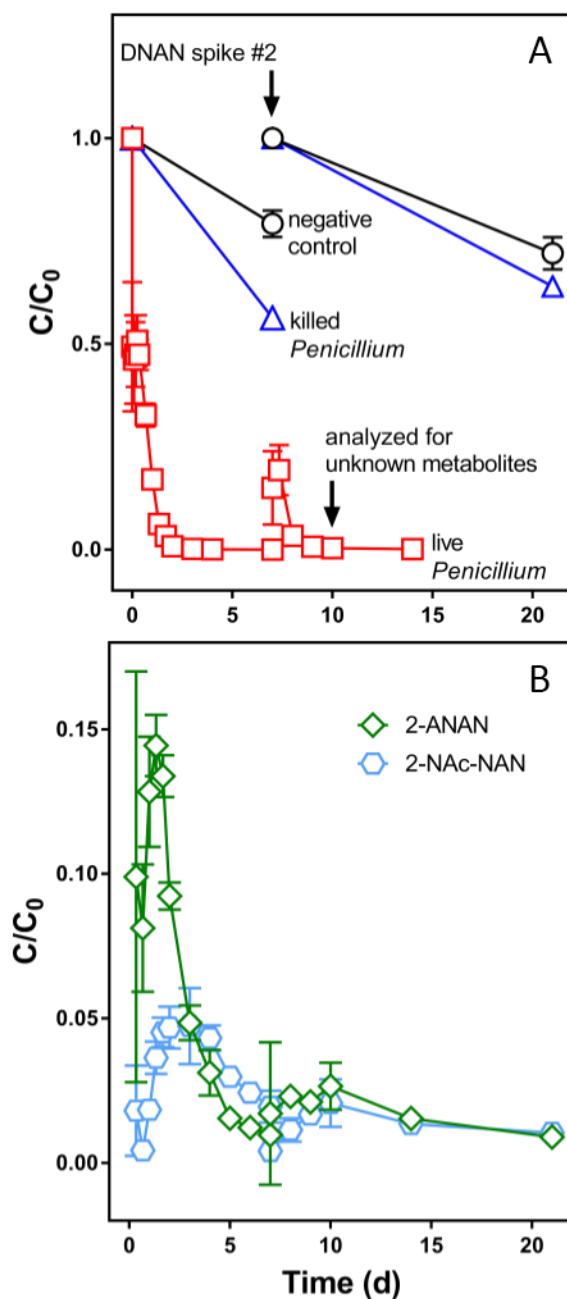


Figure 8. Time series of (a) 10 mg/L DNAN degradation and (b) metabolite formation over 21 days of incubation at 30 °C with *Penicillium* sp. KH1 in the metabolomics experiment. Error bars represent one standard deviation from the mean. Metabolomics analysis was executed on media after ten days of incubation with an additional DNAN spike after seven days.

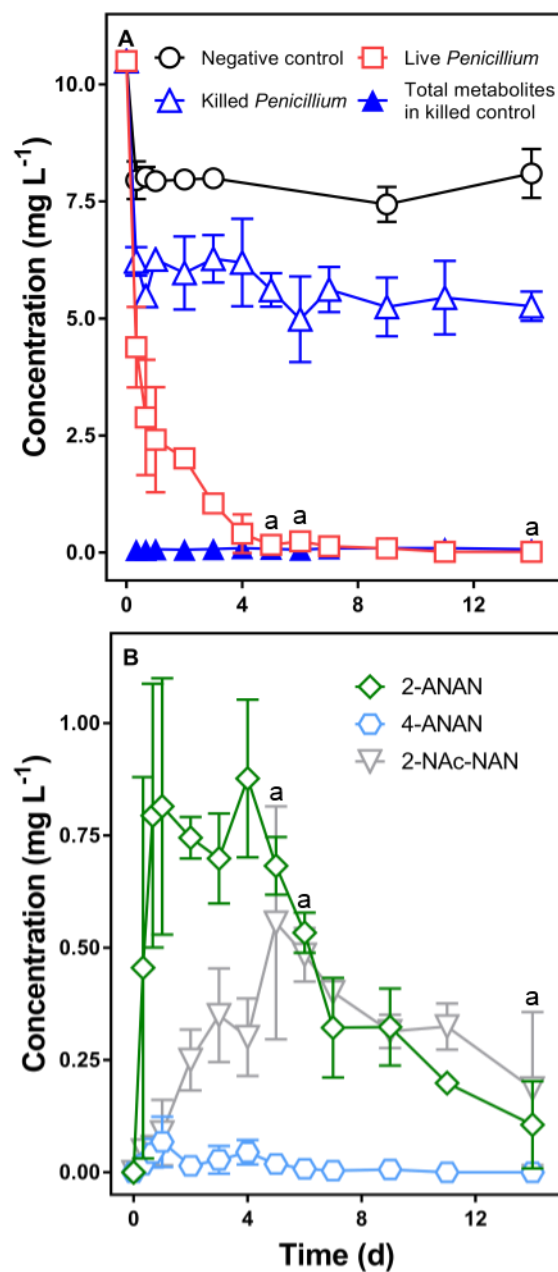


Figure 9. Time series of (A) 10 mg/L DNAN degradation and (B) metabolite formation over fourteen days of incubation at 30 °C with *Penicillium* sp. KH1 (n=3, <sup>a</sup>denotes n=2). The sum of 2-ANAN, 2-ANP, 4-ANAN, 4-ANP, DNP and 2-NAc-NAN in the killed control is represented with closed blue triangles (n=1). Error bars represent one standard deviation from the mean.

Table 5. Transformations of various DNAN metabolites resulting from 16 hours of incubation of strain KH1.

Starting substrate	Resulting metabolite				
	2-ANP	2-ANAN	4-ANP	4-ANAN	2-NAc-NAN
DNAN	Yes	Yes	Yes	Yes	Yes
DNP	Yes	No	Yes	No	No
2-ANP	N/A	No	No	No	No
2-ANAN	Yes	N/A	No	No	Yes
4-ANP	No	No	N/A	No	No
4-ANAN	No	No	No	N/A	No
2-NAc-NAN	No	No	No	No	N/A

Our previous work demonstrated the biotic production of 4-ANAN in a *Rhizobium* sp.<sup>27</sup> Here, 4-ANAN and 2-ANAN were also observed to result from nitroreduction of DNAN (Figure 9B). 2-ANAN is the most commonly detected transformation product of DNAN and has been observed to result from soil and sludge cultures, as well as abiotic reduction<sup>19, 25, 28</sup>. Note that 2-ANAN and 4-ANAN have also been abbreviated as MENA and iMENA, respectively, in other literature<sup>25, 26</sup>; here, we chose this convention to more easily relate isomeric TPs explicitly to the *ortho* and *para* nitro groups of DNAN. DNP, resulting from demethylation of the methoxy group of DNAN, is a TP of DNAN in mammalian systems,<sup>17, 109</sup> and was observed transiently in the treatment along with low levels of 4-ANP and 2-ANP (Table 5).

When strain KH1 was incubated with DNP as the starting substrate, 2-ANP and 4-ANP were formed, while separate incubations with 2-ANAN yielded 2-ANP as well (Table 5). However, when the starting substrate was 4-ANAN, the compound was not demethylated to form 4-ANP. These incubations indicate that demethylation and *o*-nitroreduction are parallel degradation pathways that can occur simultaneously and *p*-nitroreduction precludes demethylation. In general, 2-ANAN was observed in quantities at least two orders of magnitude greater than those of DNP and 4-ANAN (Figure 9B, DNP not shown), indicating that *ortho* reduction of DNAN was the most dominant transformation pathway as previously observed abiotically and biologically, both in the presence and absence of O<sub>2</sub><sup>19, 25, 26, 28</sup>. DNAN dimers have been observed in other studies<sup>25, 26</sup> and are quite commonly formed from TNT<sup>34, 110</sup>; however, no DNAN dimers were observed in our study.

### *Metabolite identification*

After ten days of incubation with DNAN, including an additional spike after seven days, bioreactors were analyzed for unknown metabolite identification. Accurate mass data and untargeted metabolomics-based analysis revealed 16 additional compounds that were in the treatments but absent in the fungal reactors without DNAN (Table 6). Each compound contained the corresponding mass shifts consistent with the stable isotope labeling of the starting substrate, confirming that these were metabolites of DNAN. The accurate mass data for the <sup>15</sup>N<sub>2</sub>- and <sup>13</sup>C<sub>6</sub>-labeled DNAN metabolites can be found in



Table 6. DNAN metabolites determined from LC-QToF. Each accurate mass value is the average of six biological replicates.

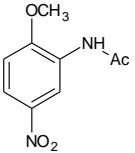
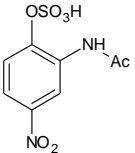
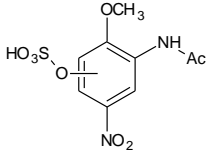
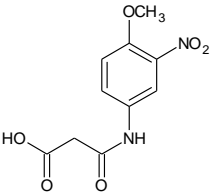
	proposed structure	confidence level <sup>a</sup>	RT (min)	ESI	ion formula	proposed ion	accurate mass	deviation (mDa (ppm))	fragment mass <sup>b</sup>	fragment formula	proposed fragment ion <sup>d</sup>		
M210, 2-NAC-NAN		1. Synthesized standard, HR-MS, MS/MS, RT	2.78	+	C <sub>9</sub> H <sub>11</sub> N <sub>2</sub> O <sub>4</sub>	[M+H] <sup>+</sup>	211.0713	-0.6 (-2.8)	169.0627	C <sub>7</sub> H <sub>9</sub> N <sub>2</sub> O <sub>3</sub>	[M+H <sub>2</sub> -Ac] <sup>+</sup>		
				-	C <sub>9</sub> H <sub>9</sub> N <sub>2</sub> O <sub>4</sub>	[M-H] <sup>-</sup>	209.0561	-0.1 (-0.5)	177.0299	C <sub>8</sub> H <sub>5</sub> N <sub>2</sub> O <sub>3</sub>	[M-OCH <sub>3</sub> ] <sup>-</sup>		
M276		2b. HR-MS, MS/MS, diagnostic fragment, relative RT, putative pathways	1.86	-	C <sub>8</sub> H <sub>7</sub> N <sub>2</sub> O <sub>7</sub> S	[M-H] <sup>-</sup>	274.9976	0.2 (0.7)	195.0411	C <sub>8</sub> H <sub>7</sub> N <sub>2</sub> O <sub>4</sub>	[M-H-HSO <sub>3</sub> ] <sup>-</sup>		
									153	N/A	[M-Ac-SO <sub>3</sub> ] <sup>-</sup>		
									123	N/A	Ambiguous		
									46	N/A	[NO <sub>2</sub> ] <sup>-</sup>		
M306		3. HR-MS, MS/MS, diagnostic fragment	1.50	-	C <sub>9</sub> H <sub>9</sub> N <sub>2</sub> O <sub>8</sub> S	[M-H] <sup>-</sup>	305.0063	-1.7 (-5.6)	225.0498	C <sub>9</sub> H <sub>9</sub> N <sub>2</sub> O <sub>5</sub>	[M-H-HSO <sub>3</sub> ] <sup>-</sup>		
									153.0212	C <sub>6</sub> H <sub>5</sub> N <sub>2</sub> O <sub>3</sub>	[M-OCH <sub>3</sub> -Ac-HSO <sub>3</sub> ] <sup>-</sup>		
									210	N/A	[M-H-HSO <sub>3</sub> -CH <sub>3</sub> ] <sup>-</sup>		
									168	N/A	[M-HSO <sub>3</sub> -CH <sub>3</sub> -Ac] <sup>-</sup>		
									180	N/A	[M-HSO <sub>3</sub> -NO <sub>2</sub> ] <sup>-</sup>		
M254a		3. HR-MS, MS/MS, diagnostic fragment	2.04 <sup>c</sup>	+	C <sub>10</sub> H <sub>11</sub> N <sub>2</sub> O <sub>6</sub>	[M+H] <sup>+</sup>	255.0648	3.1 (12.2)	237	N/A	[M+H-H <sub>2</sub> O] <sup>+</sup>		
										209	N/A	[M+H-CH <sub>2</sub> O <sub>2</sub> ] <sup>+</sup>	
											96	N/A	Ambiguous
			1.45	-	C <sub>9</sub> H <sub>9</sub> N <sub>2</sub> O <sub>4</sub>	[M-H-CO <sub>2</sub> ] <sup>-</sup>	209.0564	0.2 (1.0)	167.0450	C <sub>7</sub> H <sub>7</sub> N <sub>2</sub> O <sub>3</sub>	[M-H-C <sub>3</sub> H <sub>3</sub> O <sub>3</sub> ] <sup>-</sup>		
											152.0219	C <sub>6</sub> H <sub>4</sub> N <sub>2</sub> O <sub>3</sub>	[M-H-C <sub>3</sub> H <sub>3</sub> O <sub>3</sub> -CH <sub>3</sub> ] <sup>-</sup>



Table 6. (continued)

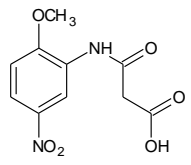
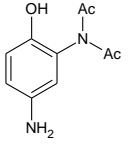
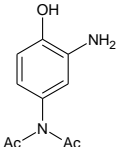
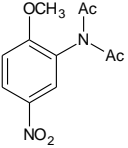
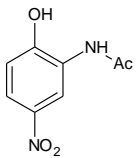
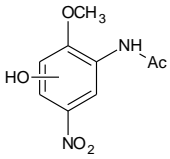
	proposed structure	confidence level <sup>a</sup>	RT (min)	ESI	ion formula	proposed ion	accurate mass	deviation (mDa (ppm))	fragment mass <sup>b</sup>	fragment formula	proposed fragment ion <sup>d</sup>
M254b		3. HR-MS, MS/MS, diagnostic fragment	2.28 <sup>c</sup>	+	C <sub>10</sub> H <sub>11</sub> N <sub>2</sub> O <sub>6</sub>	[M+H] <sup>+</sup>	255.0669	5.2 (20.4)			
			1.72	-	C <sub>10</sub> H <sub>9</sub> N <sub>2</sub> O <sub>6</sub>	[M-H] <sup>-</sup>	253.0431	-3.0 (-11.9)	191	N/A	Ambiguous
					C <sub>9</sub> H <sub>9</sub> N <sub>2</sub> O <sub>4</sub>	[M-H-CO <sub>2</sub> ] <sup>-</sup>	209.0549	-1.3 (-6.2)	167.0456	C <sub>7</sub> H <sub>7</sub> N <sub>2</sub> O <sub>3</sub>	[M-H-C <sub>3</sub> H <sub>3</sub> O <sub>3</sub> ] <sup>-</sup>
									152.0219	C <sub>6</sub> H <sub>4</sub> N <sub>2</sub> O <sub>3</sub>	[M-H-C <sub>3</sub> H <sub>3</sub> O <sub>3</sub> -CH <sub>3</sub> ] <sup>-</sup>
M208a		4. HR-MS	0.67	-	C <sub>10</sub> H <sub>11</sub> N <sub>2</sub> O <sub>3</sub>	[M-H] <sup>-</sup>	207.0755	-1.5 (-7.2)	165.0560	C <sub>8</sub> H <sub>9</sub> N <sub>2</sub> O <sub>2</sub>	[M-H-H <sub>2</sub> O] <sup>-</sup>
M208b		4. HR-MS	0.72	-	C <sub>10</sub> H <sub>11</sub> N <sub>2</sub> O <sub>3</sub>	[M-H] <sup>-</sup>	207.0756	-1.4 (-6.8)			
M208a or b	N/A	4. HR-MS	1.31 <sup>c</sup>	+	C <sub>10</sub> H <sub>13</sub> N <sub>2</sub> O <sub>3</sub>	[M+H] <sup>+</sup>	209.0939	1.3 (6.2)			
M196a	See Figure 12	4. HR-MS, MS/MS	1.00	-	C <sub>8</sub> H <sub>7</sub> N <sub>2</sub> O <sub>4</sub>	[M-H] <sup>-</sup>	195.0411	0.5 (2.6)	153.0311	C <sub>6</sub> H <sub>5</sub> N <sub>2</sub> O <sub>3</sub>	[M-Ac] <sup>-</sup>
M252		4. HR-MS	1.09	+	C <sub>11</sub> H <sub>13</sub> N <sub>2</sub> O <sub>5</sub>	[M+H] <sup>+</sup>	253.0802	-2.2 (-8.7)			
M196b	See Figure 11	4. HR-MS, MS/MS	1.13	-	C <sub>8</sub> H <sub>7</sub> N <sub>2</sub> O <sub>4</sub>	[M-H] <sup>-</sup>	195.0393	-1.3 (-6.7)	177.0294	C <sub>8</sub> H <sub>5</sub> N <sub>2</sub> O <sub>3</sub>	[M-H-H <sub>2</sub> O] <sup>-</sup>
									123.0325	C <sub>6</sub> H <sub>5</sub> NO <sub>2</sub>	[M-Ac-NO] <sup>-</sup>

Table 6. (continued)

	proposed structure	confidence level <sup>a</sup>	RT (min)	ESI	ion formula	proposed ion	accurate mass	deviation (mDa (ppm))	fragment mass <sup>b</sup>	fragment formula	proposed fragment ion <sup>d</sup>
M196d	See Figure 12	4. HR-MS	1.31	-	C <sub>8</sub> H <sub>7</sub> N <sub>2</sub> O <sub>4</sub>	[M-H] <sup>-</sup>	195.0405	-0.1 (-0.5)			
M196f		4. HR-MS, RT relative to M276	2.00	-	C <sub>8</sub> H <sub>7</sub> N <sub>2</sub> O <sub>4</sub>	[M-H] <sup>-</sup>	195.0404	-0.2 (-1.0)			
M226		4. HR-MS, putative pathways	2.29	-	C <sub>9</sub> H <sub>9</sub> N <sub>2</sub> O <sub>5</sub>	[M-H] <sup>-</sup>	225.0513	0.2 (0.9)			
M280	Ambiguous	5. HR-MS	2.30	-	Ambiguous	[M+H] <sup>+</sup>	278.9735	N/A			
M368	Ambiguous	5. HR-MS	2.18	+	Ambiguous	[M+H] <sup>+</sup>	369.1450	N/A			

<sup>a</sup>Confidence levels assigned as suggested by <sup>111</sup>

<sup>b</sup>Nominal mass fragment indicates LC-MS/MS data. Accurate mass indicates LC-QToF fragment

<sup>c</sup>Indicates a different retention time was observed in the separate positive and negative ionization chromatography runs. Because the pH of the mobile phases was lower for positive ionization, these compounds were presumably protonated in the positive ionization run condition, resulting in longer retention times

<sup>d</sup>Ac represents the acetyl moiety of the formula CH<sub>3</sub>CO

Table 7. [<sup>15</sup>N<sub>2</sub>]DNAN metabolites determined from LC-QToF. Accurate mass values are the mean of 3 biological replicates.

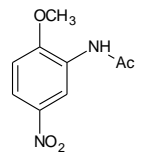
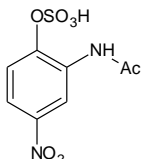
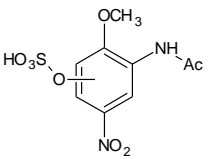
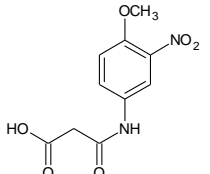
proposed structure	confidence level <sup>a</sup>	RT (min)	ESI	ion formula	proposed ion	accurate mass	deviation (mDa (ppm))	fragment mass <sup>b</sup>	fragment formula	proposed fragment ion
	1. Synthesized standard, HR-MS, MS/MS, RT	2.78	+	C <sub>9</sub> H <sub>11</sub> <sup>15</sup> N <sub>2</sub> O <sub>4</sub>	[M+H] <sup>+</sup>	213.0661	0.1 (0.5)	171.0547	C <sub>7</sub> H <sub>9</sub> N <sub>2</sub> O <sub>3</sub>	[M+H <sub>2</sub> -Ac] <sup>+</sup>
			-	C <sub>9</sub> H <sub>9</sub> <sup>15</sup> N <sub>2</sub> O <sub>4</sub>	[M-H] <sup>-</sup>	211.0500	0.3 (1.4)	179.0241	C <sub>8</sub> H <sub>5</sub> N <sub>2</sub> O <sub>3</sub>	[M-OCH <sub>3</sub> ] <sup>-</sup>
	2b. HR-MS, MS/MS, diagnostic fragment, relative RT, putative pathways	1.86	-	C <sub>8</sub> H <sub>7</sub> <sup>15</sup> N <sub>2</sub> O <sub>7</sub> S	[M-H] <sup>-</sup>	276.9922	0.7 (2.5)	197.0357	C <sub>8</sub> H <sub>7</sub> N <sub>2</sub> O <sub>4</sub>	[M-H-HSO <sub>3</sub> ] <sup>-</sup>
								155	N/A	[M-Ac-SO <sub>3</sub> ] <sup>-</sup>
								124	N/A	Ambiguous
								47	N/A	[ <sup>15</sup> NO <sub>2</sub> ] <sup>-</sup>
	3. HR-MS, MS/MS, diagnostic fragment	1.50	-	C <sub>9</sub> H <sub>9</sub> <sup>15</sup> N <sub>2</sub> O <sub>8</sub> S	[M-H] <sup>-</sup>	306.9996	-2.4 (-7.8)	227.0440	C <sub>9</sub> H <sub>9</sub> N <sub>2</sub> O <sub>5</sub>	[M-H-HSO <sub>3</sub> ] <sup>-</sup>
								155.0239	C <sub>6</sub> H <sub>5</sub> N <sub>2</sub> O <sub>3</sub>	[M-OCH <sub>3</sub> -Ac-HSO <sub>3</sub> ] <sup>-</sup>
								212	N/A	[M-H-HSO <sub>3</sub> -CH <sub>3</sub> ] <sup>-</sup>
								170	N/A	[M-HSO <sub>3</sub> -CH <sub>3</sub> -Ac] <sup>-</sup>
								181	N/A	[M-HSO <sub>3</sub> - <sup>15</sup> NO <sub>2</sub> ] <sup>-</sup>
	3. HR-MS, MS/MS, diagnostic fragment	2.04 <sup>c</sup>	+	C <sub>10</sub> H <sub>11</sub> <sup>15</sup> N <sub>2</sub> O <sub>6</sub>	[M+H] <sup>+</sup>	257.0556	-0.2 (-0.8)	239	N/A	[M+H-H <sub>2</sub> O] <sup>+</sup>
								211	N/A	[M+H-CH <sub>2</sub> O <sub>2</sub> ] <sup>+</sup>
		1.45	-	C <sub>9</sub> H <sub>9</sub> <sup>15</sup> N <sub>2</sub> O <sub>4</sub>	[M-H-CO <sub>2</sub> ] <sup>-</sup>	211.0503	1.3 (6.2)	169.0390	C <sub>7</sub> H <sub>7</sub> N <sub>2</sub> O <sub>3</sub>	[M-H-C <sub>3</sub> H <sub>3</sub> O <sub>3</sub> ] <sup>-</sup>
								154.0160	C <sub>6</sub> H <sub>4</sub> N <sub>2</sub> O <sub>3</sub>	[M-H-C <sub>3</sub> H <sub>3</sub> O <sub>3</sub> -CH <sub>3</sub> ] <sup>-</sup>

Table 7. (continued)

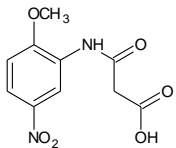
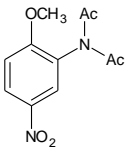
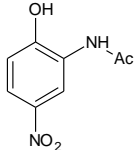
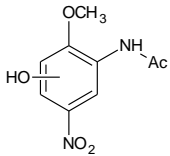
proposed structure	confidence level <sup>1</sup>	RT (min)	ESI	ion formula	proposed ion	accurate mass	deviation (mDa (ppm))	fragment mass <sup>2</sup>	fragment formula	proposed fragment ion	
	3. HR-MS, MS/MS, diagnostic fragment	2.28 <sup>c</sup>	+	C <sub>10</sub> H <sub>11</sub> <sup>15</sup> N <sub>2</sub> O <sub>6</sub>	[M+H] <sup>+</sup>	257.0556	-0.2 (-0.8)				
		1.72	-	C <sub>10</sub> H <sub>9</sub> <sup>15</sup> N <sub>2</sub> O <sub>6</sub>	[M-H] <sup>-</sup>	255.0416	1.5 (5.9)	193	N/A	Ambiguous	
				C <sub>9</sub> H <sub>9</sub> <sup>15</sup> N <sub>2</sub> O <sub>4</sub>	[M-H-CO <sub>2</sub> ] <sup>-</sup>	211.0498	-0.5 (-2.4)	169.0402	C <sub>7</sub> H <sub>7</sub> N <sub>2</sub> O <sub>3</sub>	[M-H-C <sub>3</sub> H <sub>3</sub> O <sub>3</sub> ] <sup>-</sup>	
								154.0163	C <sub>6</sub> H <sub>4</sub> N <sub>2</sub> O <sub>3</sub>	[M-H-C <sub>3</sub> H <sub>3</sub> O <sub>3</sub> -CH <sub>3</sub> ] <sup>-</sup>	
M208a	4. HR-MS	0.67	-	C <sub>10</sub> H <sub>11</sub> <sup>15</sup> N <sub>2</sub> O <sub>3</sub>	[M-H] <sup>-</sup>	209.0703	-0.7 (-3.3)	167.0587	C <sub>8</sub> H <sub>9</sub> N <sub>2</sub> O <sub>2</sub>	[M-H-H <sub>2</sub> O] <sup>-</sup>	
M208b	4. HR-MS	0.72	-	C <sub>10</sub> H <sub>11</sub> <sup>15</sup> N <sub>2</sub> O <sub>3</sub>	[M-H] <sup>-</sup>	209.0677	-3.3 (-15.8)				
M208a or b	N/A	5. HR-MS	1.31 <sup>c</sup>	+	Ambiguous	[M+H] <sup>+</sup>	211.1011	N/A			
M196a	<i>para</i> reduced See Table 5	4. HR-MS, MS/MS	1.00	-	C <sub>8</sub> H <sub>7</sub> <sup>15</sup> N <sub>2</sub> O <sub>4</sub>	[M-H] <sup>-</sup>	197.0345	-0.2 (-1.0)	155.0234	C <sub>6</sub> H <sub>5</sub> N <sub>2</sub> O <sub>3</sub>	[M-Ac] <sup>-</sup>
M252		4. HR-MS	1.09	+	C <sub>11</sub> H <sub>13</sub> <sup>15</sup> N <sub>2</sub> O <sub>5</sub>	[M+H] <sup>+</sup>	255.0789	2.3 (9.0)			
M196b	<i>ortho</i> reduced See Table 5	4. HR-MS, MS/MS	1.13	-	C <sub>8</sub> H <sub>7</sub> <sup>15</sup> N <sub>2</sub> O <sub>4</sub>	[M-H] <sup>-</sup>	197.0336	-1.1 (-5.6)	179.0237	C <sub>8</sub> H <sub>5</sub> N <sub>2</sub> O <sub>3</sub>	[M-H-H <sub>2</sub> O] <sup>-</sup>
									124	N/A	[M-H-C <sub>2</sub> H <sub>2</sub> NO <sub>2</sub> ] <sup>-</sup>

Table 7. (continued)

	proposed structure	confidence level <sup>1</sup>	RT (min)	ESI	ion formula	proposed ion	accurate mass	deviation (mDa (ppm))	fragment mass <sup>2</sup>	fragment formula	proposed fragment ion
M196d	<i>ortho</i> reduced See Table 5	4. HR-MS	1.31	-	C <sub>8</sub> H <sub>7</sub> <sup>15</sup> N <sub>2</sub> O <sub>4</sub>	[M-H] <sup>-</sup>	197.0333	-1.4 (-7.1)			
M196f		4. HR-MS, RT relative to M276	2.00	-	C <sub>8</sub> H <sub>7</sub> <sup>15</sup> N <sub>2</sub> O <sub>4</sub>	[M-H] <sup>-</sup>	197.0323	-2.4 (-12.2)			
M226		4. HR-MS, putative pathways	2.29	-	C <sub>9</sub> H <sub>9</sub> <sup>15</sup> N <sub>2</sub> O <sub>5</sub>	[M-H] <sup>-</sup>	227.0473	2.1 (9.2)			
M280	Ambiguous	5. HR-MS	2.30	-	Ambiguous	[M-H] <sup>-</sup>	280.9699	N/A			
M368	Ambiguous	5. HR-MS	2.18	+	Ambiguous	[M+H] <sup>+</sup>	371.1339	N/A			

<sup>a</sup>Confidence levels assigned as suggested in <sup>111</sup>

<sup>b</sup>Nominal mass fragment indicates LC-MS/MS data. Accurate mass indicates LC-QToF fragment

<sup>c</sup>Indicates a different retention time was observed in the separate positive and negative ionization chromatography runs. Since the pH of the mobile phases were lower for positive ionization, these compounds were presumably protonated in the positive ionization run condition, resulting in longer retention times

Table 8. [ $^{13}\text{C}_6$ ]DNAN metabolites determined from LC-QToF. Accurate mass values are the mean of 3 biological replicates.

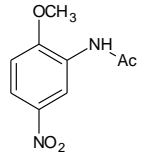
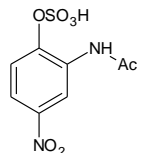
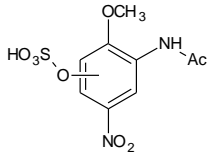
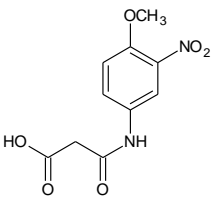
proposed structure	confidence level <sup>a</sup>	RT (min)	ESI	ion formula	proposed ion	accurate mass	deviation (mDa (ppm))	fragment mass <sup>b</sup>	fragment formula	proposed fragment ion <sup>d</sup>
	1. Synthesized standard, HR-MS, MS/MS, RT	2.78	+	$^{13}\text{C}_6\text{C}_3\text{H}_{11}\text{N}_2\text{O}_4$	$[\text{M}+\text{H}]^+$	217.0910	-1.0 (-4.6)	175.0807	$\text{C}_7\text{H}_9\text{N}_2\text{O}_3$	$[\text{M}+\text{H}_2-\text{Ac}]^+$
			-	$^{13}\text{C}_6\text{C}_3\text{H}_9\text{N}_2\text{O}_4$	$[\text{M}-\text{H}]^-$	215.0757	-0.7 (-3.3)	183.0497	$\text{C}_8\text{H}_5\text{N}_2\text{O}_3$	$[\text{M}-\text{OCH}_3]^-$
	2b. HR-MS, MS/MS, diagnostic fragment, relative RT, putative pathways	1.86	-	$^{13}\text{C}_6\text{C}_2\text{H}_7\text{N}_2\text{O}_7\text{S}$	$[\text{M}-\text{H}]^-$	281.0174	-0.1 (-0.4)	201.0611	$\text{C}_8\text{H}_7\text{N}_2\text{O}_4$	$[\text{M}-\text{H}-\text{HSO}_3]^-$
								159	N/A	$[\text{M}-\text{Ac}-\text{SO}_3]^-$
								129	N/A	Ambiguous
								46	N/A	$[\text{NO}_2]^-$
	3. HR-MS, MS/MS, diagnostic fragment	1.50	-	$^{13}\text{C}_6\text{C}_3\text{H}_9\text{N}_2\text{O}_8\text{S}$	$[\text{M}-\text{H}]^-$	311.0250	-3.1 (-10.0)	231.0693	$\text{C}_9\text{H}_9\text{N}_2\text{O}_5$	$[\text{M}-\text{H}-\text{HSO}_3]^-$
								159.0498	$\text{C}_6\text{H}_5\text{N}_2\text{O}_3$	$[\text{M}-\text{OCH}_3-\text{Ac}-\text{HSO}_3]^-$
								216	N/A	$[\text{M}-\text{H}-\text{HSO}_3-\text{CH}_3]^-$
								174	N/A	$[\text{M}-\text{HSO}_3-\text{CH}_3-\text{Ac}]^-$
								186	N/A	$[\text{M}-\text{HSO}_3-\text{NO}_2]^-$
	3. HR-MS, MS/MS, diagnostic fragment	2.04 <sup>c</sup>	+	$^{13}\text{C}_6\text{C}_4\text{H}_{11}\text{N}_2\text{O}_6$	$[\text{M}+\text{H}]^+$	261.0820	0.2 (0.8)	243	N/A	$[\text{M}+\text{H}-\text{H}_2\text{O}]^+$
		1.45	-	$^{13}\text{C}_6\text{C}_3\text{H}_9\text{N}_2\text{O}_4$	$[\text{M}-\text{H}-\text{CO}_2]^-$	215.0800	3.6 (16.7)	215	N/A	$[\text{M}+\text{H}-\text{CH}_2\text{O}_2]^+$
								101	N/A	Ambiguous
								173.0654	$\text{C}_7\text{H}_7\text{N}_2\text{O}_3$	$[\text{M}-\text{H}-\text{C}_3\text{H}_3\text{O}_3]^-$
		158.0421	$\text{C}_6\text{H}_4\text{N}_2\text{O}_3$	$[\text{M}-\text{H}-\text{C}_3\text{H}_3\text{O}_3-\text{CH}_3]^-$						

Table 8. (continued)

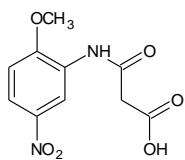
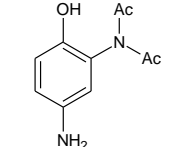
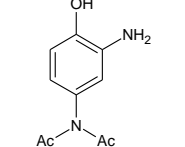
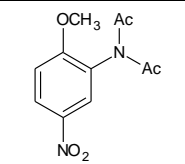
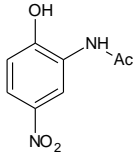
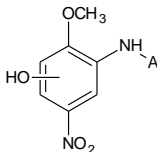
	proposed structure	confidence level <sup>a</sup>	RT (min)	ESI	ion formula	proposed ion	accurate mass	deviation (mDa (ppm))	fragment mass <sup>b</sup>	fragment formula	proposed fragment ion <sup>d</sup>
M254b		3. HR-MS, MS/MS, diagnostic fragment	2.28 <sup>c</sup>	+	<sup>13</sup> C <sub>6</sub> C <sub>4</sub> H <sub>11</sub> N <sub>2</sub> O <sub>6</sub>	[M+H] <sup>+</sup>	261.0864	4.6 (17.6)			
			1.72	-	<sup>13</sup> C <sub>6</sub> C <sub>4</sub> H <sub>9</sub> N <sub>2</sub> O <sub>6</sub>	[M-H] <sup>-</sup>	259.0619	-4.3 (-16.6)	197	N/A	Ambiguous
					<sup>13</sup> C <sub>6</sub> C <sub>3</sub> H <sub>9</sub> N <sub>2</sub> O <sub>4</sub>	[M-H-CO <sub>2</sub> ] <sup>-</sup>	215.0774	1.0 (4.6)	173.0650	C <sub>7</sub> H <sub>7</sub> N <sub>2</sub> O <sub>3</sub>	[M-H-C <sub>3</sub> H <sub>3</sub> O <sub>3</sub> ] <sup>-</sup>
									158.0421	C <sub>6</sub> H <sub>4</sub> N <sub>2</sub> O <sub>3</sub>	[M-H-C <sub>3</sub> H <sub>3</sub> O <sub>3</sub> -CH <sub>3</sub> ] <sup>-</sup>
M208a		4. HR-MS	0.67	-	<sup>13</sup> C <sub>6</sub> C <sub>4</sub> H <sub>11</sub> N <sub>2</sub> O <sub>3</sub>	[M-H] <sup>-</sup>	213.0950	-2.1 (-9.9)	171.0871	C <sub>8</sub> H <sub>9</sub> N <sub>2</sub> O <sub>2</sub>	[M-H-H <sub>2</sub> O] <sup>-</sup>
M208b		4. HR-MS	0.72	-	<sup>13</sup> C <sub>6</sub> C <sub>4</sub> H <sub>11</sub> N <sub>2</sub> O <sub>3</sub>	[M-H] <sup>-</sup>	213.0980	0.9 (4.2)			
M208a or b	N/A	5. HR-MS	1.31 <sup>c</sup>	+	Ambiguous	[M+H] <sup>+</sup>	215.1231	N/A			
M196a	<i>para</i> reduced See Table 5	4. HR-MS, MS/MS	1.00	-	<sup>13</sup> C <sub>6</sub> C <sub>2</sub> H <sub>7</sub> N <sub>2</sub> O <sub>4</sub>	[M-H] <sup>-</sup>	201.0604	-0.3 (-1.5)	159.0499	C <sub>6</sub> H <sub>5</sub> N <sub>2</sub> O <sub>3</sub>	[M-Ac] <sup>-</sup>
M252		4. HR-MS	1.09	+	<sup>13</sup> C <sub>6</sub> C <sub>5</sub> H <sub>13</sub> N <sub>2</sub> O <sub>5</sub>	[M+H] <sup>+</sup>	253.1000	-2.6 (-10.0)			
M196b	<i>ortho</i> reduced See Table 5	4. HR-MS, MS/MS	1.13	-	<sup>13</sup> C <sub>6</sub> C <sub>2</sub> H <sub>7</sub> N <sub>2</sub> O <sub>4</sub>	[M-H] <sup>-</sup>	201.0594	-1.3 (-6.5)	183.0503	C <sub>8</sub> H <sub>5</sub> N <sub>2</sub> O <sub>3</sub>	[M-H-H <sub>2</sub> O] <sup>-</sup>
									129.0525	C <sub>6</sub> H <sub>5</sub> NO <sub>2</sub>	[M-H-C <sub>2</sub> H <sub>2</sub> NO <sub>2</sub> ] <sup>-</sup>

Table 8. (continued)

	proposed structure	confidence level <sup>a</sup>	RT (min)	ESI	ion formula	proposed ion	accurate mass	deviation (mDa (ppm))	fragment mass <sup>b</sup>	fragment formula	proposed fragment ion <sup>d</sup>
M196d	<i>ortho</i> reduced See Table 5	5. HR-MS	1.31	-	Ambiguous	[M-H] <sup>-</sup>	201.0368	N/A			
M196f		4. HR-MS, RT relative to M276	2.00	-	<sup>13</sup> C <sub>6</sub> C <sub>3</sub> H <sub>7</sub> N <sub>2</sub> O <sub>4</sub>	[M-H] <sup>-</sup>	201.0587	-2.0 (-9.9)			
M226		4. HR-MS, putative pathways	2.29	-	<sup>13</sup> C <sub>6</sub> C <sub>3</sub> H <sub>9</sub> N <sub>2</sub> O <sub>5</sub>	[M-H] <sup>-</sup>	231.0692	-2.1 (-9.1)			
M280	Ambiguous	5. HR-MS	2.30	-	Ambiguous	[M-H] <sup>-</sup>	284.9922	N/A			
M368	Ambiguous	5. HR-MS	2.18	+	Ambiguous	[M+H] <sup>+</sup>	375.1632	N/A			

<sup>a</sup>Confidence levels assigned as suggested in <sup>111</sup>

<sup>b</sup>Nominal mass fragment indicates LC-MS/MS data. Accurate mass indicates LC-QToF fragment

<sup>c</sup>Indicates a different retention time was observed in the separate positive and negative ionization chromatography runs. Since the pH of the mobile phases were lower for positive ionization, these compounds were presumably protonated in the positive ionization run condition, resulting in longer retention times



*DNAN is acetylated and hydroxylated by Penicillium*

The metabolite detected at  $m/z$  211.0729 (along with the corresponding mass label shifts) was hypothesized to be 2-(*N*-acetyl)amino-4-nitroanisole (2-NAc-NAN), and the compound was confirmed by a synthesized standard (M210, Table 6). This compound has been observed in two of the three previous investigations of DNAN degradation by an isolated culture<sup>27, 28</sup>. After initial formation over the first five days of exposure, the concentration of 2-NAc-NAN (M210) decreased and then plateaued (Figure 9B). When strain KH1 was incubated with 2-ANAN, direct amine acetylation was observed to form M210. This is in contrast to the findings of Perreault and co-workers, who observed hydroxylamine acetylation with subsequent de-hydroxylation to form 2-NAc-NAN<sup>28</sup>. The *N*-acetylation reaction is known to be catalyzed by *N*-acetyltransferases, which are ubiquitous in fellow plant-derived Ascomycota fungi<sup>112</sup> and detoxify a range of other aromatic amines<sup>108</sup>. An ascomycete fungus detoxified soil artificially contaminated by 3,4-dichloroaniline by *N*-acetylation to the extent that plants could then grow, indicating that this reaction likely reduces the toxicity of the DNAN metabolite<sup>108</sup>.

2,4-Diaminoanisole was not detected by high resolution mass spectrometry, which is consistent with previous studies in aerobic systems<sup>19, 25, 26</sup>. However, two observed metabolites may have resulted from dual nitro group reductions (M208a and M208b, Table 2). Since 2-NAc-NAN was not demethylated by strain KH1 (Table 5), metabolites 208a and 208b are proposed to result from demethylation of DNAN followed by two successive acetylations of the primary amine group. These *N*-acetyl groups would withdraw electrons from the aromatic ring and promote further reduction of the remaining nitro group to yield M208a and M208b. The intermediate nitro-containing compounds were not detected, but these intermediates would be subject to amide hydrolysis to yield M196e and M196f or reduction to yield the isomers of M208. A third metabolite (M252) was detected that is proposed to result from multiple *N*-acetylations; this specific case is *N*-acetylation of 2-NAc-NAN (M210). Since 4-(*N*-acetyl)amino-2-nitroanisole was not detected, it is logical that only one isomer of M252 (presumably *o*-reduced) was detected. An additional metabolite (M226) had the formula C<sub>9</sub>H<sub>9</sub>N<sub>2</sub>O<sub>5</sub>, and is proposed to result from ring hydroxylation of 2-NAc-NAN (M210).

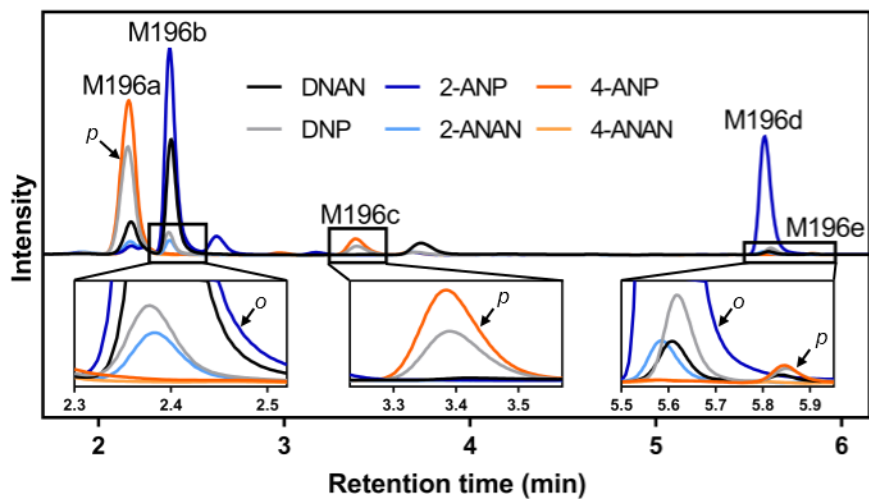


Figure 11. LC-MS chromatogram of  $m/z$  195 in ESI mode illustrating that isomeric starting substrates confirm five isomers of M196 resulting from either *ortho* (*o*) or *para* (*p*) nitro-reduction of DNAN.

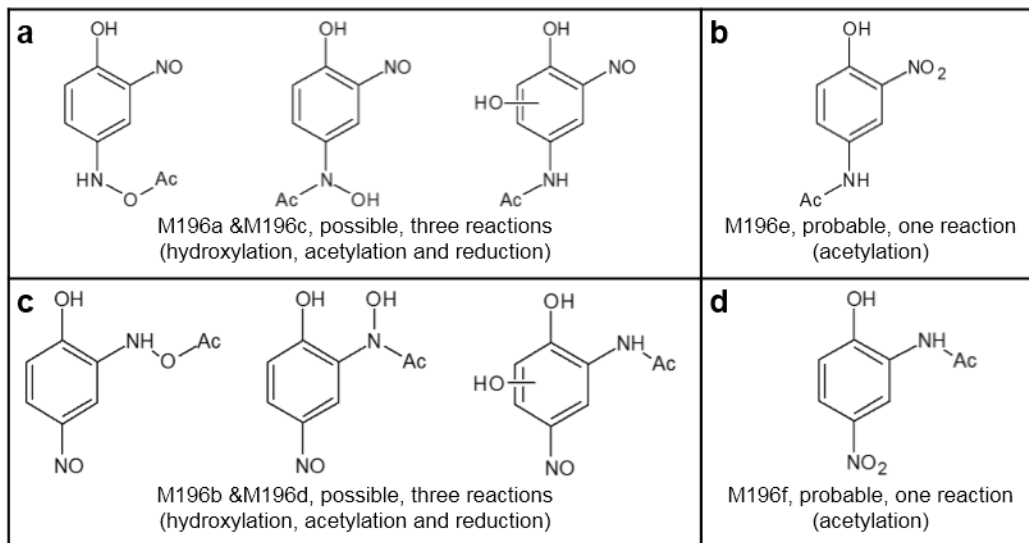


Figure 12. Possible structures for the six isomers of M196 and reactions required for formation from the corresponding amino-nitrophenol.

### *Six isomers of M196 have ambiguous structures*

Six isomers ( $m/z$  195), designated M196a to M196f, were detected in ESI<sup>-</sup> mode using selected ion monitoring (SIM) LC-MS (Figure 11) and/or LC-QToF. Multiple primary substrates were utilized to facilitate metabolite elucidation. M196a, c, and d were formed by demethylation and subsequently reduction at the *para* position because these metabolites resulted from 4-ANP and DNP, but not 4-ANAN. After strain KH1 was incubated with DNP, 2-ANAN, and 2-ANP, the same two isomers (M196b and e) of  $m/z$  195 were detected. This demonstrated that M196b and M196e resulted from both demethylation and *o*-nitroreduction of DNAN in parallel. Finally, incubations with 2-NAc-NAN and 4-ANAN yielded no isomers of M196, indicating that demethylation of DNAN occurs before *p*-nitroreduction and *o*-acetylation (Figure 11).

Four of the isomers of M196 were detected by LC-QToF after ten days of incubation with DNAN and were assigned the formula C<sub>8</sub>H<sub>8</sub>N<sub>2</sub>O<sub>4</sub>. M196b showed a neutral loss of H<sub>2</sub>O, as previously observed for aromatic hydroxyl groups<sup>113</sup>. In addition, M196b had a fragment of [M-Ac-NO]<sup>-</sup> (C<sub>6</sub>H<sub>5</sub>NO<sub>2</sub>), consistent with the nitroso-containing structures presented in Fig. 3a and c. None of the M196 isomers were detected in ESI<sup>+</sup> mode which strongly suggests an absence of primary amine functional groups. The lack of ESI<sup>+</sup> ionization, and the observation that M196a-e resulted from demethylated substrates points to the formation of three pairs of analogous *para*- and *ortho*-reduced isomers structures (Figure 12). The peak areas of the M196a-e isomers were monitored over time on LC-MS (SIM), but only M196b and M196d were detected in measurable quantities when DNAN was the initial substrate (Figure 13). Similar to the proportion of 2-ANAN to 4-ANAN, *o*-nitroreduced M196 isomers were formed in more substantial quantities than their analogous *para* isomers.

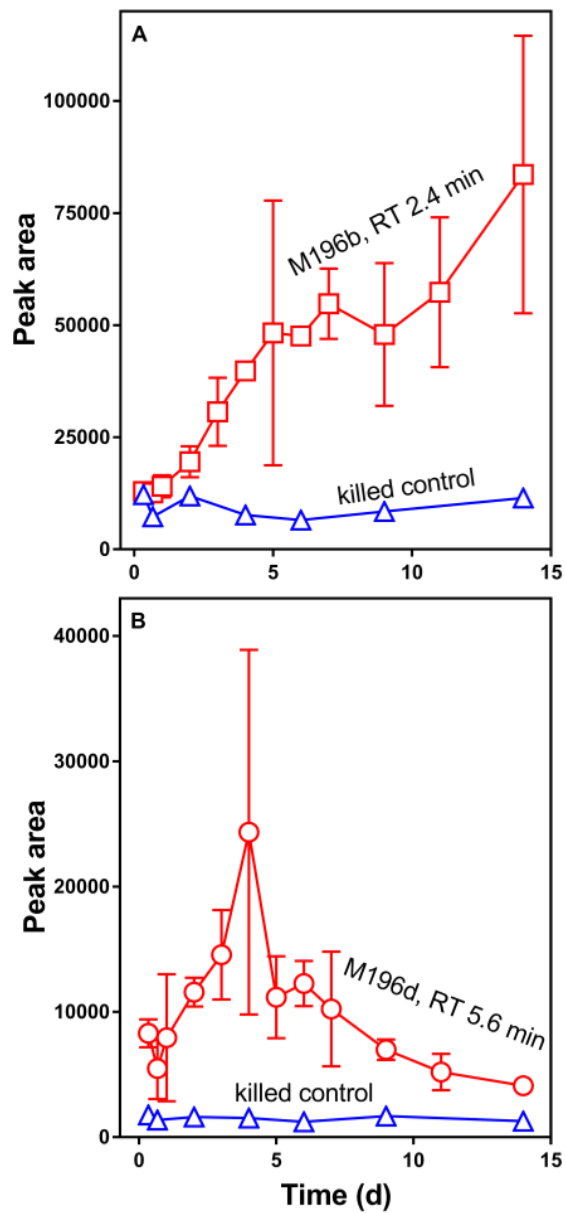


Figure 13. LC-MS (SIM) peak areas over time of  $m/z$  195 in ESI mode for metabolite (A) M196b and (B) M196d produced from DNAN by *Penicillium* sp. KH1. Error bars are one standard deviation from the mean ( $n=3$ ,  $n=2$  days 5, 6, and 14). The open triangles

are the concentrations in the killed control media (n=1).

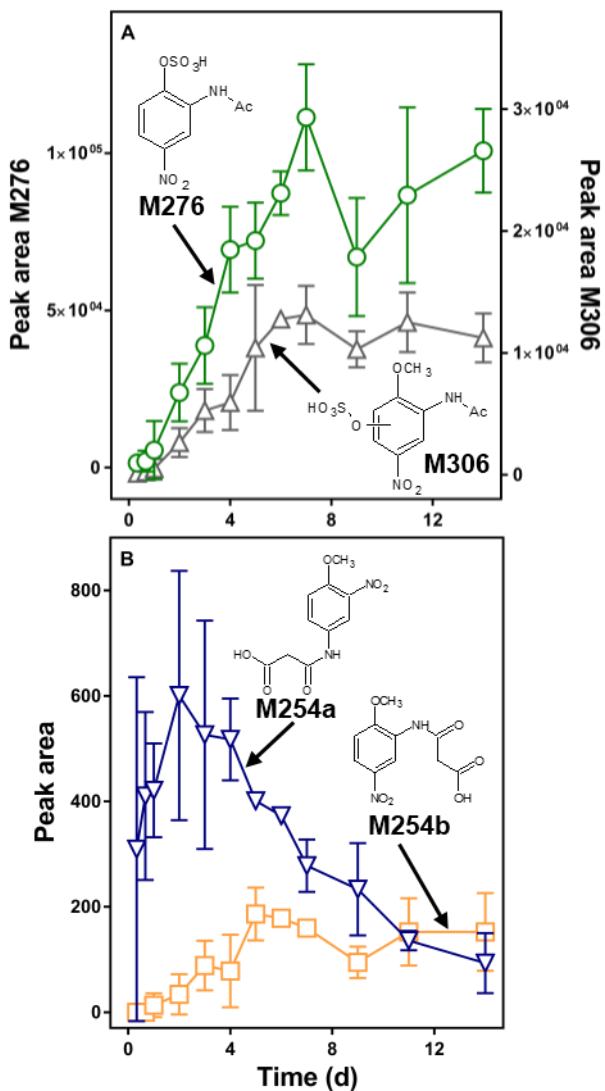


Figure 14. Concentration trends of (A) sulfated and (B) malonylated DNAN metabolites as demonstrated by LC-MS/MS peak areas. Error bars represent one standard deviation from the mean (n=3, n=2 days 5, 6 and 14).

### *Nitro-reduction products of DNAN are sulfated*

A metabolite ( $C_8H_8N_2O_7S$ ), designated M276 (Table 6), is hypothesized to result from sulfation of M196f. This compound had a major fragment of  $m/z$  195.0414,  $[M-H-HSO_3]^-$ , with unlabeled isotopes and 197.0376 and 201.0616 with the  $^{15}N_2$ - and  $^{13}C_6$ -labels, respectively. A fragment of  $[M-H-HSO_3]^-$  is diagnostic of a sulfate attached to an  $sp^2$  carbon<sup>114</sup>, which suggests the phenolic group was sulfated. The *ortho*-nitro group of M276 was reduced as evidenced by incubations with DNAN, DNP, 2-ANP, 2-ANAN that yielded this compound and incubations with 4-ANP and 4-ANAN that did not produce M276 (Table 5). Metabolite M196f was the only isomer of M196 with a longer retention time than M276 which is consistent with an expected increase in polarity due to sulfation. M276 contained a nitro group (Table 6), suggesting that M196f was the precursor to M276 with the structure shown in Fig. 3d. Finally, M276 was not observed when strain KH1 was incubated with 2-Nac-NAN, suggesting that DNAN is demethylated initially, and then acetylated and sulfated to form M276.

A metabolite, designated M306 ( $C_9H_9N_2O_8S$ ), is proposed to result from *ortho*-nitroreduction, acetylation, hydroxylation of the aromatic ring, and then sulfation of the phenolic group. M306 had the diagnostic fragment,  $[M-H-HSO_3]^-$ , that is characteristic of a sulfate group directly attached to an aromatic carbon, and M306 would directly result from sulfation of M226. Sulfated metabolite peak areas increased over time suggesting they are “dead-end” products (Figure 14A). Sulfation is a well-known detoxification strategy for xenobiotics, especially sulfation of hydroxyl groups<sup>114</sup>. This reaction greatly increases solubility, making elimination of the product easier, and, therefore, sulfated products are generally not subject to further degradation<sup>98</sup>.

### *Amino-nitroanisoles are malonylated*

Two additional isomeric metabolites (M254a and M254b), concluded to be malonylated amino-nitroanisoles, were detected in  $ESI^+$  and  $ESI^-$  and assigned the formula  $C_{10}H_{10}N_2O_6$ . Evidence for the structure of these metabolites was collected *via* LC-MS/MS. In  $ESI^-$  mode, the  $[M-H]^-$  ion was detected at  $m/z$  253. With higher source energy, the predominant signal was  $[M-H-44]^-$  at  $m/z$  209, which has been shown to be diagnostic of a loss of the carboxyl group in *N*-malonylated lysine in peptides<sup>115</sup>. In fact, the  $[M-H]^-$  ion was below detection for M254a (Table 6) on the LC-QToF, while  $[M-H-$

$\text{CO}_2^-$  was the base peak. An LC-MS/MS product scan of the parent  $[\text{M}-\text{H}]^-$  ions revealed fragments of  $m/z$  167 and 152 resulting from both isomers. These fragments represent a loss of malonate ( $m/z$  167) and a loss of malonate and a methyl group ( $m/z$  152).

A recent study of amine transformation in sludge found that the secondary amine of ortho-chlorophenylpiperazine most likely underwent malonylation. This and other *N*-acylations were implicated as important and previously overlooked xenobiotic amine transformation pathways<sup>116</sup>. Plant-associated fungi have been shown to perform the *N*-malonylation reaction on structurally similar aryl amines produced by plants to kill unwanted microorganisms. The fungi have evolved to detoxify these aryl amines, so M254a and b likely result from this known malonyl-transferase-mediated reaction<sup>112</sup>. All of the *N*-acylated metabolites are likely to undergo amide hydrolysis and be back-transformed to primary and secondary amines<sup>117</sup>, which may explain why most did not accumulate in the media (Figure 9B, Figure 13B, and Figure 14B).

## Conclusions

This is the first report we are aware of that demonstrated DNAN degradation by a fungus. *Penicillium* sp. KH1 isolated from willow tree cuttings quickly degraded DNAN in solution. Thirteen previously unknown degradation products were identified and confirmed with stable isotope-labeled substrate. DNAN was transformed *via* many reaction pathways including *ortho*- and *para*-nitroreduction, demethylation, acetylation, hydroxylation, malonylation, and sulfation. Transformation of DNAN by the fungus did result in degradation of the parent compound, but also formed metabolites of unknown persistence and toxicity. Further work would be needed to implement remediation with *Penicillium* sp. KH1. Finally, incubation with metabolites as primary substrates is an effective way to confirm metabolite isomerism and elucidate metabolic pathways.



## CHAPTER 4: METABOLISM AND PHOTOLYSIS OF 2,4-DINITROANISOLE IN ARABIDOPSIS

This chapter has been peer-reviewed and published in *Environmental Science & Technology*, **2017**, *51*(23), pp 13714–13722, doi: 10.1021/acs.est.7b04220

### Introduction

Explosive compounds contaminate millions of land acres globally, primarily through releases at military training facilities (e.g., as unexploded ordnance) and at production and disposal facilities.<sup>2, 17</sup> Utilization of the most common explosives, 2,4,6-trinitrotoluene (TNT) and hexahydro-1,3,5-trinitro-1,3,5-triazine (RDX), is projected to decrease as insensitive munitions gain favor in new melt cast explosives formulations.<sup>17, 19</sup> For example, the formulation “IMX-101,” comprised of 2,4-dinitroanisole (DNAN), nitrotriazolone, and nitroguanidine, provides a similar explosive force to TNT, but with a decreased sensitivity to shocks that can trigger unintended detonations.<sup>20</sup> DNAN ( $S_w = 276 \text{ mg L}^{-1}$ ), used in at least six modern explosives formulations, is considerably more water-soluble than TNT and RDX ( $S_w = 100$  and  $60 \text{ mg L}^{-1}$ , respectively), which elevates concern for groundwater contamination.<sup>20, 95, 118, 119</sup> DNAN is also less sorptive than TNT and RDX, which makes contaminant plume migration more likely while rendering site cleanup more difficult and expensive.<sup>19</sup> Remediation of explosives is typically achieved by costly *ex situ* methods, such as pump and treat or incineration.<sup>6</sup> Alternatively, *in situ* bioremediation is potentially less expensive, and biotic systems have been used to remediate legacy explosives such as TNT and RDX.<sup>6, 11, 12, 15, 16, 83, 84, 96, 97, 120, 121</sup>

One biotic remediation approach, phytoremediation, is the use of plants to metabolize or even sequester harmful chemicals irreversibly into biomass.<sup>122</sup> When exposed to organic contaminants, plants may metabolize the compound following the conceptual framework called the “green liver” model. The green liver model posits that xenobiotics are functionalized in phase I (e.g., hydroxylation, nitro-reduction, demethylation). In phase II metabolism, plants conjugate large, water-soluble moieties, such as glucose onto the new functional group. Plants can also perform phase II conjugation without phase I functionalization if the original compound contains a sufficiently reactive moiety.<sup>16, 122, 123</sup> The phase II metabolites are subject to further

degradation or permanent sequestration to cell walls or vacuoles in phase III of metabolism, which make plants a promising option for long-term contaminant remediation.<sup>11, 16, 83, 122, 124</sup> Specifically with regards to explosives, plants can functionalize TNT via nitro group reductions to hydroxylamines and amines prior to conjugation with glutathione and sugars – precursors to non-extractable, covalently-bound TNT residues, containing and detoxifying the explosives.<sup>5, 11, 16, 83, 125</sup> Additionally, plants facilitate the degradation of photo-labile explosives such as RDX through uptake, translocation to leaves, and subsequent photolysis. In one study, sunlight exposure degraded RDX within reed canary grass leaves, while in the absence of sunlight, the grass did not metabolize RDX.<sup>126</sup> In another study, both light and *Populus* tissue culture cells were required for RDX mineralization, indicating a light-induced transformation inside the plant cells.<sup>13</sup> Despite these promising results, the role of sunlight in phytoremediation (i.e., photophotolysis) has largely been overlooked for other compounds.<sup>127</sup>

Although photolysis and metabolism in plants has been demonstrated for RDX and TNT, respectively, there is little data available on plant metabolism of DNAN and the potential to clean up DNAN-contaminated sites with phytoremediation. A limited number of studies have investigated DNAN chemical and biochemical transformations, soil binding behavior, and ecotoxicity.<sup>17, 19, 25-27, 33, 39, 62</sup> One study reported DNAN in grass shoots and roots, but no mass balance was reported and no transformation products were measured.<sup>36</sup> Another study observed DNAN metabolism in ryegrass where DNAN was reduced to 2-amino-4-nitroanisole (2-ANAN) and further conjugated to unknown, acid-hydrolysable products, possibly sugars.<sup>17</sup> However, it remains unknown whether plant metabolites of *any* xenobiotics can undergo photolysis inside photosynthetic tissues, potentially altering the phytoremediation process. We are unaware of any previous reports of DNAN, or DNAN metabolite, photolysis inside plant tissues despite knowledge that DNAN, and a model plant metabolite of DNAN (4-nitrophenyl- $\beta$ -D-glucopyranoside), are photolyzed in aqueous solution.<sup>19, 128</sup> Here, we report DNAN metabolism and photolysis within the model plant *Arabidopsis*.

## Materials & Methods

### Chemicals

All reagents and standards were used as received with sources and purities listed in Table 9. [ $^{13}\text{C}_6$ ]DNAN (>99%) and [ $^{15}\text{N}_2$ ]DNAN (>99%) were synthesized as previously described.<sup>27</sup> Liquid chromatography solvents (Optima grade) were purchased from Fisher Scientific (Waltham, MA).

Table 9. Chemicals and reagents utilized.

IUPAC name	Abbreviation	CAS #	Purity	Source
2,4-dinitroanisole	DNAN	119-27-7	98%	Alfa Aesar
2,4-dinitrophenol	DNP	51-28-5	Analytical standard	Restek
2-methoxy-5-nitroaniline	2-ANAN	99-59-2	Analytical standard	SPEXOrganics
4-methoxy-3-nitroaniline	4-ANAN	577-72-0	97%	Accela ChemBio Co.
2-amino-4-nitrophenol	2-ANP	99-57-0	99%	Acros Organics
4-amino-2-nitrophenol	4-ANP	119-34-6	99%	Acros Organics
2-(N-acetyl)amino-4-nitroanisole	2-NAc-NAN	N/A	>99%	Synthesized, see Appendix A
Sucrose	N/A	57-50-1	ACS	Fisher Scientific
2-(N-morpholino)ethanesulfonic acid	MES	4432-31-9	≥99%	Research Products International Corp.
Sodium Nitrite- $^{15}\text{N}$	$^{15}\text{NO}_2$	68378-96-1	98%+ atom	Cambridge Isotope Laboratories
2,3-diaminonaphthalene	DAN	771-97-1	97%	Alfa Aesar
Ammonium acetate	$\text{NH}_4\text{OAc}$	631-61-8	Optima LC/MS	Fisher Scientific

### *Experimental Design: Plant growth conditions*

*Arabidopsis thaliana* (Col-0) was studied due to its extensive use and characterization in basic research and to compare with previous studies on *Arabidopsis* metabolism of explosives.<sup>5, 16, 129, 130</sup> Before exposure to DNAN, *Arabidopsis thaliana* (Col-0) seeds were sterilized using a bleach solution and stratified for 1-5 days in sterilized deionized (DI) water at 4 °C.<sup>129</sup> After stratification, seeds or seedlings were placed into Magenta™ boxes (Magenta LLC., Lockport, IL) containing 25 mL of filter-sterilized (0.2 µm, cellulose nitrate, Nalgene, Rochester, NY) Murashige and Skoog (MS) basal medium.<sup>129</sup> MS basal medium was prepared as follows (per liter of deionized water): 5.0 g sucrose, 4.43 g MS salts plus vitamins (Caisson labs, Smithfield, UT), 0.5 g 2-(N-morpholino)ethanesulfonic acid hydrate (MES). We adjusted the pH to 5.7 using 1 M KOH. The boxes were incubated in a growth chamber (Percival Scientific, Perry, IA) with a diurnal cycle of 16 hours of light (23 °C) and 8 hours of dark (21 °C) at 50% relative humidity. At the basal medium surface, the light intensity was  $140 \pm 19 \mu\text{mol photons m}^{-2} \text{ s}^{-1}$  (photosynthetically active range) as measured three times per week by a quantum light sensor (LI-COR, Lincoln, NE).

### *DNAN and metabolite mass balance*

To determine a DNAN mass balance in plant media and tissues, hydroponic cultures of *Arabidopsis* were sacrificed every 12 hours over three days of DNAN exposure. Plants (n = 25 seeds per box) were exposed to DNAN after 14 days of seed germination and growth, at which point the medium in each Magenta™ box (n = 18) was replaced with fresh, sterile medium (25 mL) spiked with 125 nmoles DNAN (dissolved in 250 µL methanol, 1% v/v) to achieve a nominal concentration of 5 µM (1 mg/L). This relatively high DNAN concentration was selected to facilitate metabolite identification after preliminary uptake experiments indicated no visible physiological plant effects at 5 (Figure 16). Every 12 hours, randomly selected, whole Magenta™ boxes were sacrificially harvested in triplicate. Control boxes, containing MS medium and DNAN, but no plants, were simultaneously harvested in duplicate. Hydroponic media was analyzed by mass spectrometry and plant tissues were extracted as described below.

### *Metabolite identification experiments*

Metabolites of DNAN were identified using an untargeted metabolomics approach, enhanced by stable-isotope labeled DNAN. Three exposure conditions (n = 12 boxes, 25 seeds per box) were conducted simultaneously: 1) non-labeled DNAN with [<sup>13</sup>C<sub>6</sub>]DNAN (31 nmoles each), 2) non-labeled DNAN with [<sup>15</sup>N<sub>2</sub>]DNAN (31 nmoles each), and 3) no added DNAN. After 14 days of germination and growth, the MS medium was replaced with fresh medium (25 mL) containing non-labeled DNAN and labeled DNAN (dissolved in methanol) as above to a nominal concentration of 2.5 μM. The equivalent volume of methanol (250 μL, 1% v/v) was added to the no-DNAN controls. After 48 hours, quadruplicate boxes of each treatment type were harvested, extracted, and analyzed by liquid chromatography high-resolution mass spectrometry with data processing via metabolomics software as described below.

### *Photolysis experiments*

Irradiation experiments used an Atlas Suntest CPS+ solar simulator (Atlas Material Testing Technology, Mount Prospect, IL) with a xenon lamp and an Atlas UV Suntest filter to simulate the emission spectrum of natural sunlight at an irradiance of 750 W/m<sup>2</sup> (Figure 15) and the irradiation chamber was cooled to 19.9 ± 0.6 °C during experiments using a portable air conditioning unit. To determine if DNAN and its metabolites were photolyzed inside leaves, we exposed *Arabidopsis* plants to DNAN and then exposed the leaves to simulated sunlight. *Arabidopsis* seeds were sterilized and stratified in the same manner as described above. Next, approximately 1000 seeds were placed into MS medium (150 mL) in a foam-stoppered, 500 mL flask. The flask was incubated in the growth chamber on a shaker table (120 rpm). After seven days, germinated seedlings were placed into Magenta™ boxes (n = 20 per box) with 25 mL of fresh MS medium. After seven days of additional growth, the seedlings were exposed to 5 μM [<sup>15</sup>N<sub>2</sub>]DNAN in 25 mL of fresh MS medium. After 48 hours in the growth chamber, leaves were excised from roots, and the leaves from each Magenta™ box were divided into two groups. The “irradiation treatment” leaves were placed into cork-stoppered quartz tubes positioned at 30° from horizontal within the solar simulator. The “non-irradiated control” leaves were placed into sealed 2 mL vials wrapped in aluminum foil before positioning

inside the solar simulator. Each hour, triplicate sets of irradiated and non-irradiated leaves were removed from the solar simulator and the fresh weight was recorded before lyophilization. In a separate experiment to examine DNAN transformation products from solar irradiation of *Arabidopsis* leaves, 125 nmoles of DNAN was added to each box (n=10 boxes, 20 seedlings each) to a nominal concentration of 5  $\mu$ M. After two days of DNAN exposure, excised leaves were divided into irradiated and non-irradiated groups. Leaves were either exposed to simulated sunlight or kept in the dark for three hours before freeze-drying, solvent extraction, analysis, and data processing.

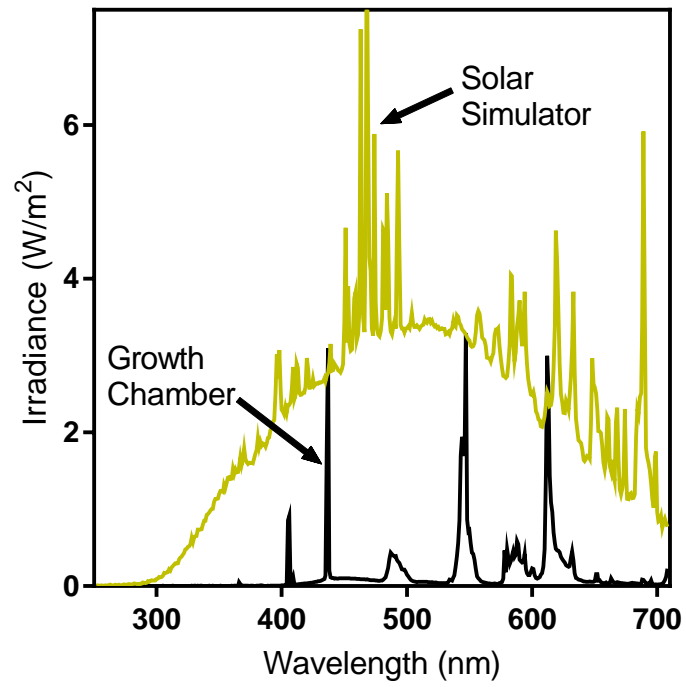


Figure 15. Irradiance of Suntest CPS+ at 750 W/m<sup>2</sup> and growth chamber lights as measured by a spectral radiometer (International Light Technologies, Peabody, MA).

### *Liquid chromatography and mass spectrometry*

Quantitative mass spectrometry analyses were performed on a liquid chromatograph (Agilent model 1260, Santa Clara, CA) and triple-quadrupole (LC-QQQ) mass spectrometer (Agilent model 6460) equipped with a Jet Stream electrospray ionization (ESI) source. Samples in the auto-sampler tray were maintained at 8 °C. DNAN and other metabolites were quantified in ESI negative (ESI<sup>-</sup>) and positive (ESI<sup>+</sup>) modes and verified with a second fragment ion using the mass transitions, analytical columns, and mobile phase conditions outlined in Table 10. DNAN was quantified using a six-standard, [<sup>13</sup>C<sub>6</sub>]DNAN internal standard-normalized, external calibration curve run before each batch. Amino-nitroanisoles were quantified by an external calibration curve of the respective standards diluted from stock solutions, without adjusting for the internal standard due to separate runs in different ionization modes from DNAN. Agilent MassHunter Quantitative Analysis software was used to fit a linear calibration curve. For quality control, three to four check standards from the calibration curve were analyzed per batch (25-75 samples) to ensure consistent detector response. A deionized (DI) water blank was run every five injections to ensure there was no sample carry-over contamination. Analyses requiring accurate mass data were performed by ultraperformance liquid chromatograph with a quadrupole time-of-flight (LC-QToF) mass spectrometer or an Orbitrap (LC-Orbitrap) mass spectrometer.

### *QTOF Parameters for untargeted metabolomics*

To identify DNAN metabolites in whole plant extracts, we used a Waters (Milford, MA) Acquity ultraperformance liquid chromatography (UPLC) instrument with a quadrupole-time-of-flight mass spectrometer (Acquity QToF Premier). An Acquity UPLC HSS T3 column (2.1 mm x 100 mm, 1.8 μm) heated to 60 °C (0.6 mL/min) was used. Leucine enkephalin was infused (10 μL/min) as the lock mass and samples were analyzed (in separate runs) in ESI<sup>-</sup> and ESI<sup>+</sup> modes. A mass to charge (m/z) range of 40–1000, a scan rate of 0.2 s/scan and a sampling cone voltage of 30 were used for ESI<sup>-</sup> mode. A scan rate of 0.15 s/scan and a sampling cone voltage of 23 were used for ESI<sup>+</sup> mode. Samples in the auto-sampler tray were maintained at 8 °C. The mobile phase was (A) 95% DI water with 5% acetonitrile and (B) 95% acetonitrile and 5% DI water, both containing 5



mM ammonium acetate for ESI<sup>-</sup>. For ESI<sup>+</sup> mode, 0.05% formic acid was added to both mobile phases. The mobile phase gradient was: 0 min, 0% B; linear to 7 min, 100% B; 9 min, 100% B; 9.1 min 0% B; 13 min 0% B. The desolvation gas (400 °C) flow was 800 L/h and the capillary voltage was 2.5 kV.

*Orbitrap parameters for tandem mass spectrometry and formula assignment*

To elucidate accurate mass fragments of DNAN metabolites, we used a Thermo Scientific (Waltham, MA), Q Exactive quadrupole-Orbitrap mass spectrometer after separation with a Thermo Ultimate 3000 UHPLC+ Focused at the Center For Mass Spectrometry and Proteomics at the University of Minnesota. We used an Acquity UPLC HSS T3 column (2.1 mm x 100 mm, 1.8 µm) heated to 60 °C (0.4 mL/min). The mobile phase for positive mode was DI/ACN containing 10 mM ammonium acetate, and the gradient was as follows (% ACN): 0 min, 2%; linear to 3 min, 5%; linear to 11 min, 98%; 12 min, 98%, 13 min, 2%; 15 min 2%. For negative mode, the same gradient was used with 10 mM ammonium acetate in MeOH as the organic phase. The mass range was 65-975m/z and targeted MS/MS was conducted with a ramped normalized collision energy of 10, 35, 45.

Table 10. LC-QQQ parameters

LC-QQQ, Agilent 1260 LC and Agilent 6460 QQQ, Agilent Poroshell 120 EC-C18 (3x50 mm, 2.7 µm) with 3x5 mm guard column and 0.5 mL/min flow rate (35 °C), 10 µL injection					
Analyte	ESI mode	LOQ <sup>a</sup> (ppb)	Mass transitions (m/z)	Mobile Phases (A/B)	Gradient Time %B
DNAN	-	5	183>109 183>123	DI/MeOH 10mM ammonium acetate in both	0 10 5 95 7 95 7.1 10 12 10
[ <sup>15</sup> N <sub>2</sub> ]DNAN	-	5	185>110 185>123		
[ <sup>13</sup> C <sub>6</sub> ]DNAN	-	5	189>114 189>129		
DNP	-	0.5	183>109 183>123		
2-ANAN	+	0.5	169.1>123 169.1>108	DI/ACN 0.1% formic acid in both	0 5 3 5 10 15 11 98 13 98 13.1 5 17 5
4-ANAN	+	0.5	169.1>122.0 169.1>94.1		
2-amino-4-nitrophenol	+	1	155.1>109 155.1>92		
4-amino-2-nitrophenol	+	1	155.1>109 155.1>80.1		
2-(N-acetyl)amino-4-nitroanisole	+	10	211.07>169.1 211.07>123		
M330	+	N/A	331>169.1 331>123		
[ <sup>15</sup> N <sub>2</sub> ]M330	+	N/A	333>171 333>124		
M568	+	N/A	569.2>321 569.2>304 569.2>289		
M524	-	N/A	523.2>303		
			523.2>289		
			523.2>273		

<sup>a</sup>Limit of quantification defined here as lowest concentration used in a linear calibration curve

*Plant tissue extraction, metabolite hydrolysis, and nitrite derivitization*

At each sampling time, plant tissue was removed from the medium and dabbed dry with a Kimwipe (Kimberly-Clark, Irving, TX). The plant tissue was placed into a 2 mL vial (safe-lock, Eppendorf) and the fresh weight was recorded before freezing (-80 °C) and subsequent lyophilization (FreeZone 6, Labconco, Kansas City, MO) for 13-16 hours. The dry weight (52-75 mg, mean: 69 mg dry weight for whole plants; 10-17 mg, mean: 13 mg for leaf fractions) of the freeze-dried tissue was recorded and a single stainless steel ball (5 mm) and 1 mL water:methanol (1:1) mixture were added to each vial. The vials were frozen (-80 °C), thawed, and homogenized by a mixer mill (Retsch, Haan, Germany) for 5 min at 30 Hz. The vials were then sonicated for 10 min, vortexed for 30 s and centrifuged at 13,000g for 10 min. Finally, the supernatant was removed and syringe-filtered (0.22 µm, PES, Chemglass Life Sciences, Vineland, NJ). The tissue was extracted without the freeze-thaw step two additional times with 500 µL of water:methanol (1:1) and the supernatants were combined.<sup>129</sup> Samples for metabolite identification were extracted only once, with 1 mL of water:methanol (1:1) mixture. Reported concentrations of DNAN and metabolites were corrected for a  $95.7 \pm 0.6$  % extraction efficiency (determined from spike recoveries on unexposed plant tissues after three extractions). An internal standard (250 nM [<sup>13</sup>C<sub>6</sub>]DNAN final concentration) was added after extracts were diluted (with DI water) to fall within the calibrated range of the mass spectrometer. In a preliminary test for sorption of DNAN to Magenta boxes, we decanted DNAN-containing media from two boxes, rinsed the boxes with 1 mL of water:methanol (1:1), and analyzed this fraction for DNAN. This procedure resulted in negligible recovery of DNAN (< 0.1%), therefore, we concluded that DNAN sorption to the boxes was not important and did not repeat the procedure for each experiment.

For glycosylated metabolite analysis, tissue extracts were prepared as above and hydrolyzed with acid prior to analysis for released 2-ANAN by adding 30 µL of sample, 30 µL DI water, and 30 µL of 1.5N HCl to a 150 µL vial insert inside a 2 mL LC autosampler vial. The extracts were incubated at 45 °C for 5 min and analyzed immediately by LC-QQQ. Isotope-labeled nitrite (<sup>15</sup>NO<sub>2</sub><sup>-</sup>) was measured by LC-QQQ after derivitization with 2,3-diaminonaphthalene (DAN) using a method modified from Nussler, et al.<sup>131</sup> Briefly, 5 µL of leaf extract was diluted with 95 µL of DI water prior to

derivitization with 50  $\mu\text{L}$  of DAN (158  $\mu\text{M}$  in 0.62 N HCl) and 50  $\mu\text{L}$  of 1.5N HCl for 10 minutes at room temperature. To quench the reaction, 20  $\mu\text{L}$  of 1N NaOH was added and the samples were incubated at 8  $^{\circ}\text{C}$  for at least 90 minutes prior to analysis. Labeled nitrite in plant extracts was calibrated to derivitized standards with a known amount of spiked  $^{15}\text{NO}_2^-$  in DI water and 1.1  $\mu\text{M}$   $\text{NO}_2^-$  as a background concentration similar to plant extracts.

#### *Unknown metabolite identification and statistical analysis*

Full-scan LC-QToF data of whole plant extracts were collected for ten minutes, converted to netCDF format by Databridge software (Waters, Milford, MA) and uploaded to XCMS Online<sup>104</sup> for an untargeted metabolomics approach to metabolite elucidation. This study examined compounds resulting from DNAN transformation as confirmed by stable-isotope labeled substrates, and, as such, was not a comprehensive metabolomics investigation. Three DNAN isotopologues (i.e., unlabeled DNAN, [ $^{13}\text{C}_6$ ]DNAN, and [ $^{15}\text{N}_2$ ]DNAN) were used to allow unambiguous identification of metabolites derived from DNAN and to provide orthogonal data sets. Full XCMS Online parameters are detailed in Table S3. Elemental formulas were assigned based on the averaged accurate mass of all biological replicates using Thermo Xcalibur software. Raw, time-series concentration data were compared for significant differences using a two-sided, matched-pairs Student's t-test ( $\alpha = 0.05$ ,  $p < 0.05$ ). Figures were produced and statistical analysis was conducted using GraphPad Prism 7.00 and PerkinElmer Chemdraw Prime 16.0.1.4.

## Results and Discussion

### *Arabidopsis* takes up and metabolizes DNAN

To determine if *Arabidopsis* can take up and metabolize DNAN, plants were exposed to DNAN for three days in hydroponic medium under sterile conditions. Plants quickly took up DNAN from solution, with 67% of DNAN mass removed over 72 hours (Figure 17). In a no-plant control, some DNAN was transformed, presumably due to photolysis because DNAN is stable in solution in the dark, and DNAN was not sorbed to Magenta boxes.<sup>19</sup> However, the DNAN concentration in planted media was significantly different from the controls ( $p = 0.0005$ ,  $n = 6$  pairs). *Arabidopsis* removed DNAN from the hydroponic medium with pseudo-first order kinetics ( $k_{\text{obs}} = 0.33 \pm 0.03 \text{ d}^{-1}$ ). DNAN uptake by *Arabidopsis* is consistent with previous work where DNAN was detected in grass grown on soil amended with DNAN, as well as with other studies of plant metabolism of xenobiotics.<sup>17, 36, 123, 129, 130</sup> Of the DNAN taken up from solution, a maximum of 13% was found within the plant tissues after 12 hours, suggesting that DNAN was extensively metabolized. We detected 2-ANAN and 4-amino-2-nitroanisole (4-ANAN) in plant tissue and media at low levels (Figure 18), indicating that *Arabidopsis* reduced both nitro groups. The *ortho* reduction product was present in 4-5 times the abundance of the *para* reduction product, consistent with other studies of DNAN transformation.<sup>19, 25, 26, 33</sup> Acid hydrolysis of extracts increased the 2-ANAN concentration, suggesting a conjugated product similar to that found in ryegrass (Figure S4).<sup>17</sup>

Despite – or as a result of – their immobile nature, plants have adapted diverse enzymes for detoxifying xenobiotic compounds.<sup>122</sup> Indeed, *Arabidopsis* has over 60 genes encoding cytochrome P450 enzymes and metabolizes a variety of chemicals.<sup>124</sup> For example, *Arabidopsis* quickly assimilates and metabolizes benzotriazole and 2-mercaptobenzothiazole in hydroponic media, while carrots and horseradish conjugate the antibacterial agent triclosan.<sup>123, 129, 130, 132</sup> *Arabidopsis* also takes up and transforms the structurally similar TNT.<sup>5, 16</sup> While the detected phase I and phase II metabolites were not unexpected based on the green liver model and plant metabolism of TNT, the low mass balance of DNAN and phase I metabolites from LC-QQQ analysis indicated that further investigation was required to identify unknown DNAN metabolites.

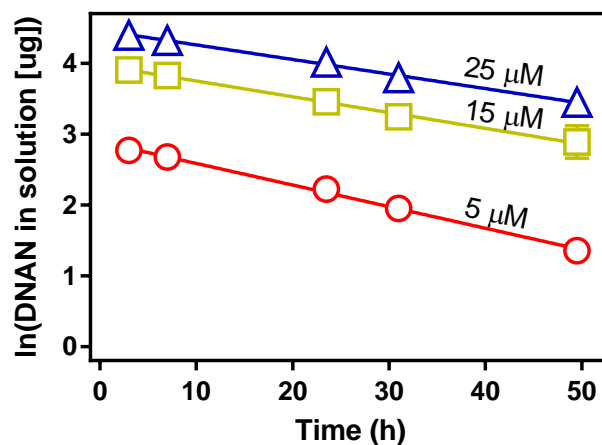


Figure 16. DNAN uptake kinetics at varying initial concentrations (n=3). Error bars of one standard deviation from the mean of triplicate flasks are not shown because they are smaller than the symbols. Experiments were conducted with 20 seedlings in 25 mL of MS media shaking at 120 rpm in 50 mL Erlenmeyer flasks after 14 days of pre-growth. DNAN was added in MeOH and an equivalent amount of MeOH was added to all conditions. Samples (0.5 mL) were withdrawn, analyzed by HPLC, and were not corrected for evaporation. Lines are simple linear regression ( $R^2 = 0.997$  for all three), indicating pseudo-first-order uptake kinetics. The slopes of the linear regression ( $k_{obs}$ ) were significantly different between the three initial concentrations ( $p < 0.0001$ );  $k_{obs,5\mu M} = 0.031 \pm 0.001 \text{ h}^{-1}$ ,  $k_{obs,15\mu M} = 0.022 \pm 0.001 \text{ h}^{-1}$ ,  $k_{obs,25\mu M} = 0.021 \pm 0.001 \text{ h}^{-1}$ . The difference in observed rates is most likely due to DNAN toxicity. Plants showed minor chlorosis at  $15\mu M$  initial DNAN and some chlorosis and plant death at  $25\mu M$  initial DNAN, so  $5\mu M$  was selected for further experiments.

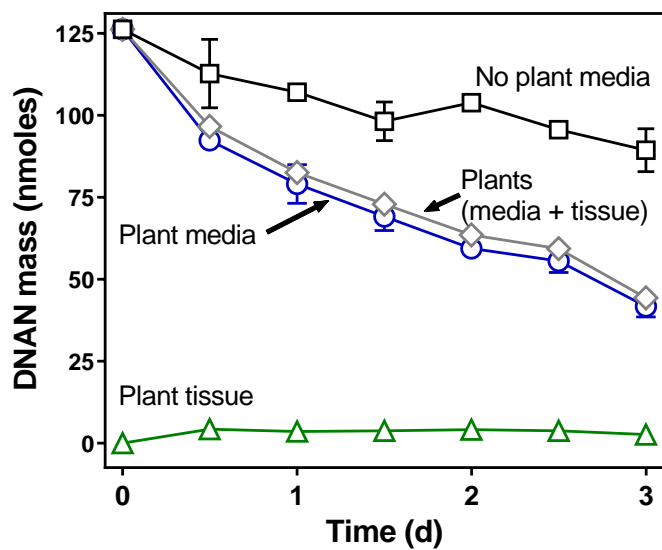


Figure 17. DNAN mass in hydroponic media and *Arabidopsis* whole plant tissue as a function of time. Error bars are  $\pm$  standard error of the mean ( $n = 3$  plant tissue and media,  $n = 2$  media, no plant control) and are not displayed when within the markers.

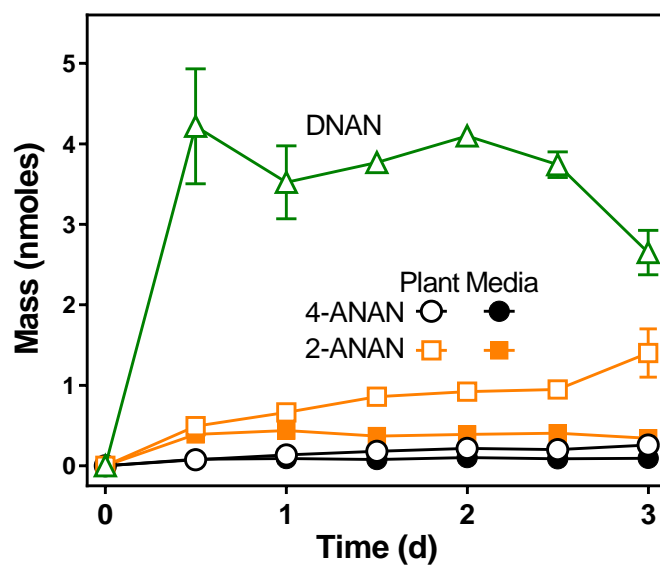


Figure 18. Mass of DNAN and phase I metabolites in plant tissues and media. DNAN data are the same as Figure 1 from manuscript, zoomed in on the y-axis for detail. Error bars are  $\pm$  standard error of the mean ( $n=3$ ) and are not displayed when smaller than the symbol.



Table 11. Summary of phase II DNAN metabolites identified in *Arabidopsis* plant tissue after 48 hours of exposure.

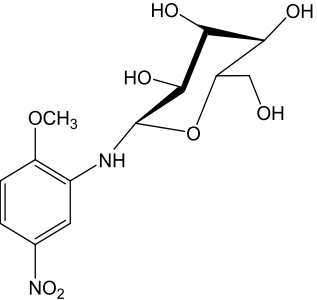
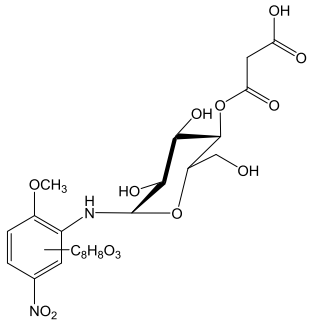
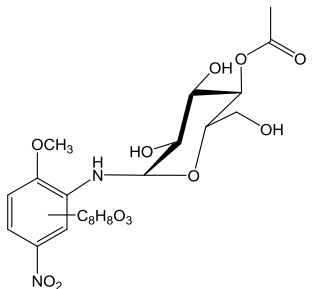
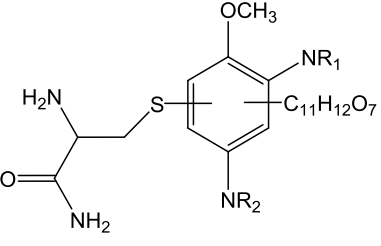
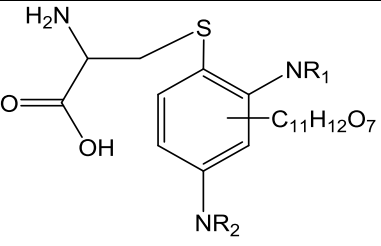
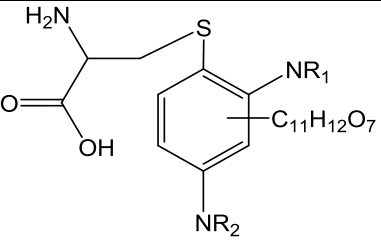
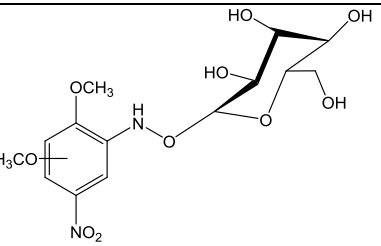
metabolite	proposed structure <sup>a</sup>	confidence level <sup>b</sup>	RT (min)	proposed ion	proposed ion formula	accurate mass	deviation mDa (ppm)	fragments (nominal m/z)
M330		2	3.4	[M+H] <sup>+</sup>	C <sub>13</sub> H <sub>19</sub> N <sub>2</sub> O <sub>8</sub>	331.1129	1.3 (3.8)	169
M568		3	4.4	[M+H] <sup>+</sup>	C <sub>24</sub> H <sub>29</sub> N <sub>2</sub> O <sub>14</sub>	569.1604	1.5 (2.6)	321
								304
								289
								274
M524		3	3.9	[M-H] <sup>-</sup>	C <sub>23</sub> H <sub>27</sub> N <sub>2</sub> O <sub>12</sub>	523.1573	0.9 (1.7)	319
								303
								289
								152

Table 11. (continued)

M699		3	3.0	[M+H] <sup>+</sup>	C <sub>28</sub> H <sub>38</sub> N <sub>5</sub> O <sub>14</sub> S	700.2117	-0.6 (0.9)	393
								308
								274
								130
				[M-H] <sup>-</sup>	C <sub>28</sub> H <sub>36</sub> N <sub>5</sub> O <sub>14</sub> S	698.1992	-1.3 (1.8)	306
								272
				143				
				128				
M669		3	3.1	[M+H] <sup>+</sup>	C <sub>27</sub> H <sub>36</sub> N <sub>5</sub> O <sub>13</sub> S	670.2013	1.7 (2.6)	363
								308
								145
								130
				[M-H] <sup>-</sup>	C <sub>27</sub> H <sub>34</sub> N <sub>5</sub> O <sub>13</sub> S	668.1886	1.2 (1.8)	306
								272
				143				
				128				

Table 11. (continued)

M513		4	3.4	[M+H] <sup>+</sup>	C <sub>21</sub> H <sub>28</sub> N <sub>3</sub> O <sub>10</sub> S	514.1484	1.1 (2.2)	N/A
				[M-H] <sup>-</sup>	C <sub>21</sub> H <sub>26</sub> N <sub>3</sub> O <sub>10</sub> S	512.1347	0.8 (1.6)	
M483a		4	3.4	[M+H] <sup>+</sup>	C <sub>20</sub> H <sub>26</sub> N <sub>3</sub> O <sub>9</sub> S	484.1379	1.1 (2.2)	N/A
				[M-H] <sup>-</sup>	C <sub>20</sub> H <sub>24</sub> N <sub>3</sub> O <sub>9</sub> S	482.1244	1.1 (2.2)	
M483b		4	3.5	[M+H] <sup>+</sup>	C <sub>20</sub> H <sub>26</sub> N <sub>3</sub> O <sub>9</sub> S	484.1354	3.6 (7.4)	N/A
				[M-H] <sup>-</sup>	C <sub>20</sub> H <sub>24</sub> N <sub>3</sub> O <sub>9</sub> S	482.1243	1.0 (2.0)	
M376		4	2.4	[M-H] <sup>-</sup>	C <sub>14</sub> H <sub>19</sub> N <sub>2</sub> O <sub>10</sub>	375.1041	-0.1 (0.4)	N/A
M808	N/A	5	2.4	N/A	N/A	807.1708	N/A	N/A

<sup>a</sup> R<sub>1</sub> and R<sub>2</sub> are H<sub>2</sub> in these structural approximations, and β-D-glucopyranoside is presented as the conjugated hexose sugar moiety. These structures represent the potential variety of nitro-reduction states, hexose sugars, and conjugation locations (i.e., positional isomers) that cannot be determined by mass spectrometry alone. <sup>b</sup>confidence was assigned using the Schymanski, et al. framework, briefly, 2: probable structure, 3: tentative candidate, 4: unequivocal molecular formula, 5: exact mass only.<sup>111</sup>

Table 12. Summary of [<sup>15</sup>N<sub>2</sub>]DNAN metabolites identified in *Arabidopsis* plant tissue after 48 hours of exposure.

metabolite	confidence level	RT (min)	proposed ion	proposed ion formula	accurate mass	deviation mDa (ppm)	fragments (nominal m/z)
M330	2	3.4	[M+H] <sup>+</sup>	C <sub>13</sub> H <sub>19</sub> <sup>15</sup> N <sub>2</sub> O <sub>8</sub>	333.1070	0.67 (2.0)	171
M568	3	4.4	[M+H] <sup>+</sup>	C <sub>24</sub> H <sub>29</sub> <sup>15</sup> N <sub>2</sub> O <sub>14</sub>	571.1545	0.90 (1.6)	323
							306
							291
							275
M524	3	3.9	[M-H] <sup>-</sup>	C <sub>23</sub> H <sub>27</sub> <sup>15</sup> N <sub>2</sub> O <sub>12</sub>	525.1513	1.4 (2.6)	321
							305
							291
							154
M699	3	3.0	[M+H] <sup>+</sup>	C <sub>28</sub> H <sub>38</sub> <sup>15</sup> N <sub>2</sub> <sup>14</sup> N <sub>3</sub> O <sub>14</sub> S	702.2057	1.4 (2.0)	395, plus same as Table 1
			[M-H] <sup>-</sup>	C <sub>28</sub> H <sub>36</sub> <sup>15</sup> N <sub>2</sub> <sup>14</sup> N <sub>3</sub> O <sub>14</sub> S	700.1936	2.1 (3.0)	
M669	3	3.1	[M+H] <sup>+</sup>	C <sub>27</sub> H <sub>36</sub> <sup>15</sup> N <sub>2</sub> <sup>14</sup> N <sub>3</sub> O <sub>13</sub> S	672.1951	1.5 (2.2)	365, plus same as Table 1
			[M-H] <sup>-</sup>	C <sub>27</sub> H <sub>34</sub> <sup>15</sup> N <sub>2</sub> <sup>14</sup> N <sub>3</sub> O <sub>13</sub> S	670.1825	1.6 (2.4)	
M513	4	3.4	[M+H] <sup>+</sup>	C <sub>21</sub> H <sub>28</sub> <sup>15</sup> N <sub>2</sub> <sup>14</sup> N <sub>1</sub> O <sub>10</sub> S	516.1423	0.76 (1.5)	N/A
			[M-H] <sup>-</sup>	C <sub>21</sub> H <sub>26</sub> <sup>15</sup> N <sub>2</sub> <sup>14</sup> N <sub>1</sub> O <sub>10</sub> S	514.1286	1.2 (2.3)	
M483a	4	3.4	[M+H] <sup>+</sup>	C <sub>20</sub> H <sub>26</sub> <sup>15</sup> N <sub>2</sub> <sup>14</sup> N <sub>1</sub> O <sub>9</sub> S	486.1321	0.40 (0.82)	N/A
			[M-H] <sup>-</sup>	C <sub>20</sub> H <sub>24</sub> <sup>15</sup> N <sub>2</sub> <sup>14</sup> N <sub>1</sub> O <sub>9</sub> S	484.1183	1.5 (3.0)	
M483b	4	3.5	[M+H] <sup>+</sup>	C <sub>20</sub> H <sub>26</sub> <sup>15</sup> N <sub>2</sub> <sup>14</sup> N <sub>1</sub> O <sub>9</sub> S	486.1323	0.20 (0.40)	N/A
			[M-H] <sup>-</sup>	C <sub>20</sub> H <sub>24</sub> <sup>15</sup> N <sub>2</sub> <sup>14</sup> N <sub>1</sub> O <sub>9</sub> S	484.1185	1.7 (3.4)	
M375	4	2.4	[M-H] <sup>-</sup>	C <sub>14</sub> H <sub>19</sub> <sup>15</sup> N <sub>2</sub> O <sub>10</sub>	377.0973	0.19 (0.51)	N/A
M808	5	2.4	N/A	N/A	809.1894	N/A	N/A

Table 13. Summary of [<sup>13</sup>C<sub>6</sub>]DNAN metabolites identified in *Arabidopsis* plant tissue after 48 hours of exposure.

metabolite	confidence level	RT (min)	proposed ion	proposed ion formula	accurate mass	deviation mDa (ppm)	fragments (nominal m/z)
M330	2	3.4	[M+H] <sup>+</sup>	<sup>13</sup> C <sub>6</sub> C <sub>7</sub> H <sub>19</sub> N <sub>2</sub> O <sub>8</sub>	337.1332	1.1 (3.3)	175
M568	3	4.4	[M+H] <sup>+</sup>	<sup>13</sup> C <sub>6</sub> C <sub>18</sub> H <sub>29</sub> N <sub>2</sub> O <sub>14</sub>	575.1804	1.1 (1.8)	327
							310
							295
							280
M524	3	3.9	[M-H] <sup>-</sup>	<sup>13</sup> C <sub>6</sub> C <sub>17</sub> H <sub>27</sub> N <sub>2</sub> O <sub>12</sub>	529.1774	1.4 (2.7)	325
							309
							295
							158
M699	3	3.0	[M+H] <sup>+</sup>	<sup>13</sup> C <sub>6</sub> C <sub>22</sub> H <sub>38</sub> N <sub>5</sub> O <sub>14</sub> S	706.2317	1.5 (2.1)	399, plus same as Table 1
			[M-H] <sup>-</sup>	<sup>13</sup> C <sub>6</sub> C <sub>22</sub> H <sub>36</sub> N <sub>5</sub> O <sub>14</sub> S	704.219	1.5 (2.1)	
M669	3	3.1	[M+H] <sup>+</sup>	<sup>13</sup> C <sub>6</sub> C <sub>21</sub> H <sub>36</sub> N <sub>5</sub> O <sub>13</sub> S	676.2214	1.2 (1.8)	369, plus same as Table 1
			[M-H] <sup>-</sup>	<sup>13</sup> C <sub>6</sub> C <sub>21</sub> H <sub>34</sub> N <sub>5</sub> O <sub>13</sub> S	674.2080	1.0 (1.5)	
M513	4	3.4	[M+H] <sup>+</sup>	<sup>13</sup> C <sub>6</sub> C <sub>15</sub> H <sub>28</sub> N <sub>3</sub> O <sub>10</sub> S	520.1684	0.72 (1.4)	N/A
			[M-H] <sup>-</sup>	<sup>13</sup> C <sub>6</sub> C <sub>15</sub> H <sub>26</sub> N <sub>3</sub> O <sub>10</sub> S	518.1539	0.43 (0.83)	
M483a	4	3.4	[M+H] <sup>+</sup>	<sup>13</sup> C <sub>6</sub> C <sub>14</sub> H <sub>26</sub> N <sub>3</sub> O <sub>9</sub> S	490.1578	0.76 (1.5)	N/A
			[M-H] <sup>-</sup>	<sup>13</sup> C <sub>6</sub> C <sub>14</sub> H <sub>24</sub> N <sub>3</sub> O <sub>9</sub> S	488.1446	1.7 (3.5)	
M483b	4	3.5	[M+H] <sup>+</sup>	<sup>13</sup> C <sub>6</sub> C <sub>14</sub> H <sub>26</sub> N <sub>3</sub> O <sub>9</sub> S	490.1583	0.23 (0.52)	N/A
			[M-H] <sup>-</sup>	<sup>13</sup> C <sub>6</sub> C <sub>14</sub> H <sub>24</sub> N <sub>3</sub> O <sub>9</sub> S	488.1446	1.7 (3.5)	
M375	N/A	N/A	N/A	N/A	nd	N/A	N/A
M808	5	2.4	N/A	N/A	813.2102	N/A	N/A

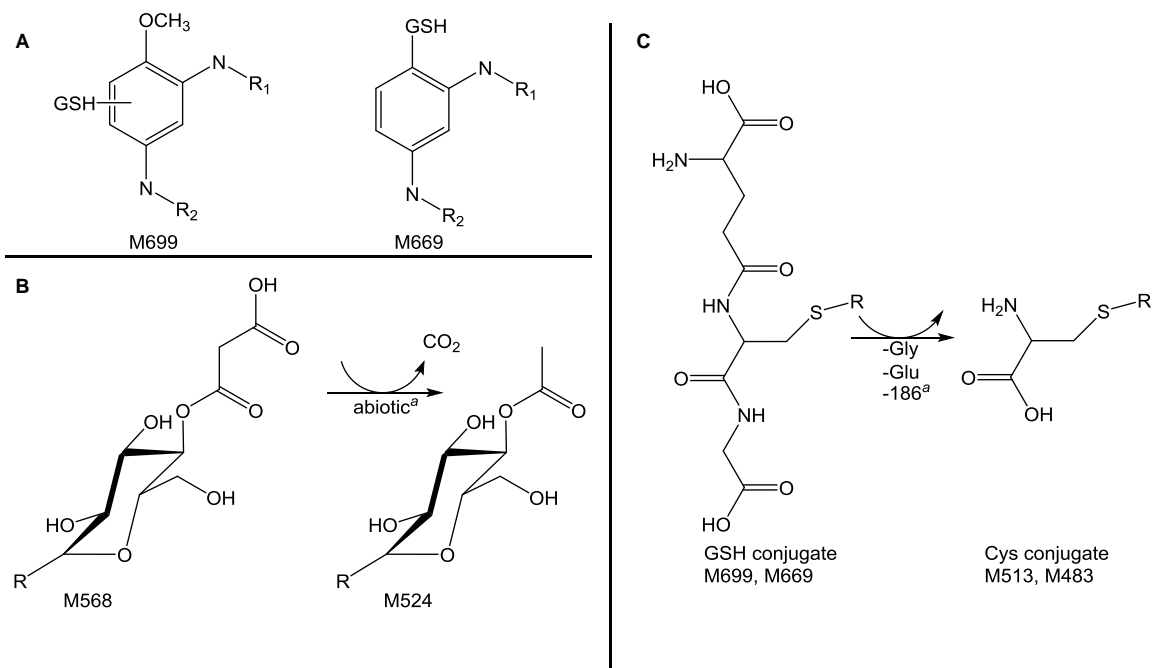


Figure 19. Proposed relationships between some identified DNAN metabolites in *Arabidopsis*. A) Proposed glutathione conjugation B) abiotic decarboxylation of M568 to yield M524 C) glutathione degradation to cysteinyl metabolites. Abbreviations: GSH (glutathione), Cys (cysteine), R (unknown moiety). <sup>a</sup>ref. 134.

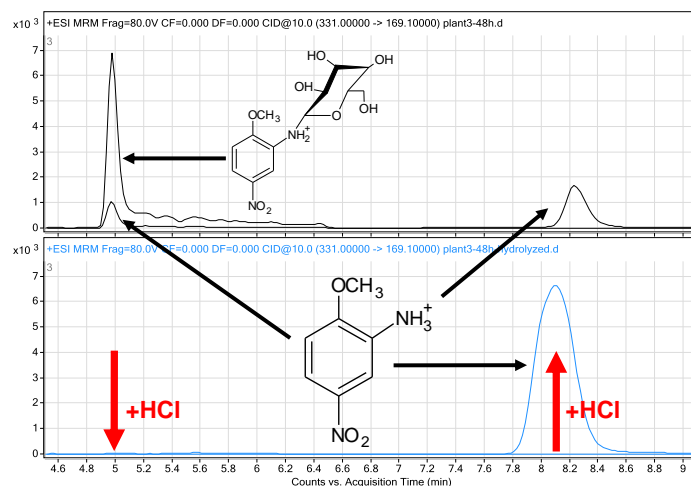


Figure 20. Hydrolysis of metabolite M330 to yield 2-ANAN. Shown are LC-MS/MS chromatograms of M330 in plant extract before (black lines, top panel) and after (blue lines, bottom panel) acid hydrolysis. M330 had a retention time of 5.0 minutes, while 2-ANAN had a retention time of about 8.1 minutes. The chromatograms shown are 331>169.1 for M330 and 169.1>108.0 for 2-ANAN. Some 2-ANAN is observed at 5 minutes due to in-source fragmentation of M330.

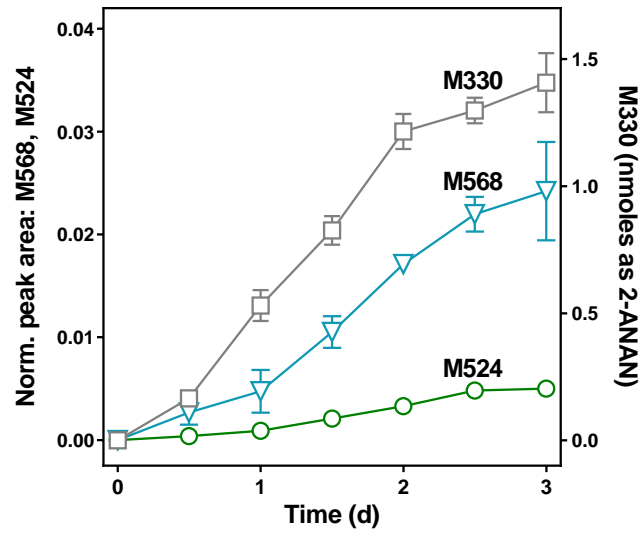


Figure 21. Metabolite formation over time in whole plant tissues. M568 and M524 are expressed as LC-QQQ peak area of metabolite normalized to internal standard [<sup>13</sup>C<sub>6</sub>]DNAN and dry weight of plant material (mg). M330 is quantified as peak area quantified with a 2-ANAN calibration curve. Error bars are ± standard error of the mean (n = 3) and are not displayed when within the markers.



*Arabidopsis* conjugates DNAN with sugars and glutathione

To detect DNAN transformation products, we utilized an untargeted metabolomics approach, which identified sugar conjugates M330, M568, M524, and M376 and glutathione conjugates M699 and M669 (Table 11, Figure 19). All discovered metabolites were confirmed using stable isotope-labeled DNAN, and the metabolites in Table 1 each contained all respective stable isotopes (see Tables S4 and S5 for labeled metabolites). DNAN metabolites contained all the original isotope labels, indicating that *Arabidopsis* did not mineralize the aromatic ring of DNAN, nor did the plants remove the original nitrogen atoms from DNAN. These sugar and glutathione conjugates are therefore consistent with the green liver model of plant metabolism.

DNAN metabolites M669 and M699 both contained multiple characteristic glutathione mass fragments in both ESI<sup>+</sup> and ESI<sup>-</sup> mode (Table 11). The observed mass fragments indicate that the glutathionyl group was conjugated to an aromatic or benzylic group.<sup>133</sup> In addition, the molecular masses of metabolites M669 and M699 differ by an average  $m/z$  of 30.0105 corresponding to a neutral loss of CH<sub>2</sub>O ( $m/z$  30.0106). We hypothesize that M699 results from direct conjugation to the aromatic ring at a previously unsubstituted position, and that M669 results from a sulfhydryl substitution for the DNAN methoxy group (Figure 19A). Glutathione conjugation is a well-known detoxification process for electrophilic xenobiotics, including nitro-aromatics and resulting hydroxylamine reduction products.<sup>16</sup> Furthermore, glutathione conjugates of DNAN are consistent with a specific pathway that *Arabidopsis* utilizes to detoxify TNT via glutathione transferases (GSTs). Importantly, an isolated GST catalyzed denitration of TNT, which would increase bioavailability and significantly decrease the toxicity of the TNT metabolite.<sup>16</sup> However, our observed products retained both original nitrogen atoms as confirmed with <sup>15</sup>N-labeled DNAN.

The identification of M483 and M513 (Table 11) suggests that the glutathione metabolites were further degraded to S-cysteinyl conjugates. This process has been described for glutathione conjugates of the herbicide safener, fenclorim, among other compounds, and has been attributed to intra-vacuolar peptidases, which successively cleave the glyciny and glutamyl moieties from the attached glutathione (Figure 19B).<sup>124,</sup>

<sup>134</sup> Although the mass fragments enabled us to classify these metabolites as glutathione

and cysteine conjugates, the transformation pathways and ultimate molecular structures could not be definitively determined.

In addition to glutathione conjugation, detoxification of metabolites with sugar moieties is a common pathway in plants that occurs on aromatic hydroxyl or amino groups.<sup>123, 135-137</sup> Conjugation proceeds without prior phase I functionalization (e.g., refs 123, 129, 132) or after a phase I reaction.<sup>5</sup> Conjugation with sugars decreases toxicity of the compound and these phase II metabolites are likely intermediates to permanently bound residues.<sup>83, 137</sup> Glucosyltransferases in *Arabidopsis* also conjugate TNT reduction products, forming *C*-, *O*-, and *N*-glycosidic conjugates, and  $\beta$ -D-glucopyranosides are common hexose sugar stereoisomers utilized by plants to detoxify organic contaminants.<sup>5, 123</sup>

Here, the neutral losses observed for both M524 and M568 indicate a glycosylated and further conjugated sugar. M568 has a neutral loss of 248, indicative of a malonylated hexose sugar ( $m/z$  162+86).<sup>123</sup> Malonylation is known to signal vacuolar sequestration in *Arabidopsis*, and is commonly observed in plant metabolism of glycosyl-conjugates.<sup>123, 134</sup> M524 has a neutral loss of 204, corresponding to a loss of acetyl-hexose (162+42) and contains the same aglycone moiety as M568. The mass difference between M568 and M524 ( $\Delta m/z$  43.9875) is equivalent to CO<sub>2</sub> ( $m/z$  43.9898). Abiotic decarboxylation of a malonyl-glycoside to yield the acetyl-glycoside has been observed for other *Arabidopsis* metabolites, which we believe to occur with M568, yielding M524 (Figure 19C).<sup>134</sup> To further investigate the identity of M330, we hydrolyzed plant extracts and analyzed the resulting solution by LC-QQQ. Under acidic conditions, a decrease of M330 was concomitant with an increase in 2-ANAN, further validating the structure of M330 as a hexose-conjugate of 2-ANAN (Figure 20). We quantified M330 redundantly using LC-QQQ peak area of M330 calibrated to 2-ANAN peak area and by measuring 2-ANAN resulting from acid hydrolysis of the plant extracts. The first method assumed that M330 and 2-ANAN had the same ionization efficiencies, and therefore detector response, per mole of mass. This assumption is supported by a study where acylated amines had an average mass spectrometer detector response factor of 1.5 times when compared to the unconjugated amine, providing an approximation of transformation product mass.<sup>116</sup> The second method quantified M330 as 2-ANAN assuming complete acid hydrolysis, no

other loss of 2-ANAN, and no ion suppression in the mass spectrometer. The two methods similarly found that M330 made up 1.7% or 1.8% of the DNAN mass taken up after 3 days, respectively.

#### *Glycosylated metabolites accumulate over three days*

We measured each metabolite in whole plants and hydroponic media over three days of DNAN exposure. While ten phase II conjugates of DNAN were detected by LC-QToF and LC-Orbitrap, we were unable to detect some metabolites by LC-QQQ. In contrast, some glycosylated metabolites (M524, M568, and M330) accumulated over the 72-hour exposure (Figure 21). Similarly, a glycosylated metabolite accumulated over time when *Arabidopsis* metabolized benzotriazole and the metabolite was released into the media.<sup>129</sup> Here, little M330 accumulated in the media, but plant tissues contained M330 at levels comparable to DNAN and 2-ANAN. The mass balance after three days was low (i.e., 8% of DNAN taken up), suggesting that DNAN conjugates were sequestered into cell walls or vacuoles through phase III metabolism, similar to TNT in other plants.<sup>138</sup> For example, hybrid poplar trees sequestered about half of [<sup>14</sup>C]TNT to non-extractable residues, and 27% of <sup>14</sup>C from [<sup>14</sup>C]TNT was covalently bound to lignin in wheat.<sup>11, 139</sup> *Arabidopsis* also quickly and extensively metabolizes naproxen and diclofenac to non-extractable residues.<sup>140, 141</sup> In addition to phase III metabolism, the low mass balance could be the result of unidentified and non-extractable bound residues, incorrect assumptions in the M330 mass approximation, low ionization efficiency of identified metabolites, or in-source fragmentation of identified or other non-identified conjugated metabolites.

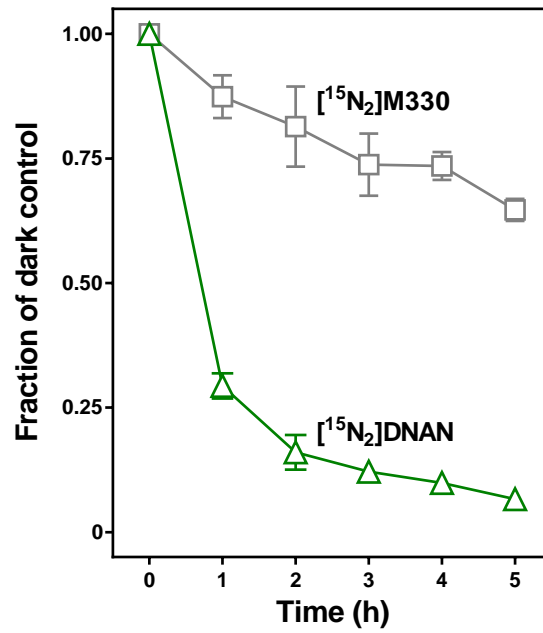


Figure 22. DNAN and M330 in *Arabidopsis* leaves during exposure to simulated sunlight (20 °C, 750 W/m<sup>2</sup>). Data are LC-QQQ peak area of compounds in light-exposed leaf extracts normalized to foil-wrapped, dark control extracts and dry weight. Error bars are  $\pm$  standard error of the mean (n = 3) and are not displayed when within the markers.

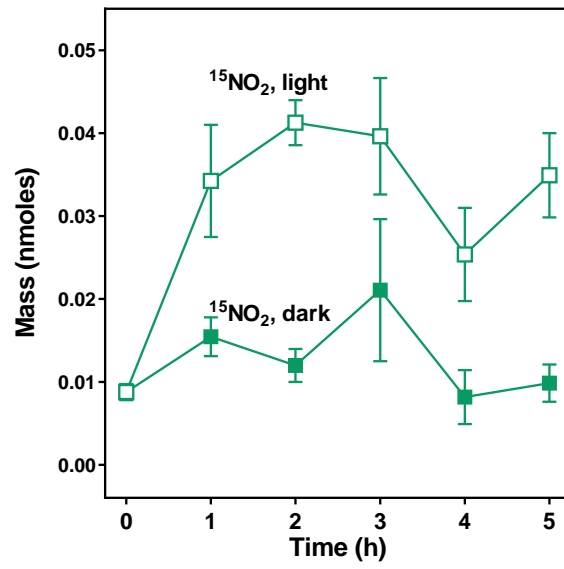


Figure 23.  $^{15}\text{NO}_2^-$  measured in leaf extracts exposed to simulated sunlight or in the dark. Error bars are  $\pm$  standard error of the mean (n = 3).

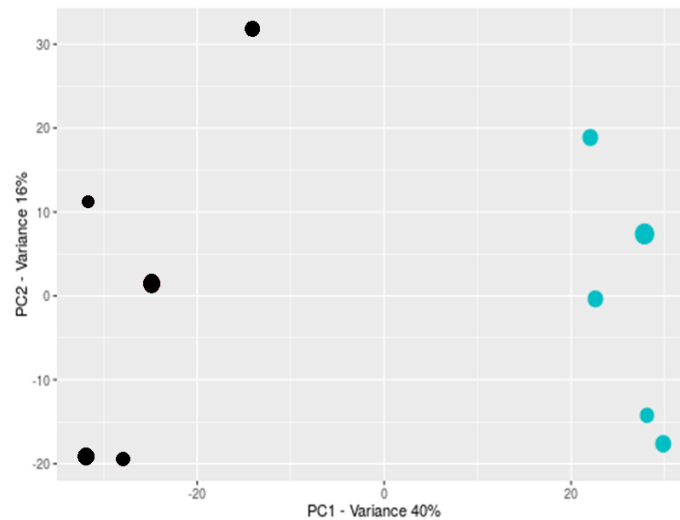


Figure 24. Principal components plot of photolyzed leaves (teal circles) compared to dark-control leaves (black circles) after 3 hours of simulated sunlight exposure, extraction, and analysis by LC-MS/QToF and XCMS online. The two treatments yielded two distinct groupings, but no photo-products of DNAN could be identified besides nitrite.

*[<sup>15</sup>N<sub>2</sub>]DNAN and glycosylated [<sup>15</sup>N<sub>2</sub>]DNAN metabolite are photolyzed in leaves to yield <sup>15</sup>NO<sub>2</sub><sup>-</sup>*

To determine the potential for DNAN and DNAN metabolites to be photolyzed inside plants, we subjected *Arabidopsis* leaves to simulated sunlight after two days of exposure to [<sup>15</sup>N<sub>2</sub>]DNAN in a growth chamber. The [<sup>15</sup>N<sub>2</sub>]DNAN and [<sup>15</sup>N<sub>2</sub>]M330 metabolite were significantly photolyzed compared to foil wrapped controls ( $p < 0.001$  and  $p = 0.005$ , respectively, matched pairs Student's t-test for  $n = 5$  triplicate pairs (Figure 22)). The DNAN in the leaf fraction at the beginning of the simulated sunlight experiment was 0.7% of the total amount taken up by the plants after two days, which is 8.1% of the DNAN detected in the whole plants in the mass balance experiment. Other metabolites were not detected in the leaf fractions. Besides RDX photolysis in grass blades and poplar tissues, *in planta* photolysis has not been investigated for other compounds to our knowledge.<sup>24,25</sup> In fact, a recent review of plant uptake of pharmaceuticals and personal care products stated “we are not aware of any studies confirming photodegradation of contaminants within plants.”<sup>127</sup> One recent study speculated that photolysis inside leaves could alter sulfamethoxazole concentrations in lettuce and strawberry shoots, but the effect was not investigated.<sup>142</sup> Therefore, we believe this is the first demonstration of photolysis of a plant xenobiotic metabolite *in planta*. DNAN is directly photolyzed in solution to yield nitrite and nitrate.<sup>62</sup> Therefore, we measured <sup>15</sup>NO<sub>2</sub><sup>-</sup> evolution in photolyzed leaves exposed to [<sup>15</sup>N<sub>2</sub>]DNAN (Figure 23). The results clearly show that <sup>15</sup>NO<sub>2</sub><sup>-</sup> is present in higher concentrations in light-exposed leaves than in dark controls ( $p < 0.0001$ ,  $n = 5$  triplicate pairs), albeit at low concentrations. The production of <sup>15</sup>N-labeled nitrite indicates that [<sup>15</sup>N<sub>2</sub>]DNAN, or its metabolites, are denitrated by light inside the plant leaves. The concentration of <sup>15</sup>NO<sub>2</sub><sup>-</sup> corresponded well with the amount of [<sup>15</sup>N<sub>2</sub>]DNAN that was degraded, reaching a maximum of 77% of the initial [<sup>15</sup>N<sub>2</sub>]DNAN concentration in the leaf on a molar basis. Interestingly, this denitration process occurred abiotically, and we did not detect any plant metabolites with only one <sup>15</sup>N label (Table 11 and Table 12). Since nitro groups impart toxicity and stability through resonance, the observed denitration represents an important step towards detoxifying DNAN.<sup>16</sup> Some photolysis of DNAN and its metabolites in the growth chamber is unavoidable, which likely why some <sup>15</sup>NO<sub>2</sub><sup>-</sup> was detected in dark control leaves. However, there was not a

significant difference in unlabeled  $\text{NO}_2^-$  in the dark and light-exposed plants ( $p = 0.81$ ), further confirming that the  $^{15}\text{NO}_2^-$  resulted from labeled DNAN. The decrease in nitrite after two hours of photolysis is likely due to oxidation of nitrite to nitrate, observed during DNAN photolysis in aqueous solution, but we were not able to accurately quantify nitrate at these levels using a reduction step before derivitization.<sup>62</sup> In addition to photo-oxidation, nitrite and nitrate could be incorporated into other plant molecules, contributing to the observed decrease in nitrite. Light-exposed leaves grouped differently than dark-control leaves in a principal components analysis (Figure 24), but additional photolysis products could not be identified by the untargeted metabolomics approach described above. Further studies would be required to identify the metabolite photo-products. Despite the observed photolysis of DNAN and M330, sudden exposure of the plant leaves to higher levels of UV may overestimate the level of DNAN photolysis occurring in the field. Plants can adapt to higher levels of UV radiation by producing carotenoids to attenuate some UV excitation, and sudden oxidative stress response could alter the transformation of the compounds as well.<sup>143, 144</sup>

## Conclusions

Knowledge of DNAN plant uptake and transformation products will inform phytoremediation feasibility assessments for DNAN-contaminated sites. Our work, and the work of others, showed plants take up DNAN from contaminated soil and water, but further work with field-relevant species are required to confirm the benefits of DNAN phytoremediation.<sup>17, 36</sup> Beyond phytoremediation, plants can also be used as inexpensive sensors to monitor contaminant presence and concentration gradients without costly and invasive sampling techniques.<sup>145-148</sup> Our work suggests that measuring 2-ANAN or DNAN inside plant tissues would under-predict actual DNAN uptake and metabolism, making correlations to porewater DNAN concentration problematic without further investigation and result in conservative estimates of phytoremediation efficacy. Our discovery of photo-denitration of DNAN indicates that photolysis may be an overlooked mechanism for transforming and detoxifying contaminants taken up by plants under field conditions. Although a minor proportion of the DNAN was transformed *via* this pathway,



the mechanism could be more important for non-metabolized compounds or photoactive metabolites that would otherwise be shielded from sunlight in soil or porewater.

## CHAPTER 5: PHOTOLYSIS OF 3-NITRO-1,2,4-TRIAZOL-5-ONE AND NITROGUANIDINE: MECHANISMS AND PRODUCTS

### Introduction

Traditional munitions (e.g., trinitrotoluene (TNT) and hexahydro-1,3,5-trinitro-1,3,5-triazine (RDX)) are known to contaminate soil and water with well-known recalcitrance, toxicity, mutagenicity, and wide-spread contamination.<sup>4</sup> These conventional explosives are now being replaced with new, insensitive explosives to increase soldier safety during storage, transport, and use.<sup>19</sup> The new compounds such as 3-nitro-1,2,4-triazol-5-one (NTO) and nitroguanidine (NQ), have similar explosive performance to RDX and TNT, respectively, but are less likely to accidentally detonate. Despite tremendous safety benefits, NTO and NQ are much more water-soluble than their predecessors and have relatively uncharacterized and potentially problematic environmental behavior. For example, NTO undergoes little to no degradation in aerobic soil and only minimally sorbs to soil columns, and NTO is 166 and 277 times more water-soluble than TNT and RDX, respectively.<sup>18, 20, 61, 76</sup>

In preliminary studies, the acute toxicity, mutagenicity, and genotoxicity of NTO and NQ appear to be less than traditional explosive compounds, but NTO yielded reproductive effects in male rats at high concentrations.<sup>47, 51, 149</sup> Recent data also suggest that toxicity from NTO and NQ to *Ceriodaphnia dubia* increases 1000-fold upon photolysis, and only a small fraction of NTO was degraded during the photolysis period examined.<sup>38</sup> NQ photolysate is also toxic to zebrafish embryos.<sup>150</sup> Few photolysis products have been identified, making attribution of the increased aquatic toxicity problematic. Both compounds are known to produce nitrite and nitrate upon photolysis. There are conflicting reports about the organic products from NQ photolysis, including cyanamide, hydroxy-guanidine, or more recently, stoichiometric guanidine.<sup>23, 56, 80</sup> NTO apparently produces CO<sub>2</sub> or other volatile organics upon extended irradiation, with another study finding hydroxy-triazolone and potential nitric oxide formation.<sup>23, 74</sup>

Given the conflicting reports of photolysis products and mechanisms, along with the surprising reinitiation of guanidine to form NQ, our purpose was to investigate the conditions under which NQ and NTO are photolyzed. Here, we evaluate NTO and NQ

photolysis with regards to direct and indirect mechanisms and products to determine treatment methods and environmental fate of the two compounds.

## **Materials & Methods**

*Chemicals – NTO synthesis and characterization performed by Xueshu Li and Hans-Joachim Lehmler*

Chemicals and reagents were obtained commercially and used as received. NTO was synthesized *via* 1,2,4-triazolone (TO) as follows:<sup>151</sup> semicarbazide hydrochloride (16.7 g, 0.15 mol) was added to a stirred solution of formic acid (24 mL). After the semicarbazide hydrochloride had dissolved completely, the reaction mixture was heated under reflux for 2 hours. Excess formic acid was removed under reduced pressure and the crude product was recrystallized from ethanol to obtain 12 g (crude yield: 94%) TO as a white solid. TO (12 g, 140 mmol) was added in small aliquots to fuming nitric acid (60 mL) at 0 °C, and the reaction mixture was heated to 70 °C for 16 h. An exothermic reaction occurred with the evolution of brown fumes and formation of a precipitate. The reaction mixture was cooled in an ice bath, and the precipitate was filtered off and washed with ice cold water to remove excess nitric acid. The crude product was recrystallized from water to give 7.82 g (yield: 42%) NTO as a white solid. Full <sup>1</sup>H and <sup>13</sup>C NMR and high-resolution mass spectrometry characterization can be found in Appendix A.

### *Photolysis experiments*

For most experiments, we used an Atlas Suntest CPS+ solar simulator (Atlas Material Testing Technology, Mount Prospect, IL, USA) with a xenon lamp and an Atlas UV Suntest filter maintained at 35 °C to simulate the emission spectrum of natural sunlight at an irradiance of 750 W/m<sup>2</sup> (Figure 25). Solutions contained 5-25 mM buffer (acetic acid, pH 5; phosphate, pH 2, 6-8, 12; borate, pH 8.5-11). Solutions of Suwannee River Natural Organic Matter (SRNOM) were used in indirect photodegradation experiments as a model of aquatic chromophoric dissolved organic matter (DOM).<sup>152, 153</sup> SRNOM solutions were prepared according to Chu et al., and frozen aliquots were thawed and used the day of the experiment.<sup>154</sup> The final concentration of the SRNOM stock solution (54.4 mg C L<sup>-1</sup>) was measured using a total organic carbon (TOC) analyzer (TOC-V,

Shimadzu, Kyoto, Japan) calibrated to a TOC standard solution of potassium hydrogen phthalate (Ricca, Arlington, TX). For direct and indirect photolysis experiments, aqueous solutions contained 10  $\mu\text{M}$  NTO and were sparged with air for at least 30 seconds. Solutions were photolyzed in quartz tubes (O.D., 14 mm; I.D., 12 mm; V, 9 mL) stoppered with cork. Subsamples of 500  $\mu\text{L}$  were withdrawn for HPLC analysis and stored at 4  $^{\circ}\text{C}$  until analysis. Quantum yields were determined using an actinometer of *para*-nitroanisole and pyridine.<sup>155</sup>

#### *Light screening calculations*

Indirect photolysis rates and solutions with 5 mM 2,4-hexadienoic acid (sorbic acid) were corrected for light screening as follows.<sup>156</sup> UV-Vis spectra of SRNOM and sorbic acid solutions were collected on a spectrophotometer (Hach, Loveland, CO) in a quartz cuvette with a path length of 1 cm. We then calculated the wavelength-dependent screening factor ( $S_{\lambda}$ ) according to the following equation:

$$S_{\lambda} = \frac{1 - 10^{-A_{\lambda}}}{2.303A_{\lambda}}$$

where  $A_{\lambda}$  is the solution absorbance. We summed the light intensity from the solar simulator over 290 – 455 nm ( $L_{total}$ ) and corrected the observed rates for solution screening factor according to the following equation:

$$k_{obs,corr} = \frac{k_{obs}}{\sum_{\lambda=290}^{455} \frac{S_{\lambda}L_{\lambda}}{L_{total}}}$$

where  $k_{obs,corr}$  is the corrected pseudo-first order rate constant,  $k_{obs}$  is the observed pseudo-first order rate constant, and  $L_{\lambda}$  is the light intensity at the respective wavelength.

#### *Transformation product identification*

To identify transformation products, we photolyzed 100  $\mu\text{M}$  NTO solutions containing 10 mM volatile buffer (pH 5, acetic acid; pH 9, ammonium acetate) in cork-

stoppered quartz tubes in the solar simulator. Tubes were irradiated alongside buffers without NTO, and aliquots were withdrawn at time 0, 1, 2 and 8 hrs of photolysis. The sub-samples were stored at -20 °C until analysis by LC-QToF scanning from  $m/z$  40-600 with a 0.2 mL min<sup>-1</sup> flow rate on a graphite column (Hypercarb, ThermoFisher, 100 x 2.1 mm, 5 µm particle size). The mobile phase consisted of DI water (A) and acetonitrile with 100% A held for 2 min, 90% A at 4 min, 60% A at 8 min held until 9 min, and then returned to 100% A at 9.1 min. The column was equilibrated for 8.5 min before the next analysis injection. These conditions did not reveal any novel transformation products.

#### *Singlet oxygen and hydroxyl radical second-order rate constants*

To determine the second-order reaction rate constant of NTO with <sup>1</sup>O<sub>2</sub>,  $k^1_{O_2}$ , we simultaneously photolyzed 20 µM solutions of either NTO or furfuryl alcohol (FFA) containing 5 µM Rose Bengal in 5 mM borate buffer at pH 8.5. Rose Bengal was used as a sensitizer to produce singlet oxygen and FFA has a known reaction rate with singlet oxygen,  $k^1_{O_2} = 1.27 \times 10^8 \text{ M}^{-1} \text{ s}^{-1}$  at 35 °C.<sup>157</sup> We utilized a 200 W xenon lamp (Oriel Instruments, Irvine CA, USA) with a 400 nm cut off filter (Figure 25) to minimize direct photolysis, and no degradation occurred in controls without Rose Bengal.

To determine the second-order reaction rate constant of NTO with •OH,  $k_{OH}$ , we used a competition kinetics approach. We photolyzed a solution containing 10 mM NaNO<sub>3</sub> with 10 µM of both NTO and *para*-chlorobenzoic acid (pCBA) in 5 mM phosphate buffer at pH 7. The nitrate produces •OH, while pCBA reacts with a known  $k_{OH}$ . The concentration of NTO was corrected for direct photolysis according to Wenk et al., and  $k_{OH,NTO}$  was calculated using the slope of a linear regression of the equation

$$\ln\left(\frac{[NTO]_t}{[NTO]_0}\right) = \frac{k_{OH,NTO}}{k_{OH,pCBA}} \ln\left(\frac{[pCBA]_t}{[pCBA]_0}\right)$$

where  $k_{OH,pCBA}$  is  $5 \times 10^9 \text{ M}^{-1} \text{ s}^{-1}$ .<sup>158, 159</sup>

### *Probing mechanisms of direct photolysis*

To determine the mechanisms by which NTO was directly photolyzed, we conducted experiments with sodium azide (1 mM) to quench singlet oxygen or sorbic acid (5 mM) to quench triplet excited state NTO.<sup>160, 161</sup> We also sparged solutions with nitrogen gas, oxygen gas, or air for at least 30 seconds prior to irradiation. The nitrogen and oxygen sparged solutions were stoppered with rubber septa and sampled with a needle syringe throughout the experiment to maintain the respective headspace and solution oxygen composition. In addition, we photolyzed FFA (20  $\mu$ M) and pCBA (10  $\mu$ M) with and without NTO as a probe for singlet oxygen and hydroxyl radicals, respectively, to determine if NTO sensitized the formation of these reactive oxygen species (ROS) upon photolysis.<sup>157, 159, 160</sup> These experiments were conducted with 10  $\mu$ M NTO in 5 mM borate buffer at pH 8.5.

### *Analytical methods*

NTO, NQ, pCBA, and FFA were measured quantitatively by HPLC-DAD (Model 1260 Infinity, Agilent Technologies, Santa Clara, CA). Hydroxy-triazolone was measured by LC-MS/MS (Model 1260 Infinity and model 6460 triple quadrupole MS, Agilent Technologies, Santa Clara, CA). Analyses utilizing high-resolution mass spectrometry were carried out on a QToF Premier (Waters, Milford, MA) coupled to an ultra-high performance liquid chromatograph (Waters Acquity). Nitrite and nitrate were measured by an Ion Chromatograph (Dionex ICS-2100, Thermo Scientific). Ammonium was measured by derivitization with an *o*-phthaldialdehyde (OPA) reagent and fluorescence measurement with excitation at 350 nm and fluorescence at 410-450 nm using a fluorometer (Trilogy, Turner Designs, San Jose, CA). The OPA reagent consisted of 21 mM borate buffer, 63  $\mu$ M sodium sulfite, and 50 mL L<sup>-1</sup> of a 298 mM OPA stock solution in ethanol. For ammonium analysis, 0.8 mL of sample and 0.2 mL of OPA reagent were added to a cuvette, which was incubated at room temperature for 2 hours and the samples were read on the fluorometer. Figures and statistics were produced using GraphPad Prism 7.00. Confidence intervals were determined from the slope of a linear regression of log-normalized concentration data of first-order reactions.

## Results & Discussion

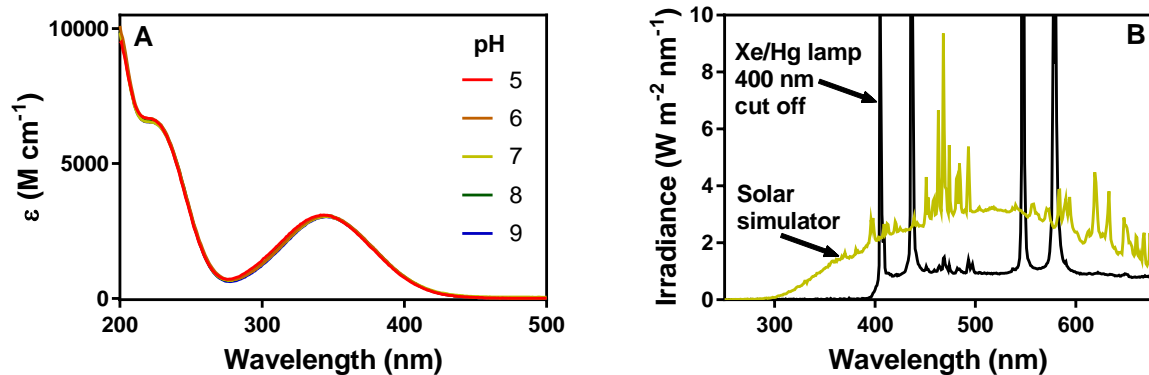


Figure 25. A) molar extinction coefficient of NTO from pH 5 to 9 and B) spectral irradiance of the solar simulator ( $750\text{ W/m}^2$ ) and the 200 W Xe/Hg lamp with a 400 nm cutoff filter.

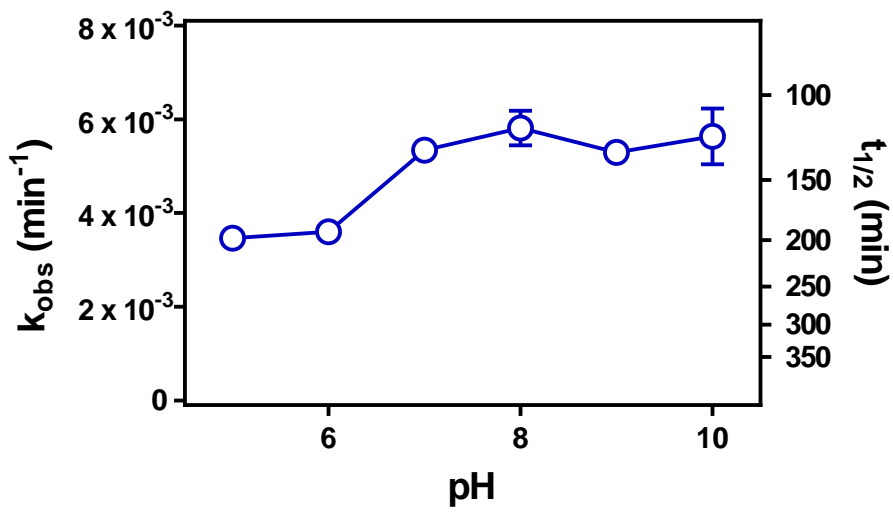


Figure 26. Observed pseudo-first-order rates and half-life of direct photolysis of NTO from pH 5-10 (25 mM buffer, 10  $\mu$ M NTO, sparged with air). Error bars are standard error of the mean of two replicates and are not shown when within the symbol.



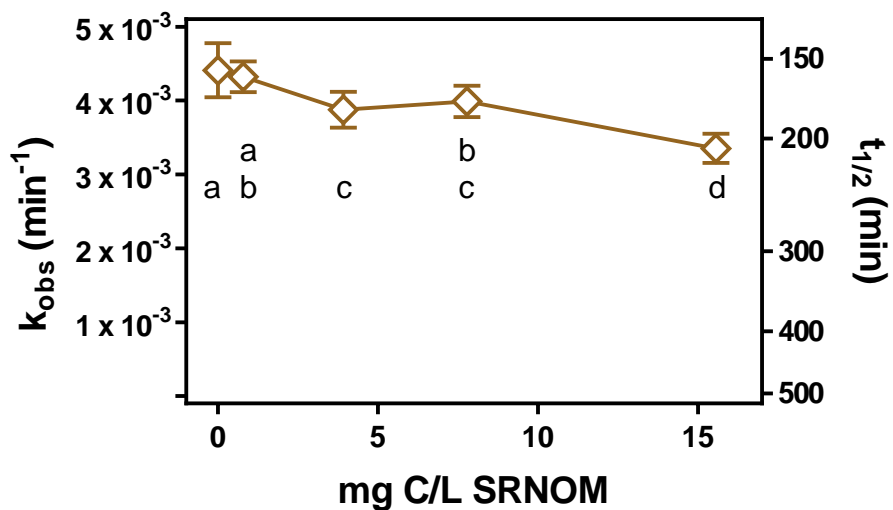


Figure 27. Rates of indirect photolysis of NTO with respect to SRNOM concentration (10  $\mu\text{M}$  NTO, 5 mM borate buffer, pH 8.5). Rates are corrected for light screening, and error bars are 95% confidence intervals. A one-way ANOVA determined a statistical significance among rates ( $p < 0.001$ ) and letters indicate significantly different groups by a post-hoc Tukey multiple comparisons test ( $\alpha = 0.05$ ).

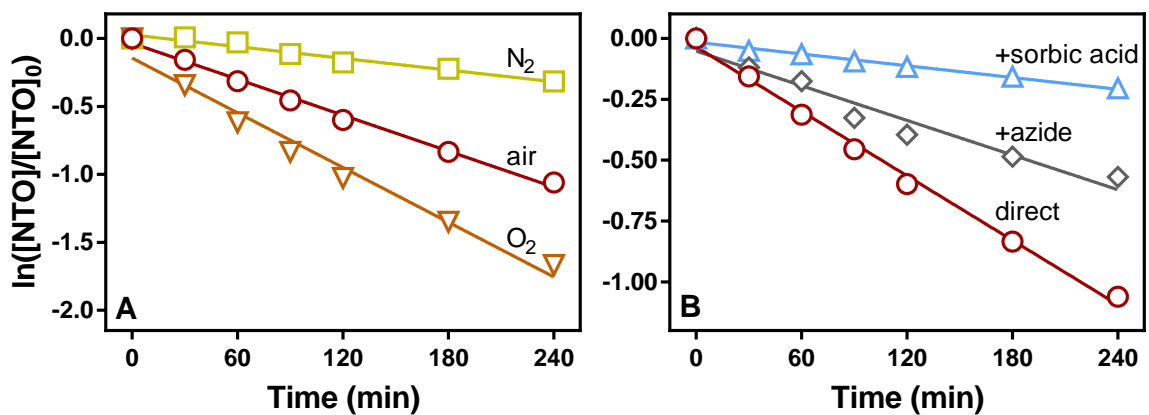


Figure 28. Probing mechanisms of NTO (10  $\mu$ M) direct photolysis. A) direct photolysis of NTO with varied dissolved oxygen regimes. B) direct photolysis of NTO with and without quenchers of singlet oxygen (1 mM sodium azide) or excited triplet states (5 mM sorbic acid). Lines are linear regression of natural log-transformed data.

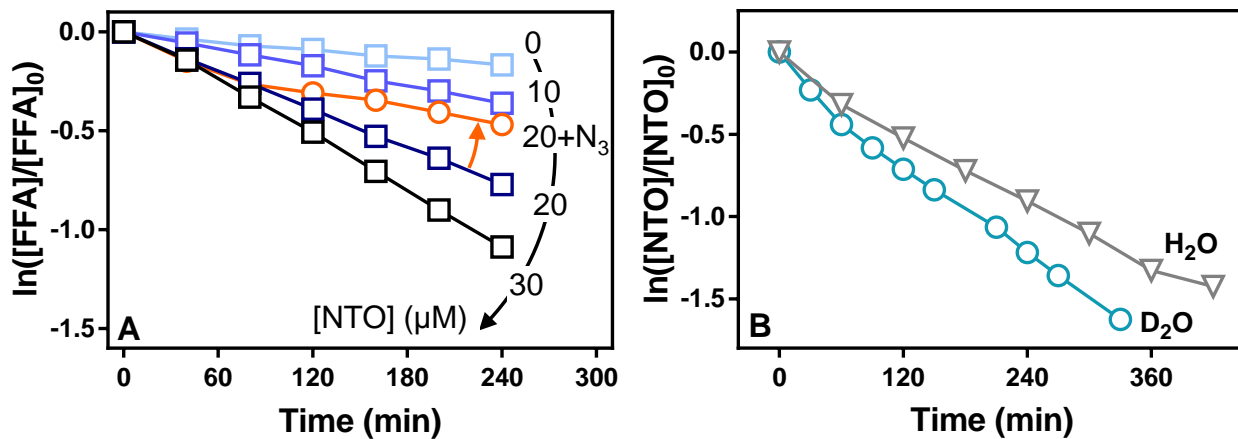


Figure 29. Production of  $^1\text{O}_2$  by NTO as demonstrated by A) photodegradation of 20  $\mu\text{M}$  FFA in the presence of varying concentrations of NTO and 1 mM sodium azide ( $\text{pH}$  8.5) and B) photolysis of NTO in  $\text{D}_2\text{O}$  and  $\text{H}_2\text{O}$  ( $\text{pH}$  7,  $\text{pD}$  7.4).

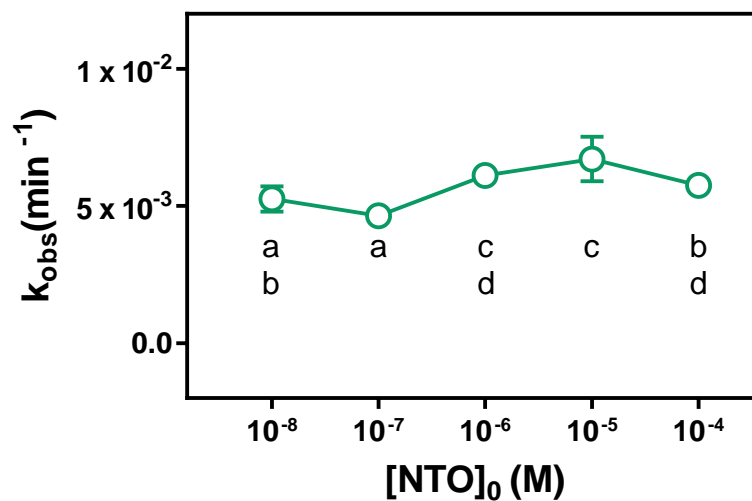


Figure 30. Observed, pseudo-first-order rate constants of NTO direct photolysis with initial concentrations spanning four orders of magnitude (pH 8, 25 mM phosphate buffer). Error bars are 95% confidence intervals and are not displayed when within the symbols. A one-way ANOVA determined a statistical significance among rates ( $p < 0.001$ ) and letters indicate significantly different groups by a post-hoc Tukey multiple comparisons test ( $\alpha = 0.05$ ).

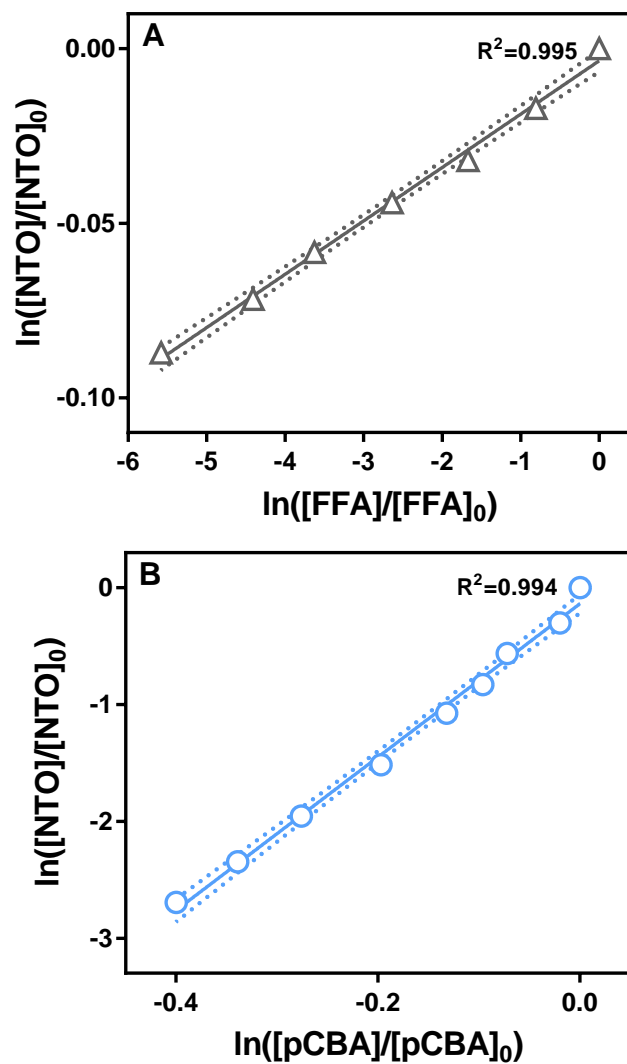


Figure 31. Determination of 2<sup>nd</sup>-order reaction rate constants of NTO with A) singlet oxygen using FFA as a probe and B) hydroxyl radical using pCBA and a competition kinetics approach. Solid lines are linear regression and dotted lines are 95% confidence intervals.

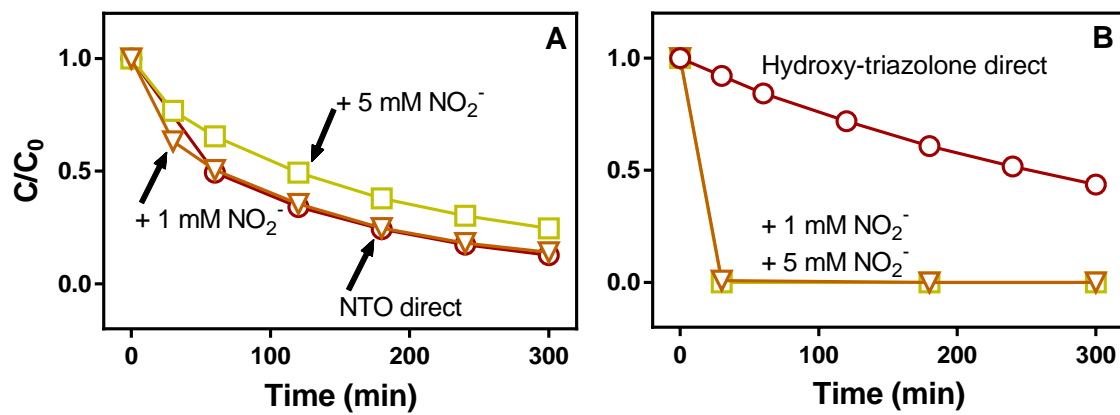


Figure 32. Effect of nitrite on A) NTO and B) hydroxyl-triazolone photolysis.

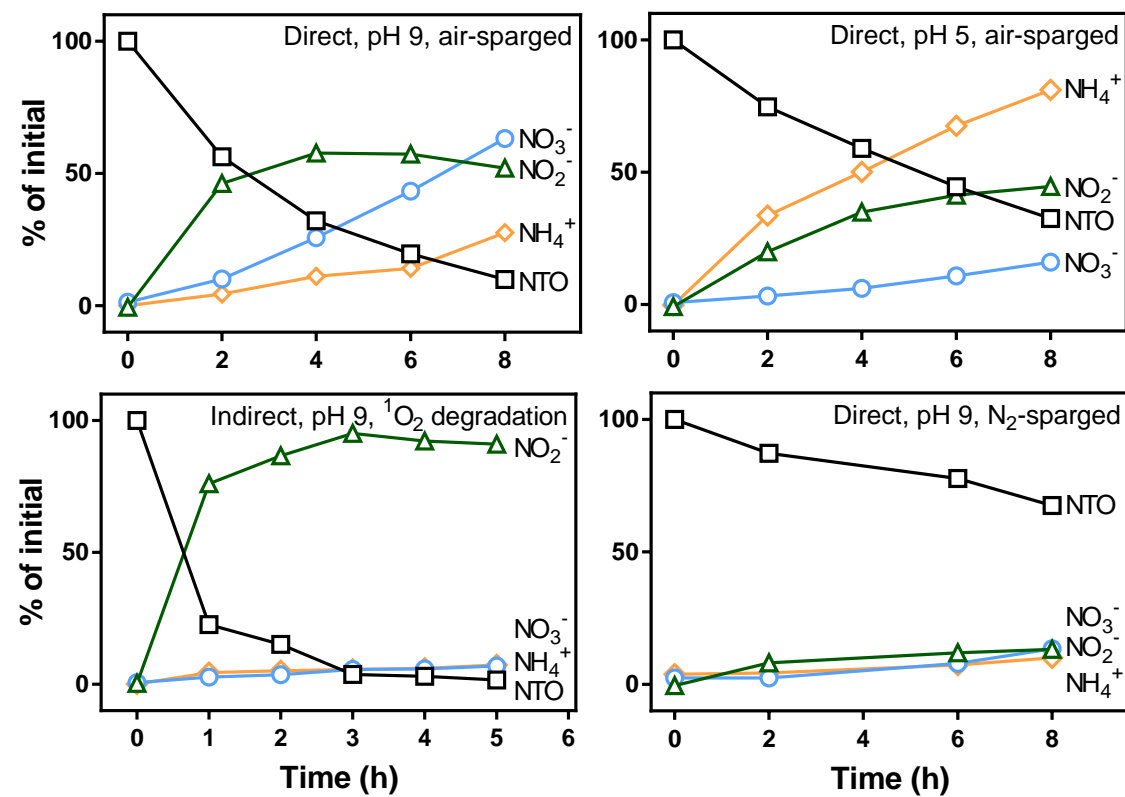


Figure 33. Photolysis and inorganic nitrogen products from photolysis of 100  $\mu$ M NTO under varying initial conditions.

To determine the effect of pH on rates of direct photolysis, we photolyzed NTO in solutions ranging from pH 5-10 (Figure 26). Interestingly, the rate of photolysis increased at neutral and higher pH (7-10) when compared to pH 5 and 6 (Figure 26). This trend was not expected based on the uniformity of the UV-Vis spectra of NTO across the pH range (Figure 25A). In addition, the pKa of NTO is 3.76, suggesting that some unexpected mechanism besides the absorbance of NTO is responsible for the increase in reaction rate at pH above 6.<sup>20</sup>

To evaluate the impact of dissolved organic matter on NTO photolysis, we photolyzed NTO in solutions of SRNOM (0-15.5 mg C/L). As the concentration of SRNOM increased, the rate of NTO photolysis decreased, even when the rate was corrected for light screening (Figure 27). The observed decrease in NTO degradation indicates that indirect photolysis mediated by DOM does not enhance observed rates of NTO photolysis. This result could be due to the antioxidant properties of SRNOM, i.e., the SRNOM may reduce intermediates of NTO photo-oxidation.<sup>158, 162-164</sup> For example, tryptophan photolysis proceeds through a radical cation that is quenched by NOM.<sup>165</sup> A similar process could happen with NTO, where a radical intermediate is quenched by redox-active moieties in the SRNOM. We investigated the pH dependence of photolysis and quenching effect of SRNOM using several methods to probe the mechanisms of direct photolysis including variable oxygen saturation and quenchers of specific reactive species. We found that both azide and sorbic acid slowed the direct photolysis of NTO (Figure 28A). The dramatic decrease in NTO direct photolysis with sorbic acid present indicates that NTO photolysis proceeds through a triplet excited state.<sup>161</sup> Since singlet oxygen is formed from triplet excited states, sorbic acid quenches both reactions mediated by triplet excited states, and prevents singlet oxygen formation.<sup>166</sup> Direct photolysis of NTO was slower with azide present, suggesting that singlet oxygen may play a role in direct photolysis of NTO because azide is known to physically quench singlet oxygen.<sup>153, 160</sup>

An increase in dissolved oxygen increased the rate of NTO photolysis (Figure 28B). Interestingly, sparging the solution with nitrogen gas resulted in the same rate of transformation as adding 1mM sodium azide to quench singlet oxygen ( $p=0.467$ , F-test on slope of linear regression). However, both N<sub>2</sub> sparging and azide quenching to eliminate singlet oxygen formation have confounding effects.<sup>166</sup> Firstly, the sodium azide added (1



mM) is only estimated to quench 60% of singlet oxygen formed, which means that singlet oxygen could still be forming and degrading NTO under these conditions.<sup>152</sup> In the case of N<sub>2</sub> sparging, the lack of O<sub>2</sub> prevents formation of singlet oxygen, but because O<sub>2</sub> quenches <sup>3</sup>DOM\*, this condition potentially eliminates a major sink for excited triplet state NTO. Without O<sub>2</sub>, excited triplet state NTO is not quenched by oxygen, theoretically facilitating faster degradation. Similar results have been observed for photolysis of the phytoestrogens genistein and daidzein, which were quenched by sorbic acid in deionized water, and the reaction also slowed under deoxygenated conditions.<sup>160</sup>

Once we hypothesized that NTO sensitizes ROS formation upon irradiation, we further evaluated the role of singlet oxygen and hydroxyl radical in the direct photolysis of NTO. We photolyzed FFA with varying amounts of NTO and sodium azide present in aqueous solution (Figure 29A). The presence of NTO dramatically enhanced the degradation of FFA, a well-characterized probe for singlet oxygen degradation.<sup>152, 159, 160</sup> FFA is also known to react with hydroxyl radical, so we conducted a similar experiment with pCBA, a probe for hydroxyl radicals. Overall, little pCBA was degraded in the presence or absence of NTO. While the presence of NTO did slightly enhance the rate of pCBA degradation (p=0.011, paired t-test of initial concentration-normalized data), the steady-state concentration of hydroxyl radicals was calculated to be only  $3 \times 10^{-16}$  M using the equation:

$$[R]_{ss} = \frac{k_{obs}^{probe}}{k_{OH,1O2}} \quad (1)$$

where R is the concentration of radical species in M,  $k_{obs}$  is the observed reaction rate of the probe compound, and  $k_{OH,1O2}$  is the known second-order reaction rate of pCBA. FFA is known to react with hydroxyl radical at the rate of  $1.5 \times 10^{10} \text{ M}^{-1} \text{ s}^{-1}$ , but the concentration of <sup>•</sup>OH determined from the pCBA experiment would only result in minor FFA degradation (i.e.,  $k_{obs,FFA}/k_{calc,OH,FFA} = \sim 12$ ).<sup>152</sup> To further confirm singlet oxygen formation, we also photolyzed NTO in D<sub>2</sub>O (Figure 29B). Water quenches singlet oxygen, and D<sub>2</sub>O is often used to extend the lifetime of singlet oxygen molecules.<sup>159</sup> The reaction in D<sub>2</sub>O was faster than in water, further confirming that direct photolysis of NTO produces singlet oxygen (p<0.001, F-test comparing pseudo-first-order rate constants).

In addition to producing singlet oxygen, NTO is degraded by singlet oxygen (Figure 31A). We conducted an experiment to determine the 2<sup>nd</sup>-order reaction rate constant of NTO with singlet oxygen using Rose Bengal as a sensitizer and FFA as a probe, and found an estimated rate constant of  $2.0 \times 10^6 \text{ M}^{-1} \text{ s}^{-1}$ . Because NTO itself reacts with singlet oxygen, it was not unsurprising that sparging the solution with O<sub>2</sub> prior to irradiation increased the direct photolysis rate of NTO, and that eliminating oxygen also slowed the reaction. We also measured the 2<sup>nd</sup>-order reaction rate constant of NTO with regards to hydroxyl radicals to be  $3.3 \times 10^{10} \text{ M}^{-1} \text{ s}^{-1}$  using competition kinetics with pCBA as a probe (Figure 31) and nitrate as a sensitizer.<sup>158, 159</sup>

To determine the effect of more environmentally-relevant initial concentrations of NTO on the observed rate of photolysis, we exposed NTO solutions ranging from 0.01-100  $\mu\text{M}$  (1.3-13000  $\mu\text{g/L}$ ). Even at the lower concentrations, the observed rate was similar among all concentrations tested (Figure 30). An ANOVA analysis did reveal significant differences among rates ( $p < 0.001$ ), but the magnitude of the differences was small, and the rate at lowest concentration (10 nM) was not significantly different from the rate at the highest concentration (100  $\mu\text{M}$ ) according to a post-hoc Tukey multiple comparisons test. The observed similarity among the concentration range tested, including at environmentally relevant levels, indicated that the photolysis times are reasonable predictors of environmental fate characteristics of NTO in surface waters. The similarity in reaction rates at low concentrations may indicate that the rate limiting step of photolysis is absorbance of a photon or intersystem crossing to a triplet state before further reactions. Therefore, different mechanisms (e.g., direct photolysis vs. singlet oxygen degradation) may be occurring at lower concentrations compared to higher concentrations, while the overall rate remains similar due to the rate limiting first step. Further work would be needed to confirm this hypothesis, for example, investigating photoproduct distributions at various concentrations.

In terms of transformation products, we observed that NTO photolysis produced nitrite, ammonia, nitrate and hydroxy-triazolone, consistent with other studies.<sup>23, 74</sup> Because hydroxy-triazolone did not accumulate during the photolysis, we photolyzed hydroxy-triazolone directly and with initial added nitrite to determine if nitrite facilitated indirect photolysis of hydroxy-triazolone (Figure 32B). Not only was hydroxy-triazolone

directly photolyzed, but nitrite greatly increased the rate of hydroxy-triazolone loss, confirming that observation that hydroxy-triazolone was only present in low concentrations as a reactive intermediate. In addition to direct and nitrite-mediated indirect photolysis, hydroxy-triazolone is degraded quickly by singlet oxygen, further indicating why this compound does not accumulate (Figure B6). Nitrite had no effect on NTO photolysis, and slowed the reaction when 5 mM was added (Figure 32A). Both NTO and hydroxy-triazolone formed two prominent anions after indirect photolysis in the presence of Rose Bengal, and further work should be done to determine the identity of the anions.

To further delineate the mechanisms of NTO photolysis, we compared the inorganic nitrogen products under varying conditions including pH, dissolved oxygen, and singlet oxygen degradation (Figure 33). The results indicated that nitrite is a prominent product of NTO photolysis. When subjected to singlet oxygen degradation, NTO produces nitrite in almost stoichiometric yield, with little nitrate and ammonium formation. Under direct photolysis conditions, more nitrate and ammonium are formed than by singlet oxygen. Nitrite can be photo-oxidized to nitrate, but apparently the primary products of NTO are also subject to direct photolysis to form ammonium, unlike the singlet oxygen condition. Some ammonia could have been lost in the pH 9 conditions due to volatilization, as demonstrated by the higher concentrations of ammonia at pH 5. Besides more ammonium at pH 5 compared to pH 9, the trends of inorganic nitrogen were similar across the pH difference. However, at pH 9, after 44  $\mu\text{M}$  of NTO was degraded, 56  $\mu\text{M}$  of nitrate and nitrite were formed. This mass balance is contrasted with pH 5, where after 41  $\mu\text{M}$  of NTO was degraded, exactly 41  $\mu\text{M}$  of nitrite and nitrate were formed. This difference in molar yield may indicate that an additional photolysis mechanism is occurring at higher pH, which could explain the faster degradation of NTO at pH 9 when compared to pH 5. When the solution was sparged with nitrogen gas, the rate of photolysis was much slower, and less inorganic nitrogen was formed, even when accounting for the amount NTO degraded. This finding indicates that the direct, oxygen-free photolysis reaction could form other unknown products.

The dramatic decrease in photolysis rate after nitrogen sparging along with the moderate 2<sup>nd</sup>-order reaction rate constant of NTO with singlet oxygen indicate that dissolved oxygen could play an additional role in NTO photolysis beyond formation of

singlet oxygen. For example, NDMA is photo-oxidized by a one electron transfer to dissolved oxygen, forming superoxide radical.<sup>167</sup> Superoxide is known to form by electron transfer from triplet states, in competition with energy transfer formation of singlet oxygen.<sup>168</sup> This one electron transfer mechanism from excited NTO could explain the slower rate of photolysis with natural organic matter because the NOM could quench the reaction by minimizing electron transfer.<sup>165</sup> Further work is needed to investigate the potential for superoxide formation from NTO direct photolysis.

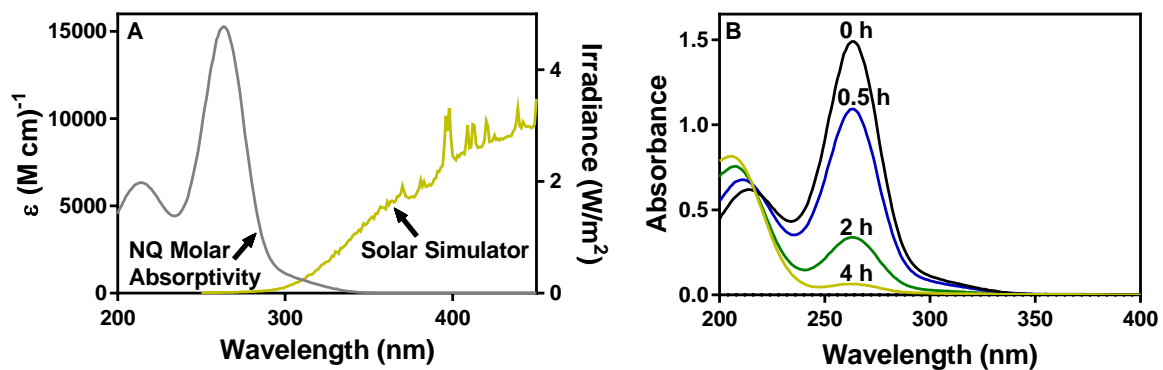


Figure 34. A) Molar absorptivity of NQ and irradiance of solar simulator. B) UV-Vis absorbance of 100  $\mu\text{M}$  NQ solution after photolysis for the indicated time.

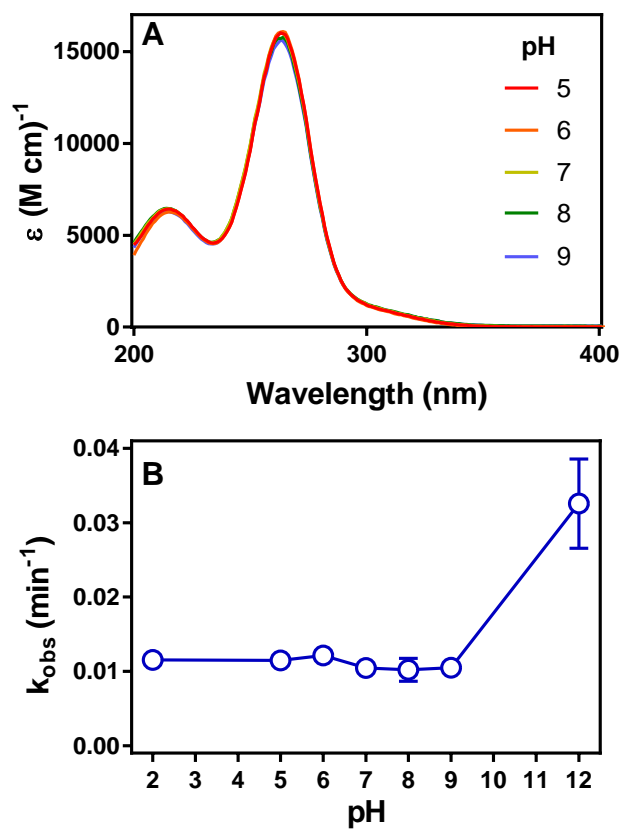


Figure 35. Variation in A) molar absorptivity from pH 5-9 and B) pseudo-first-order rate constant of NQ photolysis ( $750\text{ W/m}^2$ ,  $35\text{ }^\circ\text{C}$ ) from pH 2-12.

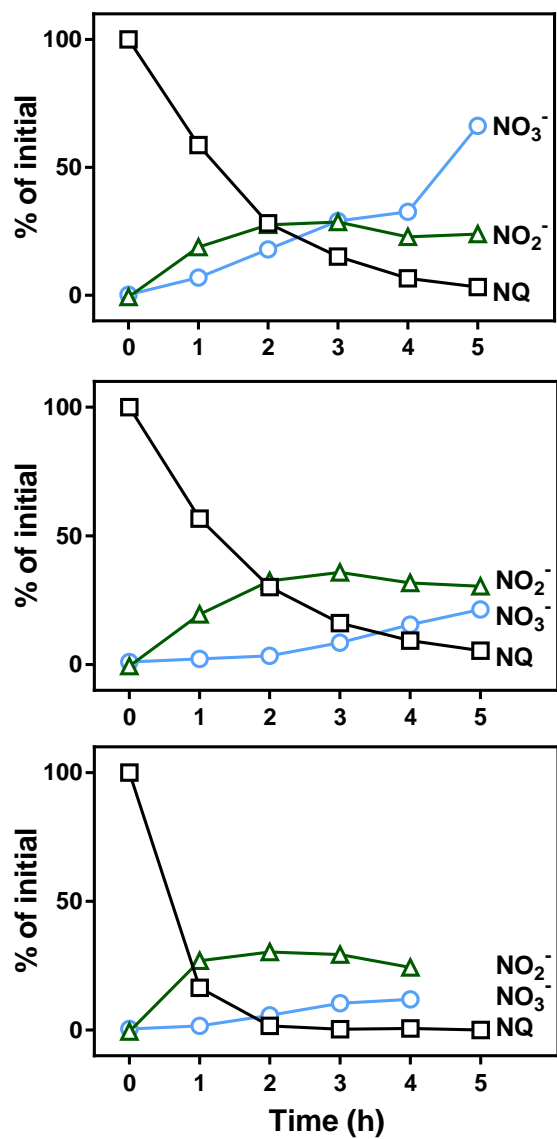


Figure 36. Production of nitrite and nitrate after five hours of NQ photolysis (100  $\mu$ M, 25 mM buffer).

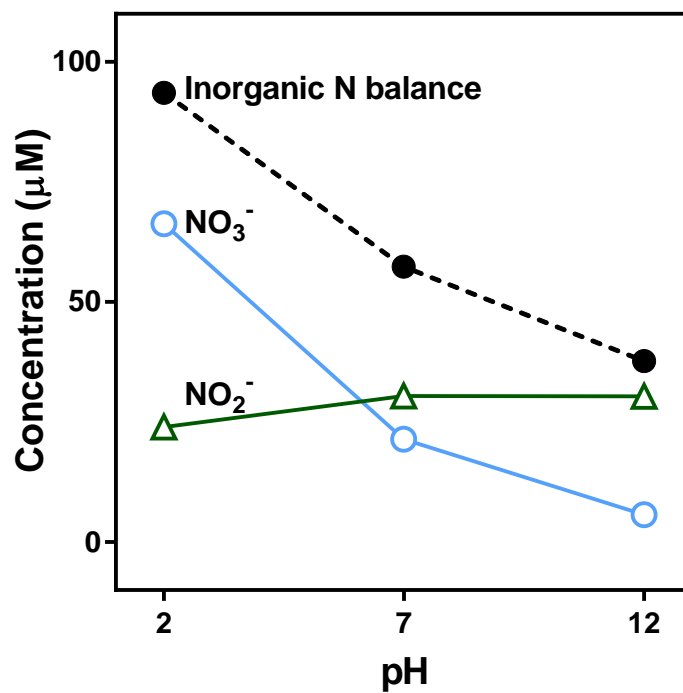


Figure 37. Summary of nitrite and nitrate yield from data in Figure 36 after 95% degradation of NQ.



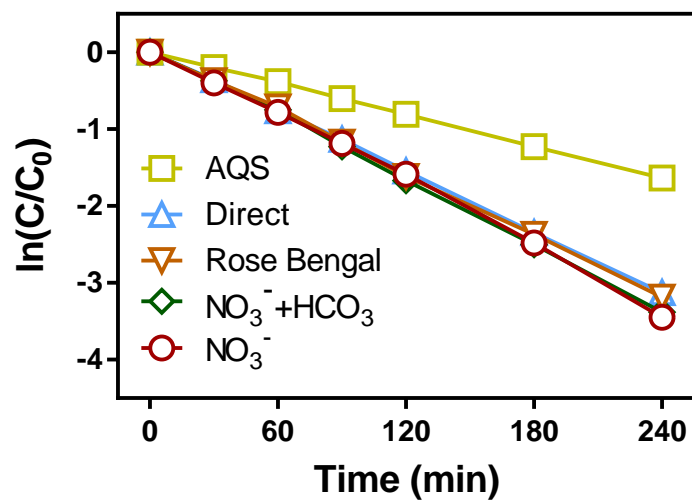


Figure 38. Preliminary experiments with photo-sensitizers to determine if NQ is reactive with any photo-produced reactive intermediates, i.e., if NQ would be subject to indirect photolysis.

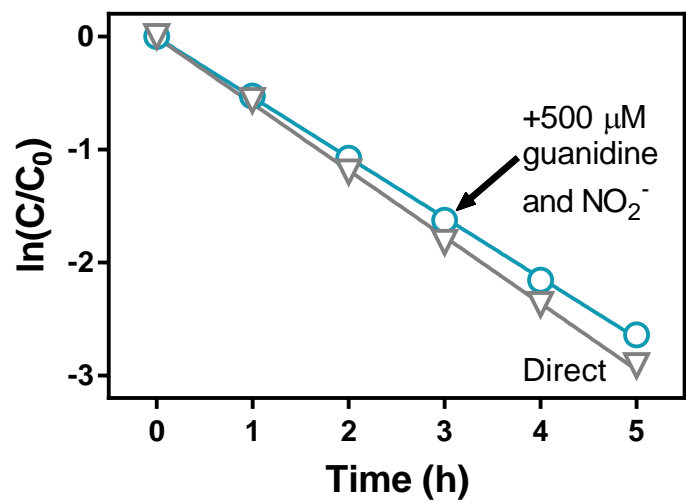


Figure 39. Photolysis of 100 μM NQ in the presence and absence of 500 μM guanidine and nitrite. Lines are linear regression of the log-normalized data.

Nitroguanidine has a UV-Vis absorbance maxima of 265 nm and the molar absorptivity of NQ overlaps with that of the solar simulator (Figure 34A). Consistent with the large absorptivity in the UV region, NQ is amenable to photo degradation, especially by UV light.<sup>23, 56, 80</sup> We found that after four hours of photolysis, NQ absorbance decreased, but an increase in absorbance was observed below 225 nm (Figure 34B). Therefore, no refractory longer wavelength UV-Vis absorbing compounds are produced during the reaction, and the products do not absorb above the UVC region (100-280 nm). NQ does not have an ionizable functional group in the neutral pH range, and the absorbance of 100  $\mu$ M NQ does not change from pH 5-9 (Figure 35A). When solutions of NQ were photolyzed for four hours with varying pH, there was no significant difference (ANOVA,  $\alpha = 0.05$ ) among the rates from pH 2-9 (Figure 35B). Similarly, the quantum yield of NQ was not significantly different as a function of pH, and the average value over the pH range was 0.0088. However, at pH 12, the observed rate of photolysis was dramatically increased, potentially due to deprotonation at the higher pH.

In terms of transformation products, a solution of 100  $\mu$ M NQ produced nitrite and nitrate after photolysis (Figure 36, Figure 37). We found that the mass balance of nitrite and nitrate varied dramatically and was dependent on solution pH. At high pH, less nitrate was formed, and the inorganic nitrogen mass balance was lower. This result is consistent with older results indicating unknown nitrogen products are formed at high pH.<sup>80</sup> Perreault et al. determined that guanidine was a stoichiometric product of NQ photolysis in IMX-101 solutions, and Burrows agreed at unbuffered pH.<sup>23, 80</sup> A conflicting report claimed that hydroxyguanidine was a stoichiometric product of NQ photolysis in unbuffered solution.<sup>56</sup> Further study is warranted to determine the exact mechanisms of photolysis, the effect of pH on NQ photolysis, and the product distribution from NQ photolysis. These studies should help clear up the conflicting results of previous studies, to determine process control parameters for treatment of NQ by UV, and to understand how NQ will break down in sunlight surface waters.

To determine the propensity of NQ for indirect photolysis in surface water with DOM, we photolyzed NQ with a variety of photosensitizers to produce reactive intermediates (Figure 38). Overall, there was little effect of photosensitizers. Adding nitrate to generate hydroxyl radicals produced a slightly increased rate compared to direct photolysis.

Additional carbonate did not further increase the reaction rate. The fact that carbonate did not increase the reaction rate indicated that either the reaction of NQ with  $\cdot\text{OH}$  is faster than carbonate radical with  $\cdot\text{OH}$ , or that NQ is not reactive with  $\cdot\text{CO}_3$ . To test this hypothesis, we performed a competition kinetics experiment with pCBA and found the 2<sup>nd</sup>-order reaction rate of NQ to be  $1.2 \times 10^{11}$ . The observed  $k_{OH}$  for NQ is faster than the rates of carbonate and bicarbonate radical previously reported ( $3.9 \times 10^8$  and  $8.5 \times 10^6$ , respectively).<sup>169, 170</sup> Therefore, we can conclude that NQ scavenges hydroxyl radicals faster than carbonate, explaining the similar rates observed with and without carbonate. Finally, when Rose Bengal was added to produce singlet oxygen and when AQS was added as a model  $^3\text{DOM}^*$ , no effect or a slowing of the reaction rate were observed (Figure 38).

The large value for the quantum yield, relatively fast photolysis, and the absence of refractory UV-absorbing products indicates that UV treatment of NQ may be a viable technique for treating NQ-containing wastewater. Recent work has demonstrated a slower rate of photolysis of NQ when present in mixtures of IMX-101.<sup>23</sup> This study also observed renitration of guanidine when NTO and  $\text{TiO}_2$  were present in the solution. To investigate this phenomenon, I photolyzed solutions of guanidine with a variety of initial conditions to determine the potential for nitroguanidine production under environmental conditions. The results indicated that NQ can form in the presence of NTO, but very little accumulated because any NQ that formed was presumably quickly photolyzed. The results after 8 hours of photolysis are summarized in Table 14. In another experiment, I photolyzed NQ with initial guanidine and nitrite, but the results did not indicate that excess guanidine and nitrite dramatically shifted the reaction equilibrium to continually produce NQ (Figure 39).

Table 14. Summary of guanidine nitration experiments (100  $\mu\text{M}$  guanidine, 25 mM pH 7  $\text{PO}_4^-$  buffer, 8 h exposure).

Initial conditions	Guanidine formation?
20 $\mu\text{M}$ NTO	Trace
20 $\mu\text{M}$ NTO and 250 ppm $\text{CO}_3^{2-}$	Trace
1 mM $\text{NO}_2^-$	No

## CHAPTER 6: BIOTRANSFORMATION OF NTO AND DNAN BY ACCLIMATED SOIL SLURRIES AND ISOLATED SOIL BACTERIA

### Introduction

Explosive compounds contaminate millions of acres of land in the U.S. and abroad and are released to the environment primarily at military training facilities (i.e., as unexploded ordinance fragments) and at production and disposal facilities. For example, over 20 million hectares are affected by bombing and training activities in the United States alone, and concentrations of 2,4,6-trinitrotoluene (TNT) have been observed up to 143 kg kg<sup>-1</sup> in soil near unexploded ordinance.<sup>2</sup> Incinerated soil even contained 10 and 2 kg kg<sup>-1</sup> concentrations of TNT and hexahydro-1,3,5-trinitro-1,3,5-triazine (RDX), respectively, in one case.<sup>2</sup> While TNT and RDX have been the most widely used – and most widely contaminating – explosives, TNT and RDX are being phased out by safer, insensitive formulations such as IMX-101 and IMX-104.<sup>19</sup> So called “insensitive munitions explosives” formulations are making storage, handling, and transport of munitions easier. The new explosive mixtures contain compounds that are less prone to sympathetic detonation, reducing the risk of accidental explosion. While new, safer compounds, such as 3-nitro-1,2,4-triazol-5-one (NTO), are replacing legacy explosive compounds, NTO has properties that could threaten environments where NTO is released.<sup>18</sup> For example, the solubility of NTO in water is 17 g/L, over two orders of magnitude higher than RDX (60 mg/L).<sup>20</sup> The increased mobility of NTO raises concerns for NTO reaching groundwater and migrating offsite, making clean up more difficult and expensive.

Remediation of explosives can be accomplished by various techniques, including bioremediation.<sup>18, 19, 27, 28, 33, 53, 96, 121, 171</sup> Biodegradation of NTO has been shown under varying conditions. For example, rat liver microsomes degraded NTO to 3-amino-1,2,4-triazol-5-one (ATO) and urazole, while these compounds were not further transformed.<sup>44,</sup><sup>172</sup> A recent study demonstrated that NTO is reduced to ATO only under anaerobic conditions in previously uncontaminated soils. ATO is then mineralized to inorganic nitrogen, but only under aerobic conditions.<sup>18</sup> Other studies have alleged to demonstrate aerobic biodegradation, but high cell and carbon source concentrations could have led to anaerobic conditions.<sup>45, 46</sup> The unique chemistry of NTO transformation requiring redox or

oxygen cycling could lead to costly and difficult remediation, whereas true aerobic biodegradation, if possible, could be the most viable remediation strategy.

Here, we sought to understand if acclimating the soil microbial community to the presence of insensitive high explosives could lead to the capacity for aerobic biodegradation of NTO and DNAN. Along with monitoring NTO and DNAN degradation, we sought to identify biotransformation products, which may be useful for monitoring natural attenuation because NTO does not readily sorb to soils.<sup>76, 96</sup>

## **Materials & Methods**

*Synthesis and characterization of 3-nitro-1,2,4-triazol-5-one (NTO) and 3-amino-1,2,4-triazol-5-one (ATO) – NTO synthesis performed by Xueshu Li and Hans-Joachim Lehmler*

NTO was synthesized via the nitration of 1,2,4-triazolone (TO). TO was synthesized from semicarbazide hydrochloride in a one-pot reaction using excess formic acid as both reagent and solvent.<sup>151</sup> Nitration of TO with fuming nitric acid gave NTO in 42% yield. The <sup>1</sup>H and <sup>13</sup>C NMR spectra were recorded on a Bruker Avance DRX-400 spectrometer in the University of Iowa Central NMR Research Facility (Iowa City, IA, USA). DMSO-*d*<sub>6</sub> was used as the solvent for NMR. High resolution mass spectral analysis was performed on a Waters Q-ToOF Premier mass spectrometer by the High Resolution Mass Spectrometry Facility of the University of Iowa. <sup>1</sup>H NMR (400 MHz, DMSO-*d*<sub>6</sub>) δ 12.80 (br s); <sup>13</sup>C NMR (100 MHz, DMSO-*d*<sub>6</sub>) δ 154.3, 147.8; HR-MS (ESI): Calc'd for C<sub>2</sub>HN<sub>4</sub>O<sub>3</sub>: 129.0049 [M-H]<sup>-</sup>, Found: 129.0049 [M-H]<sup>-</sup>.

3-Amino-1,2,4-triazol-5-one (ATO) was synthesized from NTO following a previously described method.<sup>18</sup> Briefly, NTO (0.5 g) in methanol was reduced by hydrogen gas over a palladium catalyst in a foil-wrapped serum bottle.

### *Soil acclimation and experimental design*

Soil was collected from a private farm in Lowden, IA. The soil was sandy with a pH of 6.8, natural organic matter content of 0.3% and nitrogen content of 0.5 ppm NO<sub>3</sub>-N. About ten liters of soil was added to a five-gallon bucket. Approximately three liters of IMX-101 process water from the Iowa Army Ammunition Plant (IAAAP) was added to the soil in

December 2014. This process water contained high concentration of IMX-101 constituents as well as traditional nitroaromatic explosives, listed in Table 15.

In September of 2015, we began conducting experiments to determine if the soil slurries could degrade DNAN and NTO after nine months of acclimation to nitroaromatic contamination. Soil slurry degradation experiments were conducted in 100 mL amber serum bottles according to a previously published method.<sup>28, 53</sup> The soil was sieved on a 2 mm screen prior to experiments. Ten grams (wet weight) of soil was measured into each serum bottle, and 20 mL of minimal salts medium (MSM) was added to each bottle. The MSM contained 0.38 g K<sub>2</sub>HPO<sub>4</sub>, 0.2 g MgSO<sub>4</sub>•7H<sub>2</sub>O, and 0.05 g FeCl<sub>3</sub>•6H<sub>2</sub>O per liter of deionized water, and the pH was adjusted to 7.0 prior to autoclaving. Various carbon and nitrogen regimes were used to simulate bioaugmentation scenarios. The carbon source (C) was 10 mM glucose and 5 mM succinate, while the nitrogen source (N) was 5 mM NH<sub>4</sub>Cl. Killed biomass controls contained 500 mg L<sup>-1</sup> sodium azide. Bottles were stoppered with autoclaved glass wool plugs and shaken at 20 °C and 150 rpm. Samples of 0.5 mL were withdrawn and the concentration of explosives was measured by HPLC (UV-Vis). In May 2016, the NTO soil slurry experiments were conducted again with more replicates and sampling time points to better track the degradation of NTO. Carbon and nitrogen were added to the respective bioreactors after 15 days in addition to the start of the experiment.

After DNAN or NTO were degraded, serial dilutions of soil slurries were plated on R2A or LB agar in order to isolate explosive-degrading organisms. After three rounds of streak plating, isolates were screened for their ability to degrade DNAN and NTO in liquid MSM with and without carbon and nitrogen. NTO degraders were again streaked and we identified the strains by sequencing the genomic DNA of each degrader. Two *Bacillus* isolates were identified for further study. For further experiments, isolated colonies were inoculated into MSM media with carbon and nitrogen for biomass growth. Aliquots of exponential phase biomass were added to new bioreactors containing NTO, ATO, or urazole to determine if the isolates could degrade these compounds and to identify degradation products.

Table 15. Constituents in IAAAP wastewater (provided by IAAAP staff).

Constituent	Concentration (mg L <sup>-1</sup> )
2,4-dinitroanisole (DNAN)	148.2
3-nitro-1,2,4-triazol-5-one (NTO)	968.6
nitroguanidine (NQ)	972
2,4,6-trinitrotoluene (TNT)	63
hexahydro-1,3,5-trinitro-1,3,5-triazine (RDX)	40.6
octahydro-1,3,5,7-tetranitro-1,3,5,7-tetrazocine (HMX)	5.032
1,3,5-trinitrobenzene	0.604
2,4-dinitrophenol	1.044
3,5-dinitroaniline	0.262
4-amino-2,6-dinitrotoluene	6.166
2-amino-4,6-dinitrotoluene	4.004
2,4-dinitrotoluene	0.372



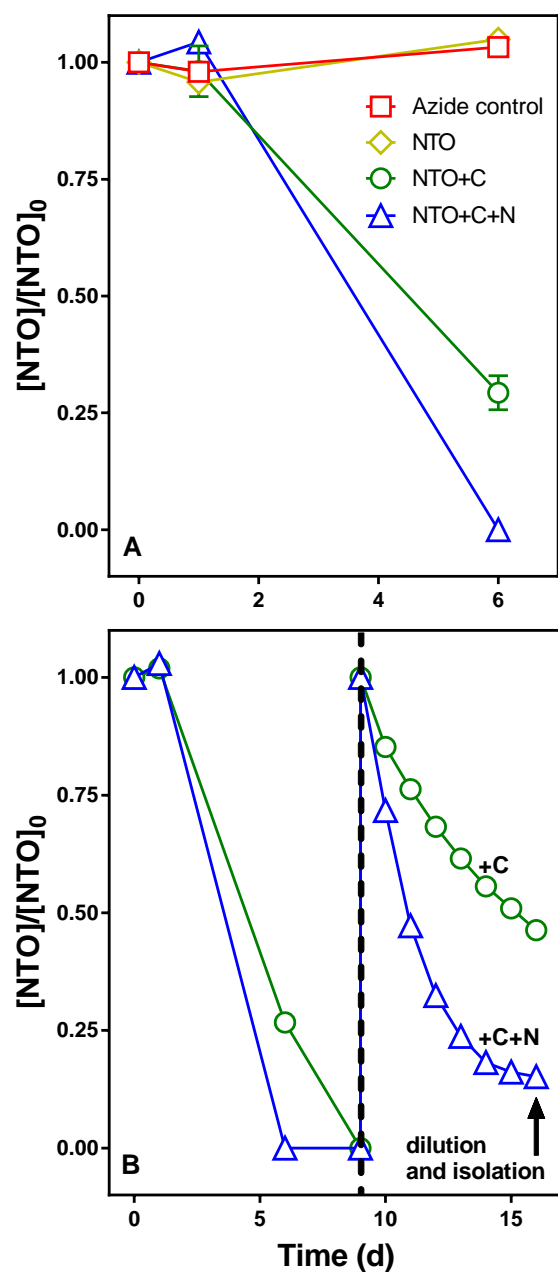


Figure 40. Preliminary NTO (5 mg L<sup>-1</sup>) degradation in minimal salts media by acclimated soil slurries. (A) n = 2 and error bars are standard deviation of the mean. Error bars are not shown when they fall inside the symbol and (B) is concentration of NTO in the soil slurries (n = 1) with carbon (C; 10 mM glucose and 5 mM succinate) and nitrogen (N; 5 mM NH<sub>4</sub>Cl), which were spiked again with NTO after nine days (indicated by the vertical dashed line). The organisms in this study were isolated from the soil slurry with added carbon and nitrogen in (B) after 16 days (indicated by the arrow).

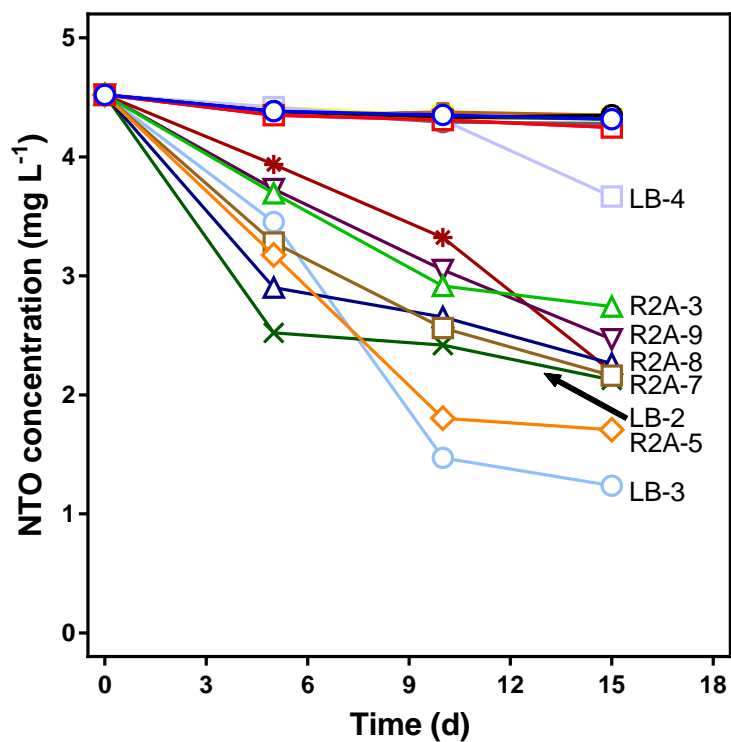


Figure 41. Screening for NTO degradation in MSM media with 10 mM glucose, 5 mM succinate, and 5 mM  $\text{NH}_4\text{Cl}$  by organisms isolated from soil slurries. The type of media the organism was isolated on is indicated in the label for each organism, and the organism numbers are arbitrary.

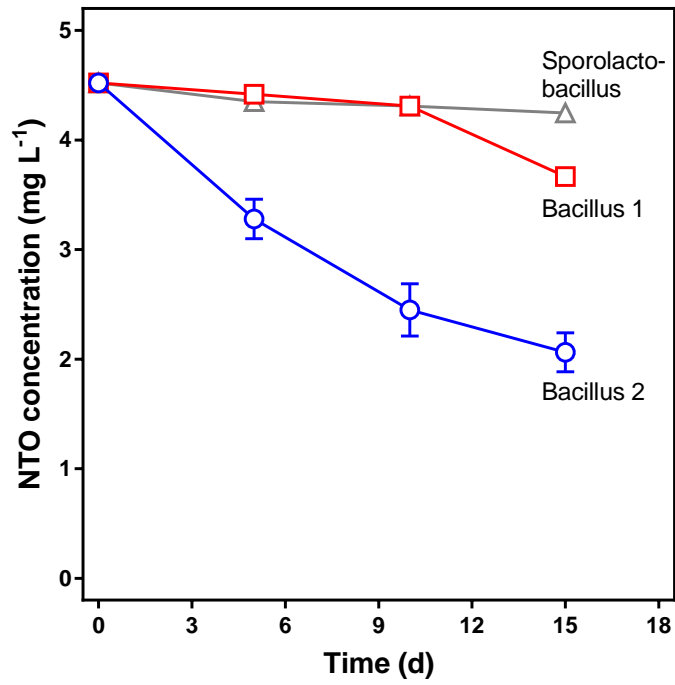


Figure 42. Data from Figure 41, averaged by organism as identified by DNA sequencing.

## Results & Discussion

In an initial screen for soil slurry degradation potential, NTO degraded quickly. Surprisingly, we observed 71% loss of NTO in the carbon amendment (C) and 100% loss of NTO in the carbon and nitrogen (C+N) amendment bioreactors, respectively after just six days (Figure 40A). This was unexpected in light of previous indications that NTO does not degrade in aerobic soil slurries.<sup>18</sup> After nine days, we added NTO to determine if the slurries could again degrade the NTO. Indeed, between nine and sixteen days, the concentration of NTO decreased in the C and the C+N bioreactors, with more degradation occurring in the bioreactor with added nitrogen (Figure 40B). After 16 days, we took serial dilutions of the C+N bioreactor to isolate organisms responsible for degrading NTO.

Eighteen organisms were isolated on R2A and LB agar, which we screened for the ability to degrade NTO in MSM with C+N (Figure 41). We then extracted the genomic DNA from these organisms and sequenced the DNA to identify the bacterial strains. The results indicated only three separate strains from the original 18 isolates: a *Sporolactobacillus* sp. and two *Bacillus* spp. The *Sporolactobacillus* did not degrade NTO, so the two *Bacillus* spp. were selected for further study (Figure 42).

When NTO was the sole carbon or nitrogen source, neither strain of *Bacillus* (B1 and B2, respectively) could transform NTO (Figure 43), indicating the degradation was co-metabolic. With carbon and nitrogen added as succinate, glucose, and ammonium chloride, both strains degraded NTO (Figure 44). While transformation of NTO by co-metabolism is in agreement with previous studies, utilization of NTO as the sole carbon or nitrogen source would be desirable for bioremediation applications.<sup>18, 46</sup> If NTO could be used as the sole source of carbon or nitrogen, full mineralization is more likely than in a co-metabolic process. Full mineralization prevents the buildup of recalcitrant intermediate compounds, likely occurs more quickly than co-metabolic processes, and may not require as much or any additional carbon or nitrogen sources to be added in a field condition.<sup>31</sup>

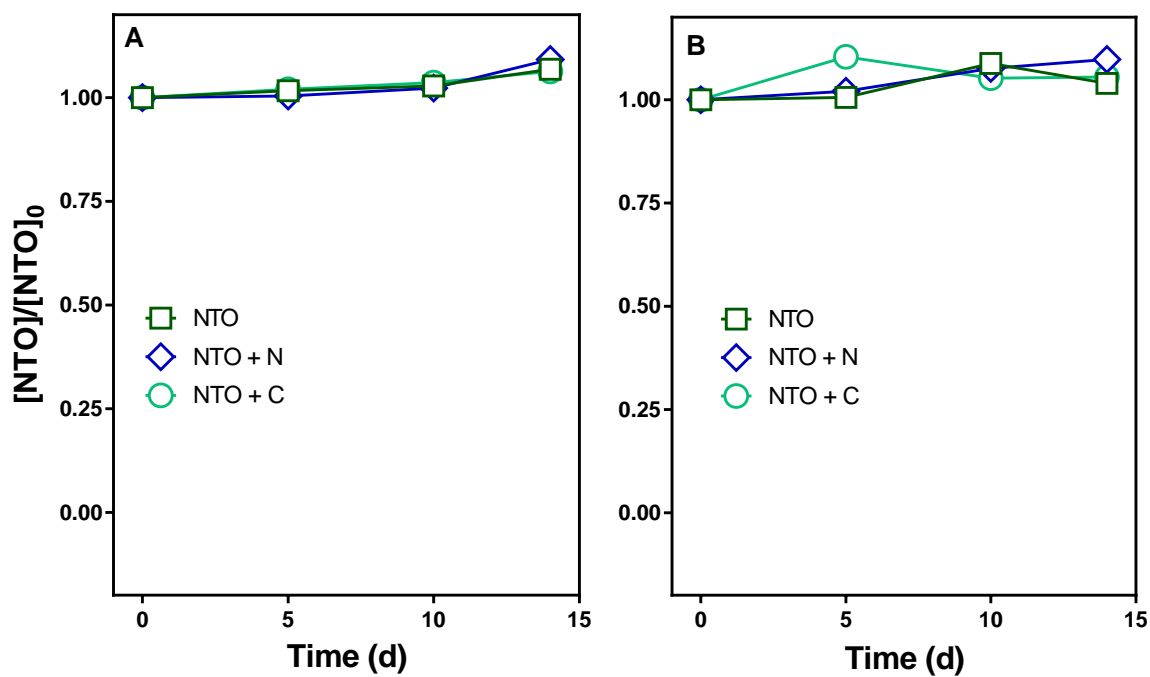


Figure 43. Neither *Bacillus* isolate (B1, panel A; B2, panel B) degraded NTO ( $5 \text{ mg L}^{-1}$ ) in minimal salts media when it was the sole source of carbon (C; 10 mM glucose and 5 mM succinate) or nitrogen (N; 5 mM  $\text{NH}_4\text{Cl}$ ). The data were not corrected for evaporation.

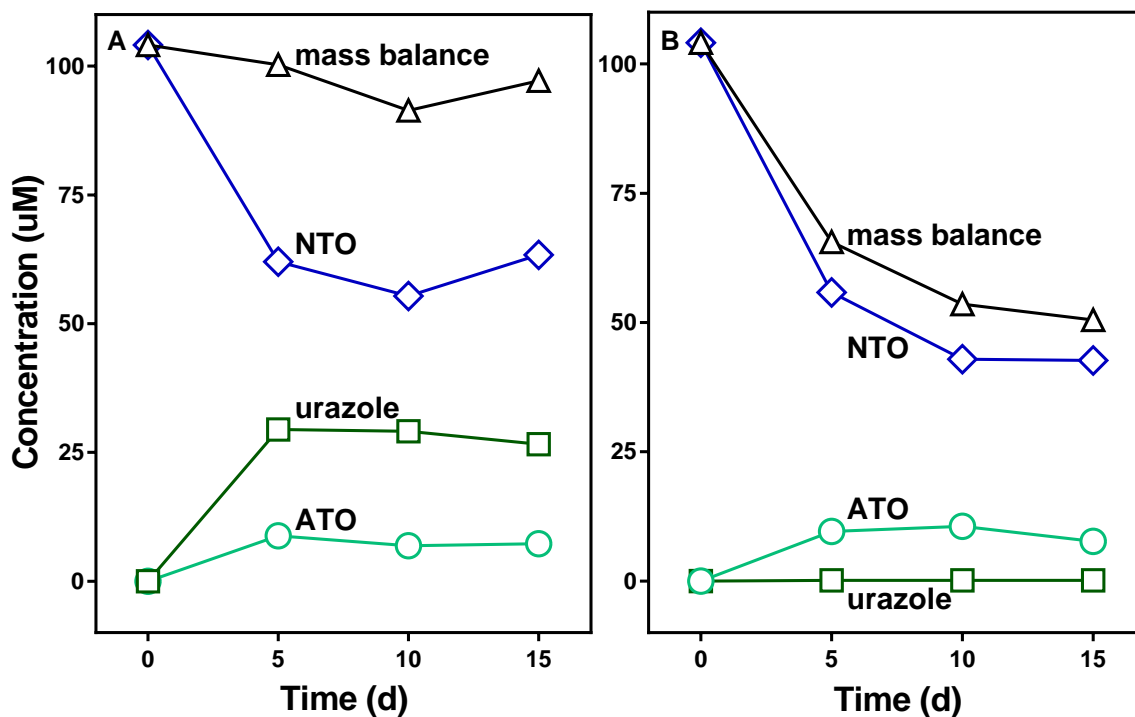


Figure 44. Degradation of NTO and resulting transformation products in minimal salts media containing 10 mM glucose, 5 mM succinate, and 5 mM  $\text{NH}_4\text{Cl}$ . A) Strain B1 produces urazole and ATO. B) Strain B2 produces some ATO and some unknown products.

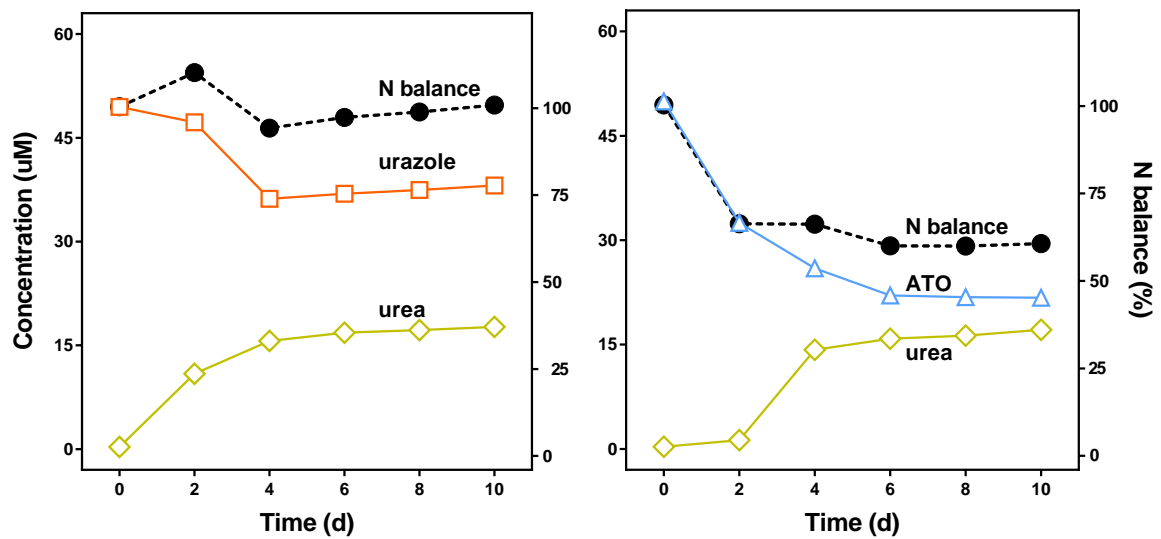


Figure 45. Degradation of urazole (left) and ATO (right) in minimal salts media containing 10 mM glucose, 5 mM succinate, and 5 mM NH<sub>4</sub>Cl by *Bacillus* sp. isolate 1 to form urea.

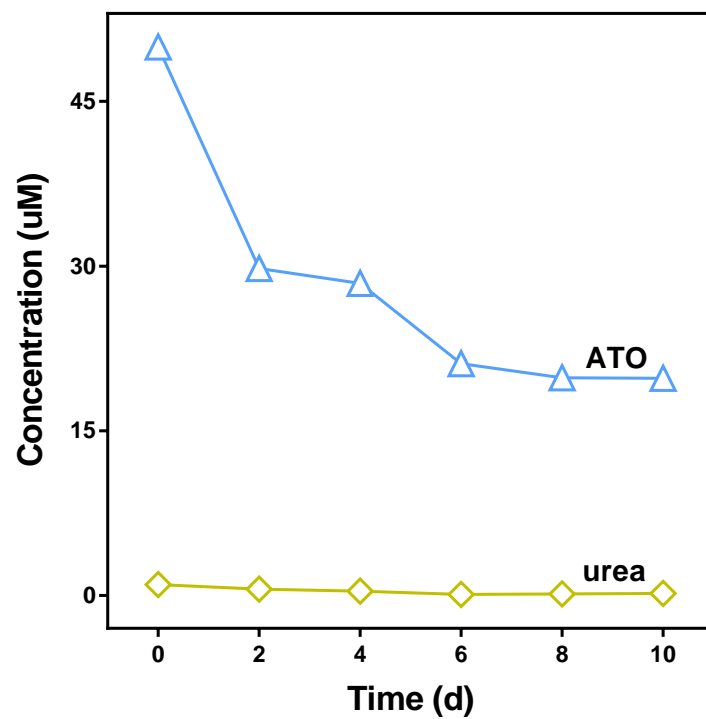


Figure 46. Degradation of ATO into unknown products by *Bacillus* sp. 2 in minimal salts medium with 10 mM glucose, 5 mM succinate, and 5 mM NH<sub>4</sub>Cl.



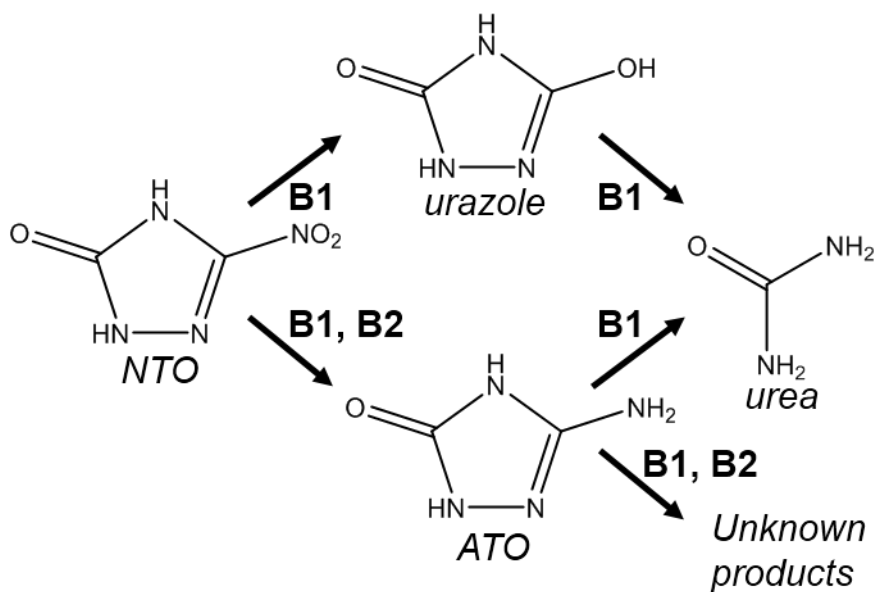


Figure 47. Putative degradation pathways of NTO by *Bacillus* spp. 1 and 2 (B1 and B2, respectively).

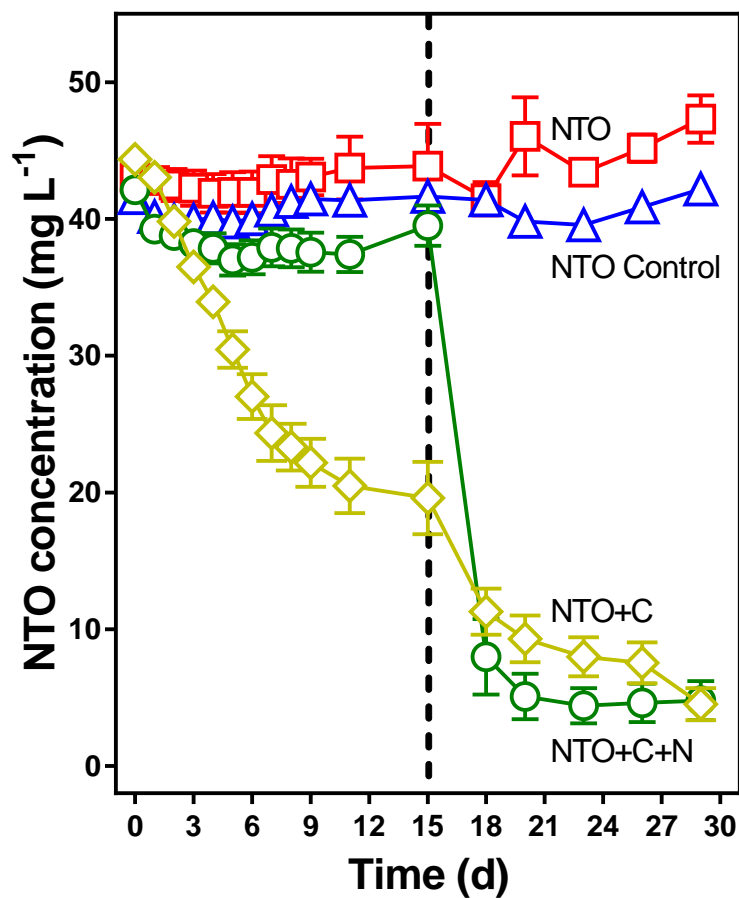


Figure 48. NTO degradation by acclimated soil slurries in minimal salts media with various carbon (C, 10 mM glucose and 5 mM succinate) and nitrogen (N, 5 mM NH<sub>4</sub>Cl) regimes (n = 3). Additional carbon and nitrogen were added at 15 days as indicated by the vertical dashed line. The NTO control contained 500 mg L<sup>-1</sup> sodium azide.

Strain B1 converted NTO into urazole (1H-1,2,4-triazole-3,5-diol) and ATO (Figure 44A). The mass balance for the reactor was high, ending at 93% after 15 days on a molar basis. While urazole has been observed as a transformation product of rat liver microsomes, this is the first time urazole has been observed as a microbial transformation product to our knowledge.<sup>172</sup> Interestingly, in aerobic incubations, rat liver microsomes formed urazole and minor amounts of ATO, similar to this study. Formation of urazole from NTO was concomitant with stoichiometric formation of nitrite.<sup>172</sup> The ability of rat liver microsomes to transform NTO to urazole was repressed by cytochrome *P*-450 inhibitors, leading to the conclusion that oxidative denitration of NTO was performed by cytochrome *P*-450s.<sup>172</sup> *Bacillus* are known to contain cytochrome *P*-450s, including a well-studied enzyme that disrupts quorum sensing by oxidizing acyl homoserine lactones produced by other bacteria and also contain an enzyme that oxidizes a bioactive, plant-produced steroid.<sup>173, 174</sup> While these two enzymes hydroxylate carbon atoms, as observed here, the target molecules are moderately hydrophobic. The previously identified enzymes would be unlikely to also oxidize the highly soluble NTO. In addition to hydroxylation, cytochrome *P*-450s have also been implicated in denitration of RDX, but in these reactions, the nitro group was removed, without hydroxylation of the substrate.<sup>175, 176</sup> The type of reaction observed for RDX by *P*-450s could have occurred here, but would require the denitration and a subsequent hydroxylation to form urazole.

In contrast to B1, strain B2 produced ATO from NTO, with no urazole detected. In addition to this difference in metabolic products, strain B2 also had a lower mass balance than strain B1. The mass balance along with the concentration profile of ATO indicates that B2 further transformed ATO to unknown products. Aerobic reduction of NTO to ATO has been claimed to occur in two studies,<sup>45, 46</sup> but a recent study questioned the aerobic nature of these experiments.<sup>18</sup> Due to high concentration of cells and carbon, Krzmarzick et al. postulated that the previous studies likely had anaerobic conditions for the reduction. In addition, Krzmarzick did not observe aerobic reduction of NTO to ATO. Here, we did not measure the oxygen content of the bioreactors, so anaerobic microenvironments could have facilitated the reduction of NTO. The predominantly oxic conditions in this study most likely facilitated further degradation of ATO, leading to a lower mass balance, similar to that observed by Krzmarzick et al.<sup>18</sup>

To determine if the strains could metabolize the identified intermediates of NTO degradation, urazole and ATO, we incubated the strains with the respective compounds in MSM with C+N (Figure 45 and Figure 46). Interestingly, B1 degraded both urazole and ATO, producing urea from both compounds. Conversion of urazole to urea by B1 was stoichiometric, with a closed mass balance. However, when B1 degraded ATO, about one-third of the nitrogen was unaccounted for by measuring only urea. When strain B2 was incubated with ATO, 60% of the ATO was transformed after ten days. While we measured urea, none was detected to be formed by strain B2. We did not incubate strain B2 with urazole because urazole was not formed from NTO by strain B2. A previous study found that ATO was mineralized to inorganic nitrogen, but we did not measure inorganic nitrogen here.<sup>18</sup> The fact that B1 could degrade both urazole and ATO, which it produced from NTO, is encouraging; strain B1 can potentially aerobically degrade NTO to urea and inorganic nitrogen. More work needs to be done to determine why urazole and ATO were not further degraded over ten days, and if urea inhibits these reactions.

Finally, the microbial degradation pathway for the two isolates is summarized in Figure 47. Further work should be undertaken to understand if the strains transform under strictly aerobic conditions or in anaerobic microenvironments. Cell-free protein extracts were prepared by sonication of pre-grown *Bacillus* cultures following a previous method, but did not transform NTO for unknown reasons, potentially due to a lack of NADPH cofactor.<sup>28</sup> Because *Bacillus* is a genus amenable to laboratory study and industrial use for its cultivability and resilience, these strains could have potential use for bioremediation with further investigation of viability, bioaugmentation requirements, and *in vivo* NTO transformation potential in inoculated soils.

In May 2016, we conducted another soil slurry degradation experiment to measure the initial degradation curve more effectively by adding more replicates and taking samples with a greater frequency. Unfortunately, the results were not consistent with the first batch of soil slurries. In the reactors with added carbon, NTO slowly degraded, while the unamended, control, and C+N bioreactors were relatively stable (Figure 48). After 15 days, we added carbon and nitrogen, and there was a dramatic decrease in NTO concentration in the C+N reactor and a renewed rate of NTO loss in the C reactor. Most probably, the decrease in NTO is due to transient anaerobic conditions. With the addition

of carbon and nitrogen, the cells that had grown in the first 15 days suddenly metabolized these nutrients, using up the available oxygen and potentially creating anaerobic conditions. Without oxygen present, NTO is readily converted to ATO in soil slurries, and this is likely what occurred when the nutrients were added.<sup>18</sup>

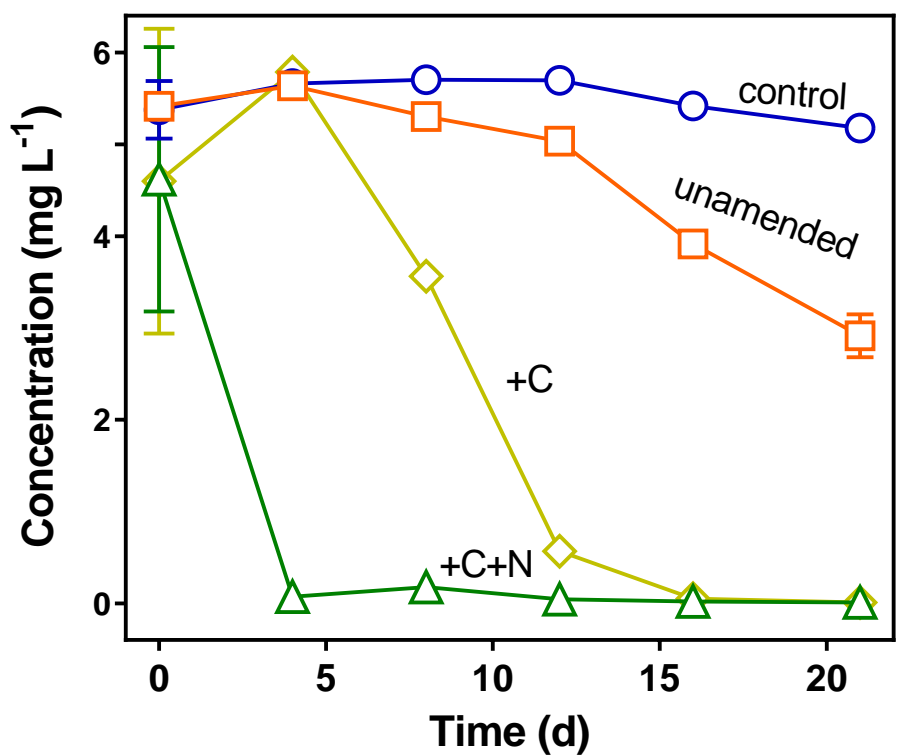


Figure 49. Degradation of DNAN by acclimated soil slurries with various carbon (C, 10 mM glucose and 5 mM succinate) and nitrogen (N, 5 mM NH<sub>4</sub>Cl) regimes in MSM media. Unamended contains DNAN and MSM, while the killed control contains DNAN, MSM, and 5 mg L<sup>-1</sup> sodium azide.

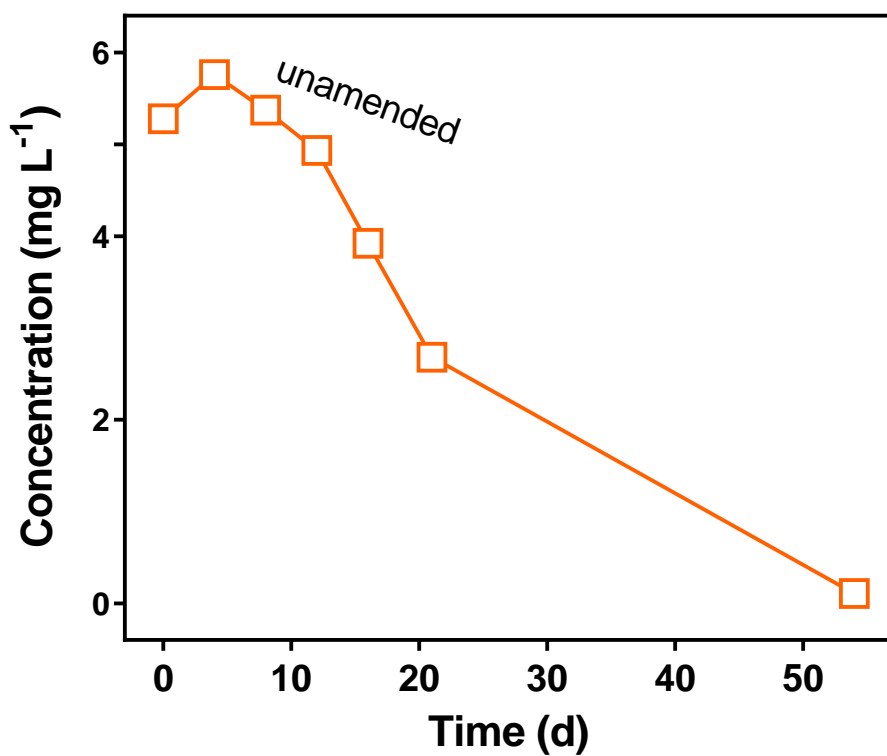


Figure 50. DNAN degradation in minimal salts media without added carbon or nitrogen from Figure 49 over a longer time period. Serial dilutions of the unamended soil slurries were taken after 54 days (after 98% DNAN degradation).

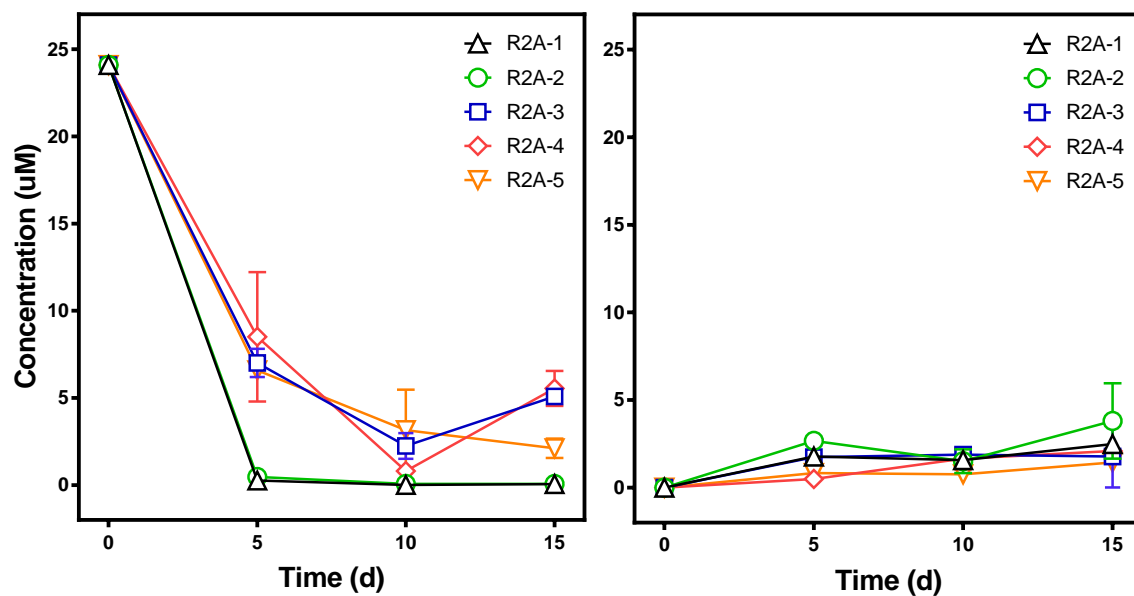


Figure 51. Degradation of DNAN (left panel) and resulting sum of 2-ANAN and 4-ANAN (right panel) in liquid media by soil slurry isolates grown on R2A agar.



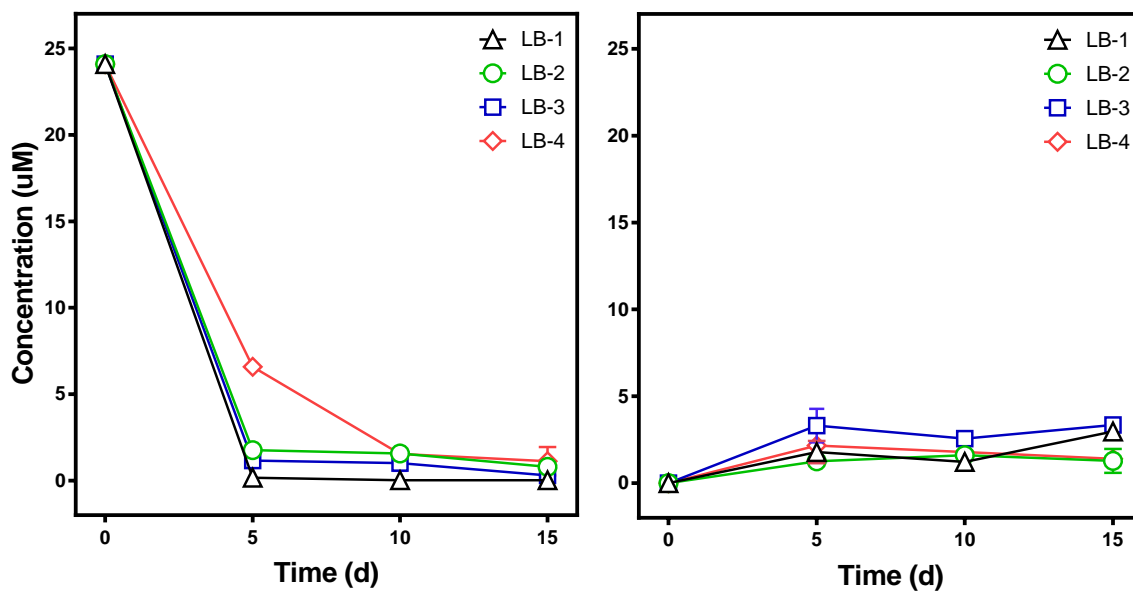


Figure 52. Degradation of DNAN (left panel) and resulting sum of 2-ANAN and 4-ANAN (right panel) in liquid media by soil slurry isolates grown on LB agar.

In addition to NTO, acclimated soil was also tested for DNAN degradation potential. All slurries except the azide control degraded DNAN within three weeks (Figure 49). Carbon and nitrogen amendments increased the rate of degradation compared to the unamended slurry, with carbon speeding the degradation and the C+N amended slurry proceeding quickly to less than 2% of the initial DNAN at the first sampling point of four days. The carbon-only amendment had a lag time of approximately four days, and then DNAN decreased through the rest of the experiment.

The soil slurry results were not surprising, and the data were strikingly similar to a previous study of unacclimated DNAN soil slurries, where added carbon increased the rate of degradation and additional nitrogen further enhanced the degradation of DNAN.<sup>28</sup> Our goal was to identify organisms that could use DNAN as the sole source of carbon and nitrogen, so we measured the DNAN in the unamended soil slurry for 54 days, until DNAN was 98% transformed (Figure 50).

Serial dilutions of the unamended soil slurry were plated on R2A and LB agar plates, and isolates were screened for their ability to degrade DNAN. Surprisingly, every isolate tested was able to transform DNAN (Figure 51, Figure 52). To determine if the bacteria simply reduced DNAN to amino reduction products, we measured 2-amino-4-nitroanisole (2-ANAN) and 4-amino-2-nitroanisole (4-ANAN) in the bioreactors (Figure 51 and Figure 52). Interestingly, little to no amino reduction products were present, indicating that the bacteria either transformed DNAN *via* a different metabolic pathway or that the amino-nitroanisoles were further degraded. These bacteria were all able to easily degrade DNAN without a buildup of ANANs. The results should be taken cautiously though, because previous studies have demonstrated a wide array of biotransformation products from DNAN, most with unknown toxicity and bioavailability.<sup>27, 28, 33</sup> Further work should be done with <sup>14</sup>C-labeled DNAN to determine if DNAN was mineralized to CO<sub>2</sub>, or if other organic products built up after DNAN disappearance. As demonstrated with various compounds, disappearance of the parent product does not indicate complete removal of risk.<sup>177-179</sup> A more in-depth understanding of the transformation pathways, formed metabolites, and necessary degradation conditions for each bacteria are needed to inform field applicability of any of the organisms for bioremediation applications.

## CHAPTER 7: CONCLUSIONS

The U.S. Army is replacing older explosives with insensitive high explosives including 2,4-dinitroanisole (DNAN), 3-nitro-1,2,4-triazol-5-one (NTO), and nitroguanidine (NQ).<sup>19</sup> These compounds are more soluble in water and less likely to sorb to soil, making groundwater contamination with the explosives likely.<sup>19, 20, 59, 61, 76</sup> Detonation of the explosives also leaves more unexploded ordnance than traditional formulations, raising concern about pollution of training range sites.<sup>23</sup> Since relatively little is known about the environmental fate and remediation of the compounds, this work aimed to understand biotic and photolytic transformations of the compounds to inform fate and transport predictions, develop remedial technologies, and to understand relevant photo-transformations in engineered and natural systems.

Based on my work on DNAN biotransformation, tracking the mass of DNAN in a given environmental system will be difficult, with low abundances of a diverse suite of metabolic products. Reduction of the *para*-nitro group of DNAN was observed in all biotic systems studied here. This reduction pathway could influence toxicity, bioavailability, and sorption characteristics of the resulting transformation products, and should not be ignored in future studies of DNAN transformation.

We isolated and cultured a *Rhizobium* sp. on solid media and in liquid media, suggesting promise for bioaugmenting soils contaminated with DNAN. A longer incubation with DNAN as the sole carbon and nitrogen source could result in DNAN mineralization, especially considering that the microbe could grow on DNAN as the sole source of carbon and nitrogen. However, the broad range of DNAN metabolites identified in this study and the lack of aromatic ring alteration with carbon and nitrogen added in this short assay suggests that the degradation pathway should be more fully elucidated before field-scale implementation of phytoremediation or bioaugmentation with *R. litchii*.

Chapter three is the first report we are aware of that demonstrated DNAN degradation by a fungus. *Penicillium* sp. KH1 isolated from willow tree cuttings quickly degraded DNAN in solution. Thirteen previously unknown degradation products were identified and confirmed with stable isotope-labeled substrate. DNAN was transformed *via* many reaction pathways including *ortho*- and *para*-nitroreduction, demethylation, acetylation,

hydroxylation, malonylation, and sulfation. Transformation of DNAN by the fungus did result in degradation of the parent compound, but also formed metabolites of unknown persistence and toxicity. Further work would be needed to implement remediation with *Penicillium* sp. KH1. Finally, incubation with metabolites as primary substrates is an effective way to confirm metabolite isomerism and elucidate metabolic pathways.

Knowledge of DNAN plant uptake and transformation products will inform phytoremediation feasibility assessments for DNAN-contaminated sites. Our work, and the work of others, showed plants take up DNAN from contaminated soil and water, but further work with field-relevant species are required to confirm the possibility of DNAN phytoremediation.<sup>17, 36</sup> Beyond phytoremediation, plants can also be used as inexpensive sensors to monitor contaminant presence and concentration gradients without costly and invasive sampling techniques.<sup>145-148</sup> Our work suggests that measuring 2-ANAN or DNAN inside plant tissues would under-predict actual DNAN uptake and metabolism, making correlations to porewater DNAN concentration problematic without further investigation, and this method would result in conservative estimates of phytoremediation efficacy. Our discovery of photo-denitration of DNAN indicates that photolysis may be an overlooked mechanism for transforming and detoxifying contaminants taken up by plants under field conditions. Although a minor proportion of the DNAN was transformed *via* this pathway, the mechanism could be more important for non-metabolized compounds or photoactive metabolites that would otherwise be shielded from sunlight in soil or porewater.

Acclimation of soil microorganisms to nitroaromatics was observed in Chapter 6. After nine months of exposure to various explosive compounds, soil slurries were able to degrade both DNAN and NTO. The observed degradation is promising and may indicate that exposed soil microorganisms can adapt to be able to degrade the new explosives under field conditions and longer-term exposures. We demonstrated NTO reduction and oxidation in air-exposed, shaking bioreactors, but potential anaerobic niches may explain the reduction of NTO to amino-triazolone (ATO). Bioaugmentation of aerobic NTO-degraders could prove an effective means for remediation of NTO, as ATO is mineralized under aerobic conditions.<sup>18</sup> To our knowledge, this is the first demonstration of aerobic oxidation of NTO to hydroxyl-triazolone (urazole) in a bacterium. This reaction has been observed in rat liver microsomes under aerobic conditions, but never demonstrated *in vivo*

or *in situ*.<sup>44</sup> Interestingly, one isolated *Bacillus* sp. degraded both hydroxyl-triazolone and ATO to urea, presumably using the same enzyme(s) to catalyze the degradation of these primary NTO metabolic products. The other *Bacillus* sp. degraded ATO to undetected products, indicating an alternate pathway of ATO degradation. Previously, ATO was shown to be mineralized in some aerobic soil slurries.<sup>18</sup>

In terms of DNAN biotransformation by soil slurries, acclimation of the soil to nitroaromatic-containing wastewater appeared to enhance the potential for DNAN bioremediation. Multiple isolates were capable of growing on DNAN as the sole carbon and nitrogen source, degrading DNAN to products other than 2-ANAN and 4-ANAN. Further work is needed to confirm mineralization of DNAN by utilizing <sup>14</sup>C-DNAN and/or tracking intermediate ring cleavage products before the organisms could be used for bioremediation.

Photolysis of NTO and NQ produced interesting results, including unexpected mechanisms of direct photolysis for both compounds. NTO produced singlet oxygen upon irradiation, and was in turn degraded by singlet oxygen. NTO potentially reacts through a radical intermediate that can be reduced back to the parent compound by dissolved organic matter. Direct photolysis of NTO potentially proceeds through a triplet excited state, which is quenched by sorbic acid. Singlet oxygenation of NTO produces nitrite in stoichiometric yield, while direct photolysis produced nitrite, nitrate, and ammonium from NTO. Photolysis of NTO also produced hydroxy-triazolone, which was degraded quickly by singlet oxygen, direct photolysis, and nitrite-mediated indirect photolysis. NQ was degraded relatively quickly in simulated sunlight, and produced nitrite, nitrate, and guanidine. The results of NQ photolysis indicate that higher pH produces volatile or unknown nitrogen-containing products, while at lower pH, the nitro group of NQ appears to remain as nitrite or nitrate.

## **Future work**

### *Bioremediation*

More research is needed to enable field remediation of the new explosives. Phytoremediation studies should focus on soil systems to understand the role of concomitant soil transformations of the compounds in addition to species-dependent

uptake and transformation pathways. DNAN remediation should be demonstrated with full mass balances, which could be aided by  $^{14}\text{C}$ -labeled DNAN. Microorganisms are clearly capable of degrading DNAN in aerobic conditions, but more work is needed to characterize enzymes and environmental conditions that promote mineralization of the compound. Bioaugmented phytoremediation may be possible, but no mineralizing endophytes have been isolated to date. More understanding is needed for DNAN degradation pathways and in bulk soils, as some  $^{14}\text{C}$ -DNAN is incorporated into humic acid, but more is irreversibly bound under anaerobic conditions than aerobic conditions. The aqueous  $^{14}\text{C}$  fraction also contains unknown polar transformation products.<sup>68</sup>

NTO bioremediation is not well understood, and requires further research. It is unclear which nitroreductase enzymes are responsible for NTO reduction to ATO. It is unclear if cytochrome *P*-450s are responsible for NTO oxidation to hydroxy-triazolone (urazole), and a completely aerobic mineralization pathway has yet to be demonstrated. Future work on NTO remediation should include assessing potential aerobic transformation of NTO. Additionally, more work is needed to evaluate irreversible incorporation of NTO into soil as bound residues, isolating and characterizing NTO-degrading organisms or consortia, and optimizing soil (or reactor) conditions for NTO biodegradation. Another area of focus could be on genetic biomarkers for ATO degradation, as some soils readily degrade ATO, but others carry out no degradation of the compound. Further, induction of NTO degradation has yet to be studied to the best of my knowledge. If enzymes responsible for NTO degradation can be identified, it may be possible to induce such enzymes using exogenously applied substrates.

NQ bioremediation is also difficult in practice. One isolate from non-contaminated soil has been shown to mineralize NQ.<sup>53</sup> But, the isolate was studied under laboratory conditions, and may not be effective in a field situation. If this specific organism is successful, monitoring ambient  $\text{N}_2\text{O}$  during bioremediation may be a potential way to track bioremediation success and progress, as  $\text{N}_2\text{O}$  was a prominent biodegradation product. For all three compounds, stable isotope fractionation would also inform field-relevant processes, enabling attribution of parent compound disappearance to biotic or abiotic processes.

Phytoremediation of DNAN, NQ and NTO was demonstrated in this work, with uptake or transformation possible in all plant systems studied here. DNAN is readily taken up and transformed by willow trees and *Arabidopsis* plants. We identified phase II metabolites of DNAN in plants, indicating that DNAN is amenable to plant degradation and detoxification. NQ is taken up and is not transformed by switchgrass under the conditions studied here, indicating that NQ concentrations in grass may be an indicator of soil and groundwater contamination. NQ may also be subject to phytophotolysis in leaf tissues because RDX has been shown to photo-degrade in grass in field conditions.<sup>126</sup> In addition to NQ, NTO was also taken up or transformed by switchgrass seedlings. Further work, especially in soil systems, is needed to inform field-relevant phytoremediation efficiencies. Plants could also be used as indicators for soil contamination by phytoforensic techniques. Future work should focus on NTO mass balances inside plants to understand if NTO is solely taken up by switchgrass or if plants transform NTO as well. Studies should also determine if NTO or NQ can be leached from dead plant material or if the compounds inside plants could pose risk for ingestion by mammals.

### *Photolysis*

For NQ, more work is needed to characterize the transformation products and mechanisms of NQ photolysis. Conflicting reports of products and photochemical breakdown of NQ under different conditions leave questions about how to treat NQ with UV, and how NQ will break down in sunlit surface waters. Work should focus on organic products, which most likely lead to the observed aquatic toxicity of photolysates. The effect of wavelength on NQ photolysis products and rates should also be investigated, as treatment by UV-LEDs could potentially prove to be a cost-effective treatment option for NQ-containing wastewaters. For NTO, further work should include identification of organic photo-transformation products, which also may be responsible for the increased aquatic toxicity of NTO after UV irradiation. Understanding the products and their occurrence under different irradiance conditions will further confirm relevant mechanisms of NTO photolysis.

Overall, the toxicity of the new explosives across all organisms is lower than the traditional compounds, but the increased opportunity for unexploded ordnance remains a

concern. Fast leaching and groundwater transport of NTO and NQ may lead to expansive groundwater plumes, making remediation of the explosives an expensive and difficult endeavor without proper management of training ranges and prevention of spills at manufacturing facilities.



## APPENDIX A: CHEMICAL SYNTHESIS AND CHARACTERIZATION

DNAN and NTO synthesis and NMR analyses were performed by Xueshu Li and Hans-Joachim Lehmler in the Department of Occupational & Environmental Health, The University of Iowa

*Synthesis and Characterization of Isotope Labeled 2,4-Dinitroanisole (DNAN)[<sup>13</sup>C<sub>6</sub>]-DNAN and [<sup>15</sup>N<sub>2</sub>]-DNAN*

### General method

The <sup>1</sup>H and <sup>13</sup>C NMR spectra were recorded on a Bruker Avance DRX-400 spectrometer in the University of Iowa Central NMR Research Facility (Iowa City, IA). Tetramethylsilane (TMS) was used as an internal standard. The HR-MS data were recorded and analyzed in the electrospray ionization mode on a Waters Q-TOF Premier mass spectrometer. The GC-MS analysis of all compounds was performed in the electron impact (EI) mode on an Agilent 6890N Gas Chromatograph coupled with an Agilent 5975 Mass Selective Detector (Agilent Technologies, CA) equipped with a Supelco SLB-5m column (5% diphenyl/95% methyl siloxane) with a dimensions of 30 m x 250 μm x 0.25 μm. The following conditions were used for the gas chromatographic analysis: starting temperature, 80 °C; final temperature, 300 °C; heating rate, 20 °C/min. The injector temperature was 280 °C and the MS temperatures were 280, 230, and 150 °C for transfer line, source, and quadrupole, respectively.

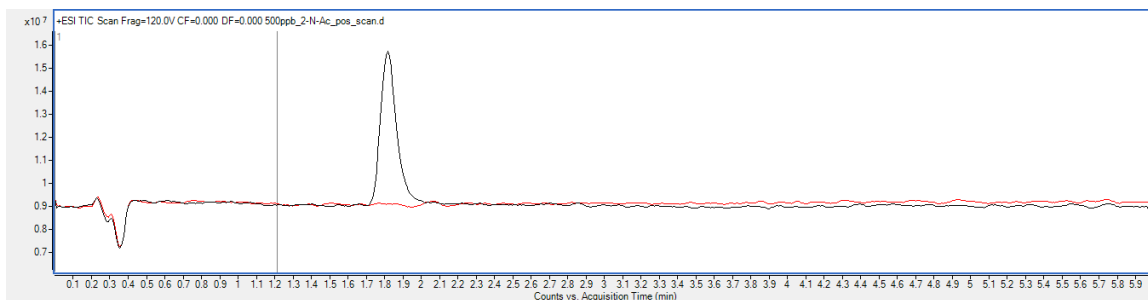


Figure A1. LC-MS scan from  $m/z$  40-500 in positive electrospray ionization mode showing the purity of 2-N-Ac-NAN synthesized as described in Chapter 2 (blank is in red).

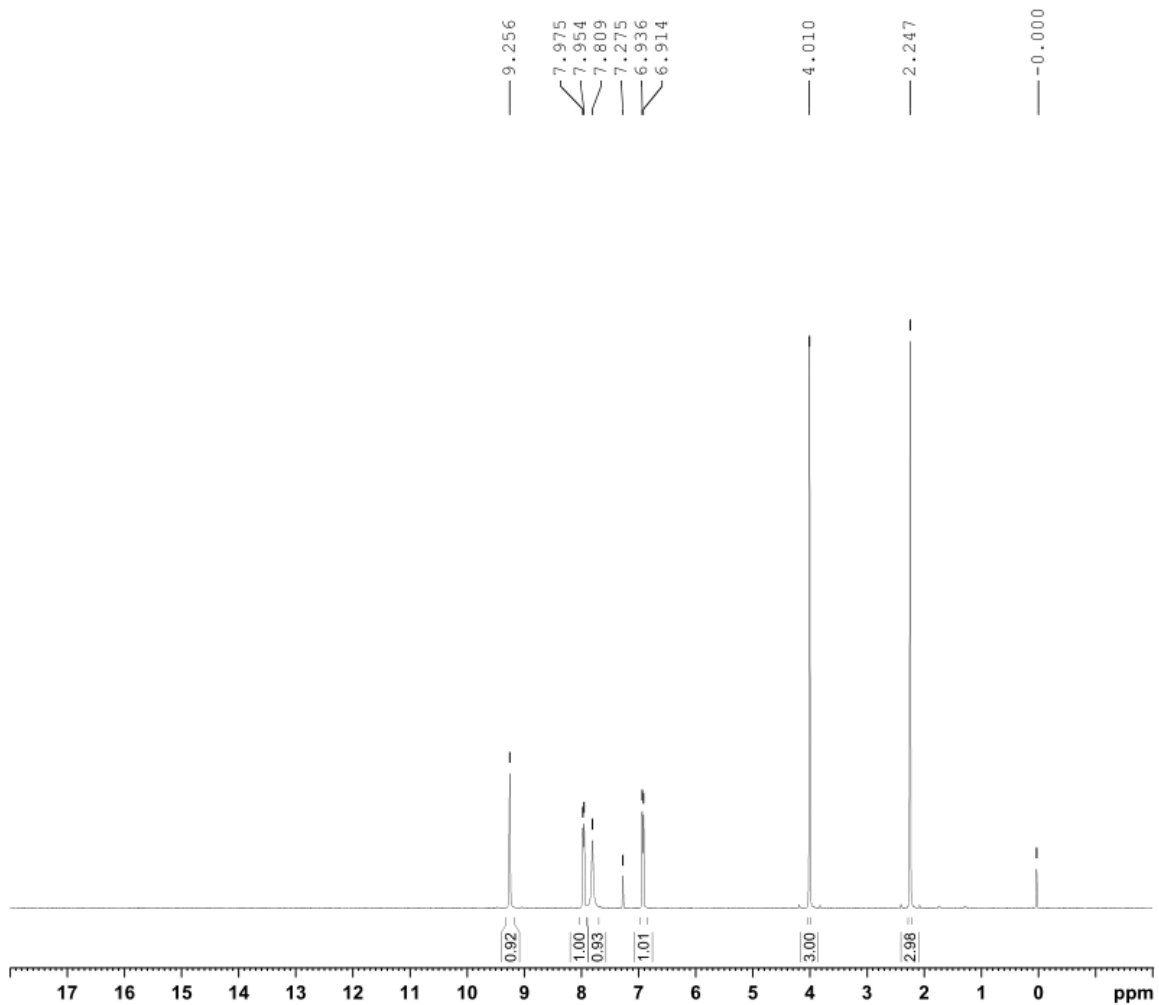


Figure A2.  $^1\text{H}$  NMR spectrum of 2-NAc-NAN.

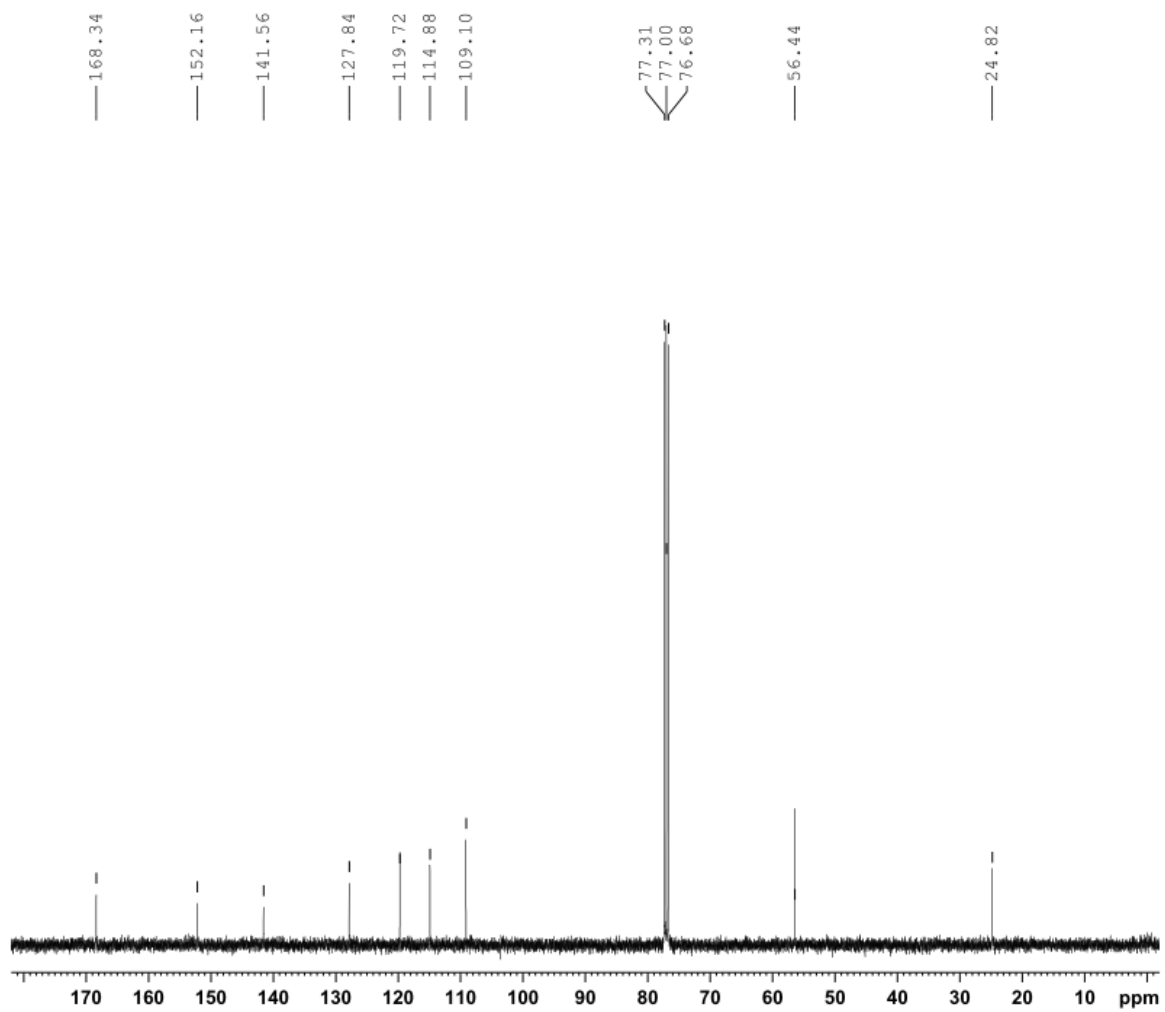


Figure A3.  $^{13}\text{C}$  NMR spectrum of 2-NAc-NAN..

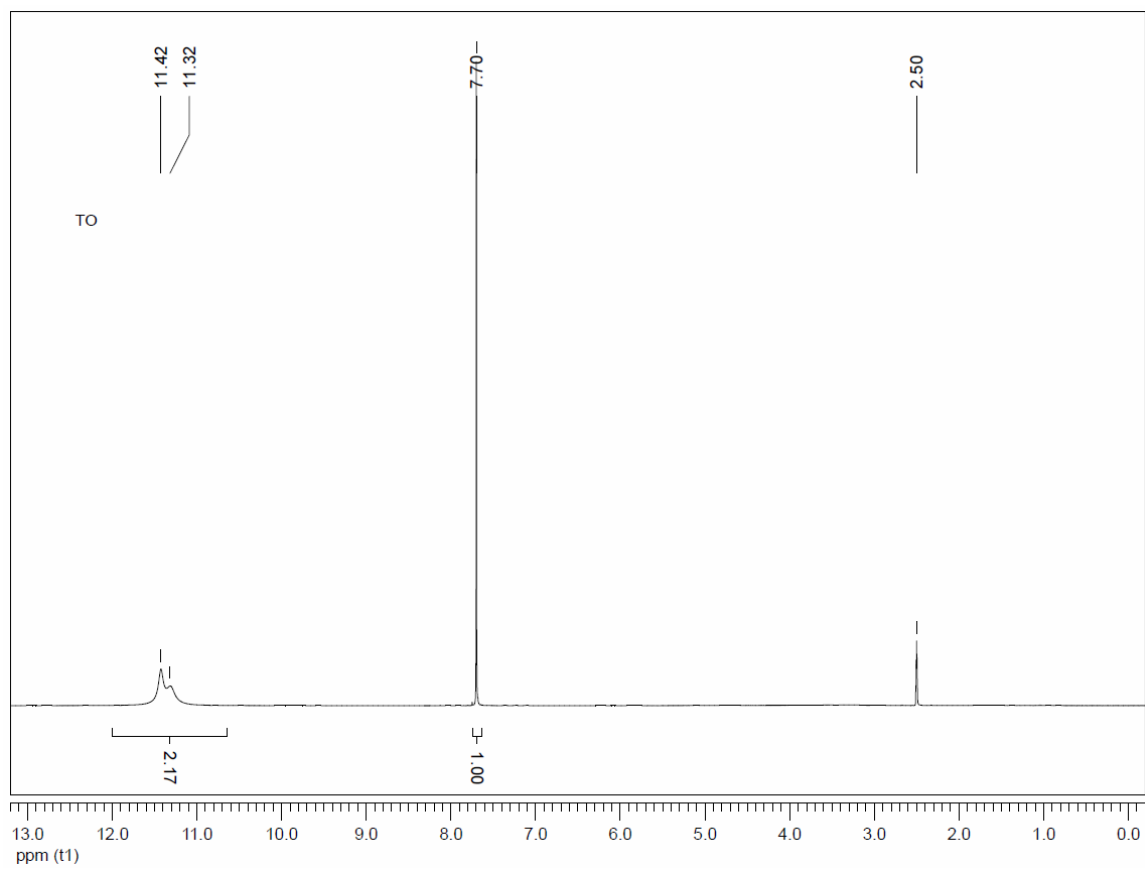


Figure A4.  $^1\text{H}$  NMR of 1,2,4-triazolone (TO).

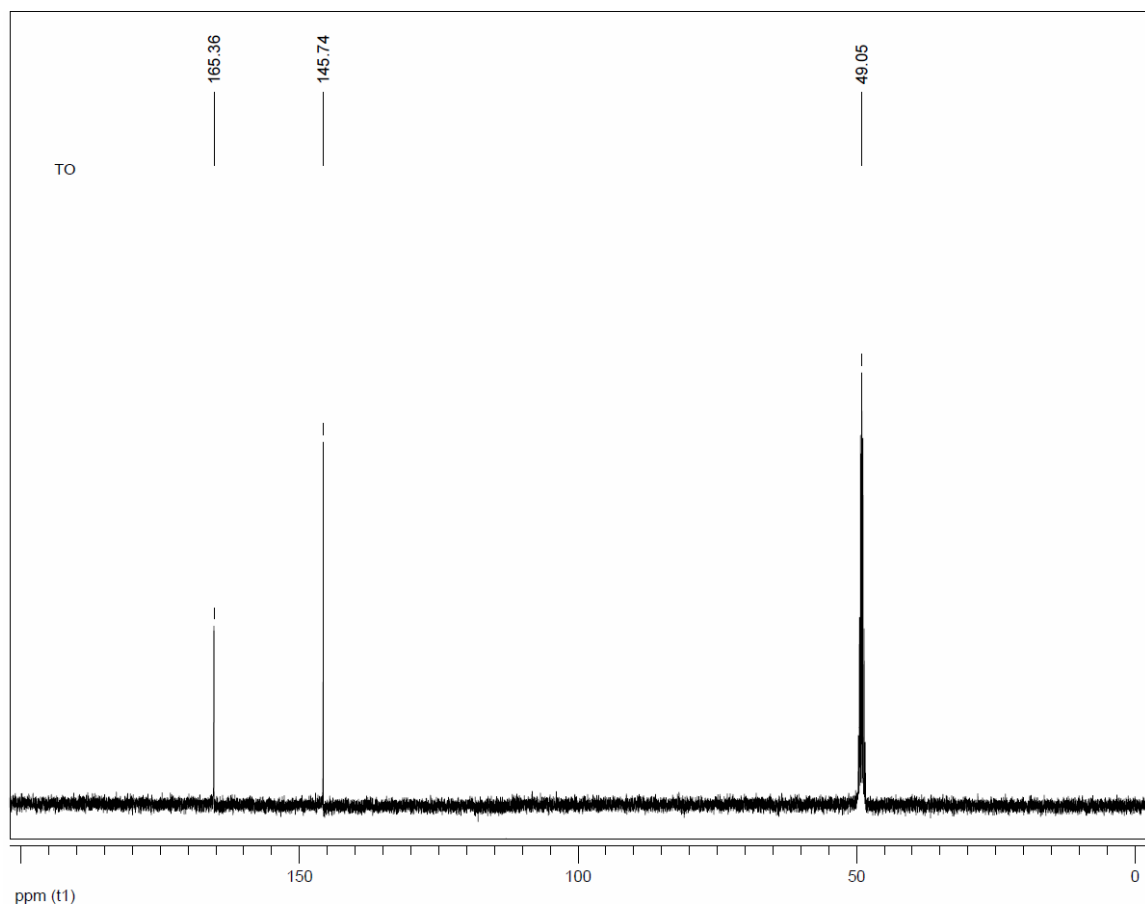


Figure A5.  $^{13}\text{C}$  NMR of 1,2,4-triazolone (TO).

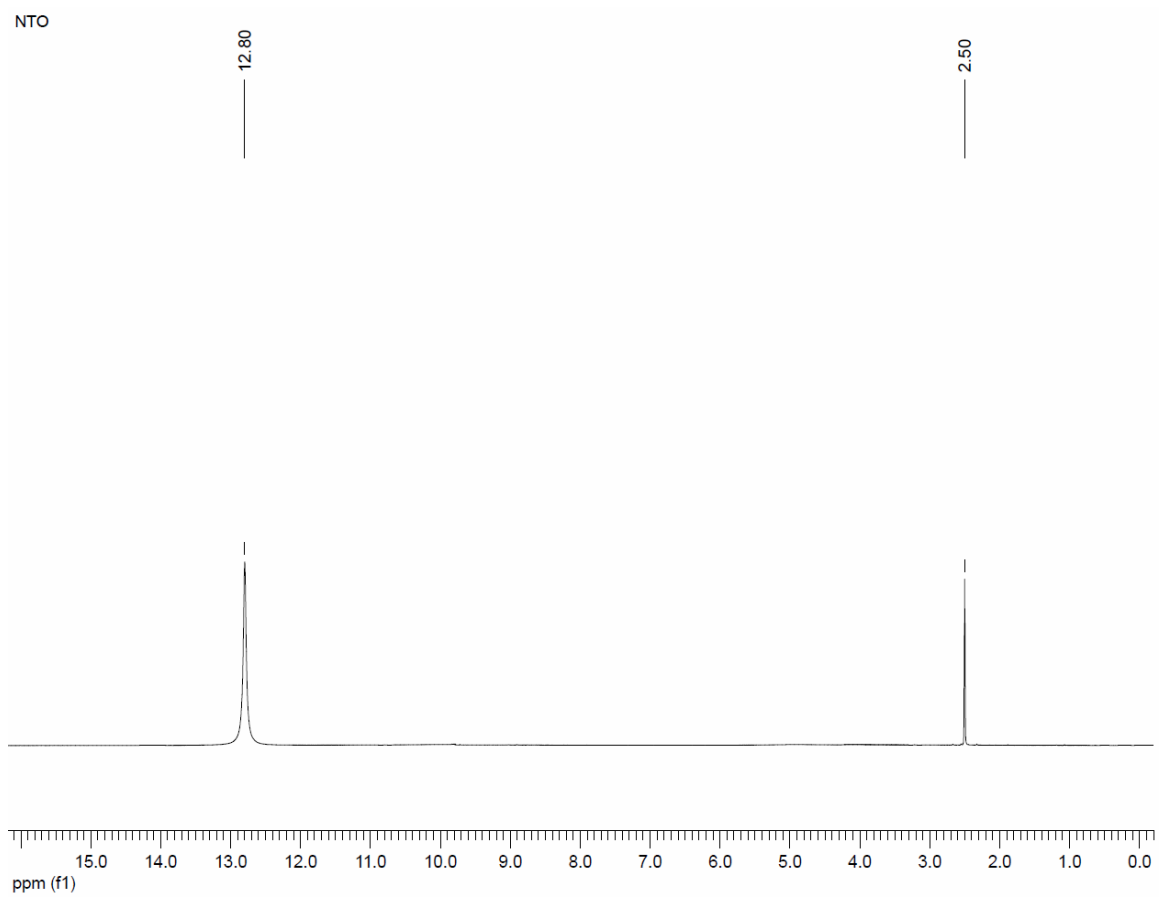


Figure A6.  $^1\text{H}$  NMR of 3-nitro-1,2,4-triazol-5-one (NTO).

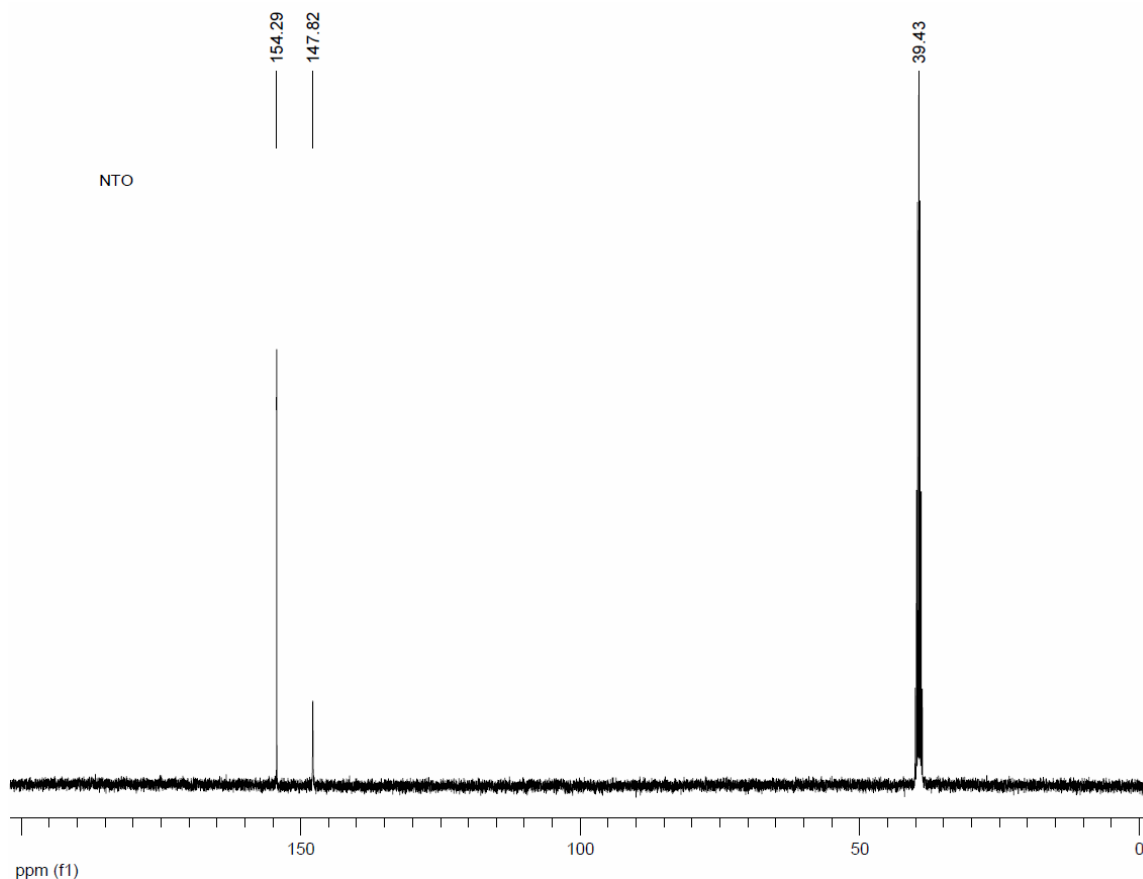


Figure A7.  $^{13}\text{C}$  NMR of 3-nitro-1,2,4-triazol-5-one (NTO).

Elemental Composition Report

Page 1

Single Mass Analysis

Tolerance = 5.0 mDa / DBE: min = -1.5, max = 100.0  
 Element prediction: Off  
 Number of isotope peaks used for i-FIT = 3

Monoisotopic Mass, Even Electron Ions  
 86 formula(e) evaluated with 3 results within limits (all results (up to 1000) for each mass)  
 Elements Used:

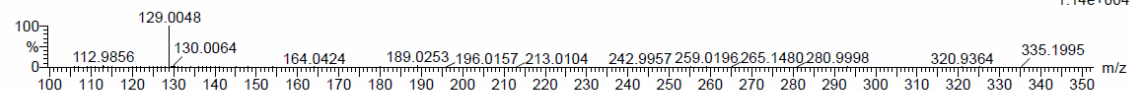
C: 0-120 H: 0-200 N: 0-20 O: 0-20

Lehmler/Li

NTO

T03311504 22 (0.441) Cm (21:34)

1: TOF MS ES-  
1.14e+004



Minimum: -1.5  
 Maximum: 100.0

Mass	Calc. Mass	mDa	PPM	DBE	i-FIT	i-FIT (Norm)	Formula
129.0049	129.0049	0.0	0.0	4.5	398.4	0.0	C2 H N4 O3
	129.0035	1.4	10.9	-0.5	401.8	3.3	C H5 O7
	129.0089	-4.0	-31.0	8.5	403.2	4.8	C7 H N2 O

Figure A8. High resolution mass spectra of 3-nitro-1,2,4-triazol-5-one (NTO).



## APPENDIX B: SUPPLEMENTARY RESULTS

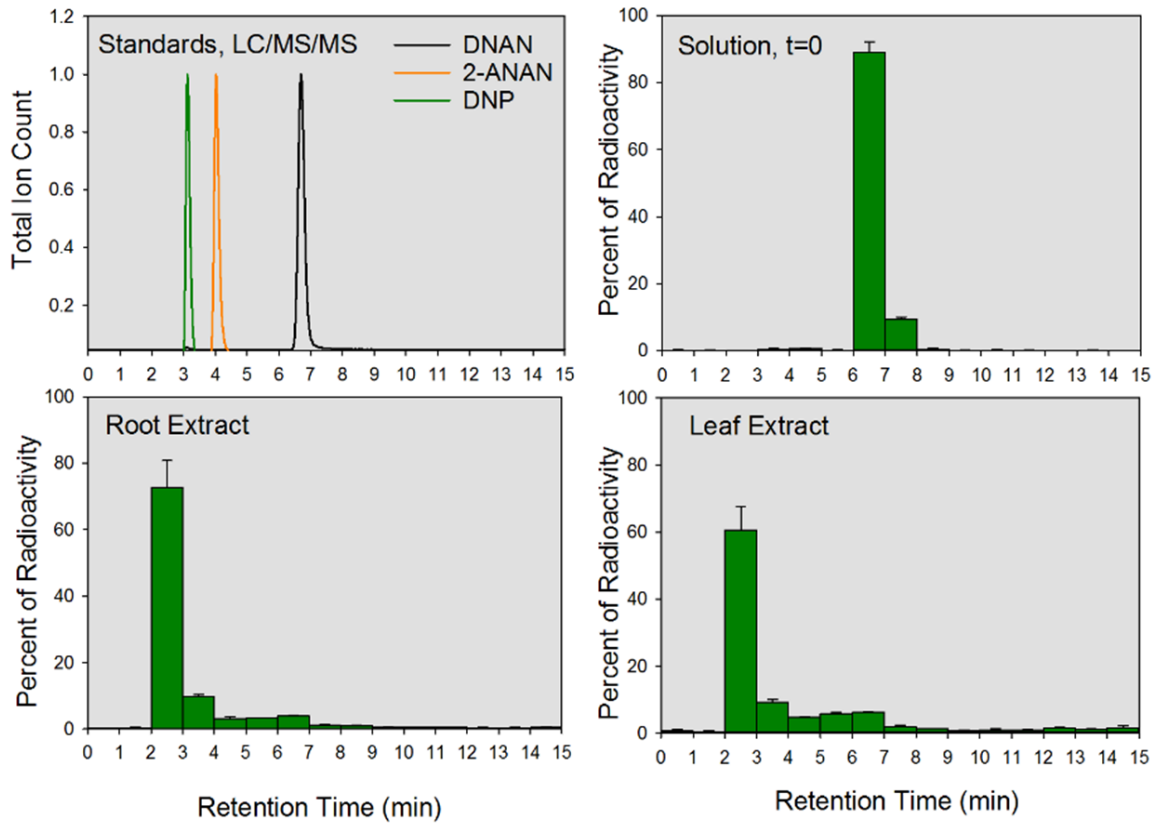


Figure B1. Radioactivity in liquid chromatography fractions from willow tree root and leaf extracts after four days of exposure to  $[^{14}\text{C}_6]\text{DNAN}$ . Both root and leaf fractions had significant transformation of DNAN indicated by shorter retention times. DNP was less than 5% of the radioactivity in the 2-4 min time bins, indicating significant unknown metabolites.

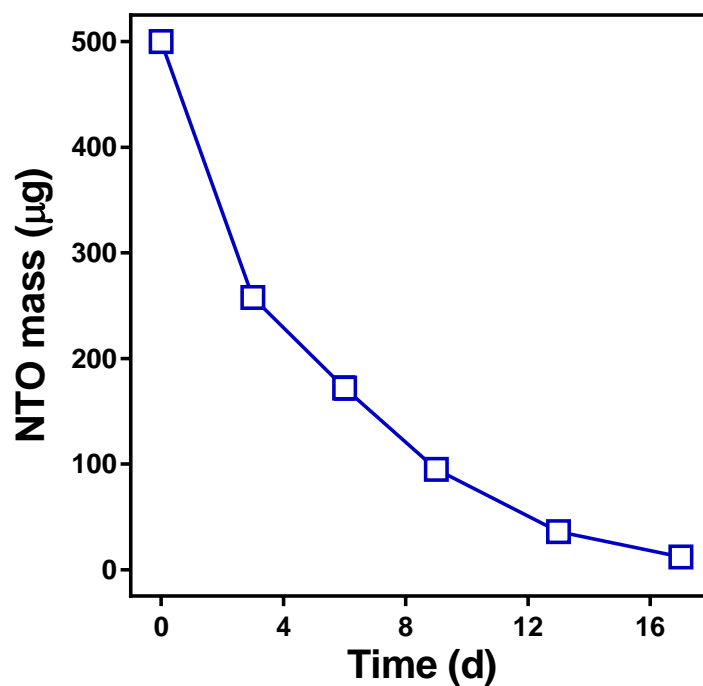


Figure B2. Uptake or root transformation of NTO by switch grass (*Panicum virgatum* ‘Alamo’). Grass was grown from seed by overnight stratification in DI water at 4 °C, and then grown in potting soil for 6 weeks. Four individual grasses were selected and transferred to 50 mL hydroponic 0.25x Hoaglands solution in a 100 mL, black-painted beaker sealed with a foam plug for two weeks of acclimation. Then, the four replicate grasses were exposed to 10 mg L<sup>-1</sup> NTO in 0.25x Hoaglands solution for 17 days, and samples were withdrawn and analyzed by HPLC over time to evaluate uptake and transformation by the switchgrass. Standard error of the means falls within the symbols.

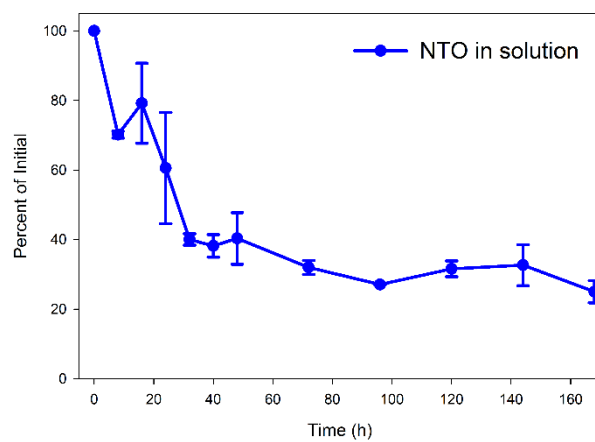


Figure B3. Degradation of  $10 \text{ mg L}^{-1}$  NTO in solution by the *Penicillium* sp. featured in chapter 3 of the thesis. Nitrite, nitrate, and urea were qualitatively identified to form from the reaction.

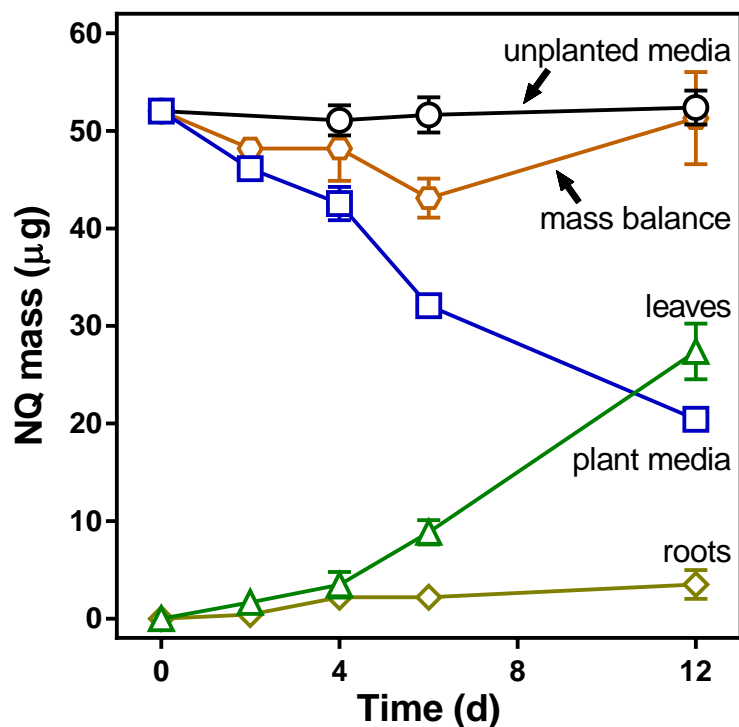


Figure B4. Uptake of  $5 \text{ mg L}^{-1}$  NQ from 0.25x Hoaglands solution by switchgrass (*Panicum virgatum* 'Alamo') and accumulation in leaf and root tissues over 12 days. Grass was grown from seed by overnight stratification in DI water at  $4 \text{ }^{\circ}\text{C}$ , and then grown in potting soil for 6 weeks. Triplicate individual grasses for each time point were selected and transferred to 10 mL hydroponic 0.25x Hoaglands solution in foil-wrapped test tubes sealed with a foam plug for two weeks of acclimation. The grasses were sacrificed in triplicate at each time point, and samples from the medium were analyzed by HPLC over time to evaluate uptake and transformation by the switchgrass. Grass leaves and roots were extracted by the method outlined in chapter 4, and the extracts were analyzed for NQ by LC-MS/MS.

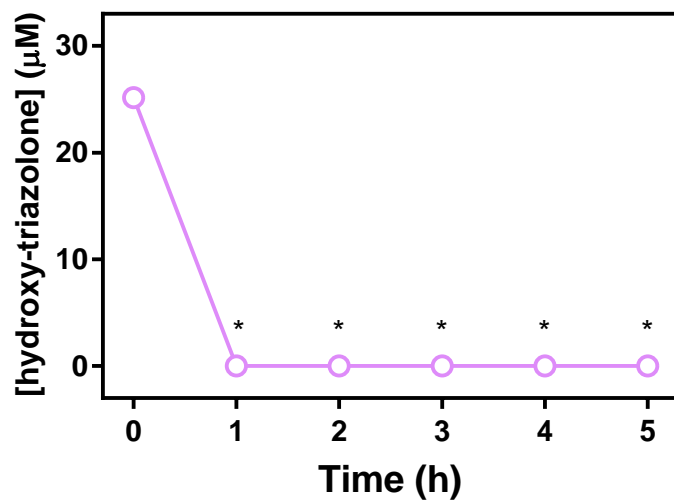


Figure B5. Indirect photolysis of hydroxyl-triazolone (25  $\mu\text{M}$ , 25 mM pH 9 borate buffer) with 10  $\mu\text{M}$  Rose Bengal to generate singlet oxygen under a 200W Xe-Hg lamp with a 400 nm cut-on filter. Asterisks indicate non-detect (LOD < 0.1  $\mu\text{M}$ ).

## REFERENCES

1. Report GAO-04-147 Military Munitions: DOD Needs to Develop a Comprehensive Approach for Cleaning Up Contaminated Sites. In, U.S. General Accounting Office **2003**.
2. Pichtel, J., Distribution and Fate of Military Explosives and Propellants in Soil: A Review. *Applied and Environmental Soil Science* **2012**, 2012, 33.
3. Rodgers, J. D.; Bunce, N. J., Treatment Methods for the Remediation of Nitroaromatic Explosives. *Water Research* **2001**, 35, (9), 2101-2111.
4. Lewis, T. A.; Newcombe, D. A.; Crawford, R. L., Bioremediation of Soils Contaminated with Explosives. *Journal of Environmental Management* **2004**, 70, (4), 291-307.
5. Gandia-Herrero, F.; Lorenz, A.; Larson, T.; Graham, I. A.; Bowles, D. J.; Rylott, E. L.; Bruce, N. C., Detoxification of the Explosive 2,4,6-Trinitrotoluene in *Arabidopsis*: Discovery of Bifunctional O- and C-Glucosyltransferases. *The Plant Journal* **2008**, 56, (6), 963-974.
6. Hannink, N. K.; Rosser, S. J.; Bruce, N. C., Phytoremediation of Explosives. *Critical Reviews in Plant Sciences* **2002**, 21, (5), 511-538.
7. Thorn, K. A.; Kennedy, K. R., <sup>15</sup>N NMR Investigation of the Covalent Binding of Reduced TNT Amines to Soil Humic Acid, Model Compounds, and Lignocellulose. *Environmental Science & Technology* **2002**, 36, (17), 3787-3796.
8. Honeycutt, M. E.; Jarvis, A. S.; McFarland, V. A., Cytotoxicity and Mutagenicity of 2,4,6-Trinitrotoluene and Its Metabolites. *Ecotoxicology and Environmental Safety* **1996**, 35, (3), 282-287.
9. Tan, E. L.; Ho, C. H.; Griest, W. H.; Tyndall, R. L., Mutagenicity of Trinitrotoluene and Its Metabolites Formed During Composting. *Journal of Toxicology and Environmental Health* **1992**, 36, (3), 165-175.
10. Burken, J. G.; Schnoor, J. L., Predictive Relationships for Uptake of Organic Contaminants by Hybrid Poplar Trees. *Environmental Science & Technology* **1998**, 32, (21), 3379-3385.
11. Thompson, P. L.; Ramer, L. A.; Schnoor, J. L., Uptake and Transformation of TNT by Hybrid Poplar Trees. *Environmental Science & Technology* **1998**, 32, (7), 975-980.
12. Thompson, P. L.; Ramer, L. A.; Schnoor, J. L., Hexahydro-1,3,5-trinitro-1,3,5-triazine Translocation in Poplar Trees. *Environmental Toxicology and Chemistry* **1999**, 18, (2), 279-284.
13. Van Aken, B.; Yoon, J. M.; Just, C. L.; Schnoor, J. L., Metabolism and Mineralization of Hexahydro-1,3,5-trinitro-1,3,5-triazine Inside Poplar Tissues (*Populus deltoides* × *nigra* DN-34). *Environmental Science & Technology* **2004**, 38, (17), 4572-4579.
14. Yoon, J. M.; Oh, B.-T.; Just, C. L.; Schnoor, J. L., Uptake and Leaching of Octahydro-1,3,5,7-tetranitro-1,3,5,7-tetrazocine by Hybrid Poplar Trees. *Environmental Science & Technology* **2002**, 36, (21), 4649-4655.

15. Rylott, E. L.; Jackson, R. G.; Edwards, J.; Womack, G. L.; Seth-Smith, H. M. B.; Rathbone, D. A.; Strand, S. E.; Bruce, N. C., An Explosive-Degrading Cytochrome P450 Activity and its Targeted Application for the Phytoremediation of RDX. *Nat Biotech* **2006**, *24*, (2), 216-219.
16. Gunning, V.; Tzafestas, K.; Sparrow, H.; Johnston, E. J.; Brentnall, A. S.; Potts, J. R.; Rylott, E. L.; Bruce, N. C., *Arabidopsis* Glutathione Transferases U24 and U25 Exhibit a Range of Detoxification Activities with the Environmental Pollutant and Explosive, 2,4,6-Trinitrotoluene. **2014**.
17. Dodard, S. G.; Sarrazin, M.; Hawari, J.; Paquet, L.; Ampleman, G.; Thiboutot, S.; Sunahara, G. I., Ecotoxicological Assessment of a High Energetic and Insensitive Munitions Compound: 2,4-Dinitroanisole (DNAN). *Journal of Hazardous Materials* **2013**, *262*, (0), 143-150.
18. Krzmarzick, M. J.; Khatiwada, R.; Olivares, C. I.; Abrell, L.; Sierra-Alvarez, R.; Chorover, J.; Field, J. A., Biotransformation and Degradation of the Insensitive Munitions Compound, 3-Nitro-1,2,4-triazol-5-one, by Soil Bacterial Communities. *Environmental Science & Technology* **2015**, *49*, (9), 5681-5688.
19. Hawari, J.; Monteil-Rivera, F.; Perreault, N. N.; Halasz, A.; Paquet, L.; Radovic-Hrapovic, Z.; Deschamps, S.; Thiboutot, S.; Ampleman, G., Environmental Fate of 2,4-Dinitroanisole (DNAN) and its Reduced Products. *Chemosphere* **2014**, *119*, (0), 16-23.
20. Taylor, S.; Park, E.; Bullion, K.; Dontsova, K., Dissolution of Three Insensitive Munitions Formulations. *Chemosphere* **2015**, *119*, (0), 342-348.
21. Davies, P. J.; Provatas, A., Characterisation of 2,4-Dinitroanisole: An Ingredient for use in Low Sensitivity Melt Cast Formulations. In Weapons System Division: Edinburgh, South Australia, **2006**.
22. Taylor, S.; Ringelberg, D. B.; Dontsova, K.; Daghlian, C. P.; Walsh, M. E.; Walsh, M. R., Insights into the Dissolution and the Three-Dimensional Structure of Insensitive Munitions Formulations. *Chemosphere* **2013**, *93*, (9), 1782-1788.
23. Halasz, A.; Hawari, J.; Perreault, N. N., New Insights into the Photochemical Degradation of the Insensitive Munition Formulation IMX-101 in Water. *Environmental Science & Technology* **2018**, *52*, (2), 589-596.
24. Liang, J.; Olivares, C.; Field, J. A.; Sierra-Alvarez, R., Microbial Toxicity of the Insensitive Munitions Compound, 2,4-Dinitroanisole (DNAN), and its Aromatic Amine Metabolites. *Journal of Hazardous Materials* **2013**, *262*, (0), 281-287.
25. Olivares, C.; Liang, J.; Abrell, L.; Sierra-Alvarez, R.; Field, J. A., Pathways of Reductive 2,4-Dinitroanisole (DNAN) Biotransformation in Sludge. *Biotechnology and Bioengineering* **2013**, *110*, (6), 1595-1604.
26. Olivares, C. I.; Abrell, L.; Khatiwada, R.; Chorover, J.; Sierra-Alvarez, R.; Field, J. A., (Bio)transformation of 2,4-Dinitroanisole (DNAN) in Soils. *Journal of Hazardous Materials* **2016**, *304*, 214-221.
27. Schroer, H. W.; Langenfeld, K. L.; Li, X.; Lehmler, H.-J.; Just, C. L., Stable Isotope-Enabled Pathway Elucidation of 2,4-Dinitroanisole Metabolized by *Rhizobium litchii*. *Environmental Science & Technology Letters* **2015**, *2*, (12), 362-366.
28. Perreault, N.; Manno, D.; Halasz, A.; Thiboutot, S.; Ampleman, G.; Hawari, J., Aerobic Biotransformation of 2,4-Dinitroanisole in Soil and Soil *Bacillus* sp. *Biodegradation* **2012**, *23*, (2), 287-295.

29. Arnett, C. M.; Rodriguez, G.; Maloney, S. W., Analysis of Bacterial Community Diversity in Anaerobic Fluidized Bed Bioreactors Treating 2,4-Dinitroanisole (DNAN) and *N*-Methyl-4-nitroaniline (MNA) Using 16S rRNA Gene Clone Libraries. *Microbes and Environments* **2009**, *24*, (1), 72-75.
30. Platten III, W. E.; Bailey, D.; Suidan, M. T.; Maloney, S. W., Biological Transformation Pathways of 2,4-Dinitroanisole and *N*-Methyl-Paranitro-Aniline in Anaerobic Fluidized-Bed Bioreactors. *Chemosphere* **2010**, *81*, (9), 1131-1136.
31. Fida, T. T.; Palamuru, S.; Pandey, G.; Spain, J. C., Aerobic Biodegradation of 2,4-Dinitroanisole by *Nocardioides* sp. Strain JS1661. *Applied and Environmental Microbiology* **2014**, *80*, (24), 7725-7731.
32. Karthikeyan, S.; Spain, J. C., Biodegradation of 2,4-Dinitroanisole (DNAN) by *Nocardioides* sp. JS1661 in Water, Soil and Bioreactors. *Journal of Hazardous Materials* **2016**, *312*, 37-44.
33. Schroer, H. W.; Langenfeld, K. L.; Li, X.; Lehmler, H.-J.; Just, C. L., Biotransformation of 2,4-Dinitroanisole by a Fungal *Penicillium* sp. *Biodegradation* **2017**, *28*, (1), 95-109.
34. Haïdour, A.; Ramos, J. L., Identification of Products Resulting from the Biological Reduction of 2,4,6-Trinitrotoluene, 2,4-Dinitrotoluene, and 2,6-Dinitrotoluene by *Pseudomonas* sp. *Environmental Science & Technology* **1996**, *30*, (7), 2365-2370.
35. Wang, C. Y.; Zheng, D.; Hughes, J. B., Stability of Hydroxylamino- and Amino-Intermediates from Reduction of 2,4,6-Trinitrotoluene, 2,4-Dinitrotoluene, and 2,6-Dinitrotoluene. *Biotechnology Letters* **2000**, *22*, (1), 15-19.
36. Richard, T.; Weidhaas, J., Dissolution, Sorption, and Phytoremediation of IMX-101 Explosive Formulation Constituents: 2,4-Dinitroanisole (DNAN), 3-Nitro-1,2,4-Triazol-5-One (NTO), and Nitroguanidine. *Journal of Hazardous Materials* **2014**, *280*, (0), 561-569.
37. Schroer, H. W.; Li, X.; Lehmler, H.-J.; Just, C. L., Metabolism and Photolysis of 2,4-Dinitroanisole in *Arabidopsis*. *Environmental Science & Technology* **2017**, *51*, (23), 13714-13722.
38. Kennedy, A. J.; Poda, A. R.; Melby, N. L.; Moores, L. C.; Jordan, S. M.; Gust, K. A.; Bednar, A. J., Aquatic Toxicity of Photo-Degraded Insensitive Munition 101 (IMX-101) Constituents. *Environmental Toxicology and Chemistry* **2017**, *36*, (8), 2050-2057.
39. Olivares, C. I.; Sierra-Alvarez, R.; Alvarez-Nieto, C.; Abrell, L.; Chorover, J.; Field, J. A., Microbial Toxicity And Characterization Of DNAN (Bio)transformation Product Mixtures. *Chemosphere* **2016**, *154*, 499-506.
40. Olivares, C. I.; Sierra-Alvarez, R.; Abrell, L.; Chorover, J.; Simonich, M.; Tanguay, R. L.; Field, J. A., Zebrafish Embryo Toxicity of Anaerobic Biotransformation Products from the Insensitive Munitions Compound 2,4-Dinitroanisole. *Environmental Toxicology and Chemistry* **2016**, *35*, (11), 2774-2781.
41. Lent, E.; Crouse, L.; Hanna, T.; Wallace, S. The Subchronic Oral Toxicity of 2,4-Dinitroanisole (DNAN) in Rats. U.S. Army Public Health Command, **2012**.
42. Kennedy, A. J.; Laird, J. G.; Lounds, C.; Gong, P.; Barker, N. D.; Brasfield, S. M.; Russell, A. L.; Johnson, M. S., Inter- and Intraspecies Chemical Sensitivity: A Case Study Using 2,4-Dinitroanisole. *Environmental Toxicology and Chemistry* **2015**, *34*, (2), 402-411.



43. Stanley, J. K.; Lotufo, G. R.; Biedenbach, J. M.; Chappell, P.; Gust, K. A., Toxicity of the Conventional Energetics TNT and RDX Relative to New Insensitive Munitions Constituents DNAN and NTO in *Rana pipiens* Tadpoles. *Environmental Toxicology and Chemistry* **2015**, *34*, (4), 873-879.
44. Le Campion, L.; Delaforge, M.; Noel, J. P.; Ouazzani, J., Metabolism of <sup>14</sup>C-Labelled 5-Nitro-1,2,4-triazol-3-one (NTO): Comparison Between Rat Liver Microsomes and Bacterial Metabolic Pathways. *Journal of Molecular Catalysis B: Enzymatic* **1998**, *5*, (1-4), 395-402.
45. Le Campion, L.; Vandais, A.; Ouazzani, J., Microbial Remediation of NTO in Aqueous Industrial Wastes. *FEMS Microbiology Letters* **1999**, *176*, (1), 197-203.
46. Richard, T.; Weidhaas, J., Biodegradation of IMX-101 Explosive Formulation Constituents: 2,4-Dinitroanisole (DNAN), 3-Nitro-1,2,4-triazol-5-one (NTO), and Nitroguanidine. *Journal of Hazardous Materials* **2014**, *280*, (0), 372-379.
47. Reddy, G.; Song, J.; Kirby, P.; Lent, E. M.; Crouse, L. C. B.; Johnson, M. S., Genotoxicity Assessment of an Energetic Propellant Compound, 3-Nitro-1,2,4-triazol-5-one (NTO). *Mutation Research/Genetic Toxicology and Environmental Mutagenesis* **2011**, *719*, (1-2), 35-40.
48. Haley, M. V.; Kuperman, R. G.; Checkai, R. T., Aquatic Toxicity of 3-Nitro-1,2,4-triazol-5-one. U.S. Army Research, Development and Engineering Command, **2009**.
49. Lotufo, G. R.; Biedenbach, J. M.; Sims, J. G.; Chappell, P.; Stanley, J. K.; Gust, K. A., Bioaccumulation Kinetics of the Conventional Energetics TNT and RDX Relative to Insensitive Munitions Constituents DNAN and NTO in *Rana pipiens* Tadpoles. *Environmental Toxicology and Chemistry* **2015**, *34*, (4), 880-886.
50. Quinn, M. J.; Bannon, D. I.; Jackovitz, A. M.; Hanna, T. L.; Shiflett, A. A.; Johnson, M. S., Assessment of 3-Nitro-1,2,4-triazol-5-one as a Potential Endocrine Disrupting Chemical in Rats Using the Hershberger and Uterotrophic Bioassays. *International Journal of Toxicology* **2014**, *33*, (5), 367-372.
51. Lent, E. M.; Crouse, L. C. B.; Wallace, S. M.; Carroll, E. E., Peri-pubertal Administration of 3-Nitro-1,2,4-Triazol-5-One (NTO) Affects Reproductive Organ Development in Male but not Female Sprague Dawley Rats. *Reproductive Toxicology* **2015**, *57*, 1-9.
52. Madeira, C. L.; Field, J. A.; Simonich, M. T.; Tanguay, R. L.; Chorover, J.; Sierra-Alvarez, R., Ecotoxicity of the Insensitive Munitions Compound 3-Nitro-1,2,4-triazol-5-one (NTO) and its Reduced Metabolite 3-Amino-1,2,4-triazol-5-one (ATO). *Journal of Hazardous Materials* **2018**, *343*, 340-346.
53. Perreault, N. N.; Halasz, A.; Manno, D.; Thiboutot, S.; Ampleman, G.; Hawari, J., Aerobic Mineralization of Nitroguanidine by *Variovorax* Strain VC1 Isolated from Soil. *Environmental Science & Technology* **2012**, *46*, (11), 6035-6040.
54. Ho, B.; Tillotson, J. A.; Kincannon, L. C.; Simboli, P. B.; Korte Jr, D. W., The Fate of Nitroguanidine in the Rat. *Fundamental and Applied Toxicology* **1988**, *10*, (3), 453-458.
55. van der Schalie, W. H. The Toxicity of Nitroguanidine and Photolyzed Nitroguanidine to Freshwater Aquatic Organisms. Army Medical Bioengineering Research and Development Laboratory, Fort Detrick MD: United States Defense Technical Information Center, **1985**.

56. Haag, W. R.; Spangord, R.; Mill, T.; Podoll, R. T.; Chou, T.-W.; Tse, D. S.; Harper, J. C., Aquatic Environmental Fate of Nitroguanidine. *Environmental Toxicology and Chemistry* **1990**, *9*, (11), 1359-1367.
57. Heitholt, J. J.; Hodgson, R. H.; Tworkoski, T. J., Toxicity and Uptake of Nitroguanidine in Plants. *Bulletin of Environmental Contamination and Toxicology* **1990**, *44*, (5), 751-758.
58. Gupta, R. K.; Korte, D. W.; Reddy, G., Mutagenic Potential of Nitroguanidine and Nitrosoguanidine in the *Drosophila melanogaster* Sex-Linked Recessive Lethal Assay. *Journal of Applied Toxicology* **1993**, *13*, (4), 231-234.
59. Mulherin, N. D.; Jenkins, T. F.; Walsh, M. E. *Stability of Nitroguanidine in Moist, Unsaturated Soils*; Engineer Research and Development Center, Hanover, NH Cold Regions Research and Engineering Lab United States Defense Technical Information Center 2005.
60. Williams, R. T.; Sisk, W. E.; MacGillivray, A. R., Degradation of Nitroguanidine Wastewater Components in Soil. *Environmental Toxicology and Chemistry* **1989**, *8*, (6), 469-475.
61. Indest, K. J.; Hancock, D. E.; Crocker, F. H.; Eberly, J. O.; Jung, C. M.; Blakeney, G. A.; Brame, J.; Chappell, M. A., Biodegradation of Insensitive Munition Formulations IMX-101 and IMX-104 in Surface Soils. *Journal of Industrial Microbiology & Biotechnology* **2017**, *44*, (7), 987-995.
62. Rao, B.; Wang, W.; Cai, Q.; Anderson, T.; Gu, B., Photochemical Transformation of the Insensitive Munitions Compound 2,4-Dinitroanisole. *Science of The Total Environment* **2013**, *443*, (0), 692-699.
63. Salter-Blanc, A. J.; Bylaska, E. J.; Ritchie, J. J.; Tratnyek, P. G., Mechanisms and Kinetics of Alkaline Hydrolysis of the Energetic Nitroaromatic Compounds 2,4,6-Trinitrotoluene (TNT) and 2,4-Dinitroanisole (DNAN). *Environmental Science & Technology* **2013**, *47*, (13), 6790-6798.
64. Sviatenko, L.; Kinney, C.; Gorb, L.; Hill, F. C.; Bednar, A. J.; Okovytyy, S.; Leszczynski, J., Comprehensive Investigations of Kinetics of Alkaline Hydrolysis of TNT (2,4,6-Trinitrotoluene), DNT (2,4-Dinitrotoluene), and DNAN (2,4-Dinitroanisole). *Environmental Science & Technology* **2014**, *48*, (17), 10465-10474.
65. Karthikeyan, S.; Kurt, Z.; Pandey, G.; Spain, J. C., Immobilized Biocatalyst for Detection and Destruction of the Insensitive Explosive, 2,4-Dinitroanisole (DNAN). *Environmental Science & Technology* **2016**, *50*, (20), 11193-11199.
66. Saad, R.; Radovic-Hrapovic, Z.; Ahvazi, B.; Thiboutot, S.; Ampleman, G.; Hawari, J., Sorption of 2,4-Dinitroanisole (DNAN) on Lignin. *Journal of Environmental Sciences* **2012**, *24*, (5), 808-813.
67. Boddu, V. M.; Abburi, K.; Fredricksen, A. J.; Maloney, S. W.; Damavarapu, R., Equilibrium and Column Adsorption Studies of 2,4-Dinitroanisole (DNAN) on Surface Modified Granular Activated Carbons. *Environmental Technology* **2009**, *30*, (2), 173-181.
68. Olivares, C. I.; Madeira, C. L.; Sierra-Alvarez, R.; Kadoya, W.; Abrell, L.; Chorover, J.; Field, J. A., Environmental Fate of <sup>14</sup>C Radiolabeled 2,4-Dinitroanisole in Soil Microcosms. *Environmental Science & Technology* **2017**, *51*, (22), 13327-13334.

69. Niedźwiecka, J. B.; Drew, S. R.; Schlautman, M. A.; Millerick, K. A.; Grubbs, E.; Tharayil, N.; Finneran, K. T., Iron and Electron Shuttle Mediated (Bio)degradation of 2,4-Dinitroanisole (DNAN). *Environmental Science & Technology* **2017**, *51*, (18), 10729-10735.
70. Shen, J.; Ou, C.; Zhou, Z.; Chen, J.; Fang, K.; Sun, X.; Li, J.; Zhou, L.; Wang, L., Pretreatment of 2,4-Dinitroanisole (DNAN) Producing Wastewater Using a Combined Zero-Valent Iron (ZVI) Reduction and Fenton Oxidation Process. *Journal of Hazardous Materials* **2013**, *260*, (0), 993-1000.
71. Salter-Blanc, A. J.; Bylaska, E. J.; Johnston, H. J.; Tratnyek, P. G., Predicting Reduction Rates of Energetic Nitroaromatic Compounds Using Calculated One-Electron Reduction Potentials. *Environmental Science & Technology* **2015**, *49*, (6), 3778-3786.
72. Salter-Blanc, A. J.; Bylaska, E. J.; Lyon, M. A.; Ness, S. C.; Tratnyek, P. G., Structure–Activity Relationships for Rates of Aromatic Amine Oxidation by Manganese Dioxide. *Environmental Science & Technology* **2016**, *50*, (10), 5094-5102.
73. Khatiwada, R.; Olivares, C.; Abrell, L.; Root, R. A.; Sierra-Alvarez, R.; Field, J. A.; Chorover, J., Oxidation of Reduced Daughter Products from 2,4-Dinitroanisole (DNAN) by Mn(IV) and Fe(III) oxides. *Chemosphere*.
74. Le Champion, L.; Giannotti, C.; Ouazzani, J., Photocatalytic Degradation of 5-Nitro-1,2,4-triazol-3-one (NTO) in Aqueous Suspension of TiO<sub>2</sub>. Comparison with Fenton Oxidation. *Chemosphere* **1999**, *38*, (7), 1561-1570.
75. Wallace, L.; Cronin, M. P.; Day, A. I.; Buck, D. P., Electrochemical Method Applicable to Treatment of Wastewater from Nitrotriazolone Production. *Environmental Science & Technology* **2009**, *43*, (6), 1993-1998.
76. Mark, N.; Arthur, J.; Dontsova, K.; Brusseau, M.; Taylor, S., Adsorption and Attenuation Behavior of 3-Nitro-1,2,4-triazol-5-one (NTO) in Eleven Soils. *Chemosphere* **2016**, *144*, 1249-1255.
77. Weiss, J. V.; Emerson, D.; Megonigal, J. P., Geochemical Control of Microbial Fe(III) Reduction Potential in Wetlands: Comparison of the Rhizosphere to Non-Rhizosphere Soil. *FEMS Microbiology Ecology* **2004**, *48*, (1), 89-100.
78. Linker, B. R.; Khatiwada, R.; Perdrial, N.; Abrell, L.; Sierra-Alvarez, R.; Field, J. A.; Chorover, J., Adsorption of Novel Insensitive Munitions Compounds at Clay Mineral and Metal Oxide Surfaces. *Environmental Chemistry* **2015**, *12*, (1), 74-84.
79. Koutsospyros, A.; Pavlov, J.; Fawcett, J.; Strickland, D.; Smolinski, B.; Braid, W., Degradation of High Energetic and Insensitive Munitions Compounds by Fe/Cu Bimetal Reduction. *Journal of Hazardous Materials* **2012**, *219–220*, (0), 75-81.
80. Burrows, W. D.; Schmidt, M. O.; Chyrek, R. H.; Noss, C. I. Photochemistry of Aqueous Nitroguanidine. Army Biomedical Research and Development Laboratory, Fort Detrick MD: United States Defense Technical Information Center, **1988**.
81. Noss, C. I.; Chyrek, R. H. Nitroguanidine Wastewater Pollution Control Technology: Phase III. Treatment with Ultraviolet Radiation, Ozone, and Hydrogen Peroxide. Army Medical Bioengineering Research and Development Laboratory, Fort Detrick MD Defense Technical Information Center, **1984**.
82. Kaplan, D. L.; Cornell, J. H.; Kaplan, A. M., Decomposition of Nitroguanidine. *Environmental Science & Technology* **1982**, *16*, (8), 488-492.

83. Bhadra, R.; Wayment, D. G.; Hughes, J. B.; Shanks, J. V., Confirmation of Conjugation Processes during TNT Metabolism by Axenic Plant Roots. *Environmental Science & Technology* **1999**, *33*, (3), 446-452.
84. Hughes, J. B.; Shanks, J.; Vanderford, M.; Lauritzen, J.; Bhadra, R., Transformation of TNT by Aquatic Plants and Plant Tissue Cultures. *Environmental Science & Technology* **1997**, *31*, (1), 266-271.
85. Doty, S. L., Enhancing Phytoremediation Through the Use of Transgenics and Endophytes. *New Phytologist* **2008**, *179*, (2), 318-333.
86. Khan, Z.; Roman, D.; Kintz, T.; delas Alas, M.; Yap, R.; Doty, S., Degradation, Phytoprotection and Phytoremediation of Phenanthrene by Endophyte *Pseudomonas putida*, PD1. *Environmental Science & Technology* **2014**, *48*, (20), 12221-12228.
87. Andreolli, M.; Lampis, S.; Poli, M.; Gullner, G.; Biró, B.; Vallini, G., Endophytic *Burkholderia fungorum* DBT1 Can Improve Phytoremediation Efficiency of Polycyclic Aromatic Hydrocarbons. *Chemosphere* **2013**, *92*, (6), 688-694.
88. van Aken, B.; Schnoor, J. L., Evidence of Perchlorate (ClO<sub>4</sub><sup>-</sup>) Reduction in Plant Tissues (Poplar Tree) Using Radio-Labeled <sup>36</sup>ClO<sub>4</sub>. *Environmental Science & Technology* **2002**, *36*, (12), 2783-2788.
89. Kang, J. W.; Khan, Z.; Doty, S. L., Biodegradation of Trichloroethylene by an Endophyte of Hybrid Poplar. *Applied and Environmental Microbiology* **2012**, *78*, (9), 3504-3507.
90. Van Aken, B.; Yoon, J. M.; Schnoor, J. L., Biodegradation of Nitro-Substituted Explosives 2,4,6-Trinitrotoluene, Hexahydro-1,3,5-Trinitro-1,3,5-Triazine, and Octahydro-1,3,5,7-Tetranitro-1,3,5-Tetrazocine by a Phytosymbiotic *Methylobacterium* sp. Associated with Poplar Tissues (*Populus deltoides* × *nigra* DN34). *Applied and Environmental Microbiology* **2004**, *70*, (1), 508-517.
91. Mu, R.; Shi, H.; Yuan, Y.; Karnjanapiboonwong, A.; Burken, J. G.; Ma, Y., Fast Separation and Quantification Method for Nitroguanidine and 2,4-Dinitroanisole by Ultrafast Liquid Chromatography–Tandem Mass Spectrometry. *Analytical Chemistry* **2012**, *84*, (7), 3427-3432.
92. Watanabe, M.; Sofuni, T.; Nohmi, T., Involvement of Cys69 Residue in the Catalytic Mechanism of N-Hydroxyarylamine O-Acetyltransferase of *Salmonella typhimurium*. Sequence Similarity at the Amino Acid Level Suggests a Common Catalytic Mechanism of Acetyltransferase for *S. typhimurium* And Higher Organisms. *Journal of Biological Chemistry* **1992**, *267*, (12), 8429-8436.
93. Payton, M.; Mushtaq, A.; Yu, T.-W.; Wu, L.-J.; Sinclair, J.; Sim, E., Eubacterial Arylamine N-Acetyltransferases – Identification and Comparison of 18 Members of the Protein Family with Conserved Active Site Cysteine, Histidine and Aspartate Residues. *Microbiology* **2001**, *147*, (5), 1137-1147.
94. Dairou, J.; Flatters, D.; Chaffotte, A. F.; Pluvinage, B.; Sim, E.; Dupret, J.-M.; Rodrigues-Lima, F., Insight into the Structure of *Mesorhizobium loti* Arylamine N-Acetyltransferase 2 (MLNAT2): A Biochemical and Computational Study. *FEBS Letters* **2006**, *580*, (7), 1780-1788.
95. Boddu, V. M.; Abburi, K.; Maloney, S. W.; Damavarapu, R., Thermophysical Properties of an Insensitive Munitions Compound, 2,4-Dinitroanisole. *Journal of Chemical & Engineering Data* **2008**, *53*, (5), 1120-1125.

96. Sheremata, T. W.; Hawari, J., Mineralization of RDX by the White Rot Fungus *Phanerochaete chrysosporium* to Carbon Dioxide and Nitrous Oxide. *Environmental Science & Technology* **2000**, *34*, (16), 3384-3388.
97. Fernando, T.; Bumpus, J. A.; Aust, S. D., Biodegradation of TNT (2,4,6-trinitrotoluene) by *Phanerochaete chrysosporium*. *Applied and Environmental Microbiology* **1990**, *56*, (6), 1666-1671.
98. Harms, H.; Schlosser, D.; Wick, L. Y., Untapped Potential: Exploiting Fungi in Bioremediation of Hazardous Chemicals. *Nat Rev Micro* **2011**, *9*, (3), 177-192.
99. Golan-Rozen, N.; Seiwert, B.; Riemenschneider, C.; Reemtsma, T.; Chefetz, B.; Hadar, Y., Transformation Pathways of the Recalcitrant Pharmaceutical Compound Carbamazepine by the White-Rot Fungus *Pleurotus ostreatus*: Effects of Growth Conditions. *Environmental Science & Technology* **2015**, *49*, (20), 12351-12362.
100. Singh, H., *Mycoremediation, Fungal Bioremediation*. John Wiley & Sons, Inc.: Hoboken, New Jersey, **2006**.
101. Ayyangar, N. R.; Srinivasan, K. V., Effect of Substituents in the Formation of Diacetanilides. *Canadian Journal of Chemistry* **1984**, *62*, (7), 1292-1296.
102. Dean, T. R.; Betancourt, D.; Menetrez, M. Y., A Rapid DNA Extraction Method for PCR Identification of Fungal Indoor Air Contaminants. *Journal of Microbiological Methods* **2004**, *56*, (3), 431-434.
103. Smit, E.; Leeftang, P.; Glandorf, B.; Dirk van Elsas, J.; Wernars, K., Analysis of Fungal Diversity in the Wheat Rhizosphere by Sequencing of Cloned PCR-Amplified Genes Encoding 18S rRNA and Temperature Gradient Gel Electrophoresis. *Applied and Environmental Microbiology* **1999**, *65*, (6), 2614-2621.
104. Gowda, H.; Ivanisevic, J.; Johnson, C. H.; Kurczy, M. E.; Benton, H. P.; Rinehart, D.; Nguyen, T.; Ray, J.; Kuehl, J.; Arevalo, B.; Westenskow, P. D.; Wang, J.; Arkin, A. P.; Deutschbauer, A. M.; Patti, G. J.; Siuzdak, G., Interactive XCMS Online: Simplifying Advanced Metabolomic Data Processing and Subsequent Statistical Analyses. *Analytical Chemistry* **2014**, *86*, (14), 6931-6939.
105. Mineralization of <sup>14</sup>C-Labelled Synthetic Lignin and Extracellular Enzyme Activities of the Wood-Colonizing Ascomycetes *Xylaria hypoxylon* and *Xylaria polymorpha*. *Applied Microbiology and Biotechnology* **2016**, *69*, (5), 573-579.
106. Baldrian, P., Fungal Laccases – Occurrence and Properties. *FEMS Microbiology Reviews* **2006**, *30*, (2), 215.
107. Scheibner, K.; Hofrichter, M.; Herre, A.; Michels, J.; Fritsche, W., Screening for Fungi Intensively Mineralizing 2,4,6-Trinitrotoluene. *Applied Microbiology and Biotechnology* **1997**, *47*, (4), 452-457.
108. Martins, M.; Rodrigues-Lima, F.; Dairou, J.; Lamouri, A.; Malagnac, F.; Silar, P.; Dupret, J.-M., An Acetyltransferase Conferring Tolerance to Toxic Aromatic Amine Chemicals. *Journal of Biological Chemistry* **2009**, *284*, (28), 18726-18733.
109. Hoyt, N.; Brunell, M.; Kroeck, K.; Hable, M.; Crouse, L.; O'Neill, A.; Bannon, D. I., Biomarkers of Oral Exposure to 3-Nitro-1,2,4-triazol-5-one (NTO) and 2,4-Dinitroanisole (DNAN) in Blood and Urine of Rhesus Macaques (*Macaca mulatta*). *Biomarkers* **2013**, *18*, (7), 587-594.
110. Wang, C. Y.; Zheng, D.; Hughes, J. B., Stability of Hydroxylamino- and Amino-Intermediates from Reduction of 2,4,6-Trinitrotoluene, 2,4-Dinitrotoluene, and 2,6-Dinitrotoluene. *Biotechnology Letters* **2000**, *22*, (1), 15-19.

111. Schymanski, E. L.; Jeon, J.; Gulde, R.; Fenner, K.; Ruff, M.; Singer, H. P.; Hollender, J., Identifying Small Molecules via High Resolution Mass Spectrometry: Communicating Confidence. *Environmental Science & Technology* **2014**, *48*, (4), 2097-2098.
112. Karagianni, E. P.; Kontomina, E.; Davis, B.; Kotseli, B.; Tsirka, T.; Garefalaki, V.; Sim, E.; Glenn, A. E.; Boukouvala, S., Homologues of Xenobiotic Metabolizing N-Acetyltransferases in Plant-Associated Fungi: Novel Functions for an Old Enzyme Family. *Scientific Reports*, Published online: 6 August 2015; | doi:10.1038/srep12900 **2015**.
113. Fabre, N.; Rustan, I.; de Hoffmann, E.; Quetin-Leclercq, J., Determination of Flavone, Flavonol, and Flavanone Aglycones by Negative Ion Liquid Chromatography Electrospray Ion Trap Mass Spectrometry. *Journal of the American Society for Mass Spectrometry* **2001**, *12*, (6), 707-715.
114. Yi, L.; Dratter, J.; Wang, C.; Tunge, J. A.; Desaire, H., Identification of Sulfation Sites of Metabolites and Prediction of the Compounds' Biological Effects. *Analytical and Bioanalytical Chemistry* **2006**, *386*, (3), 666-674.
115. Peng, C.; Lu, Z.; Xie, Z.; Cheng, Z.; Chen, Y.; Tan, M.; Luo, H.; Zhang, Y.; He, W.; Yang, K.; Zwaans, B. M. M.; Tishkoff, D.; Ho, L.; Lombard, D.; He, T.-C.; Dai, J.; Verdin, E.; Ye, Y.; Zhao, Y., The First Identification of Lysine Malonylation Substrates and Its Regulatory Enzyme. *Molecular & Cellular Proteomics : MCP* **2011**, *10*, (12), M111.012658.
116. Gulde, R.; Meier, U.; Schymanski, E. L.; Kohler, H.-P. E.; Helbling, D. E.; Derrer, S.; Rentsch, D.; Fenner, K., Systematic Exploration of Biotransformation Reactions of Amine-Containing Micropollutants in Activated Sludge. *Environmental Science & Technology* **2016**, *50*, (6), 2908-2920.
117. Helbling, D. E.; Hollender, J.; Kohler, H.-P. E.; Fenner, K., Structure-Based Interpretation of Biotransformation Pathways of Amide-Containing Compounds in Sludge-Seeded Bioreactors. *Environmental Science & Technology* **2010**, *44*, (17), 6628-6635.
118. Ro, K. S.; Venugopal, A.; Adrian, D. D.; Constant, D.; Qaisi, K.; Valsaraj, K. T.; Thibodeaux, L. J.; Roy, D., Solubility of 2,4,6-Trinitrotoluene (TNT) in Water. *Journal of Chemical & Engineering Data* **1996**, *41*, (4), 758-761.
119. Fung, V.; Schreiber, B.; Patel, C.; Samuels, P.; Vinh, P.; Zhao, X.-L. In *Process Improvement and Optimization of Insensitive Explosive IMX-101*, Insensitive Munitions & Energetic Material Technology Symposium, Las Vegas, NV, 2012; Las Vegas, NV, 2012.
120. Hughes, J. B.; Wang, C.; Yesland, K.; Richardson, A.; Bhadra, R.; Bennett, G.; Rudolph, F., Bamberger Rearrangement during TNT Metabolism by *Clostridium acetobutylicum*. *Environmental Science & Technology* **1998**, *32*, (4), 494-500.
121. Hawari, J.; Halasz, A.; Groom, C.; Deschamps, S.; Paquet, L.; Beaulieu, C.; Corriveau, A., Photodegradation of RDX in Aqueous Solution: A Mechanistic Probe for Biodegradation with *Rhodococcus* sp. *Environmental Science & Technology* **2002**, *36*, (23), 5117-5123.
122. Sandermann, H., Plant Metabolism of Xenobiotics. *Trends in Biochemical Sciences* **1992**, *17*, (2), 82-84.

123. Macherius, A.; Eggen, T.; Lorenz, W.; Moeder, M.; Ondruschka, J.; Reemtsma, T., Metabolization of the Bacteriostatic Agent Triclosan in Edible Plants and its Consequences for Plant Uptake Assessment. *Environmental Science & Technology* **2012**, *46*, (19), 10797-10804.
124. Coleman, J.; Blake-Kalff, M.; Davies, E., Detoxification of Xenobiotics by Plants: Chemical Modification and Vacuolar Compartmentation. *Trends in Plant Science* **1997**, *2*, (4), 144-151.
125. Durringer, J. M.; Morrie Craig, A.; Smith, D. J.; Chaney, R. L., Uptake and Transformation of Soil [<sup>14</sup>C]-Trinitrotoluene by Cool-Season Grasses. *Environmental Science & Technology* **2010**, *44*, (16), 6325-6330.
126. Just, C. L.; Schnoor, J. L., Phytophotolysis of Hexahydro-1,3,5-trinitro-1,3,5-triazine (RDX) in Leaves of Reed Canary Grass. *Environmental Science & Technology* **2004**, *38*, (1), 290-295.
127. Miller, E. L.; Nason, S. L.; Karthikeyan, K. G.; Pedersen, J. A., Root Uptake of Pharmaceuticals and Personal Care Product Ingredients. *Environmental Science & Technology* **2016**, *50*, (2), 525-541.
128. Alif, A.; Pilichowski, J.-F.; Boule, P., Photochemistry and Environment XIII: Phototransformation of 2-Nitrophenol in Aqueous Solution. *Journal of Photochemistry and Photobiology A: Chemistry* **1991**, *59*, (2), 209-219.
129. LeFevre, G. H.; Müller, C. E.; Li, R. J.; Luthy, R. G.; Sattely, E. S., Rapid Phytotransformation of Benzotriazole Generates Synthetic Tryptophan and Auxin Analogs in *Arabidopsis*. *Environmental Science & Technology* **2015**, *49*, (18), 10959-10968.
130. LeFevre, G. H.; Portmann, A. C.; Müller, C. E.; Sattely, E. S.; Luthy, R. G., Plant Assimilation Kinetics and Metabolism of 2-Mercaptobenzothiazole Tire Rubber Vulcanizers by *Arabidopsis*. *Environmental Science & Technology* **2016**, *50*, (13), 6762-6771.
131. Nussler, A. K.; Glanemann, M.; Schirmeier, A.; Liu, L.; Nussler, N. C., Fluorometric Measurement of Nitrite/Nitrate by 2,3-Diaminonaphthalene. *Nat. Protocols* **2006**, *1*, (5), 2223-2226.
132. Macherius, A.; Seiwert, B.; Schröder, P.; Huber, C.; Lorenz, W.; Reemtsma, T., Identification of Plant Metabolites of Environmental Contaminants by UPLC-QToF-MS: The in Vitro Metabolism of Triclosan in Horseradish. *Journal of Agricultural and Food Chemistry* **2014**, *62*, (5), 1001-1009.
133. Xie, C.; Zhong, D.; Chen, X., A Fragmentation-Based Method for the Differentiation of Glutathione Conjugates by High-Resolution Mass Spectrometry with Electrospray Ionization. *Analytica Chimica Acta* **2013**, *788*, 89-98.
134. Brazier-Hicks, M.; Evans, K. M.; Cunningham, O. D.; Hodgson, D. R. W.; Steel, P. G.; Edwards, R., Catabolism of Glutathione Conjugates in *Arabidopsis thaliana*: Role In Metabolic Reactivation of the Herbicide Safener Fenclorim. *Journal of Biological Chemistry* **2008**, *283*, (30), 21102-21112.
135. Colby, S. R., Herbicide Metabolism: N-Glycoside of Amiben Isolated from Soybean Plants. *Science* **1965**, *150*, (3696), 619-620.
136. Winkler, R.; Sandermann, H., N-Glucosyl Conjugates of Chlorinated Anilines: Spontaneous Formation and Cleavage. *Journal of Agricultural and Food Chemistry* **1992**, *40*, (10), 2008-2012.

137. McCutcheon, S. C.; Schnoor, J. L., *Phytoremediation: Transformation and control of contaminants*. John Wiley & Sons, Inc: Hoboken, New Jersey, 2003.
138. Sandermann, H., Higher Plant Metabolism of Xenobiotics: The 'Green Liver' Concept. *Pharmacogenetics* **1994**, *4*, (5), 225-241.
139. Sens, C.; Scheidemann, P.; Werner, D., The Distribution of <sup>14</sup>C-TNT in Different Biochemical Compartments of the Monocotyledonous *Triticum aestivum*. *Environmental Pollution* **1999**, *104*, (1), 113-119.
140. Fu, Q.; Zhang, J.; Borchardt, D.; Schlenk, D.; Gan, J., Direct Conjugation of Emerging Contaminants in *Arabidopsis*: Indication for an Overlooked Risk in Plants? *Environmental Science & Technology* **2017**, *51*, (11), 6071-6081.
141. Fu, Q.; Ye, Q.; Zhang, J.; Richards, J.; Borchardt, D.; Gan, J., Diclofenac in *Arabidopsis* cells: Rapid formation of conjugates. *Environmental Pollution* **2017**, *222*, (Supplement C), 383-392.
142. Hyland, K. C.; Blaine, A. C.; Higgins, C. P., Accumulation of Contaminants of Emerging Concern in Food Crops—Part 2: Plant Distribution. *Environmental Toxicology and Chemistry* **2016**, *34*, (10), 2222-2230.
143. Holt, N. E.; Zigmantas, D.; Valkunas, L.; Li, X.-P.; Niyogi, K. K.; Fleming, G. R., Carotenoid Cation Formation and the Regulation of Photosynthetic Light Harvesting. *Science* **2005**, *307*, (5708), 433.
144. Ramel, F.; Birtic, S.; Ginies, C.; Soubigou-Taconnat, L.; Triantaphylidès, C.; Havaux, M., Carotenoid Oxidation Products are Stress Signals that Mediate Gene Responses to Singlet Oxygen in Plants. *Proceedings of the National Academy of Sciences* **2012**, *109*, (14), 5535-5540.
145. Limmer, M. A.; Balouet, J.-C.; Karg, F.; Vroblesky, D. A.; Burken, J. G., Phytoscreening for Chlorinated Solvents Using Rapid in Vitro SPME Sampling: Application to Urban Plume in Verl, Germany. *Environmental Science & Technology* **2011**, *45*, (19), 8276-8282.
146. Limmer, M. A.; Shetty, M. K.; Markus, S.; Kroeker, R.; Parker, B. L.; Martinez, C.; Burken, J. G., Directional Phytoscreening: Contaminant Gradients in Trees for Plume Delineation. *Environmental Science & Technology* **2013**, *47*, (16), 9069-9076.
147. Limmer, M. A.; Holmes, A. J.; Burken, J. G., Phytomonitoring of Chlorinated Ethenes in Trees: A Four-Year Study of Seasonal Chemodynamics in Planta. *Environmental Science & Technology* **2014**, *48*, (18), 10634-10640.
148. Limmer, M. A.; West, D. M.; Mu, R.; Shi, H.; Whitlock, K.; Burken, J. G., Phytoscreening for Perchlorate: Rapid Analysis of Tree Sap. *Environmental Science: Water Research & Technology* **2015**, *1*, (2), 138-145.
149. Crouse, L. C. B.; Lent, E. M.; Leach, G. J., Oral Toxicity of 3-Nitro-1,2,4-triazol-5-one in Rats. *International Journal of Toxicology* **2015**, *34*, (1), 55-66.
150. Gust, K. A.; Stanley, J. K.; Wilbanks, M. S.; Mayo, M. L.; Chappell, P.; Jordan, S. M.; Moores, L. C.; Kennedy, A. J.; Barker, N. D., The Increased Toxicity of UV-Degraded Nitroguanidine and IMX-101 to Zebrafish Larvae: Evidence Implicating Oxidative Stress. *Aquatic Toxicology* **2017**, *190*, 228-245.
151. Mukundan, T.; Purandare, G. N.; Nair, J. K.; Pansare, S. M.; Sinha, R. K.; Singh, H., Explosive Nitrotriazolone Formulates. *Defence Science Journal; Vol 52, No 2* **2002**.



152. Chu, C.; Erickson, P. R.; Lundeen, R. A.; Stamatelatos, D.; Alaimo, P. J.; Latch, D. E.; McNeill, K., Photochemical and Nonphotochemical Transformations of Cysteine with Dissolved Organic Matter. *Environmental Science & Technology* **2016**, *50*, (12), 6363-6373.
153. Lundeen, R. A.; Chu, C.; Sander, M.; McNeill, K., Photooxidation of the Antimicrobial, Nonribosomal Peptide Bacitracin A by Singlet Oxygen under Environmentally Relevant Conditions. *Environmental Science & Technology* **2016**, *50*, (16), 8586-8595.
154. Chu, C.; Lundeen, R. A.; Remucal, C. K.; Sander, M.; McNeill, K., Enhanced Indirect Photochemical Transformation of Histidine and Histamine through Association with Chromophoric Dissolved Organic Matter. *Environmental Science & Technology* **2015**, *49*, (9), 5511-5519.
155. Laszakovits, J. R.; Berg, S. M.; Anderson, B. G.; O'Brien, J. E.; Wammer, K. H.; Sharpless, C. M., *p*-Nitroanisole/Pyridine and *p*-Nitroacetophenone/Pyridine Actinometers Revisited: Quantum Yield in Comparison to Ferrioxalate. *Environmental Science & Technology Letters* **2017**, *4*, (1), 11-14.
156. McConville, M. B.; Hubert, T. D.; Remucal, C. K., Direct Photolysis Rates and Transformation Pathways of the Lampricides TFM and Niclosamide in Simulated Sunlight. *Environmental Science & Technology* **2016**, *50*, (18), 9998-10006.
157. Appiani, E.; Ossola, R.; Latch, D. E.; Erickson, P. R.; McNeill, K., Aqueous Singlet Oxygen Reaction Kinetics of Furfuryl Alcohol: Effect of Temperature, pH, and Salt Content. *Environmental Science: Processes & Impacts* **2017**, *19*, (4), 507-516.
158. Wenk, J.; von Gunten, U.; Canonica, S., Effect of Dissolved Organic Matter on the Transformation of Contaminants Induced by Excited Triplet States and the Hydroxyl Radical. *Environmental Science & Technology* **2011**, *45*, (4), 1334-1340.
159. Prasse, C.; Wenk, J.; Jasper, J. T.; Ternes, T. A.; Sedlak, D. L., Co-occurrence of Photochemical and Microbiological Transformation Processes in Open-Water Unit Process Wetlands. *Environmental Science & Technology* **2015**, *49*, (24), 14136-14145.
160. Kelly, M. M.; Arnold, W. A., Direct and Indirect Photolysis of the Phytoestrogens Genistein and Daidzein. *Environmental Science & Technology* **2012**, *46*, (10), 5396-5403.
161. Grebel, J. E.; Pignatello, J. J.; Mitch, W. A., Sorbic Acid as a Quantitative Probe for the Formation, Scavenging And Steady-State Concentrations of the Triplet-Excited State of Organic Compounds. *Water Research* **2011**, *45*, (19), 6535-6544.
162. Canonica, S.; Laubscher, H.-U., Inhibitory Effect of Dissolved Organic Matter on Triplet-Induced Oxidation of Aquatic Contaminants. *Photochemical & Photobiological Sciences* **2008**, *7*, (5), 547-551.
163. Wenk, J.; Canonica, S., Phenolic Antioxidants Inhibit the Triplet-Induced Transformation of Anilines and Sulfonamide Antibiotics in Aqueous Solution. *Environmental Science & Technology* **2012**, *46*, (10), 5455-5462.
164. Rosario-Ortiz, F. L.; Canonica, S., Probe Compounds to Assess the Photochemical Activity of Dissolved Organic Matter. *Environmental Science & Technology* **2016**, *50*, (23), 12532-12547.
165. Felcyn, J. R.; Davis, J. C. C.; Tran, L. H.; Berude, J. C.; Latch, D. E., Aquatic Photochemistry of Isoflavone Phytoestrogens: Degradation Kinetics and Pathways. *Environmental Science & Technology* **2012**, *46*, (12), 6698-6704.

166. Lee, C.; Choi, W.; Yoon, J., UV Photolytic Mechanism of N-Nitrosodimethylamine in Water: Roles of Dissolved Oxygen and Solution pH. *Environmental Science & Technology* **2005**, *39*, (24), 9702-9709.
167. Hayyan, M.; Hashim, M. A.; AlNashef, I. M., Superoxide Ion: Generation and Chemical Implications. *Chemical Reviews* **2016**, *116*, (5), 3029-3085.
168. Janssen, E. M. L.; Erickson, P. R.; McNeill, K., Dual Roles of Dissolved Organic Matter as Sensitizer and Quencher in the Photooxidation of Tryptophan. *Environmental Science & Technology* **2014**, *48*, (9), 4916-4924.
169. Buxton, G. V.; Greenstock, C. L.; Helman, W. P.; Ross, A. B., Critical Review of Rate Constants for Reactions of Hydrated Electrons, Hydrogen Atoms and Hydroxyl Radicals ( $\cdot\text{OH}/\cdot\text{O}^-$ ) in Aqueous Solution. *Journal of Physical and Chemical Reference Data* **1988**, *17*, (2), 513-886.
170. Jasper, J. T.; Sedlak, D. L., Phototransformation of Wastewater-Derived Trace Organic Contaminants in Open-Water Unit Process Treatment Wetlands. *Environmental Science & Technology* **2013**, *47*, (19), 10781-10790.
171. Fournier, D.; Halasz, A.; Spain, J.; Spangord, R. J.; Bottaro, J. C.; Hawari, J., Biodegradation of the Hexahydro-1,3,5-Trinitro-1,3,5-Triazine Ring Cleavage Product 4-Nitro-2,4-Diazabutanal by *Phanerochaete chrysosporium*. *Applied and Environmental Microbiology* **2004**, *70*, (2), 1123-1128.
172. Le Campion, L.; Delaforge, M.; Noel, J. P.; Ouazzani, J., Metabolism of  $^{14}\text{C}$ -Labelled 5-Nitro-1,2,4-Triazol-3-One by Rat Liver Microsomes: Evidence for the Participation of Cytochrome P-450. *European Journal of Biochemistry* **1997**, *248*, (2), 401-406.
173. Chowdhary, P. K.; Keshavan, N.; Nguyen, H. Q.; Peterson, J. A.; González, J. E.; Haines, D. C., *Bacillus megaterium* CYP102A1 Oxidation of Acyl Homoserine Lactones and Acyl Homoserines. *Biochemistry* **2007**, *46*, (50), 14429-14437.
174. Brill, E.; Hannemann, F.; Zapp, J.; Brüning, G.; Jauch, J.; Bernhardt, R., A New Cytochrome P450 System from *Bacillus megaterium* DSM319 for the Hydroxylation of 11-Keto- $\beta$ -boswellic acid (KBA). *Applied Microbiology and Biotechnology* **2014**, *98*, (4), 1703-1717.
175. Bhushan, B.; Trott, S.; Spain, J. C.; Halasz, A.; Paquet, L.; Hawari, J., Biotransformation of Hexahydro-1,3,5-Trinitro-1,3,5-Triazine (RDX) by a Rabbit Liver Cytochrome P450: Insight into the Mechanism of RDX Biodegradation by *Rhodococcus* sp. Strain DN22. *Applied and Environmental Microbiology* **2003**, *69*, (3), 1347-1351.
176. Halasz, A.; Manno, D.; Perreault, N. N.; Sabbadin, F.; Bruce, N. C.; Hawari, J., Biodegradation of RDX Nitroso Products MNX and TNX by Cytochrome P450 *XplA*. *Environmental Science & Technology* **2012**, *46*, (13), 7245-7251.
177. Qu, S.; Kolodziej, E. P.; Long, S. A.; Gloer, J. B.; Patterson, E. V.; Baltrusaitis, J.; Jones, G. D.; Benchetler, P. V.; Cole, E. A.; Kimbrough, K. C.; Tarnoff, M. D.; Cwiertny, D. M., Product-to-Parent Reversion of Trenbolone: Unrecognized Risks for Endocrine Disruption. *Science* **2013**, *342*, (6156), 347.

178. Wammer, K. H.; Anderson, K. C.; Erickson, P. R.; Kliegman, S.; Moffatt, M. E.; Berg, S. M.; Heitzman, J. A.; Pflug, N. C.; McNeill, K.; Martinovic-Weigelt, D.; Abagyan, R.; Cwiertny, D. M.; Kolodziej, E. P., Environmental Photochemistry of Altrenogest: Photoisomerization to a Bioactive Product with Increased Environmental Persistence via Reversible Photohydration. *Environmental Science & Technology* **2016**, *50*, (14), 7480-7488.
179. Cwiertny, D. M.; Snyder, S. A.; Schlenk, D.; Kolodziej, E. P., Environmental Designer Drugs: When Transformation May Not Eliminate Risk. *Environmental Science & Technology* **2014**, *48*, (20), 11737-11745.